1986

Investigation of turbulence promoting inserts for augmenting heat transfer from gases in tubes

Velumylum Nirmalan
Iowa State University

Nirmalan, Velumylum

INVESTIGATION OF TURBULENCE PROMOTING INSERTS FOR AUGMENTING HEAT TRANSFER FROM GASES IN TUBES

Iowa State University PH.D. 1986

PLEASE NOTE:

In all cases this material has been filmed in the best possible way from the available copy. Problems encountered with this document have been identified here with a check mark __✓__.

1. Glossy photographs or pages _____
2. Colored illustrations, paper or print __✓__
3. Photographs with dark background __✓__
4. Illustrations are poor copy _____
5. Pages with black marks, not original copy _____
6. Print shows through as there is text on both sides of page _____
7. Indistinct, broken or small print on several pages __✓__
8. Print exceeds margin requirements _____
9. Tightly bound copy with print lost in spine _____
10. Computer printout pages with indistinct print _____
11. Page(s) _____ lacking when material received, and not available from school or author.
12. Page(s) _____ seem to be missing in numbering only as text follows.
13. Two pages numbered _____. Text follows.
14. Curling and wrinkled pages _____
15. Dissertation contains pages with print at a slant, filmed as received _____
16. Other _____

University
Microfilms
International

Investigation of turbulence promoting inserts for augmenting heat transfer from gases in tubes

by

Velumylum Nirmalan

A Dissertation Submitted to the
Graduate Faculty in Partial Fulfillment of the
Requirements for the Degree of
DOCTOR OF PHILOSOPHY

Major: Mechanical Engineering

Approved:

Signature was redacted for privacy.
In Charge of Major Work

Signature was redacted for privacy.
For the Major Department

Signature was redacted for privacy.
For the Graduate College

Iowa State University
Ames, Iowa

1986

TABLE OF CONTENTS

PAGE

DEDICATION ix

NOMENCLATURE x

I. INTRODUCTION 1

A. The Problem 1

B. Scope of Investigation 3

II. THERMAL HYDRAULIC EXPERIMENTS 5

A. Literature Survey 5

B. Experimental Apparatus 14
1. Flow system 14
2. Test section 17
3. Instrumentation 20
4. Test procedure 22
5. Data reduction 23

C. Experimental Program 28
1. Empty tube experiments 28
2. Basic thermal hydraulic experiments 32
a. Inserts tested 32
b. Results and discussion 32
3. Insert entrance length experiments 48
a. Method of testing for insert entrance effects 59
b. Results and discussion 61
4. Experiments to differentiate the effects of core and wall regions 61
a. Inserts tested 64
b. Results and discussion 64

D. General Correlations and Performance Evaluations 68
1. Empirical correlation of data 68
2. Performance evaluation 78

III. FLOW VISUALIZATION 89

A. General 89

B. Flow Visualization Experiments 89
1. Water/dye-injection technique 89
2. Oil/lamp-black technique 91

C. Observations of Flow Phenomena 93

IV. SURFACE RENEWAL/PENETRATION MODEL OF HEAT TRANSFER 104

A. Background 104

B. Turbulence Burst Phenomena 104

C. The Surface Renewal Model 107

D. Comparison of Model with Experimental Results and Discussion 113

V. CONCLUSIONS AND RECOMMENDATIONS 120

A. Conclusions 120

B. Recommendations for Future Work 123

VI. REFERENCES 124

VII. ACKNOWLEDGEMENTS 130

VIII. APPENDIX A: COMPUTER PROGRAM FOR DATA ACQUISITION AND REDUCTION 131

IX. APPENDIX B: MEASUREMENT OF INSERT TEMPERATURE TO VERIFY ASSUMPTIONS MADE TO ESTIMATE RADIANT HEAT TRANSFER FROM THE INSERT 144

A. Measurement of Insert Temperature 144

B. Results and Verification of Assumptions 145

X. APPENDIX C: SAMPLE CALCULATION AND ERROR ANALYSIS 151

XI. APPENDIX D. CALCULATIONS OF ANGLES REQUIRED FOR FABRICATING THE INSERTS 164

XII. APPENDIX E: HEAT-TRANSFER AND PRESSURE-DROP DATA 169

XIII. APPENDIX F: MULTIPLE LINEAR REGRESSION USING MATRICES . . . 186

XIV. APPENDIX G. MATHEMATICAL SOLUTIONS USED IN THE SURFACE RENEWAL/PENETRATION MODEL 189

LIST OF TABLES

PAGE

TABLE 2.1. Insert characteristics 34

TABLE 2.2. Estimates and uncertainties of constants in correlation equations 70

LIST OF FIGURES

PAGE

FIGURE 2.1. Typical configurations of (a) a wire coil, (b) a twisted tape, and (c) a bent-strip insert 6

FIGURE 2.2. Comparison of published heat-transfer data for wire-coil, twisted-tape, and bent-strip inserts 8

FIGURE 2.3. Comparison of published friction-factor data for wire-coil, twisted-tape, and bent-strip inserts 9

FIGURE 2.4. Flow system (not to scale) 15

FIGURE 2.5. Elevation view of reassembled test loop 18

FIGURE 2.6. Test section schematic (not to scale) 19

FIGURE 2.7. Heat-transfer data for smooth tube compared with the Gnielinski correlation 29

FIGURE 2.8. Friction-factor data for smooth tube compared with the Filonenko correlation 31

FIGURE 2.9. Insert geometry (not to scale) 33

FIGURE 2.10. Heat-transfer and pressure-drop data for insert A1 . . . 35

FIGURE 2.11. Heat-transfer and pressure-drop data for insert AN . . . 36

FIGURE 2.12. Heat-transfer and pressure-drop data for insert A2 . . . 37

FIGURE 2.13. Heat-transfer and pressure-drop data for insert A5 . . . 38

FIGURE 2.14. Heat-transfer and pressure-drop data for insert A4 . . . 39

FIGURE 2.15. Heat-transfer and pressure-drop data for insert A3 . . . 40

FIGURE 2.16. Heat-transfer and pressure-drop data for insert A6 . . . 41

FIGURE 2.17. Heat-transfer and pressure-drop data for insert A7 . . . 42

FIGURE 2.18. Heat-transfer and pressure-drop data for insert A8 . . . 43

FIGURE 2.19. Heat-transfer and pressure-drop data for insert A9 . . . 44

FIGURE 2.20. Heat-transfer and pressure-drop data for insert PA . . . 45

FIGURE 2.21. Effect of insert width and fabrication technique on heat-transfer coefficient 46

FIGURE 2.22. Effect of insert width and fabrication technique on friction factor 47

FIGURE 2.23. Effect of insert width and pitch on heat-transfer coefficient 49

FIGURE 2.24. Effect of insert width and pitch on friction factor . . 50

FIGURE 2.25. Effect of insert pitch on heat-transfer coefficient. Insert width = 0.875 in. 51

FIGURE 2.26. Effect of insert pitch on heat-transfer coefficient. Insert width = 0.75 in. 52

FIGURE 2.27. Effect of insert pitch on friction factor. Insert width = 0.875 in. 53

FIGURE 2.28. Effect of insert pitch on friction factor. Insert width = 0.75 in. 54

FIGURE 2.29. Effect of insert perforations on heat-transfer coefficient 55

FIGURE 2.30. Effect of insert perforations on friction factor 56

FIGURE 2.31. Effect of insert twist angle on heat-transfer coefficient 57

FIGURE 2.32. Effect of insert twist angle on friction factor 58

FIGURE 2.33. Location of insert to obtain entry region data 60

FIGURE 2.34. Insert entrance length heat-transfer data for insert A6 62

FIGURE 2.35. Insert entrance length heat-transfer data for insert A4 63

FIGURE 2.36. Inserts AW and AC. Fabricated to test core and wall region separately 65

FIGURE 2.37. Heat-transfer data for the core (AC) and wall (AW) region inserts compared with data for insert A1 66

FIGURE 2.38. Pressure-drop data for the core (AC) and wall (AW) region inserts compared with data for insert A1 67

FIGURE 2.39. Predicted data for the entry region Nusselt number (Equation 2.15) compared with the experimental data for 9 inserts 71

FIGURE 2.40. Predicted data for the developed region Nusselt number (Equation 2.15) compared with the experimental data for 9 inserts 72

FIGURE 2.41. Predicted friction-factor data (Equation 2.16) compared with the experimental data for 9 inserts 73

FIGURE 2.42. Geometry of insert B tested by Junkhan et al. (1985) . . 74

FIGURE 2.43. Insert B entry region heat-transfer data compared with prediction 75

FIGURE 2.44. Insert B developed region heat-transfer data compared with prediction 76

FIGURE 2.45. Insert B friction data compared with prediction 77

FIGURE 2.46. Predicted heat-transfer and friction-factor enhancement as a function of width-to-tube-diameter ratio 79

FIGURE 2.47. Predicted heat-transfer and friction-factor enhancement as a function of pitch-to-tube-diameter ratio 80

FIGURE 2.48. Effect of Reynolds number and W/D_i on R_2 84

FIGURE 2.49. Effect of Reynolds number and L/D_i on R_2 85

FIGURE 2.50. Effect of Reynolds number and W/D_i on R_3 87

FIGURE 2.51. Effect of Reynolds number and L/D_i on R_3 88

FIGURE 3.1. Water/dye flow visualization setup 90

FIGURE 3.2. Flow patterns obtained by using the water/dye-injection flow visualization technique. $Re_D = 1667$ . . . 94

FIGURE 3.3. Flow patterns obtained by using the oil/lamp-black technique with the glass tube. Photographed from the front 97

FIGURE 3.4. Flow patterns obtained by using the oil/lamp-black technique with the glass tube. Photographed from under the tube 98

FIGURE 3.5. Flow patterns obtained by using the oil/lamp-black technique with the glass tube. Photographed from the front 99

FIGURE 3.6. Flow patterns obtained by using the oil/lamp-black technique with the glass tube. Photographed from under the tube 100

FIGURE 3.7. Flow patterns obtained by using the oil/lamp-black technique with the split plastic tube 102

FIGURE 4.1. Turbulent burst process showing action of a fluid packet 108

FIGURE 4.2. Scatter plot of Equation 4.15 with experimental data . 115

FIGURE 4.3. Effect of insert pitch, L, on Nusselt number and comparison with Equation 4.15 117

FIGURE 4.4. Effect of insert width, W, on Nusselt number and comparison with Equation 4.15 118

FIGURE 4.5. Effect of insert twist angle, γ, on Nusselt number and comparison with Equation 4.15 119

FIGURE B.1. Comparison of estimated and measured insert temperatures 146

FIGURE B.2. Comparison of radiant heat transfer evaluated by estimation and measurement of insert temperature 148

FIGURE B.3. Comparison of convective heat transfer evaluated by estimation and measurement of insert temperature 149

FIGURE D.1. Isometric view of the insert at a bend 165

FIGURE D.2. Plan view of insert at a bend 165

FIGURE D.3. View of section ZZ 166

FIGURE D.4. View of vertical plane passing through BFC 166

FIGURE D.5. View of vertical plane passing through AD 167

DEDICATION

This dissertation is dedicated in memory of my parents,

Drs. Vethanayaki and Saravanamuttu Velumylum.

NOMENCLATURE

A	constant in correlation equation
A_i	surface area of insert in each segment, ft^2
A_s	surface area of wall in each segment, ft^2
A_t	cross-sectional area of teflon spacer, ft^2
A_x	cross-sectional flow area of calorimeter section, ft^2
B	constant in correlation equations
C	constants in correlation equations or model
C_1	proportionality constant in model
C_2	proportionality constant in model
C_D	orifice constant
c_p	specific heat of fluid packets, Btu/lbm-°F
c_{pa}	specific heat of air, Btu/lbm-°F
$c_{pa,4}$	specific heat of air in segment 4, Btu/lbm-°F
c_{pw}	specific heat of water, Btu/lbm-°F
$c_{pw,4}$	specific heat of water in segment 4, Btu/lbm-°F
D	constant in correlation equations
D_i	inside diameter of calorimeter pipe, ft
D_t	diameter of location of thermocouples in calorimeter pipe wall, ft
F_{i-s}	shape factor from insert to tube wall
f	Fanning friction factor
f_a	augmented Fanning friction factor
f_o	empty tube Fanning friction factor under R_2 or R_3 conditions

f_s	smooth tube Fanning friction factor
h_a	heat-transfer coefficient of air, Btu/hr-ft^2-°F
h_a	augmented heat-transfer coefficient, Btu/hr-ft^2-°F
$h_{a,4}$	average wall heat-transfer coefficient for air in the fourth segment, Btu/hr-ft^2-°F
$h_{i,4}$	average insert heat-transfer coefficient fcr air in the fourth segment, Btu/hr-ft^2-°F
h_o	empty tube heat-transfer coefficient, Btu/hr-ft^2-°F
k	thermal conductivity of fluid, Btu/hr-ft-°F
$k_{a,4}$	thermal conductivity of air in the fourth segment, Btu/hr-ft-°F
k_s	thermal conductivity of calorimeter wall, Btu/hr-ft-°F
k_t	thermal conductivity of teflon spacer, Btu/hr-ft-°F
L	pitch of insert, ft, as defined in Figure 2.9
L1	insert entrance length for segment 1, ft
L2	insert entrance length for segment 2, ft
L_c	axial length of a calorimeter segment, ft
L_i	insert entrance length, ft
L_t	overall length of calorimeter (distance between pressure taps), ft
m_a	mass flow rate of air, lbm/hr
m_w	mass flow rate of water, lbm/hr
N	number of tubes
Nu_a	augmented Nusselt number
Nu_D	Nusselt number based on inside pipe diameter
Nu_o	empty tube Nusselt number under R_2 or R_3 condition
Nu_s	smooth tube Nusselt number

P	pumping power, ft-lbf/sec
Pr	Prandtl number
$P(t)$	distribution function of contact time
p_{atm}	atmospheric pressure, in. of Hg
p_{st}	static pressure, in. of water
q	average heat transfer, Btu/hr
q_a	augmented heat transfer, Btu/hr
$q_{a,o}$	heat lost by air in the whole test section, Btu/hr
$q_{a,4}$	heat lost by air in segment 4, Btu/hr
$q_{c,4}$	convective heat transfer from the air to the tube wall in segment 4, Btu/hr
q_{cd}	heat transfer by conduction in the downstream calorimeter segment, Btu/hr
$q_{ci,4}$	convective heat transfer from the air to insert in segment 4, Btu/hr
q_{cu}	heat transfer by conduction in the upstream calorimeter segment, Btu/hr
$q_i(t)$	instantaneous heat transfer from fluid packet to the wall, Btu/hr
q_o	empty tube heat transfer, Btu/hr
$q_{r,4}$	radiant heat transfer from insert to wall in segment 4, Btu/hr
$q_{w,4}$	total heat gained to water in segment 4, Btu/hr
$q_{wc,4}$	heat gained by water after correction for axial conduction in segment 4, Btu/hr
$q_{w,o}$	heat gained by water in the whole test section, Btu/hr
R	universal gas constant
R^2	correlation coefficient
R_2	performance evaluation criterion under constant pressure

	drop condition
R_3	performance evaluation criterion under constant pumping power condition
Re_a	augmented Reynolds number
Re_D	Reynolds number based on inside pipe diameter
Re_o	empty tube Reynolds number
s	frequency of surface renewal, 1/sec
T	temperature of fluid packet, °F
T_{atm}	ambient room temperature, °R
$T_{a1,4}$	inlet air temperature at segment 4, °F
$T_{a2,4}$	outlet air temperature at segment 4, °F
T_b	bulk temperature of air, °R
T_b	bulk temperature of fluid packets, °F
$T_{b,4}$	bulk temperature of hot gas in segment 4, °R
T_i	temperature of eddies at first instant of renewal, °F
$T_{i,4}$	average insert temperature in segment 4, °R
T_s	tube wall (surface) temperature, °F
$T_{s,4}$	average tube wall temperature in segment 4, °R
$T_{t,4}$	average wall temperature at the thermocouple location in segment 4, °F
$T_{w1,4}$	inlet water temperature at segment 4, °F
$T_{w2,4}$	outlet water temperature at segment 4, °F
t	time of contact of a fluid packet with the tube wall, sec
t_m	mean residence time of fluid packet in tube, sec
U	overall heat-transfer coefficient, Btu/hr-ft^2-°F
u_m	mean velocity in pipe, ft/sec

W	width of insert, ft
W_{X_i}	uncertainty in any variable X_i
y	radial distance from tube wall, ft
α	thermal diffusivity, ft^2/hr
α	bending angle of insert, $^\circ$
γ	twist angle of insert, $^\circ$
Δp	measured pressure drop, in. of water
Δp_c	pressure rise due to temperature drop, lbf/ft^2
Δp_{or}	pressure drop across orifice, in. of water
ΔT	temperature difference, $^\circ F$
ΔT_{LMTD}	log mean temperature difference, $^\circ F$
ΔT_t	temperature difference across teflon spacer, $^\circ F$
ΔX	axial distance of teflon spacer, ft
δ	characteristic length of the fluid packet, ft
ε_i	emissivity of insert
ε_s	emissivity of wall
θ	bending line angle of insert, $^\circ$
μ	viscosity of fluid packet, lbm/ft-hr
$\mu_{a,\overline{4}}$	viscosity of air in segment 4, lbm/ft-hr
ρ_a	average density of air, lbm/ft^3
ρ_{a1}	inlet density of air, lbm/ft^3
ρ_{a2}	outlet density of air, lbm/ft^3
σ	Stefan-Boltzmann constant, $Btu/hr\text{-}ft^2\text{-}^\circ R^4$
ϕ	longitudinal angle of insert, $^\circ$
$\phi(L/D)$	mathematical function to correct for entry length effects

in smooth tube

I. INTRODUCTION

A. The Problem

The recent, though now nearly forgotten, energy crisis required thermal industries to give increased attention to methods of conserving energy. The thermal industry uses about 17% of the total energy consumed in the country to produce process steam and hot water (Yaverbaum, 1979). An increase in efficiency of water heating would significantly impact energy conservation nationwide.

One of the many methods used by the heating and ventilating industry for water heating involves combustion gases flowing inside water-jacketed tubes. Fire-tube boilers and domestic water heaters are familiar examples. Some representative applications of combustion gases flowing inside tubes other than the conventional usage mentioned above include (a) waste heat recovery in the chemical industry, (b) heat recovery in cogeneration systems, and (c) process gas cooling from steam/methane furnaces in the petroleum industry. If the heat transfer in any of these heat exchangers is improved by enhancing the convective heat-transfer coefficient on the gas side of the tube, the energy consumption or the required heating surface could be reduced, and thereby decreasing the cost of operation and the capital cost of the heating surface.

Enhancing or augmenting heat transfer is one of the many ways of reducing costs in the thermal industry. In recent years, the

exponential increase in the amount of published literature in the area of enhanced heat transfer (Bergles et al., 1983) indicates that enhanced heat transfer has developed into a major specialty area in heat-transfer research and development. Single-phase convective heat transfer can be enhanced by several techiques that can be broadly classified into passive and active techniques.

Some examples of passive enhancement technique include surface roughness, extended surfaces, displaced enhanced devices, and swirl flow devices. These enhancement devices augment heat transfer by disturbing the existing flow. Surface roughness is produced by knurling, corrugating, or creating repeated ribs. Rough surfaces--ranging from random sand grain type roughness to discrete protuberances--enhance heat transfer by disturbing the fluid sublayer at the surface. Displaced enhanced devices, such as baffles and mixing elements, enhance heat transfer by altering the flow at the surface by disturbing the core flow. Swirl flow devices are inserts or other geometrical device which create a rotating and/or secondary flow. Examples include vortex generators, twisted-tape inserts, and axial-core inserts.

Active augmentation techniques use additional external sources of energy to enhance convective heat transfer. Some of the commonly used techniques are surface vibration, fluid vibration, surface scraping, use of electric fields, and jet impingement.

The gas convective coefficients are normally much lower than the liquid coefficients in fire-tube boilers or water heaters. One of the

most popular and easily accomplished methods to improve the gas convection and radiation is to introduce inserts inside the tubes. Inserts can be made in an infinite variety of configurations. Commonly used insert designs include twisted ribbons or tapes of near-tube-diameter width, wire coils similar to springs, and bent-strip inserts. A typical bent-strip insert configuration is a narrow, thin metal strip bent and twisted in a zig-zag fashion to allow periodic contact with the tube wall. However, outside of the twisted-tape insert, very little fundamental work has been done to establish the heat-transfer and flow-friction data required for the design of bent-strip inserts (Junkhan et al., 1982). Hence, the present investigation concentrates on establishing the performance of bent-strip inserts.

B. Scope of Investigation

To meet the objectives of predicting the performance of bent-strip inserts, three goals were established. They were

1. To acquire heat-transfer and flow-friction data for a variety of geometrical variations of bent-strip inserts in order to formulate design equations for these inserts
2. To better understand the mechanism of enhancement of convective heat transfer by visualizing flow patterns created by the inserts
3. To devise an analytical interpretation of the results so that the mechanism of enhancement is incorporated into correlation of the heat transfer.

To meet the above goals, the following research program was conducted in the Heat Transfer Laboratory of the Department of Mechanical Engineering and Engineering Research Institute at Iowa State University. A survey of the current techniques in cooling hot gases in tubes was conducted. An experimental facility was designed and built to obtain thermal-hydraulic data from hot gases flowing inside tubes. Different geometrical variations of the bent-strip inserts were tested by using the experimental facility. The heat-transfer and friction data were used to obtain an empirical correlation to predict the performance of these inserts. At the same time, two flow visualization techniques were used to study the flow patterns created by the bent-strip inserts. They provided insight into the mechanism of enhancement. Finally, the surface renewal/penetration theory was used as a basis for a model to provide an analytically based correlation for heat transfer in tubes in the presence of bent-strip inserts.

II. THERMAL HYDRAULIC EXPERIMENTS

A. Literature Survey

A literature survey using the computerized "Bibliography on Augmentation of Convective Heat and Mass Transfer - II" (Bergles et al., 1983) has revealed only limited information regarding inserts used in the cooling of gases in tubes. The three types of turbulence-producing inserts most commonly applicable to the present study are twisted tapes, wire coils, and bent strips. Figure 2.1 shows typical configurations of a wire coil, a twisted tape, and a bent-strip insert.

As early as 1896, Whitham used "loosely fitting and gently twisted" (a 360 degree twist in 10 ft) strips made of No. 10 sheet iron. The strips were inserted into forty-four 4 in. i.d. and 20 ft long horizontal tubes of a 100-hp boiler. Whitham observed a fuel savings as high as 18% when "the boiler plant is pushed and the draught is strong." Kirov (1949), 50 years later, fitted an Economic Boiler having 76 tubes of 2.74 in. i.d. with 2.5 in. wide twisted tapes having a twist ratio of 1 turn in 1.17 ft or 1 turn in 2.33 ft. With full-length tapes, the increase in boiler efficiency was about 5% to 7% which was equivalent to a fuel saving of 7% to 10%. The increase in fan horsepower was considered negligible for the forced draft system under test; however the use of twisted tapes in a natural draft system was not advised.

Heat-transfer and flow-friction references found for various inserts are described below; these are the only cases found where air or

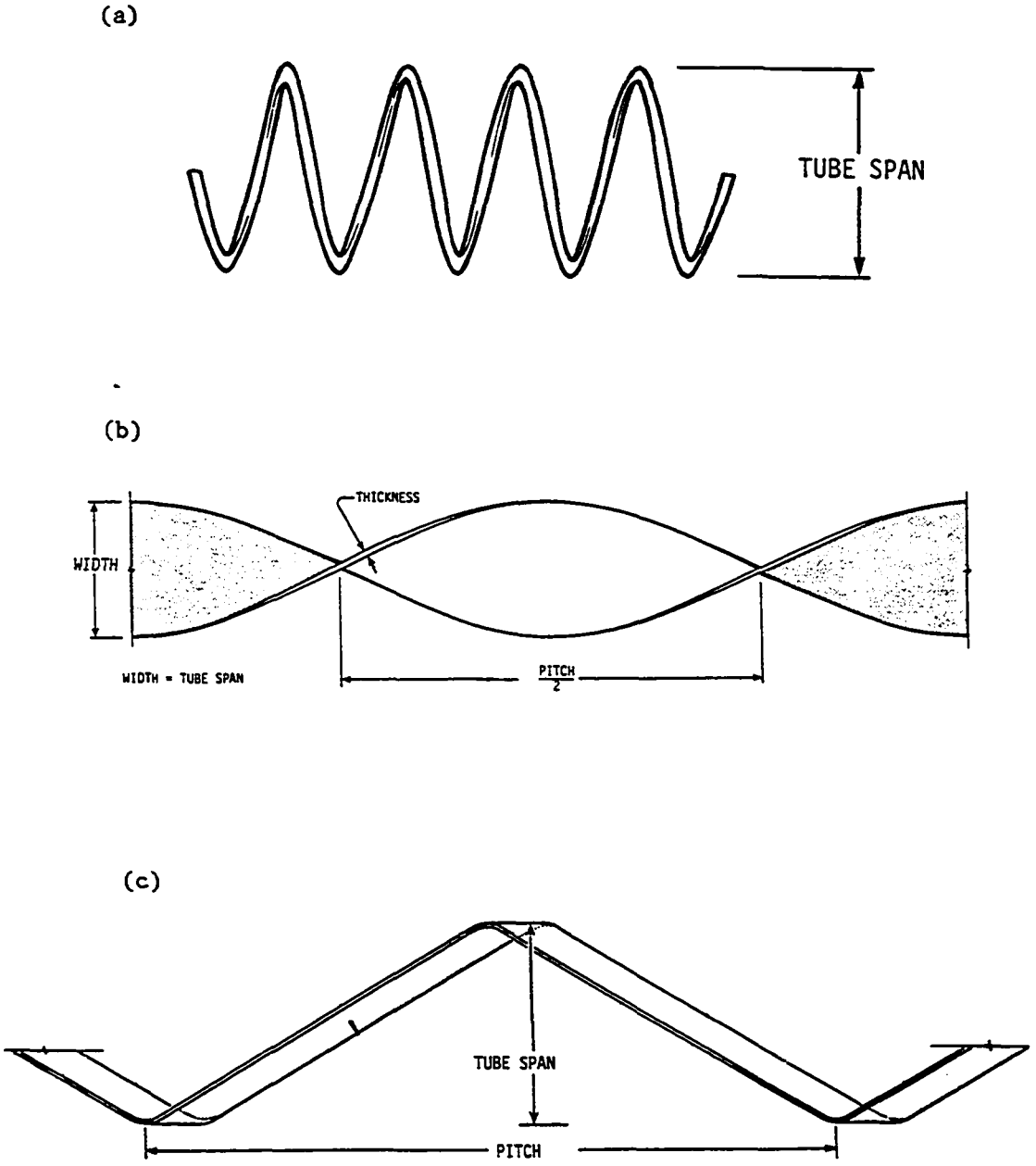

FIGURE 2.1. Typical configurations of (a) a wire coil, (b) a twisted tape, and (c) a bent-strip insert

combustion gases were used as the working fluid and cooling was present. To establish a uniform basis of comparison with the various references cited in this study, the pitch of an insert was defined as the length along the tube axis for one full twist of a twisted tape or one full cycle of a bent-strip insert as noted in Figure 2.1. The heat-transfer and pressure-drop data reported by the various investigators for these three types of inserts are compared in in Figures 2.2 and 2.3, respectively. The data are compared as Nusselt number and Fanning friction factor as a function of Reynolds number. The variation of Prandtl number was considered small enough to neglect Prandtl number in the heat transfer comparison. Pressure-drop data were corrected for momentum gain caused by the cooling.

An early but comprehensive study of twisted-tape turbulators with air cooling was reported by Royds (1921). Electrically heated air was allowed to flow through a tube of 2.31 in. i.d. and 6.58 ft length. A large number of tests were made with inlet air temperatures varying from 430°F to 1000°F. Nine different twisted tapes of width 1.94 in., sooted to simulate actual conditions, were tested with pitches varying from 10.9 to 88.9 in. The results obtained show that pitches larger than 20.0 in. had very little influence on heat transfer. Data were reported as curves of heat-transfer coefficients and of pressure drops as a function of mass velocities. The bulk temperature was assumed to be 550°F so that the data could be converted to standard dimensionless groups as presented in Figure 2.2. The pressure-drop data reported were

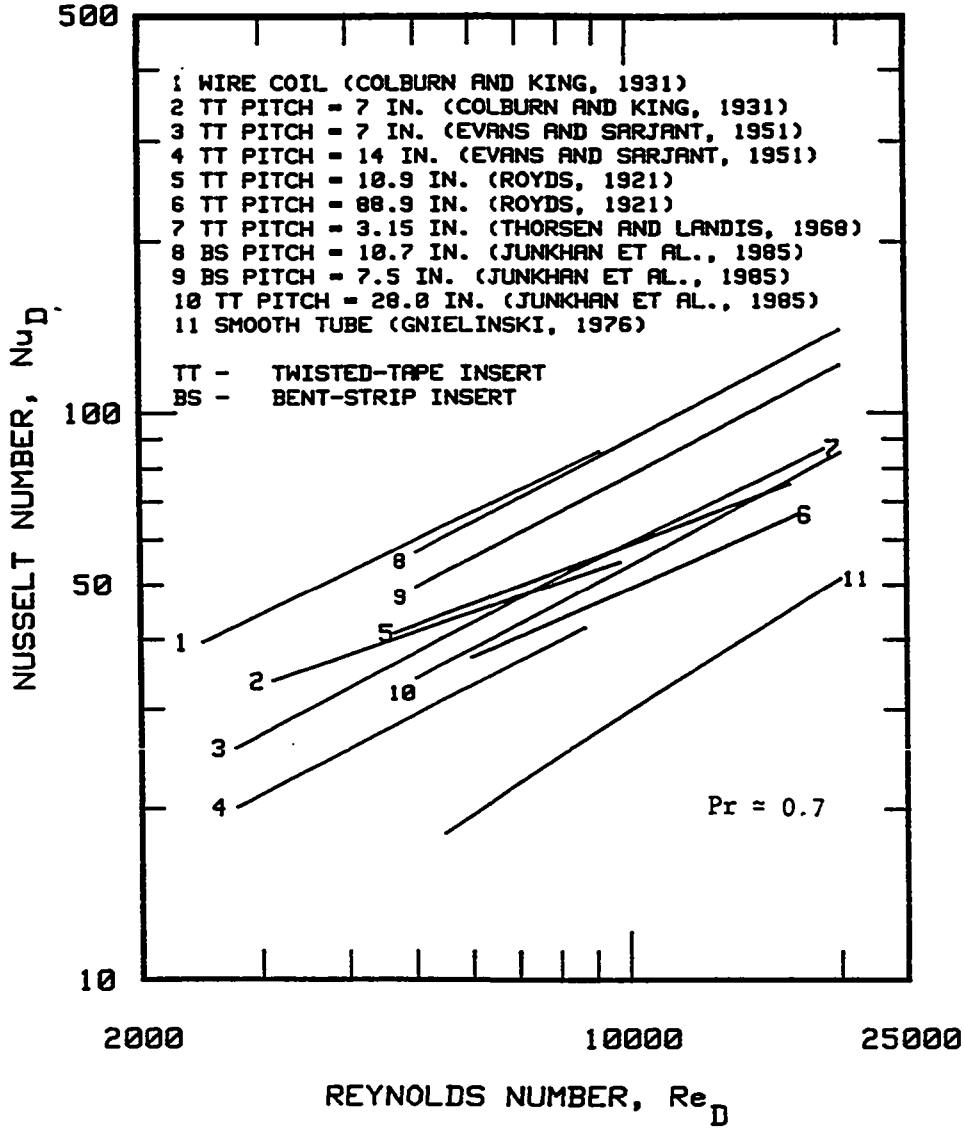

FIGURE 2.2. Comparison of published heat-transfer data for wire-coil, twisted-tape, and bent-strip inserts

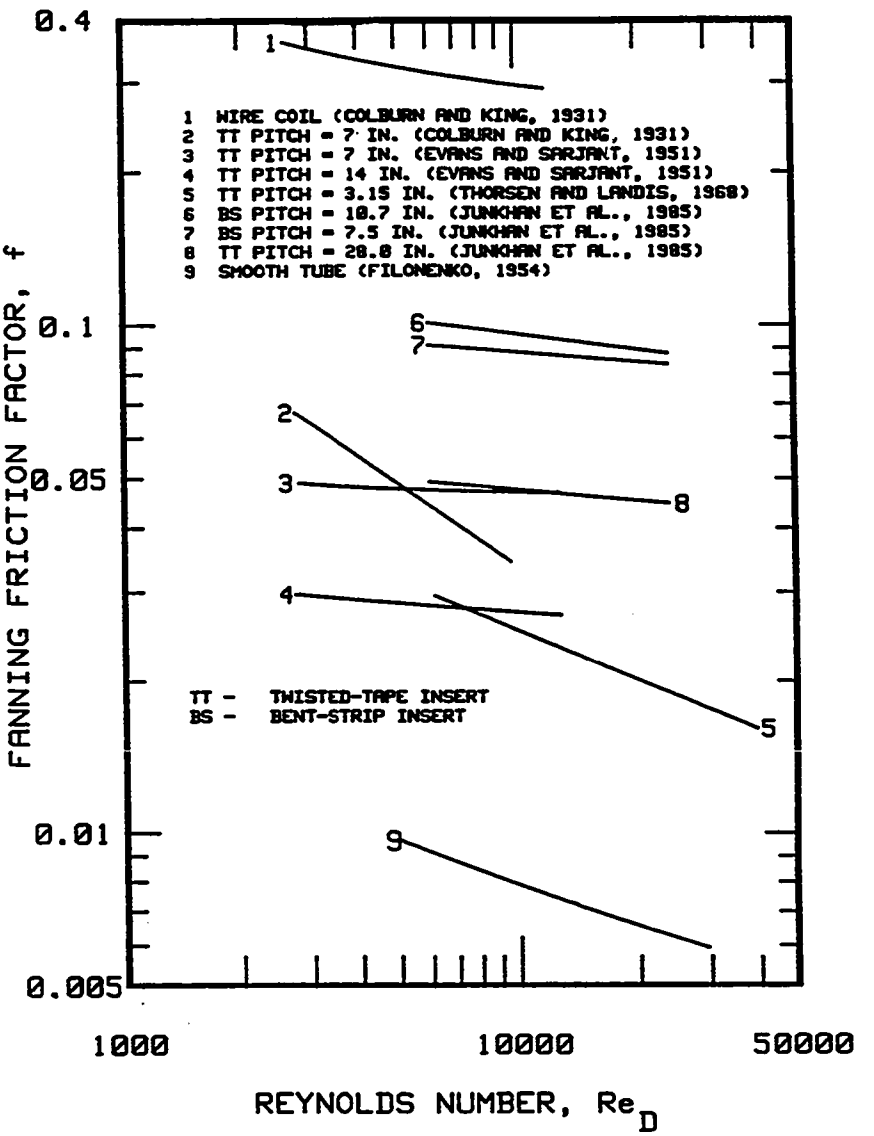

FIGURE 2.3. Comparison of published friction-factor data for wire-coil, twisted-tape, and bent-strip inserts

not corrected for momentum change caused by the temperature drop in air. Since this correction could not be calculated with the data reported, the pressure drop data are not compared in Figure 2.3.

Colburn and King (1931) investigated enhancement effects of twisted tapes and conically shaped wire coils by using hot air heated by electrical resistance heaters. The test section was water cooled by a helically wound copper tube soldered to the outside. End axial conduction gains to the test section were reduced by using guard coolers on sections of tube just upstream and downstream of the test section. Tube wall temperatures were measured on the outside wall of the tube at five equally spaced axial locations by thermocouples embedded in the solder between copper cooling coils. A traversing thermocouple was used to obtain an average inlet air temperature while the average outlet air temperature was measured by thermocouples placed in an insulated mixing chamber located on the outlet of the test section. Inlet air temperatures varied from 225°F to 734°F, and inlet wall temperatures varied from 48.6°F to 52.7°F.

Wire coils consisted of wire wound in a three dimensional conical helix, beginning with a coil essentially of the same diameter as the 2.625 in. i.d. test section and spiraling to the apex of the cone in ever-decreasing radii. The length of the cone thus formed was about 4 in. Nine of these coils were placed in the 3 ft long test section in an apex-to-base fashion. No information was given on the wire diameter and the direction of flow with respect to the cone sequence. Two full

length, snug fitting twisted tapes were also tested by Colburn and King (1931). However, only data for a 3 ft long steel tape of 7 in. pitch were tabulated. Data were reported as curves of h_a/c_{pa} and pressure drop (corrected for momentum change) as functions of mass velocity through the test section. Their data, recalculated as Nu_D and f as functions of Re_D, are compared in Figures 2.2 and 2.3.

Studies on twisted-tape enhancement were also conducted by Evans and Sarjant (1951), who used electrically heated air in a setup somewhat similar to that used by Colburn and King (1931). Twisted-tape inserts of width 2.5 in. and pitches ranging from 7 to 14 in. were tested in an 8 ft long, 3 in. i.d. test section. The outside of the tube was water cooled by helically wound copper tubing soldered on the surface. Radial gas temperature and velocity measurements were made at several axial locations so that the the bulk temperature and mean velocity could be calculated. Energy balances between cooling water gain and air energy loss were used to validate data for each run. The inlet air temperature was approximately 700°F while inlet Reynolds numbers varied from 3000 to 13,000. Results were presented as curves of the convective heat-transfer coefficients and of pressure drops as functions of Reynolds numbers for different twisted tapes and coils. Data for twisted-tape pitches of 7 and 14 in., converted to Nu_D and f as a function of Re_D, are compared in Figures 2.2 and 2.3. Bulk gas temperature was again assumed as 550°F to enable the calculation of Nusselt number and friction factor.

Evans and Sarjant attempted to separate the effects of radiation and convection in twisted-tape enhancement. While noting that their analysis was not conclusive in this respect, they estimated the maximum contribution by radiation as 25% of the measured heat-transfer coefficient when gas temperatures above about 1000°F were encountered. The contribution from radiation dropped rapidly as the gas temperature was reduced.

More recent tests of the effects of twisted tapes on cooled air flow were reported by Thorsen and Landis (1968). Inlet air temperature to a 1 in. i.d. water cooled test section ranged up to 475°F. Twisted tape pitches were 3.15, 5.17, and 8.00 in., and the tube gap was about 0.003 in. A major concern of this work was the assessment of the variable properties. A temperature-ratio correction factor was determined primarily from heating data because of the limited values of (T_s/T_b) that could be attained in cooling. The best correlation of the cooling data was achieved by ignoring the temperature-ratio correction. Heat-transfer and friction-factor data for the smallest pitch are given in Figures 2.2 and 2.3.

In a study conducted for DOE at Brookhaven National Laboratory, it was found that the addition of turbulators to residential oil-fired boilers resulted in fuel savings of 2% to 8% (McDonald et al., 1979). Details of the turbulator installation were not given in the report.

More recently, two commercial, arbitrarily designed bent-strip inserts and one twisted-tape insert were tested by Junkhan et al.

(1985). Tests were conducted using electrically heated air with inlet air temperatures around 300°F. One bent-strip insert of pitch 10.7 in. and width 0.875 in. displayed a 175% increase in the heat-transfer coefficient at a Reynolds number of 10,000, while the other insert of pitch 7.5 in. and width 0.75 in. displayed a 135% increase in the heat-transfer coefficient at the same Reynolds number. The two bent-strip inserts were made by different commercial manufacturers and bent in different fashions. The twisted tape, having a pitch of 28 in. and a width of 2.6 in, provided a 65% increase in the heat-transfer coefficient. The friction-factor increases accompanying the heat-transfer coefficients were about 1000% for the bent-strip inserts and 160% for the twisted-tape insert. The Nu_D and f data for the three inserts are alsc compared in Figures 2.2 and 2.3, respectively.

The literature was also reviewed to determine a method of obtaining an estimate of the net heat transfer due to radiation from the insert to the tube wall. Watanabe et al. (1984) indicate that a major portion of the heat transfer can be caused by radiation in the case where the fluid is being heated. In their case, the temperatures of the tube wall and the insert were of the order 1750°F. Beckermann (1984) concludes that even for small temperature differences of 40°F the radiation effects could be considerable. In his case, the temperature of the flue gas was in the range of 600°F to 1300°F. He also indicates that in the case of large tube-length-to-tube-diameter ratios, it is possible to neglect axial radiation and consider only radial radiation.

The literature reviewed above indicates that most of the research on turbulators is focused on twisted-tape inserts. Comparison of heat-transfer data in Figure 2.2 show that augmentation of heat transfer achieved by the use of bent-strip inserts is higher than twisted-tape inserts. The wire-coil inserts tested by Colburn and King (1931) attain an augmentation level marginally higher than bent-strip inserts but at a considerably higher pressure drop penalty, as seen in Figure 2.3. The review of literature shows that very little fundamental work has been done to obtain the heat transfer/flow friction basis for the design of wire-coil or bent-strip inserts. The present experimental study concentrates on establishing the heat transfer/flow friction basis for the design of bent-strip inserts.

B. Experimental Apparatus

An apparatus was developed to determine the thermal hydraulic performance of various inserts. The test apparatus consists of a blower suitable to produce flows in the Reynolds number range of 3000 to 20000, a heater box to heat the air to over 300°F, and a test section in which the actual performance of the inserts is to be evaluated. Prior to its use for insert tests, the performance of the apparatus as a smooth tube without inserts was obtained and compared with accepted correlations.

1. Flow system

The flow system that provided hot air to the test section is shown in Figure 2.4. Airflow was provided by a centrifugal blower that

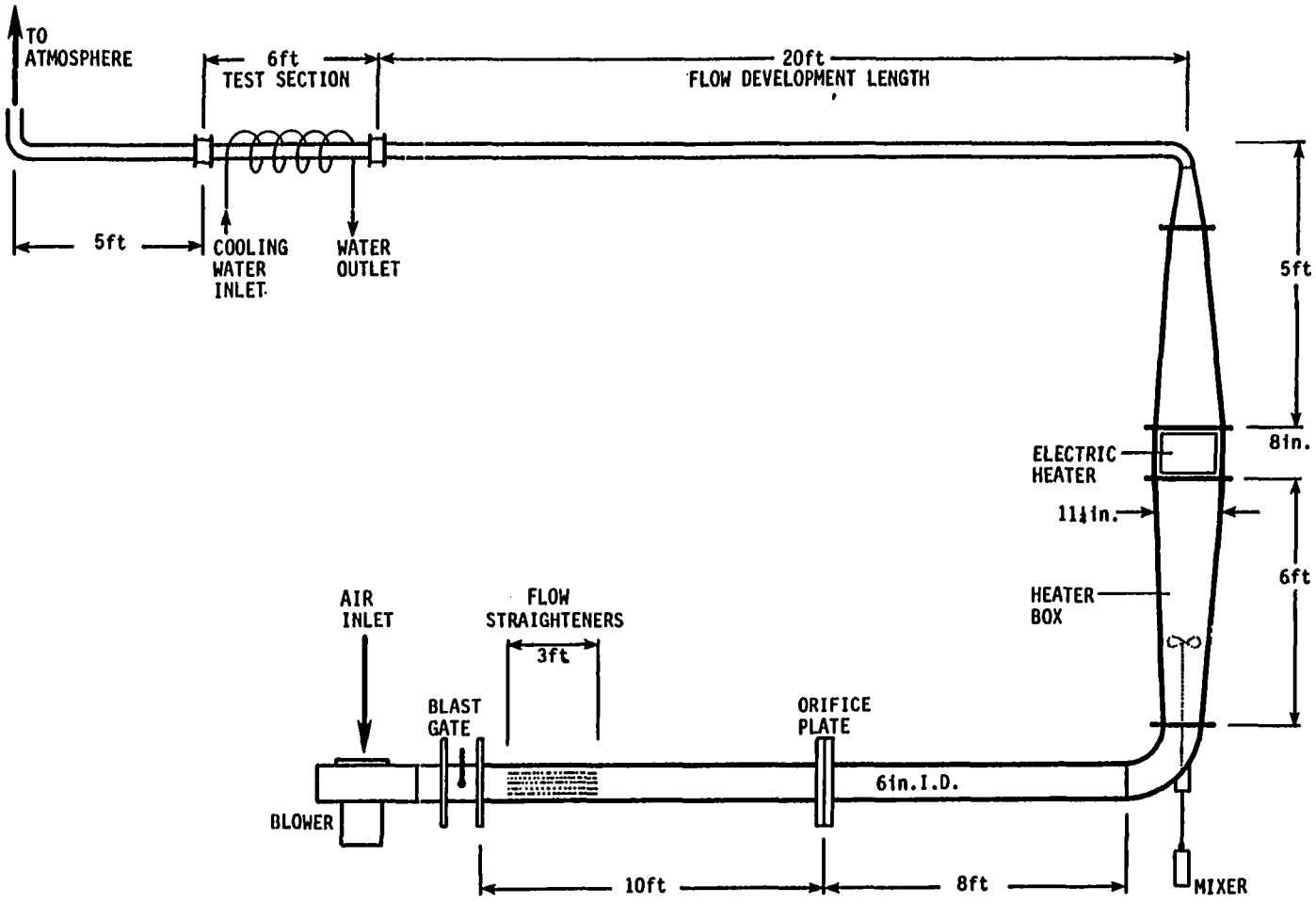

FIGURE 2.4. Flow system (not to scale)

delivered 600 SCFM at a head of 6 in. of water. After leaving the fan, the air passed through a blast gate and into a 6 in. i.d. aluminum tube. This tube contained flow straighteners consisting of 1 in. diameter and 3 ft long plastic tubes packed inside the aluminum tube. After a flow development length of 10 ft, the air entered an orifice meter. Eight feet downstream from the orifice meter, the air passed through an elbow before entering the heater box.

The heater box was fabricated from 22-gage sheet steel in three parts: an inlet rectangular diffuser section varying in cross section from 6 in. x 6 in. at the entrance to 21 in. x 11.25 in. over a length of 72 in., an 8 in. long heater housing section, and a converging section with its cross section reducing from 21 in x 11.25 in. to 6 in. x 6 in. over a length of 50 in. The housing section for the heater contained a three-phase Chromalox Process Air Duct Heater, Model ADHT-010XX, rated at 10 kW, 240 V. A General Electric motor-driven three-phase autotransformer was used to control the power to the heater. An ammeter and a voltmeter were included in the circuitry to monitor the current and voltage input to the heater. An over-temperature protector for the heater was included in the electrical circuit to shut off the electric power to the heater if a predetermined limit temperature was reached. A motorized mixer was provided to minimize thermal stratification within the heater box.

The hot air coming out of the heater box passed through a bend and entered a 2.67 in. i.d. and 20 ft long drawn-on-mandrel steel tube,

which acted as the developing length required before the hot air entered the test section. After passing through the test section, the air was exhausted into a 5 ft long pipe section before being discharged outside the building. The heater box and the pipe leading into and out of the test section were covered with a layer of calcium silicate insulation for this high temperature service. A layer of glass fiber insulation was added to reduce the heat loss to a minimum.

During the latter part of the investigation, the flow loop had to be dismantled and moved to the Heat Transfer Laboratory in the new Mechanical Engineering/Engineering Science and Mechanics Building. The configuration of the flow loop was redesigned to reduce the floor space required. In its rebuilt form, as shown in Figure 2.5, the loop was about 40 ft long with the blower at one end and the heater box at the other end. After the air was heated, the hot air proceeded through two 90-degree bends separated by a short straight section, flowed above the heater box through the test section, and was vented to the outside through the roof. Care was taken to preserve the upstream conditions for the test section.

2. Test section

The test section shown in Figure 2.6 was based on a 3 in. o.d. carbon, drawn-on-mandrel steel tube with an i.d. of 2.67 in. The tube was 71.75 in. long and was flanged at the ends to enable easy installation and removal of inserts. To facilitate the attachment of thermocouples on the tube wall, 1 in. long and 1/8 in. wide axial slots

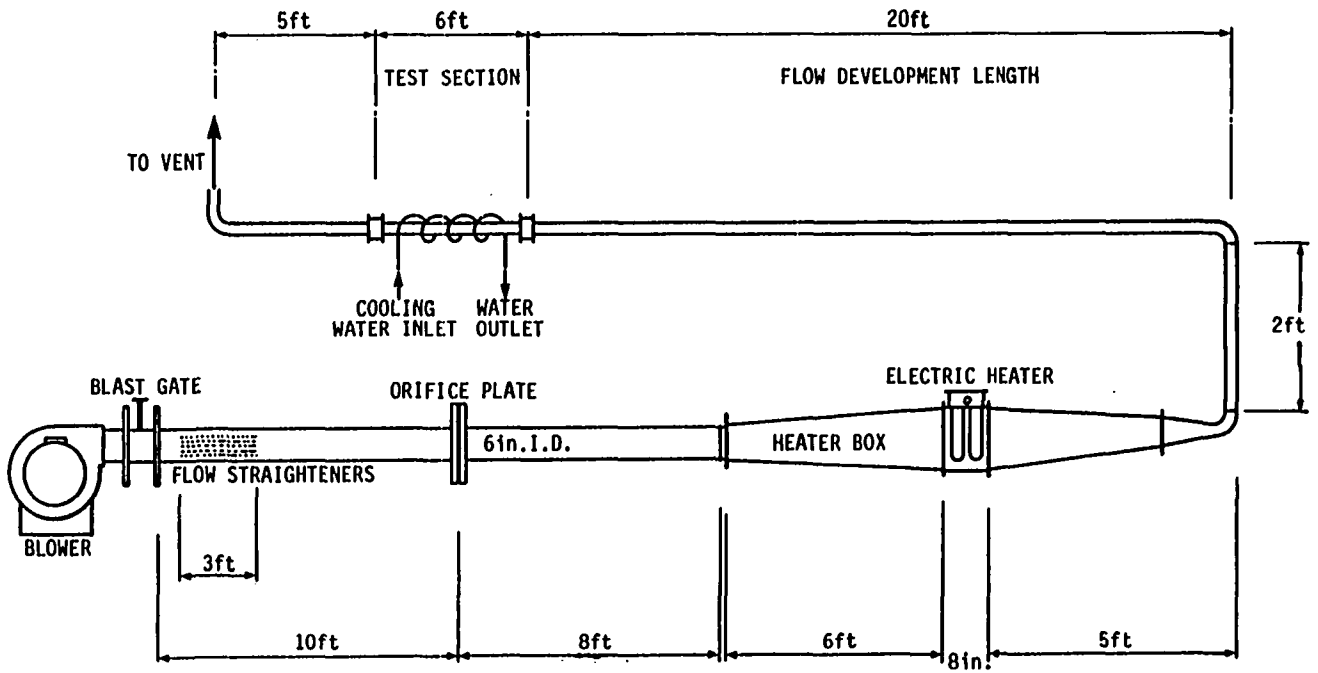

FIGURE 2.5. Elevation view of reassembled test loop

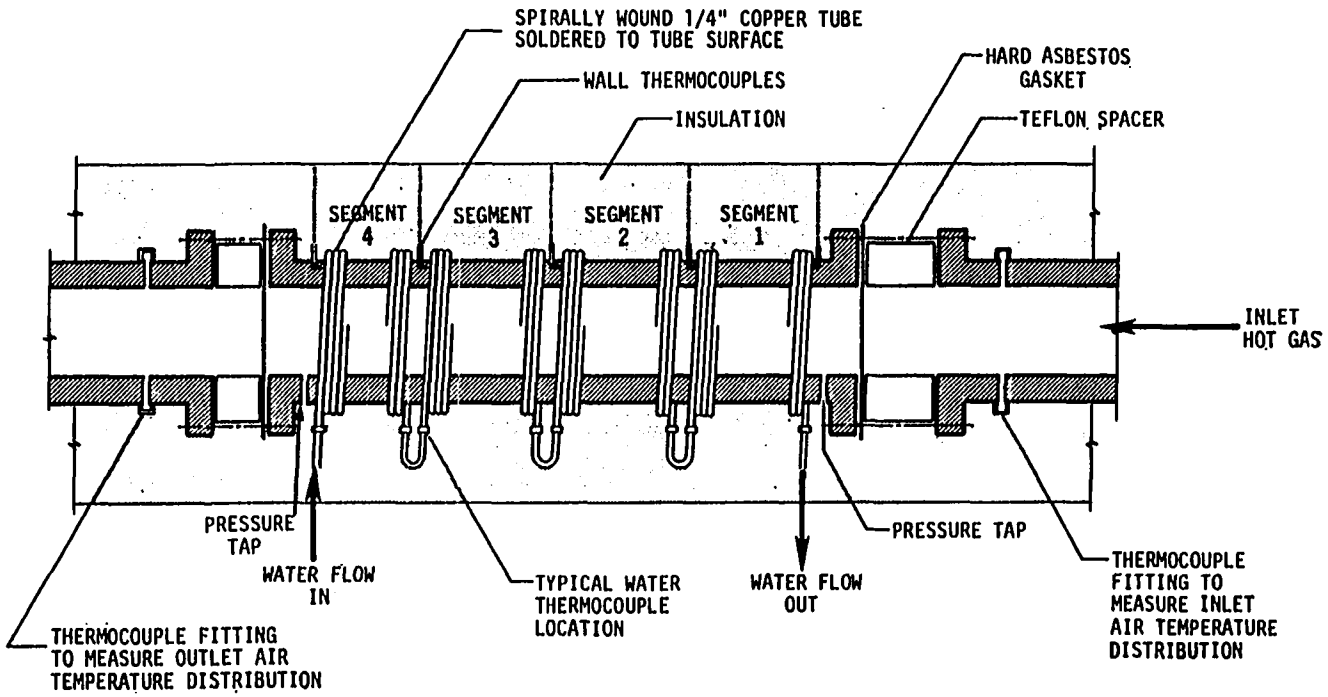

FIGURE 2.6. Test section schematic (not to scale)

were milled partway through the tube wall. These slots were provided at five axial locations corresponding to the ends of the four calorimeter segments described below. At each axial location, three slots were milled equidistant around the circumference. Also, each end of the test section was fitted with three pressure taps spaced equally around the circumference.

The water calorimeter for cooling the gas and conducting energy balances was made of 0.25 in. i.d. copper tubing wound around the tube and soldered to the outside with a low temperature (430°F) silver solder. Small 0.1 in. i.d. copper tubes were placed in the axial slots made for the thermocouples before the water calorimeter copper tubing was soldered to the outside of the test section. The calorimeter tubing was connected as four separate segments in series.

To minimize the axial conduction from the test section, teflon spacers were placed between the test section flanges and the inlet and outlet tube flanges. Finally, the test section was insulated with glass fiber.

3. Instrumentation

The basic measurements needed were the air and water mass flow rates and the various air and water bulk temperatures. Wall temperatures were also required for calculation of the heat-transfer coefficients. In addition, the pressure drop over the entire test section was required to calculate the friction factor.

Tube wall temperatures were measured with thermocouples fitted into the 15 axial slots milled partway into the test section wall. The welded thermocouple junctions were inserted into the slots through the small copper tubes passing under the calorimeter segments. The water temperature was measured by thermocouples attached to the calorimeter tubing at the inlet and outlet of each of the four calorimeter segments. The thermocouples installed as described above, permitted the determination of four sectional-average, gas-side heat-transfer coefficients. The bulk air temperatures at the inlet and outlet of the test section were measured by using four thermocouples placed at different radial locations just upstream and downstream of the test section. Also, to estimate the axial conduction at the ends of the test section, four thermocouples were placed on both sides of each teflon spacer to measure the temperature differences across the spacers. The axial conduction gains by the test section were calculated from the spacer dimensions, the thermal conductivity of the spacers, and the temperature differences across the spacers. The thermocouples were made of 28 ga chromel-alumel wire and were independently referenced to a Whittaker model BRJ14-50TP chromel-alumel 150°F constant temperature junction.

The static pressure at the test section inlet and the pressure drop across the test section were measured by using a Setra Systems model 239 differential pressure transducer. This transducer was connected via a six-channel Scanivalve to a piezometer ring attached to the pressure

taps at the inlet and outlet of the test section. To measure very small pressure differences, a Meriam model 34FB2 micromanometer, which is capable of reading 0.001 in. water, was used.

The air flow rate, controlled by the blast gate at the blower outlet, was measured by using the ASME orifice. The pressure drop across the orifice was measured by the differential pressure transducer, which was also connected via the Scanivalve to a piezometer ring attached to the pressure taps. The same system was used to measure static pressure at the orifice. The mass-flow rate was found by using standard ASME procedures and equations.

The water flow rate was measured directly using a container on a sensitive balance and a digital stopwatch. This was considered more accurate than using a rotameter because of the low water flow rate and variations in water temperature.

The outputs from the constant temperature junction and the pressure transducer were recorded digitally using a data acquisition system consisting of a Hewlett Packard (HP) 9845B Desktop computer, a HP 3495A 40-channel scanner, a HP 3456A digital voltmeter, two HP 9885M flexible disk drives, and a HP 2316G printer. Finally, the water-flow rate and atmospheric pressure were input into the computer by hand.

4. Test procedure

The test procedure consisted of starting the blower and switching on the electric heater. The air mixer in the heater box was also started at this time to reduce stratification of the low velocity flow

in the heater box. The system was allowed to heat up, a process that normally took about three hours. The air-flow rate was adjusted for a specific run requirement by setting the blast gate at the blower outlet. The data acquisition system was programmed to scan the air inlet and outlet water temperatures to determine when a steady state was obtained. The water flow was adjusted to obtain at least a 40°F temperature rise in water from test section inlet to outlet. Once steady state was obtained, temperature and pressure readings were measured in about 90 seconds by the data acquisition system.

5. Data reduction

The data acquisition program (listed in Appendix A) was used to promptly reduce the data, and the energy balance for the overall test section was checked by using the equation

$$q_{w,o} - q_{cu} - q_{cd} = q_{a,o} \tag{2.1}$$

Agreement of both sides of Equation 2.1 to within 5% was required to validate a run; however, energy balances typically agreed to within 2%.

Heat transfer to each calorimeter segment was determined by writing the energy equation for the segment. The calculation procedure was started at the fourth segment. The process of calculation described below was repeated using the inlet air temperature at one segment as the outlet air temperature for the next segment. The second and the third segments had no conduction correction; however, heat gain by the coolant in the first segment required a conduction correction similar to that used for the fourth segment.

The calculation procedure for inserts was started from the fourth segment instead of the first segment because the mixing effect of an insert reduces possible temperature stratification in the flow and thereby yields a better mixed-mean outlet air temperature. In the case of the smooth tube, the calculation procedure was started from the first segment, because this method was considered better in the case in which there was no insert in the test section.

For the fourth segment, the net energy added to the water from the air flowing in the segment was obtained from

$$q_{w,4} - q_{cd} = m_w c_{pw,4}(T_{w2,4} - T_{w1,4}) - q_{cd} \tag{2.2}$$

where q_{cd} is the estimated heat transfer to the water by conduction from the downstream ducting. Then, the air-side energy balance,

$$q_{w,4} - q_{cd} = q_{a,4} = m_a c_{pa,4}(T_{a1,4} - T_{a2,4}), \tag{2.3}$$

was used to find the air inlet temperature to the segment, $T_{a1,4}$. The convective heat transfer from the air to tube wall is given by

$$q_{c,4} = q_{a,4} - q_{r,4} \tag{2.4}$$

where $q_{r,4}$ is the radiant heat transfer from the insert to the tube wall. The average wall temperature near the surface for this segment, $T_{t,4}$, was taken as the linear average of the six wall temperature readings at the ends of each segment. The log-mean temperature difference between the bulk air temperature and the tube wall in the fourth segment was obtained by using the equation given below.

$$\Delta T_{LMTD} = \frac{(T_{a1,4}-T_{t,4}) - (T_{a2,4}-T_{t,4})}{\ell n\left(\frac{T_{a1,4} - T_{t,4}}{T_{a2,4} - T_{t,4}}\right)} \tag{2.5}$$

The overall heat-transfer coefficient times surface area from the hot air to the wall thermocouples is given by

$$(UA_s)_4 = \frac{q_{c,4}}{\Delta T_{LMTD}} = \left[\frac{1}{h_{a,4}\pi D_i L_c} + \frac{1}{2\pi k_s L_c}\ell n\left(\frac{D_t}{D_i}\right)\right]^{-1} \tag{2.6}$$

The convective heat-transfer coefficient, $h_{a,4}$, was obtained by combining Equations 2.5 and 2.6 and is given by

$$q_{c,4} = \left[\frac{1}{h_{a,4}\pi D_i L_c} + \frac{1}{2\pi k_s L_c}\ell n\left(\frac{D_t}{D_i}\right)\right]^{-1} \frac{(T_{a1,4}-T_{t,4}) - (T_{a2,4}-T_{t,4})}{\ell n\left(\frac{T_{a1,4} - T_{t,4}}{T_{a2,4} - T_{t,4}}\right)} \tag{2.7}$$

To calculate $q_{r,4}$, the radiation transfer model used to estimate the radiation heat transfer from the insert to the wall is

$$q_{r,4} = \frac{\sigma(T_{i,4}^4 - T_{s,4}^4)\, A_i}{1/F_{i-s} + (1/\varepsilon_i - 1) + (1/\varepsilon_s - 1)(A_i/A_s)} \tag{2.8}$$

where suffixes i and s are for the insert and tube wall, respectively. The shape factor, F_{i-s}, cannot be assumed to be unity as the strip insert is bent in such a fashion that it can radiate to itself. To simplify the calculation, one can assume constant wall and insert

temperatures in each segment of the test section. This is reasonable as far as the insert is concerned, since the conduction from the insert to the tube wall can be neglected because of the very small contact area between the tube wall and the insert. Data from Kreith (1962) and Feingold (1966) were used to estimate the shape factor from the insert to the wall. The insert was assumed to be two finite plates with a common edge joined at different angles depending on the pitch-to-diameter ratio.

The convective heat transfer from the hot gas to the insert is given by the following equation:

$$q_{ci,4} = h_{i,4} (T_{b,4} - T_{i,4}) \tag{2.9}$$

where the bulk air temperature, $T_{b,4}$, is the average of the inlet and the outlet air temperatures in the fourth segment. By considering an energy balance for the insert in one segment and neglecting any conduction in the insert,

$$h_{i,4}(T_{b,4} - T_{i,4}) = \frac{\sigma(T_{i,4}^4 - T_{s,4}^4)}{1/F_{i-s} + (1/\varepsilon_i - 1) + (1/\varepsilon_s - 1)(A_i/A_s)} \tag{2.10}$$

The system of Equations 2.2 through 2.10 required an iterative solution. Initially, assuming $q_{r,4} = 0$, $h_{a,4}$ was obtained in Equations 2.2-2.7. Then assuming $h_{a,4} = h_{i,4}$ in Equation 2.10, the value of $T_{i,4}$ was obtained. Equation 2.8 was used to calculate $q_{r,4}$ when the value of $T_{i,4}$ was known. The value of $q_{r,4}$ was used to correct further the

convective heat transfer from the hot gas to the tube in Equation 2.4. A new value of $h_{a,4}$ was calculated by using Equation 2.7 and was compared with the previous value. This iteration was repeated until the the value of $h_{a,4}$ converged to within 1%.

The corrections caused by radiation were about 2% to 5% of the total heat transfer for the temperature and Reynolds number ranges of this study. In order to verify the assumptions regarding the calculation procedure of the radiant component of heat transfer, the insert temperature was measured for one insert, and the radiant heat transfer from the insert to the wall was estimated. These results, given in Appendix B, indicated that by using the above assumptions the radiant component of heat transfer is underpredicted by about 30%. The most likely cause for this discrepancy is the assumption of $h_{i,4} = h_{a,4}$. However, since the total radiant component is only about 2 to 5% of the convective heat transfer, the uncertainty in the radiation correction based on these assumptions does not affect the convective heat-transfer coefficient by more than 2%.

The average Fanning friction factor is given by

$$f = \left[\Delta p - \left(\frac{m_a}{A_x}\right)^2 \left(\frac{1}{\rho_{a2}} - \frac{1}{\rho_{a1}}\right)\right] \Bigg/ \frac{4L_t \rho_a u_m^2}{D_i^2} \qquad (2.11)$$

$$f = \left[\Delta p - \left(\frac{m_a}{A_x}\right)^2 \left(\frac{1}{\rho_{a2}} - \frac{1}{\rho_{a1}}\right)\right] \left(D_i \rho_a A_x^2\right) \Big/ \left(2 m_a^2 L_t\right) \qquad (2.12)$$

where the pressure drop is corrected for the momentum change. The cross-sectional area is that of the empty tube without considering inserts. Also, in calculating the Reynolds number, no allowance was made for the blockage of the inserts. A sample calculation and the uncertainty analysis are given in Appendix C.

C. Experimental Program

1. Empty tube experiments

Before starting to evaluate the performance of the inserts, the experimental apparatus was tested for its performance as a plain tube without inserts. Average heat-transfer coefficients were determined for each calorimeter segment of the test section. The average friction factor was calculated by using the pressure drop across the test section.

The conditions just upstream of the test section approximate an almost uniform temperature gas with a fully developed velocity profile. At the cooled test section, a temperature profile develops and the heat-transfer coefficient in the first segment should be that for a developing flow. Further downstream, the temperature profile should become fully developed. This behavior is shown in the top half of Figure 2.7 where the data for segment 1 is above that for the other three segments. The average Nusselt numbers, corrected for thermal entry length effects according to curves given by Mills (1962) and property variations, are shown in the bottom half of Figure 2.7 together

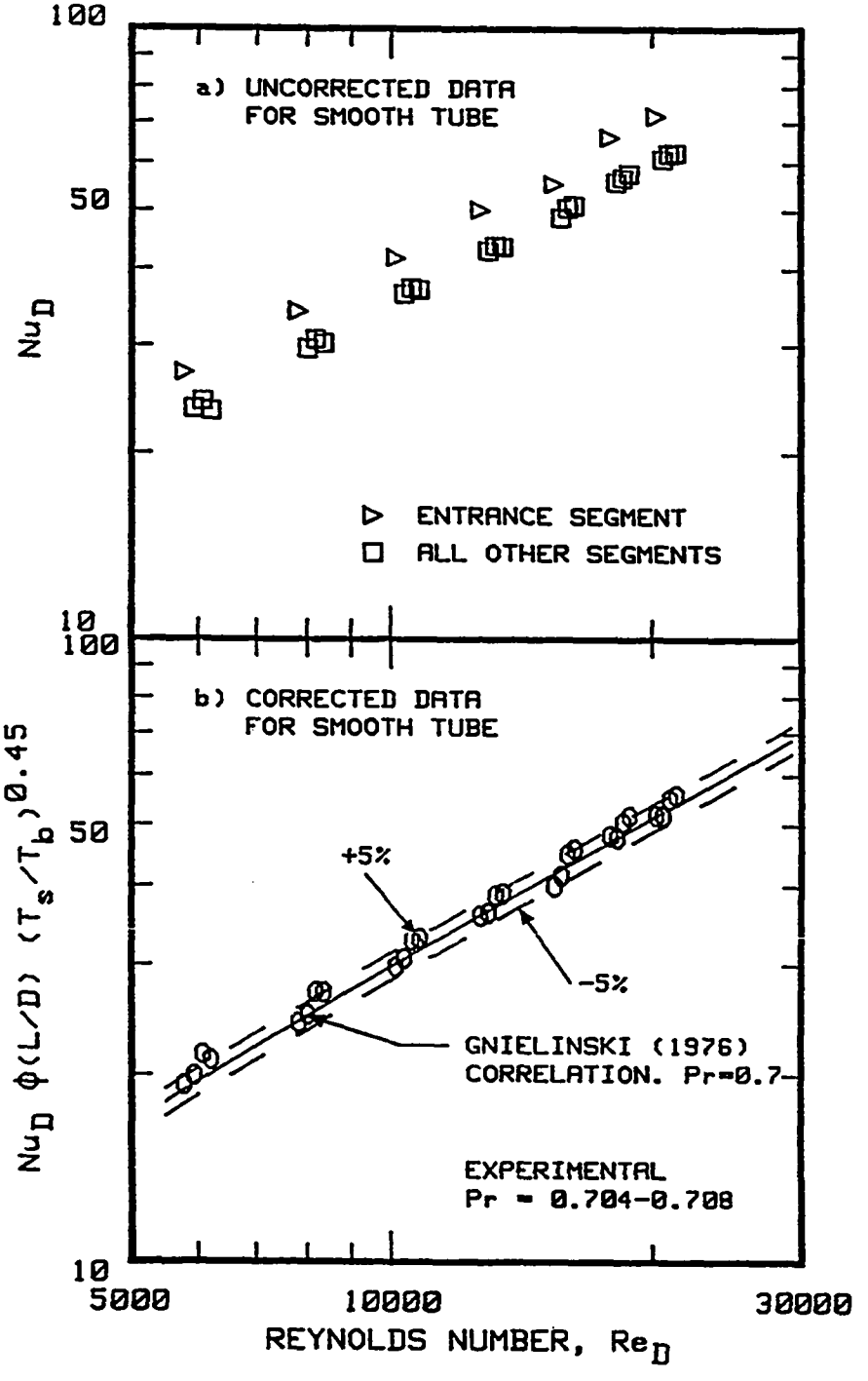

FIGURE 2.7. Heat-transfer data for smooth tube compared with the Gnielinski correlation

with a line representing the Gnielinski (1976) correlation for cooling expressed as

$$Nu_D\left(\frac{T_s}{T_b}\right)^{0.45} = \frac{(f/2)(Re_D - 1000)Pr}{1 + 12.7\sqrt{(f/2)}(Pr^{2/3} - 1)} \qquad (2.13)$$

where T_s is the average surface temperature of the inside of the tube, obtained from the the average of the six wall thermocouple readings at the ends of each segment. Shah and Johnson (1981) recommend the Gnielinski correlation for constant property fully developed turbulent flow through a smooth circular tube for Reynolds numbers ranging from 2300 to 5,000,000. To correct for property variations in cooling of air, Gnielinski recommends an exponent of -0.45 for use with his correlation.

The average Fanning friction-factor data, compared with the Filonenko (1954) correlation

$$f = [\ 1.58\ \ell n(Re_D) - 3.28\ ]^{-2} \qquad (2.14)$$

are shown in Figure 2.8 where the agreement is within ±2%. Property variation effects for the friction data have not been considered because of the uncertainty in the correction factor (Shah and Johnson, 1981). Figures 2.7 and 2.8 show that the heat-transfer data are within ±5% of the Gnielinski correlation and the friction data are within ±2% of the Filonenko correlation. This confirms the basic smooth tube performance of the test apparatus.

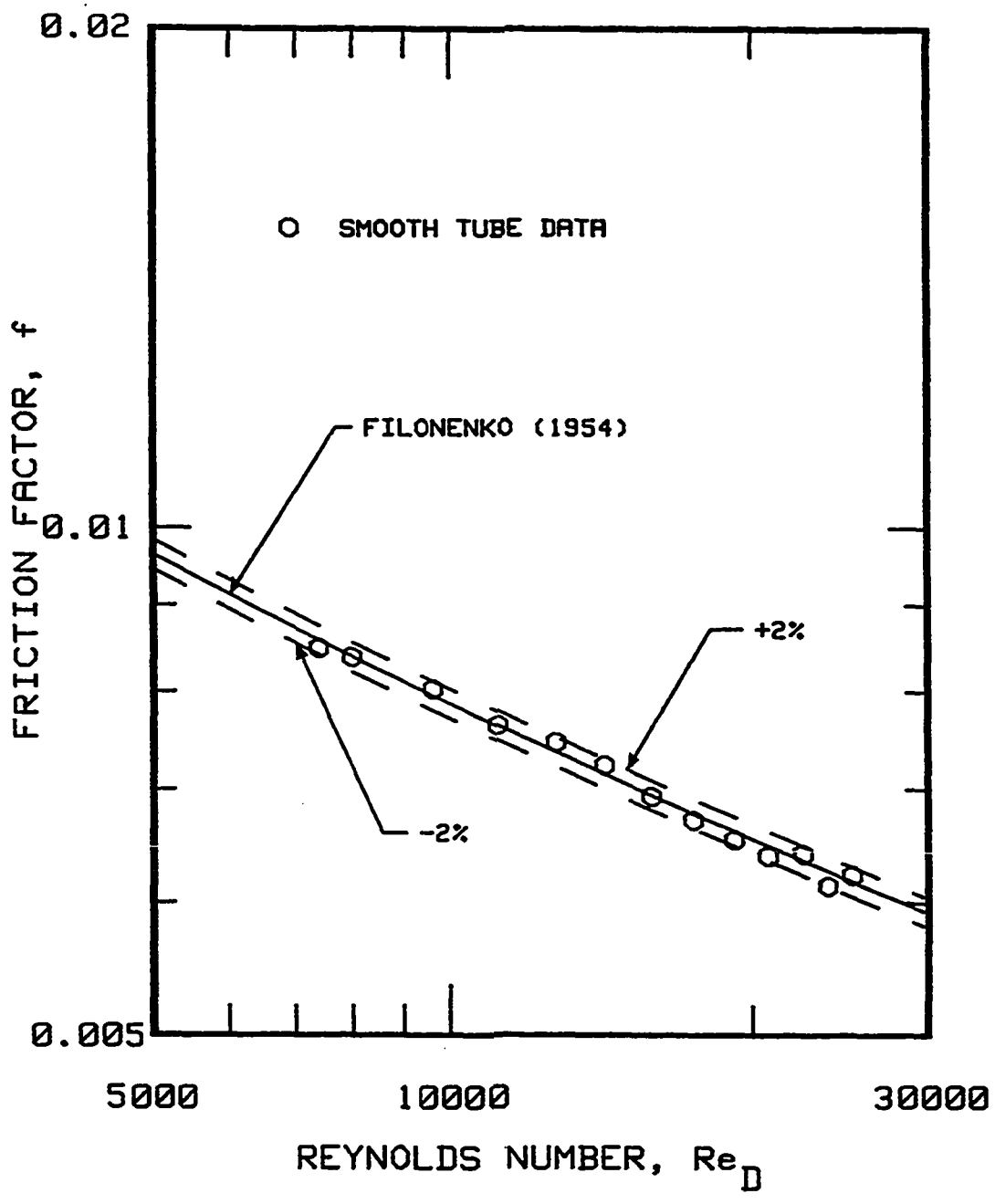

FIGURE 2.8. Friction-factor data for smooth tube compared with the Filonenko correlation

2. Basic thermal hydraulic experiments

a. Inserts tested The type of insert tested is shown in Figure 2.9. Heat-transfer and pressure-drop studies were conducted with eleven different geometrical variations of the same type of insert. Included were pitches of 6.0, 9.5, and 16.0 in., and insert widths of 0.5, 0.75, and 0.875 in., as shown in Table 2.1. Three of the 9.5 in. pitch inserts were made by a commercial manufacturer. Included was one insert fabricated from perforated steel. The other eight inserts were made at Iowa State University (ISU). One of the ISU inserts had a twist angle of 0°, while all the other inserts had a twist angle of 25°. Equations relating tube diameter, insert pitch, width, longitudinal angle and twist angle are given in Appendix D.

b. Results and discussion Nusselt numbers obtained from the tube side heat-transfer coefficients of the four segments are plotted against Reynolds numbers in Figures 2.10-2.20. The Nusselt numbers were corrected for variable properties by using the exponent -0.45 in order to compare the data with the empty tube correlation of Gnielinski (1976). The pressure-drop data, converted to the Fanning friction factor, are also plotted in these figures. Heat-transfer and pressure-drop results are given in a tabular form in Appendix E.

The heat-transfer data in Figures 2.10-2.20 show that segment 1 heat transfer is lower than the other three segments, which indicates possible thermal hydraulic entrance effects. In the following discussion, only results from the second, third, and fourth segments

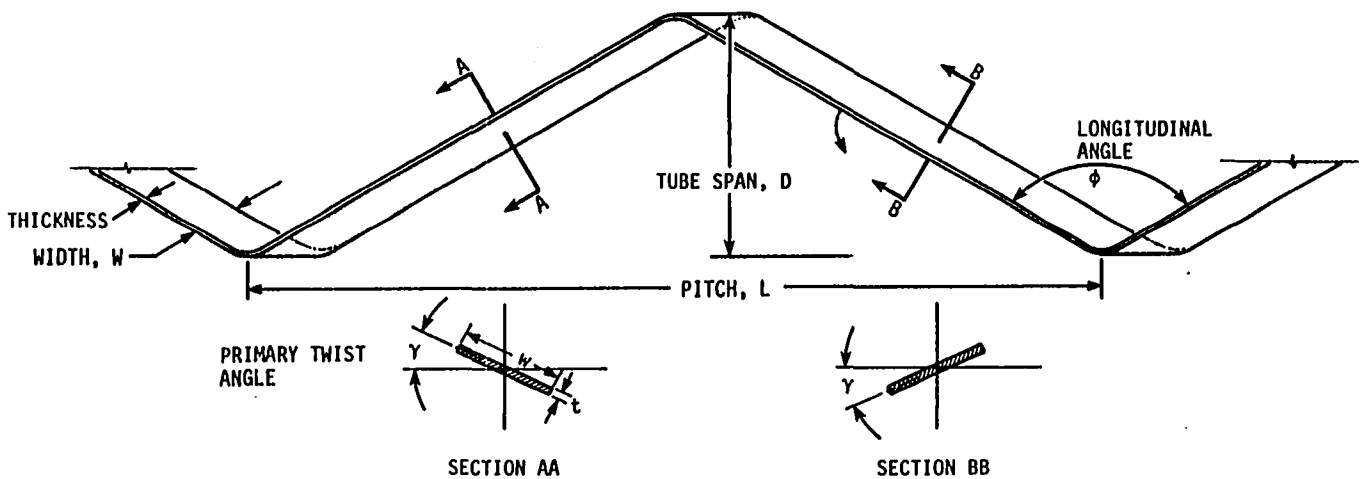

FIGURE 2.9. Insert geometry (not to scale)

TABLE 2.1. Insert characteristics

Insert Label	Pitch P (in.)	Width W (in.)	Long. Angle ϕ (°)	Twist Angle γ (°)	Manufacturer
A1	9.5	0.875	122	25	Commercial
AN	9.5	0.75	122	25	Commercial
A2	16.0	0.875	143	25	ISU
A5	16.0	0.75	143	25	ISU
A4	6.0	0.875	90	25	ISU
A3	6.0	0.75	90	25	ISU
A6	9.5	0.875	122	25	ISU
A7	9.5	0.75	122	25	ISU
A8	9.5	0.5	122	25	ISU
A9	9.5	0.75	122	0	ISU
PA	9.5	0.75	122	25	Commercial (Perforated)

have been considered; the entrance effects are considered in a later section. Figures 2.21 and 2.22 show the effect of width and fabrication technique on heat-transfer and pressure-drop data, respectively, by using the data for the inserts A6, A7, A8, A1, and AN. These inserts all have the same pitch of 9.5 in. but the widths vary as shown in the figures. From Figures 2.21 and 2.22, it is seen that the heat-transfer coefficient and friction factor decrease with decreasing width. It is also seen that the commercially manufactured inserts A1 and AN have higher heat transfer and pressure drop. Inserts A1 and A7 (also AN and A7) are identical in most dimensions, except that inserts A6 and A7 have sharp bends (radius of bend about 0.1 in.) and inserts A1 and AN have rounder bends (radius of bend about 1 in.). A least-squares line is

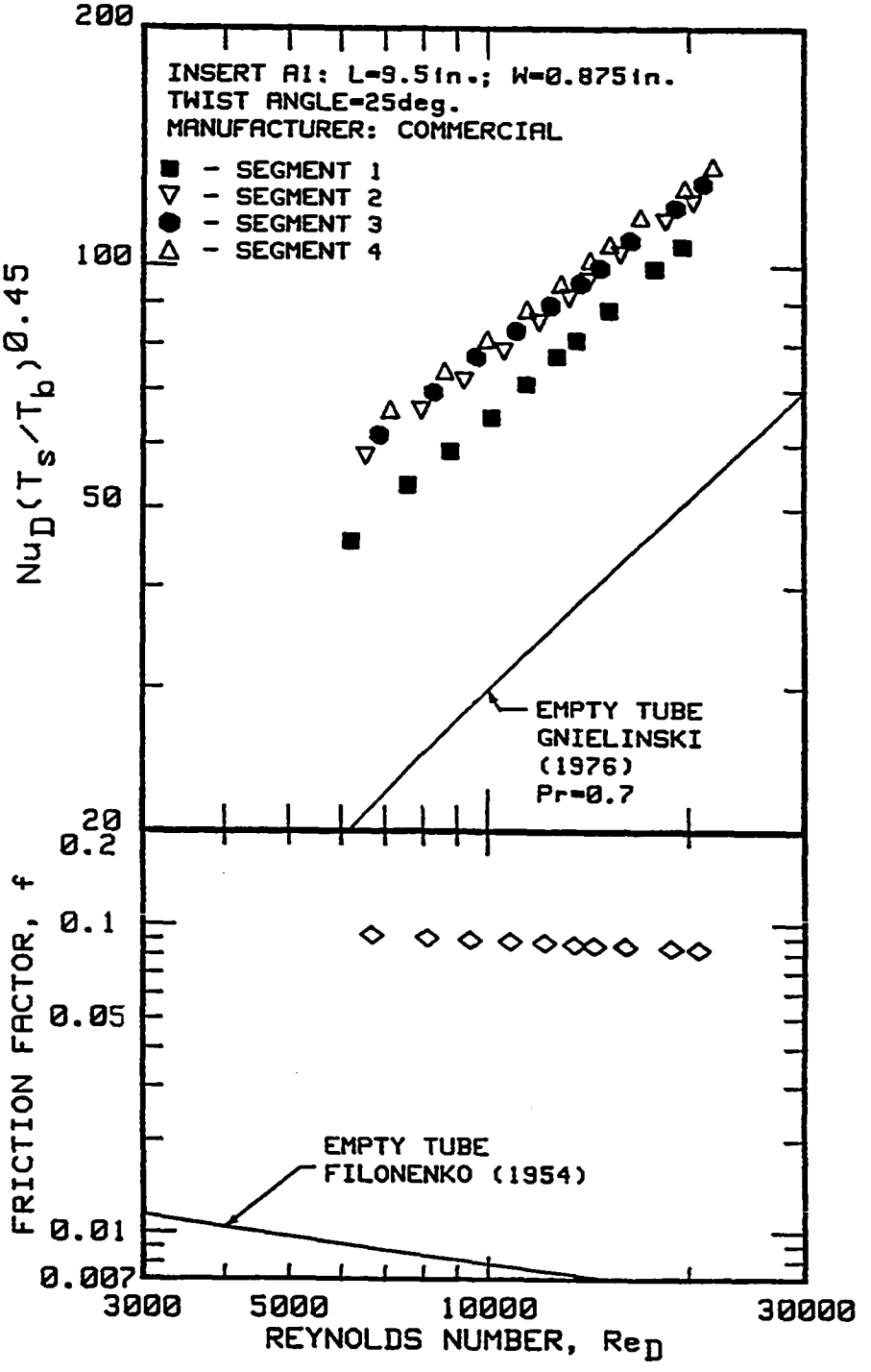

FIGURE 2.10. Heat-transfer and pressure-drop data for insert A1

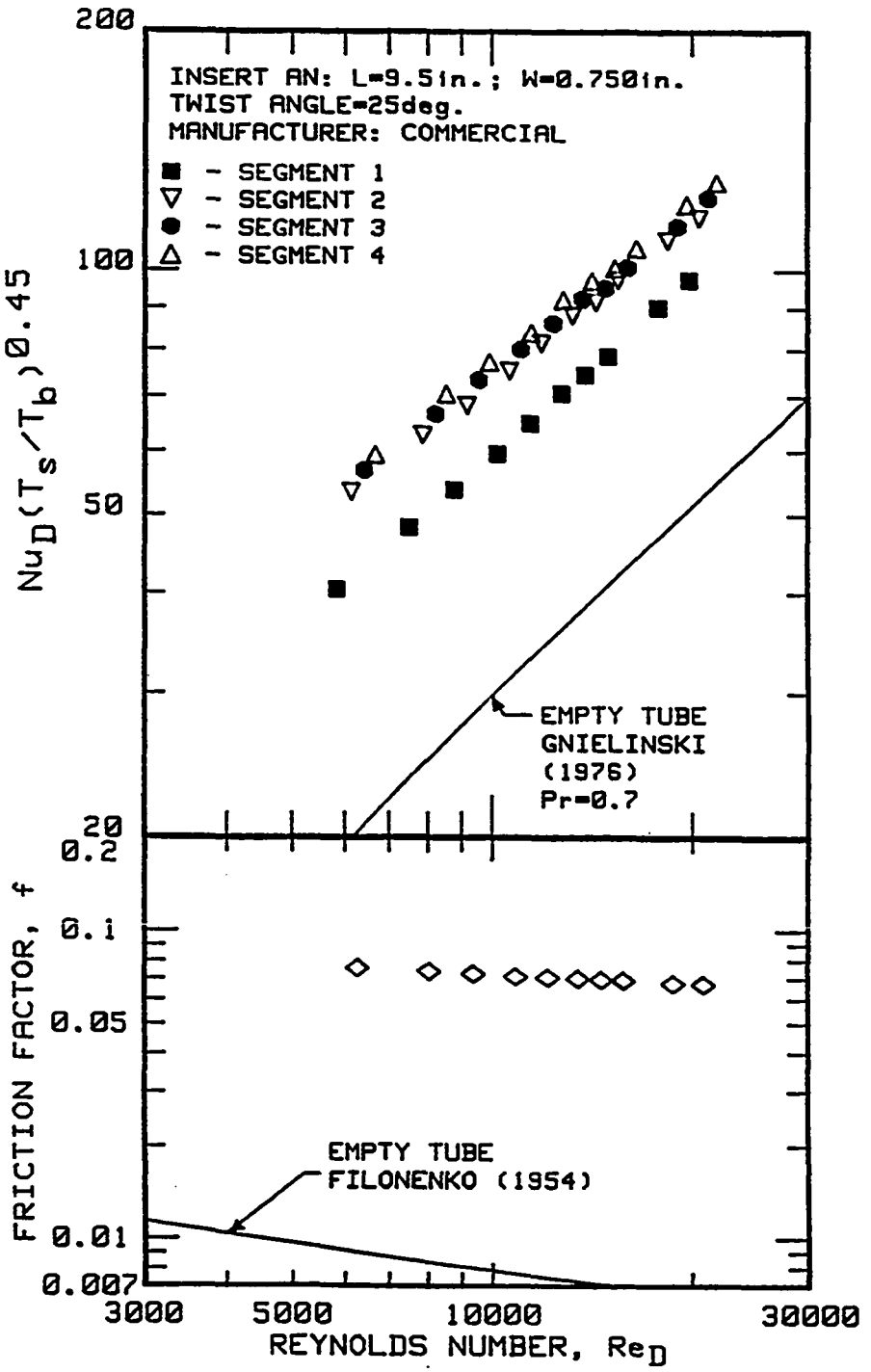

FIGURE 2.11. Heat-transfer and pressure-drop data for insert AN

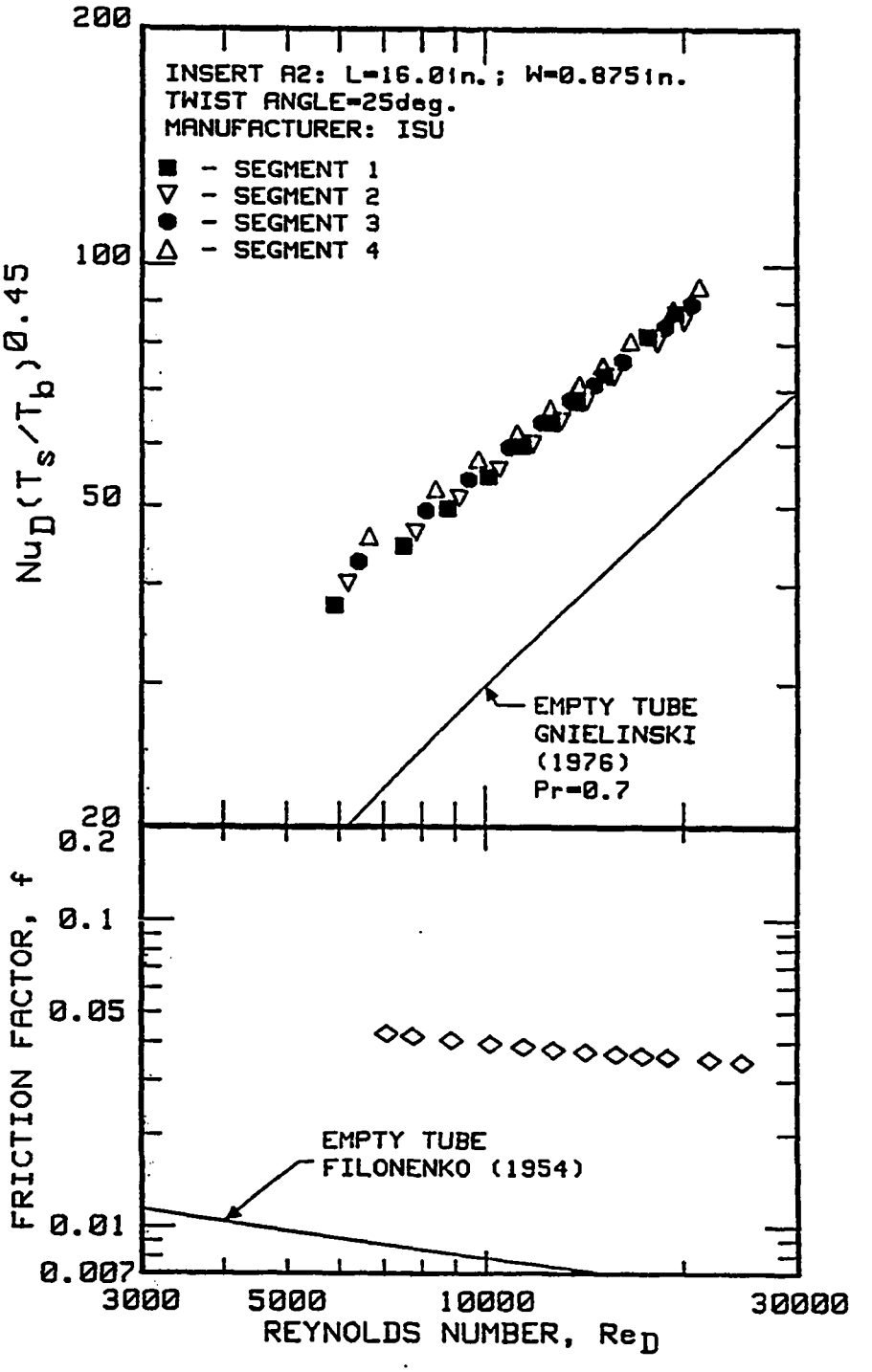

FIGURE 2.12. Heat-transfer and pressure-drop data for insert A2

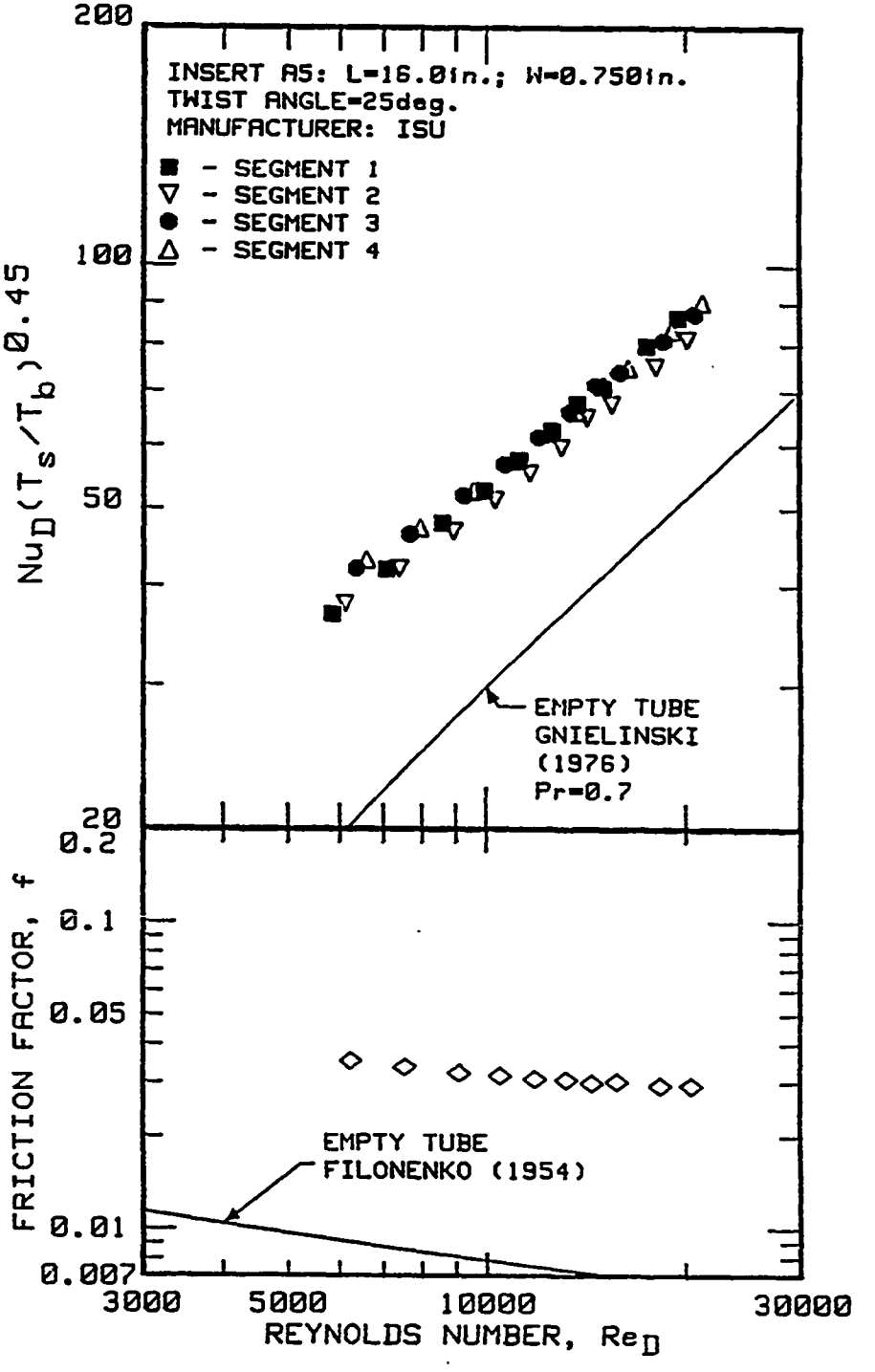

FIGURE 2.13. Heat-transfer and pressure-drop data for insert A5

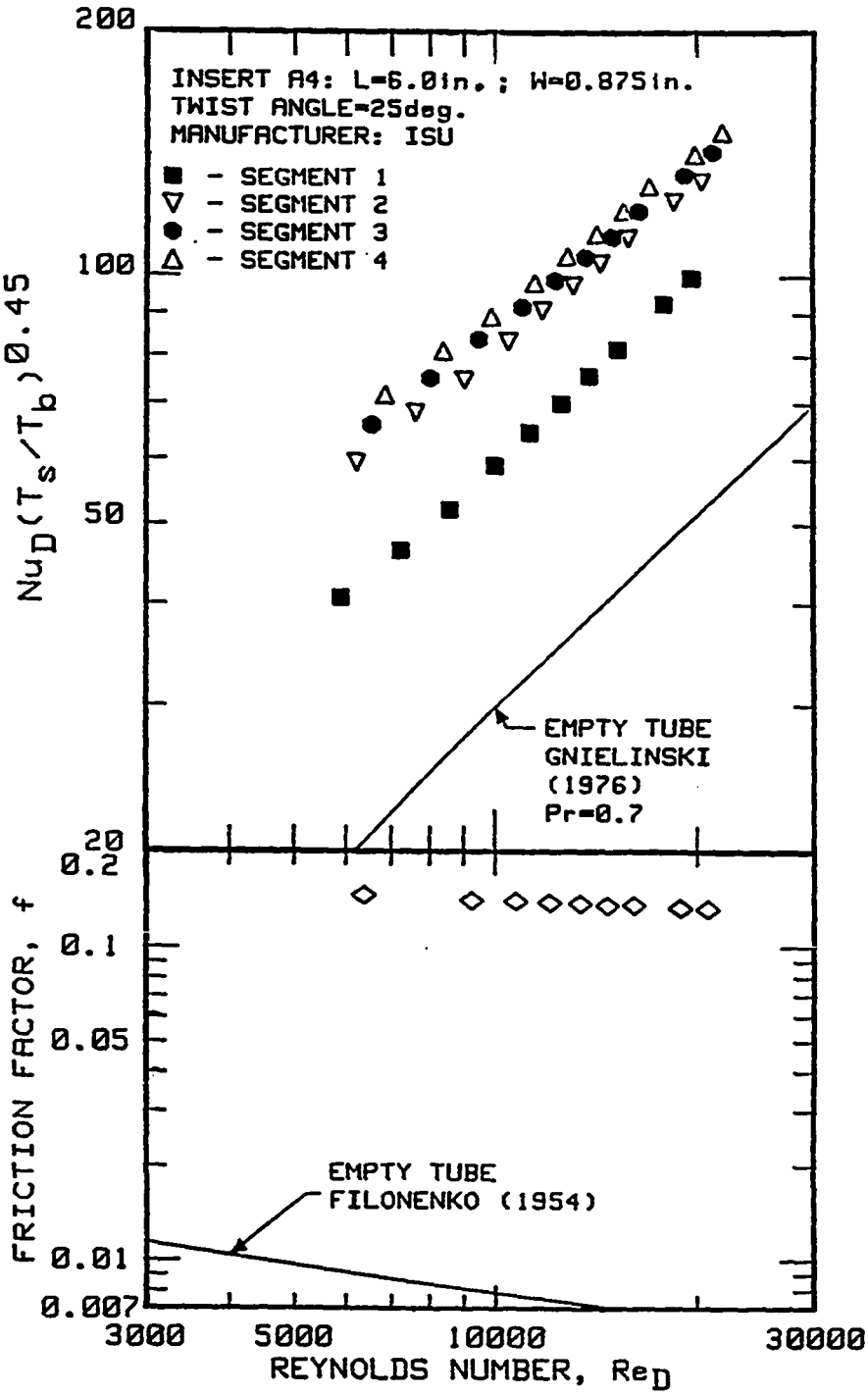

FIGURE 2.14. Heat-transfer and pressure-drop data for insert A4

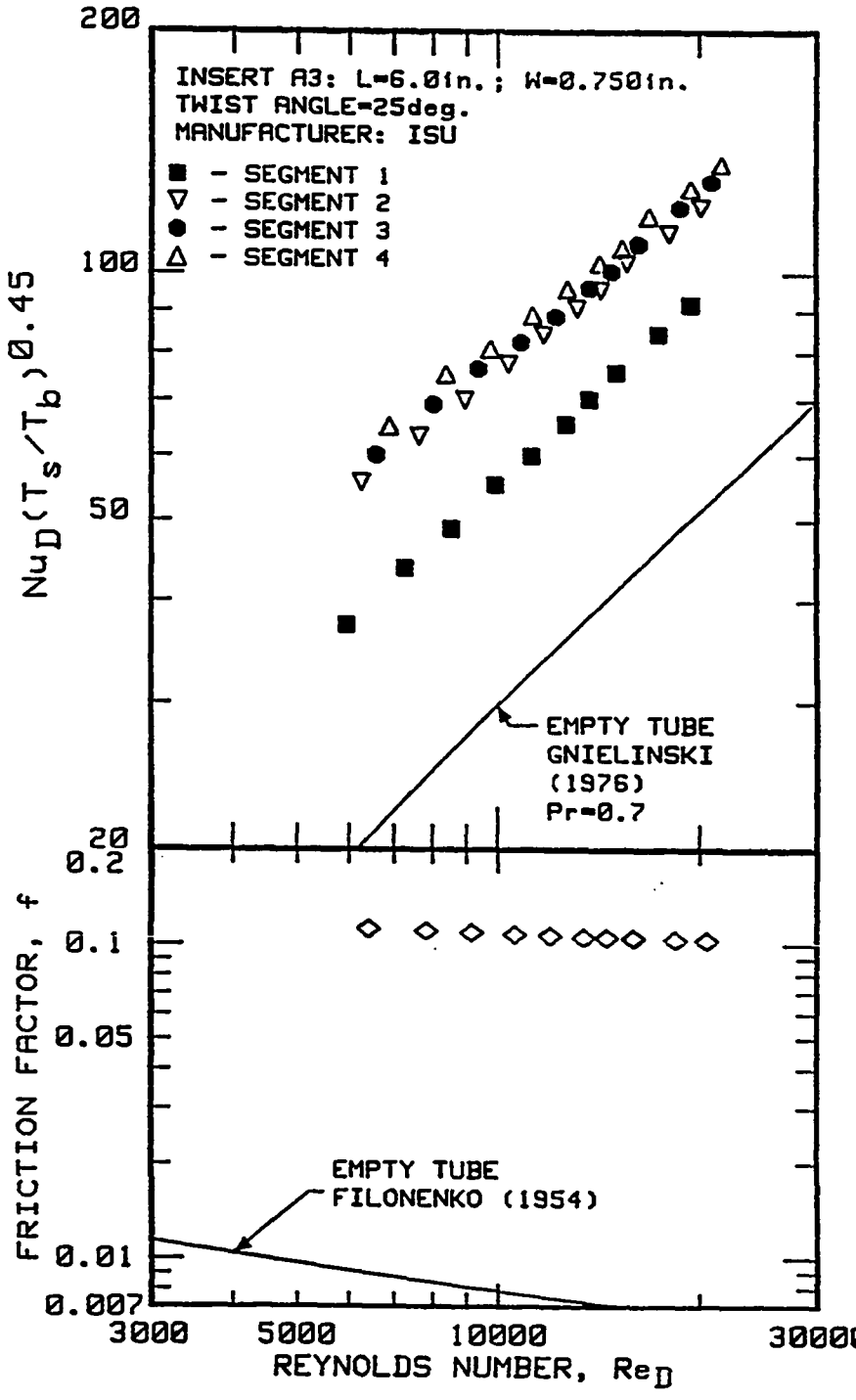

FIGURE 2.15. Heat-transfer and pressure-drop data for insert A3

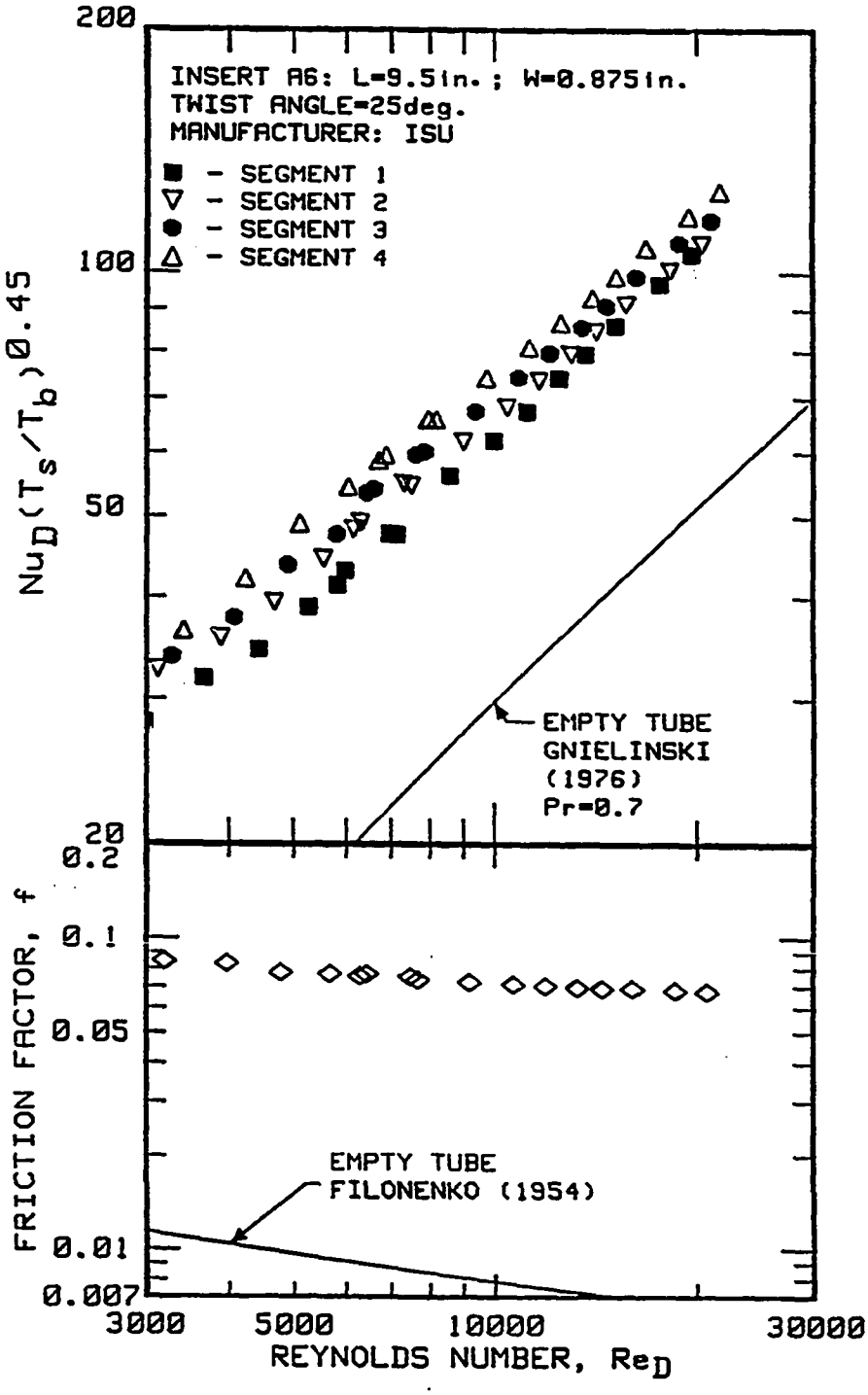

FIGURE 2.16. Heat-transfer and pressure-drop data for insert A6

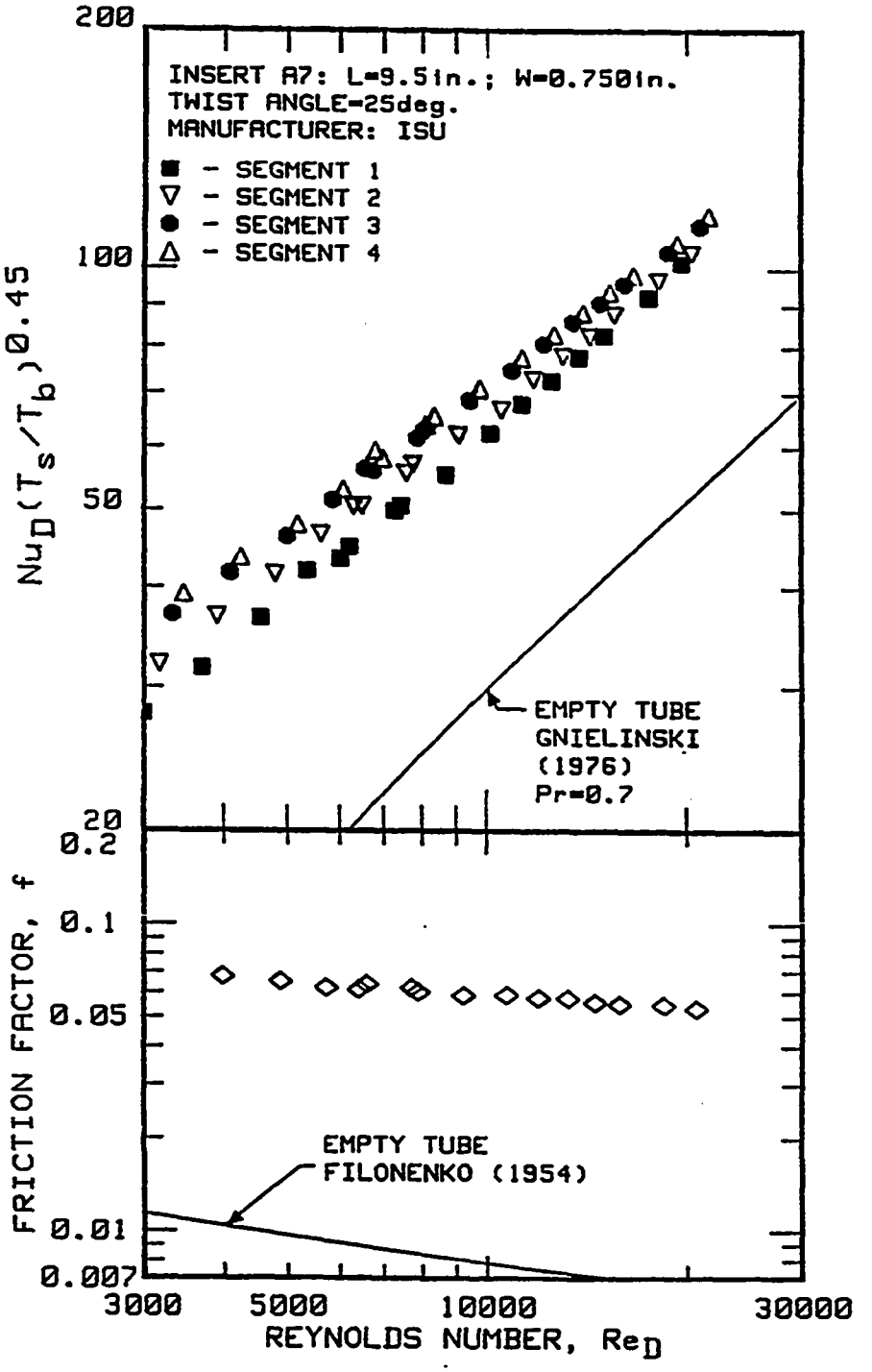

FIGURE 2.17. Heat-transfer and pressure-drop data for insert A7

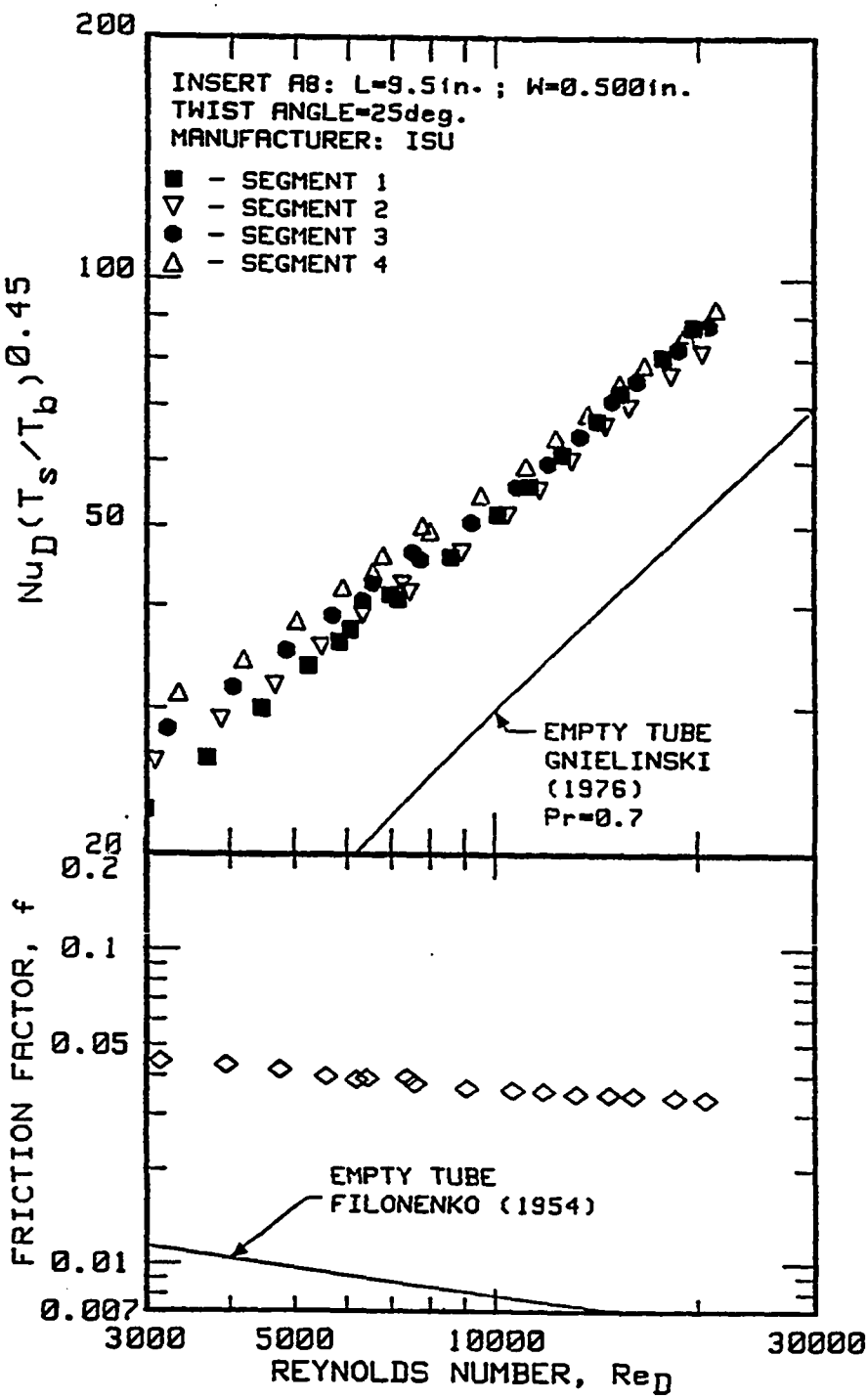

FIGURE 2.18. Heat-transfer and pressure-drop data for insert A8

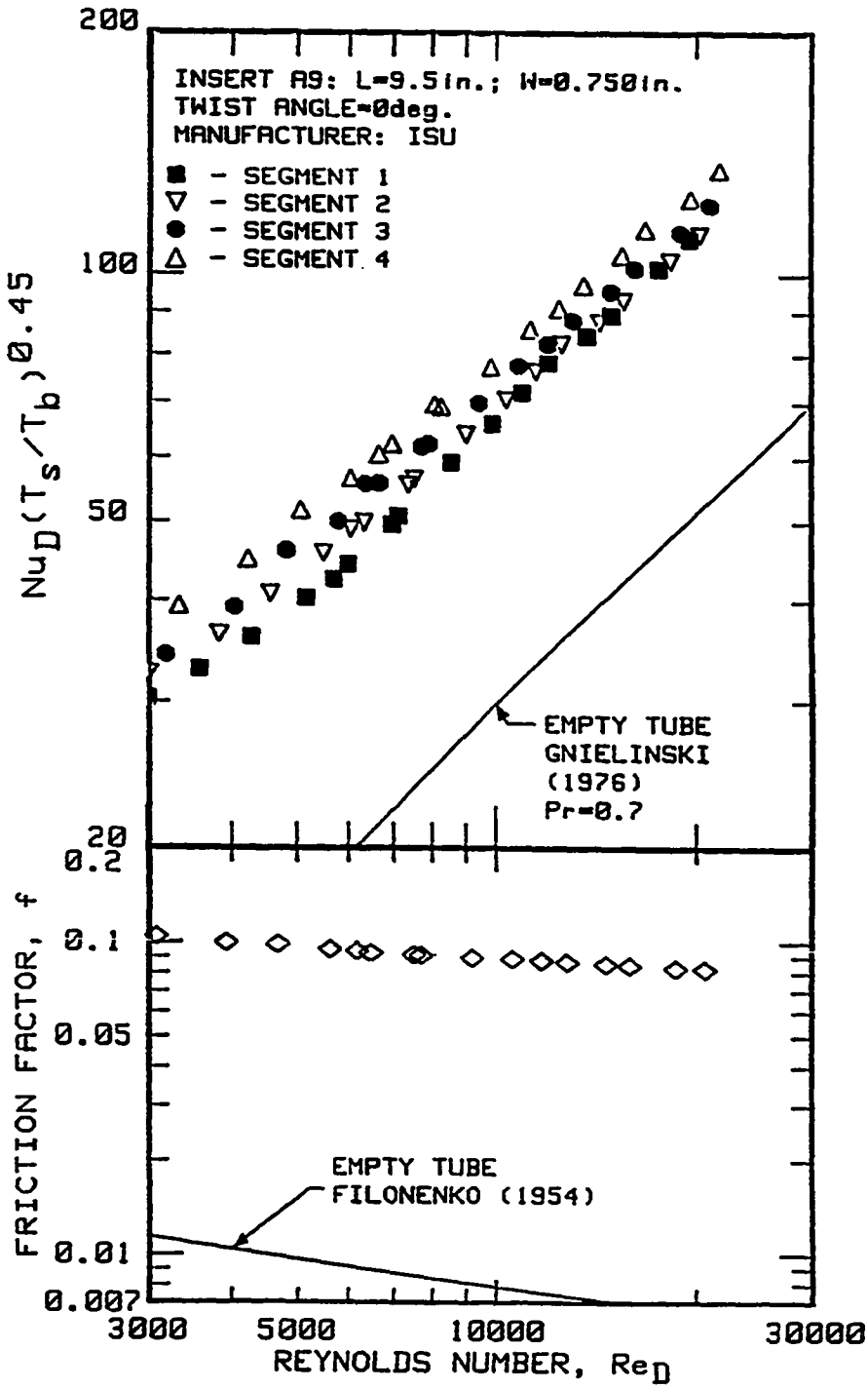

FIGURE 2.19. Heat-transfer and pressure-drop data for insert A9

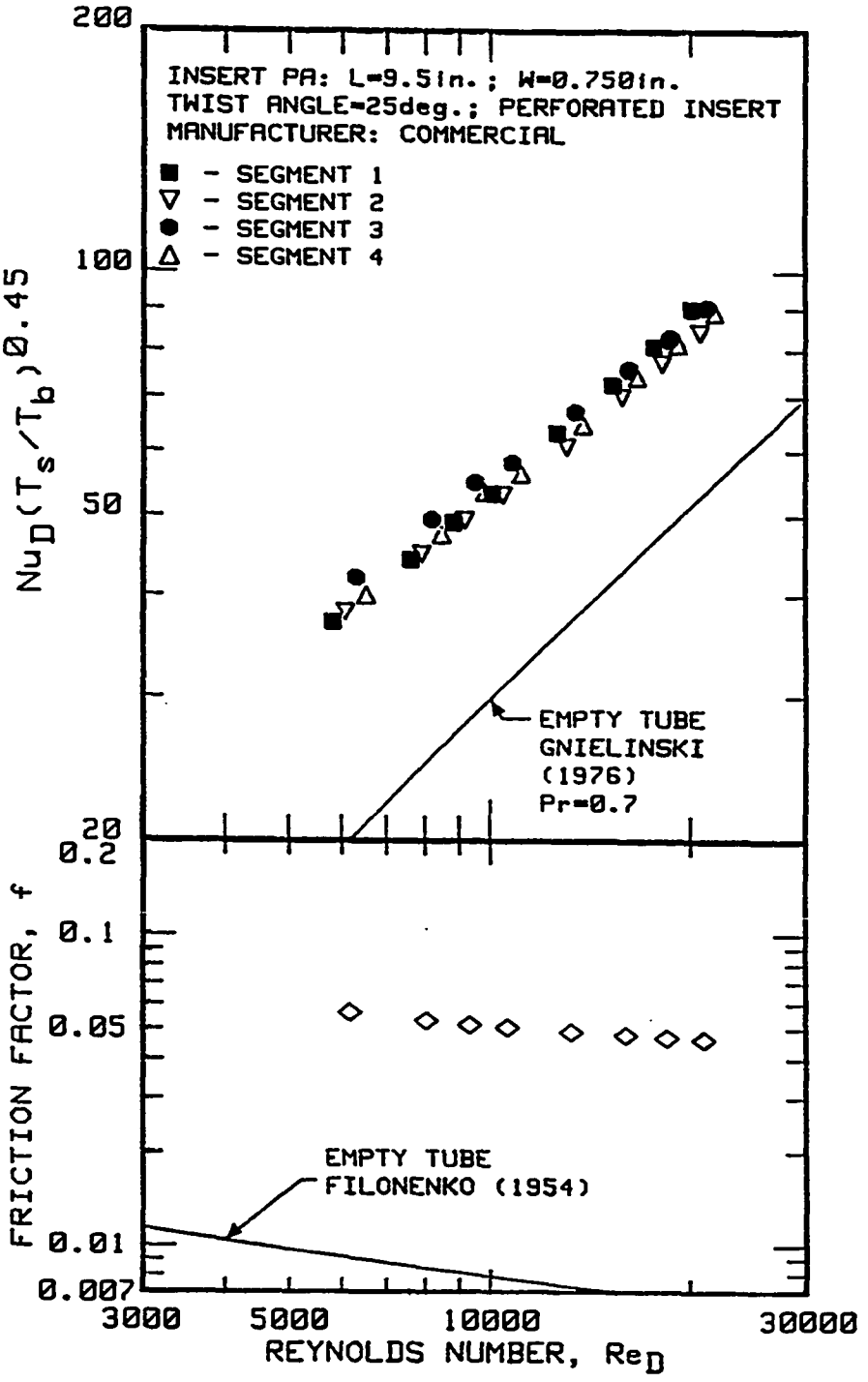

FIGURE 2.20. Heat-transfer and pressure-drop data for insert PA

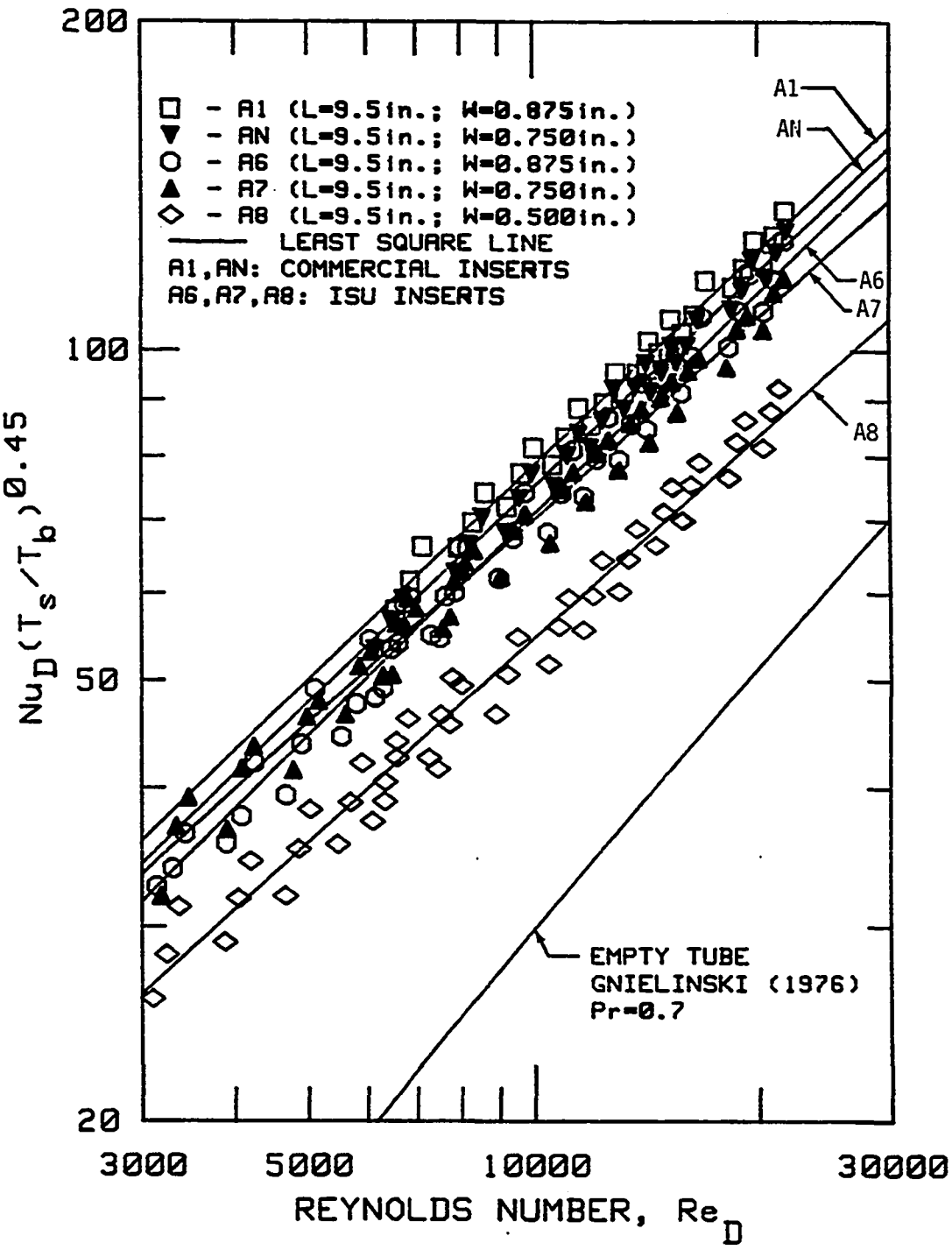

FIGURE 2.21. Effect of insert width and fabrication technique on heat-transfer coefficient

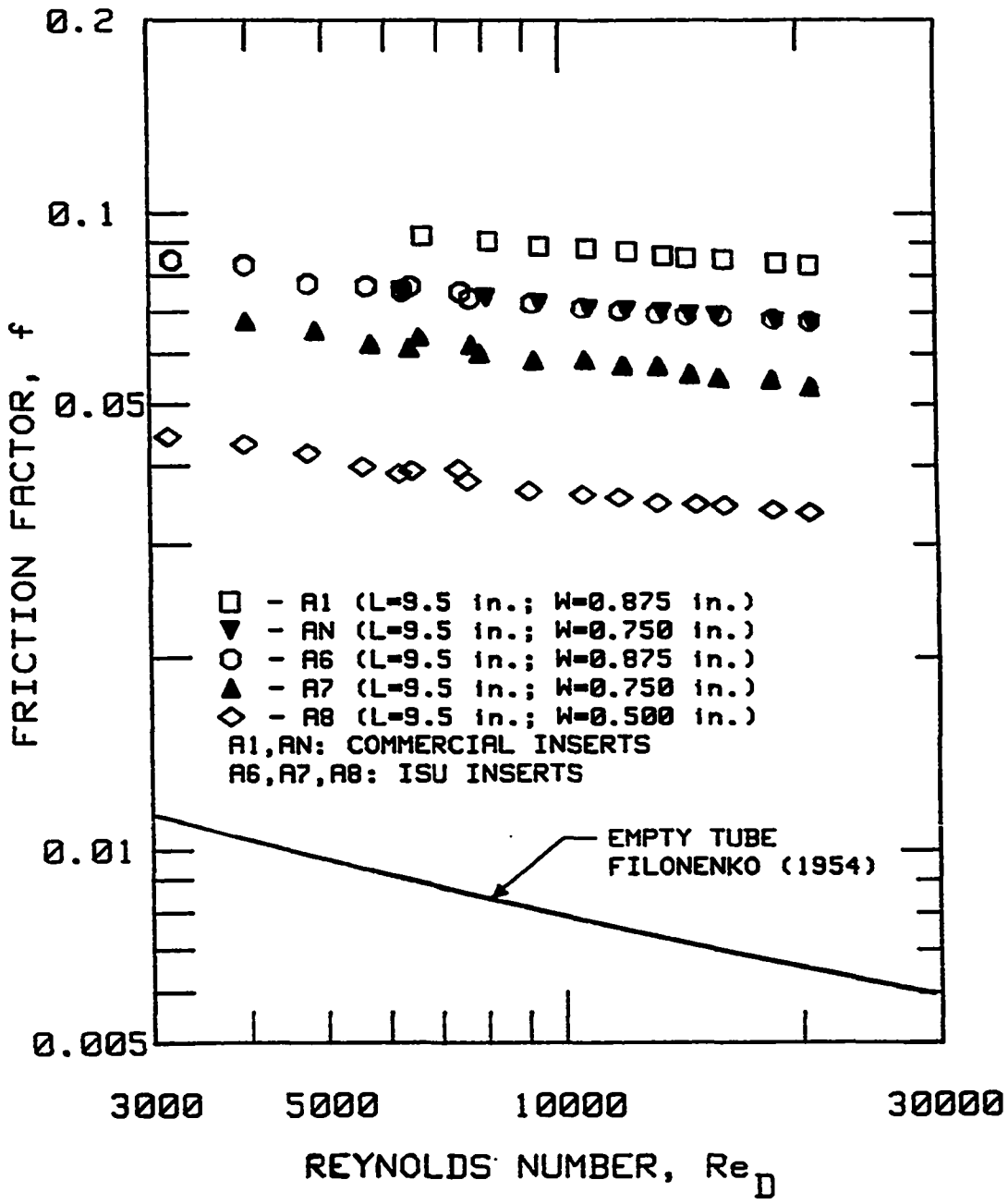

FIGURE 2.22. Effect of insert width and fabrication technique on friction factor

drawn through the data for each insert to give a better idea of the enhancement above the smooth tube base line.

Figures 2.23 and 2.24 show the heat-transfer and pressure-drop data for inserts A3, A4, A2, and A5. In addition to the effect of width, Figures 2.23 and 2.24 also show that heat transfer and pressure drop increases with decreasing pitch. This trend is shown more clearly in Figures 2.25 and 2.26, in which heat-transfer data of inserts A6, A7, and A2 (all of width 0.875 in.) and of A7, A3, and A5 (all of width 0.75 in.) are plotted, respectively, as a function of Reynolds number. For example, the data in Figures 2.21 and 2.23 show a 6% increase in Nusselt number for an increase of 17% in width. Similarly, Figure 2.25 indicates a 15% increase in Nusselt number for a 37% decrease in pitch. The same trend of an increase in friction factor with a decrease in pitch is also shown in Figures 2.27 and 2.28.

The performance of the perforated insert PA (identical to insert AN except for the perforations) is shown in Figures 2.29 and 2.30. Insert PA has a much lower heat transfer and pressure drop than insert AN. To estimate the effect of twist angle, the performances of inserts A7 and A9 are compared in Figures 2.31 and 2.32. With lower twist angles, the flow encounters a larger projected cross section of the insert, and therefore, an increase in heat transfer and pressure drop is expected.

3. Insert entrance length experiments

The flow conditions entering the test section approximate a fully developed turbulent flow velocity profile with a temperature

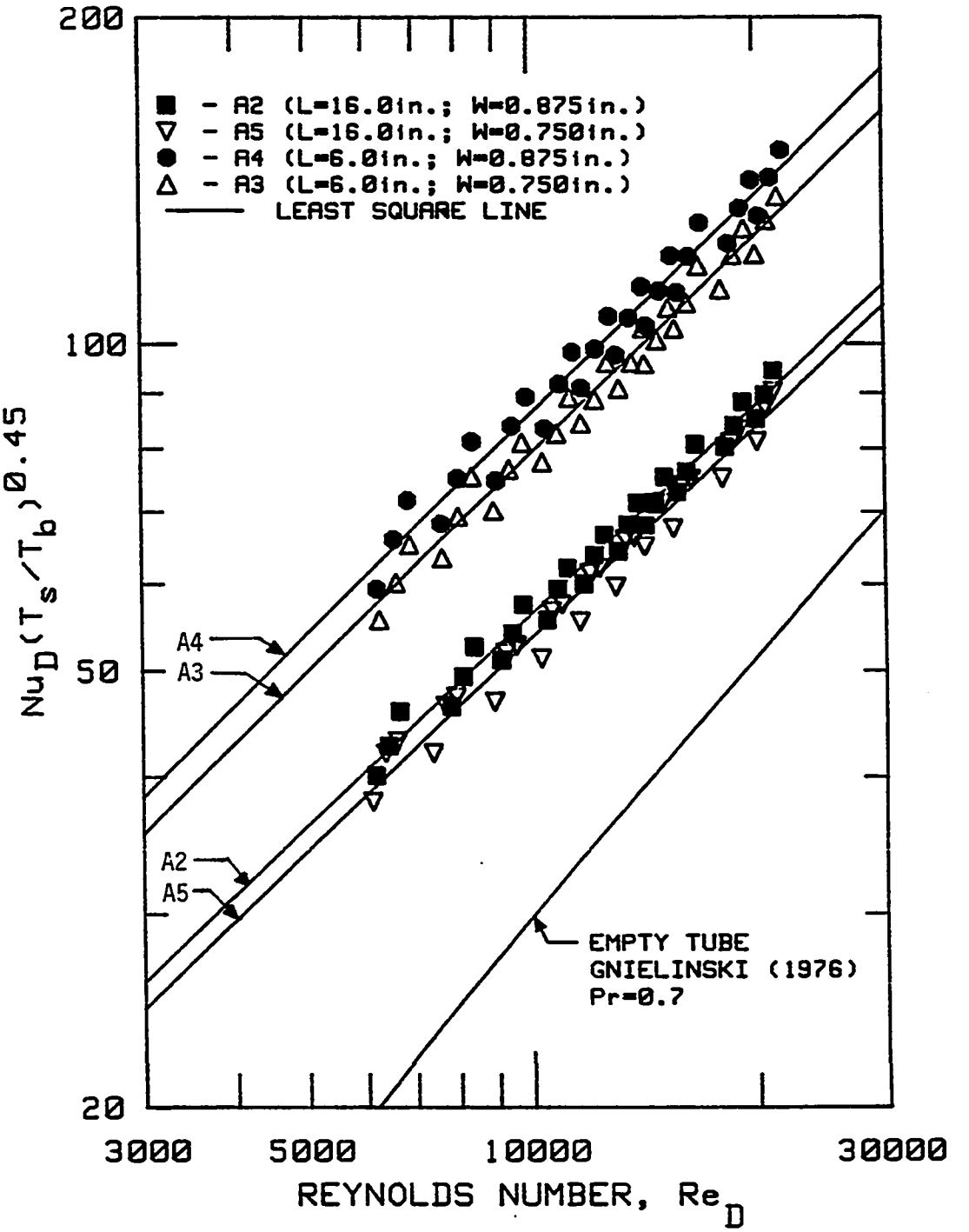

FIGURE 2.23. Effect of insert width and pitch on heat-transfer coefficient

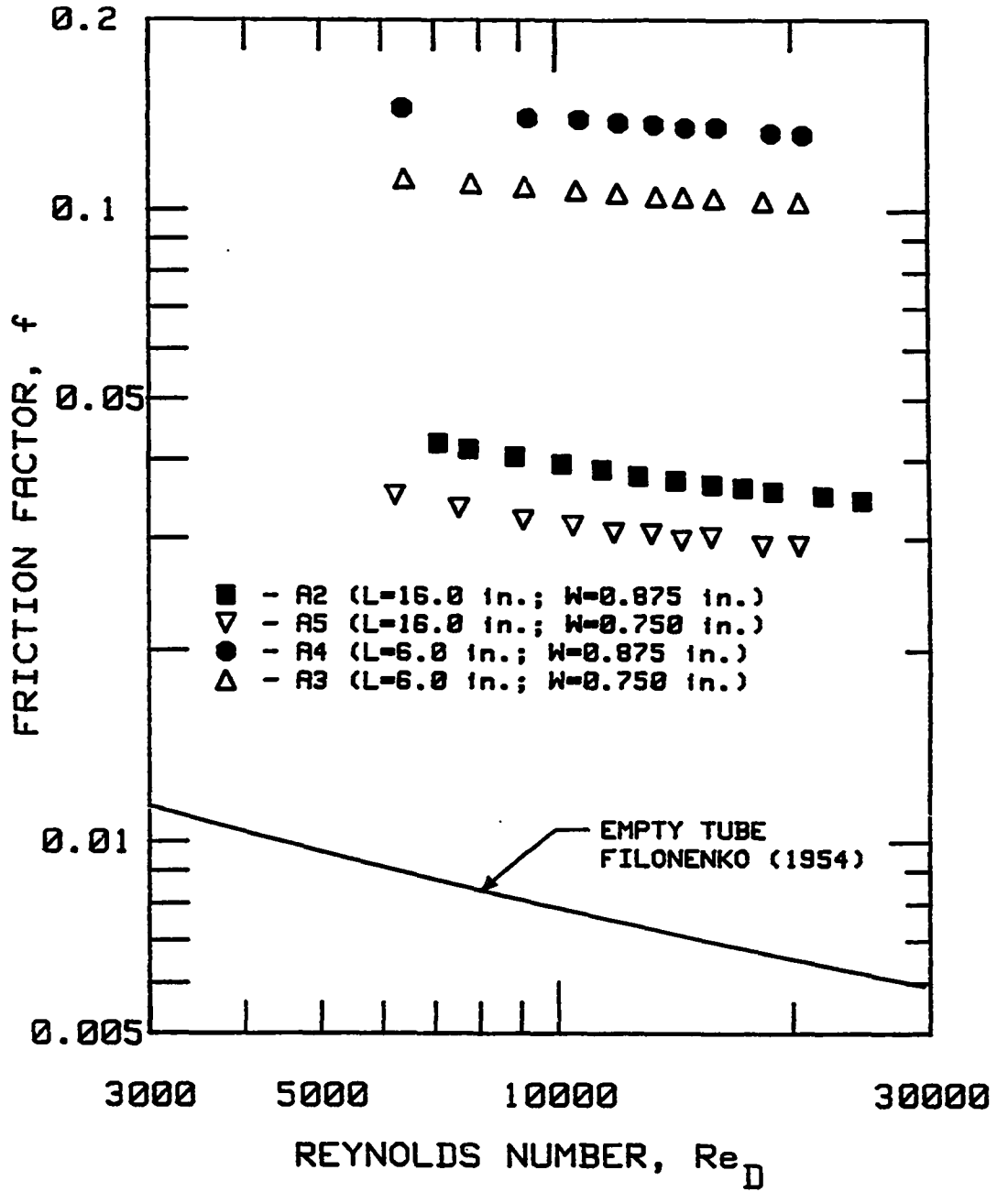

FIGURE 2.24. Effect of insert width and pitch on friction factor

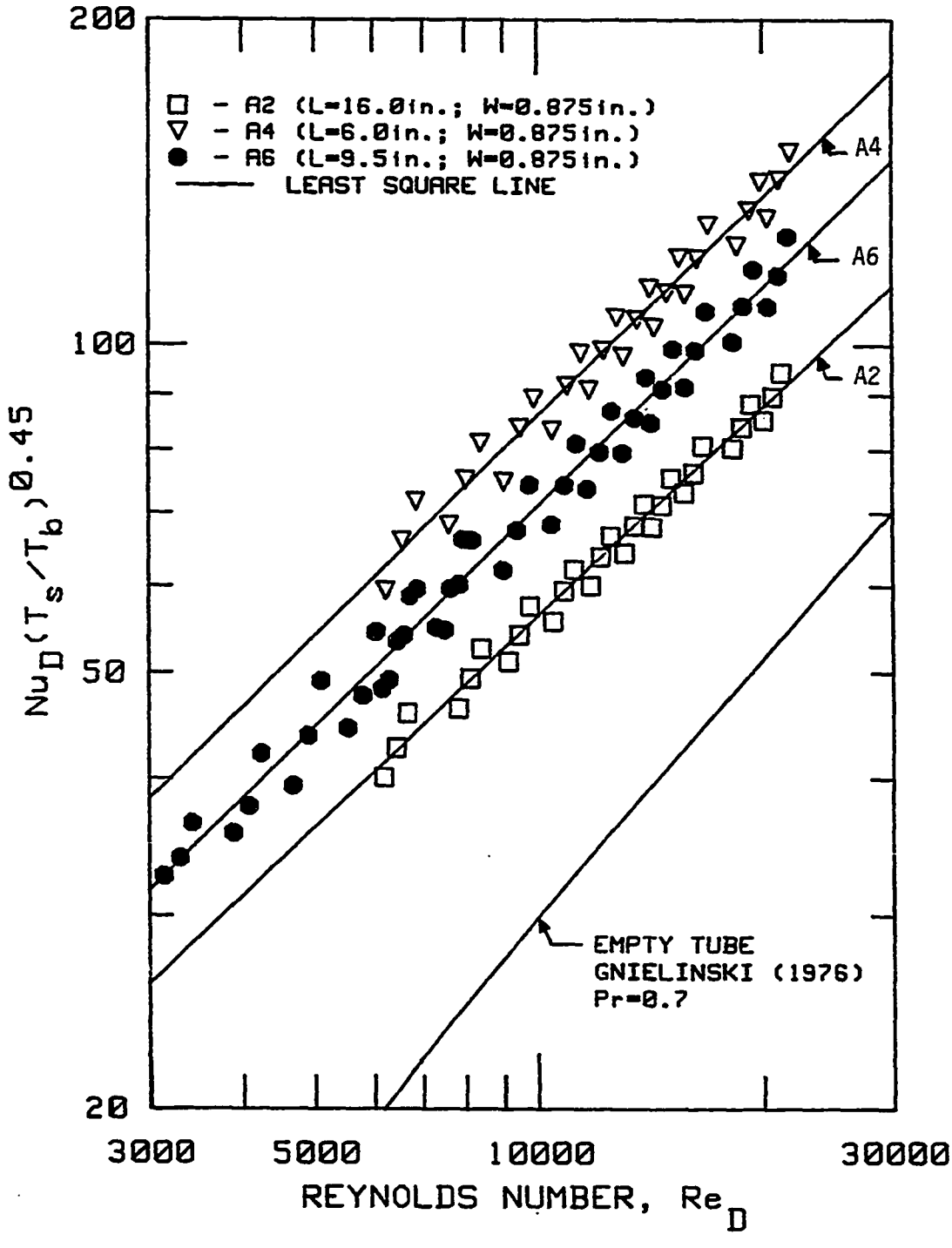

FIGURE 2.25. Effect of insert pitch on heat-transfer coefficient. Insert width = 0.875 in.

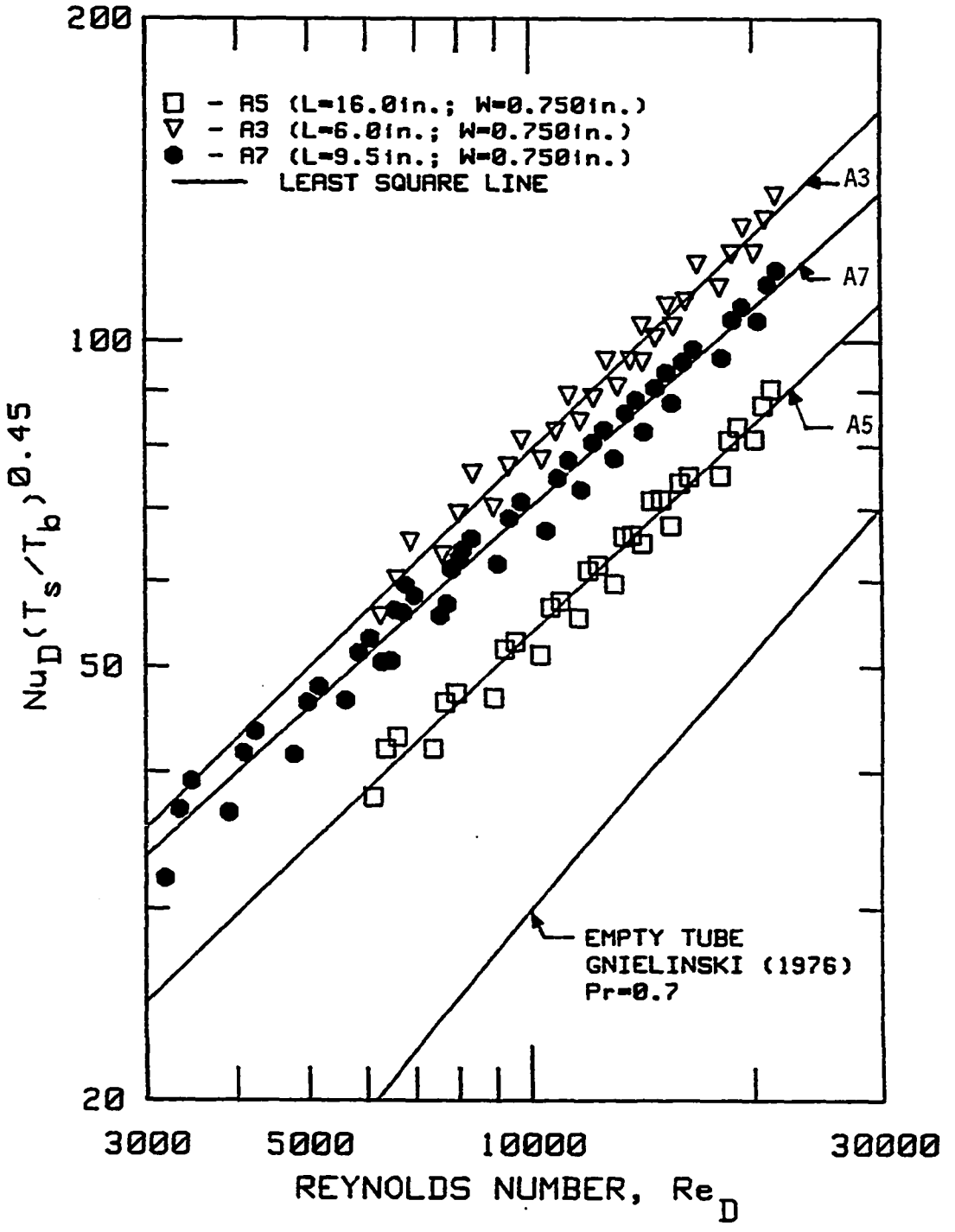

FIGURE 2.26. Effect of insert pitch on heat-transfer coefficient. Insert width = 0.75 in.

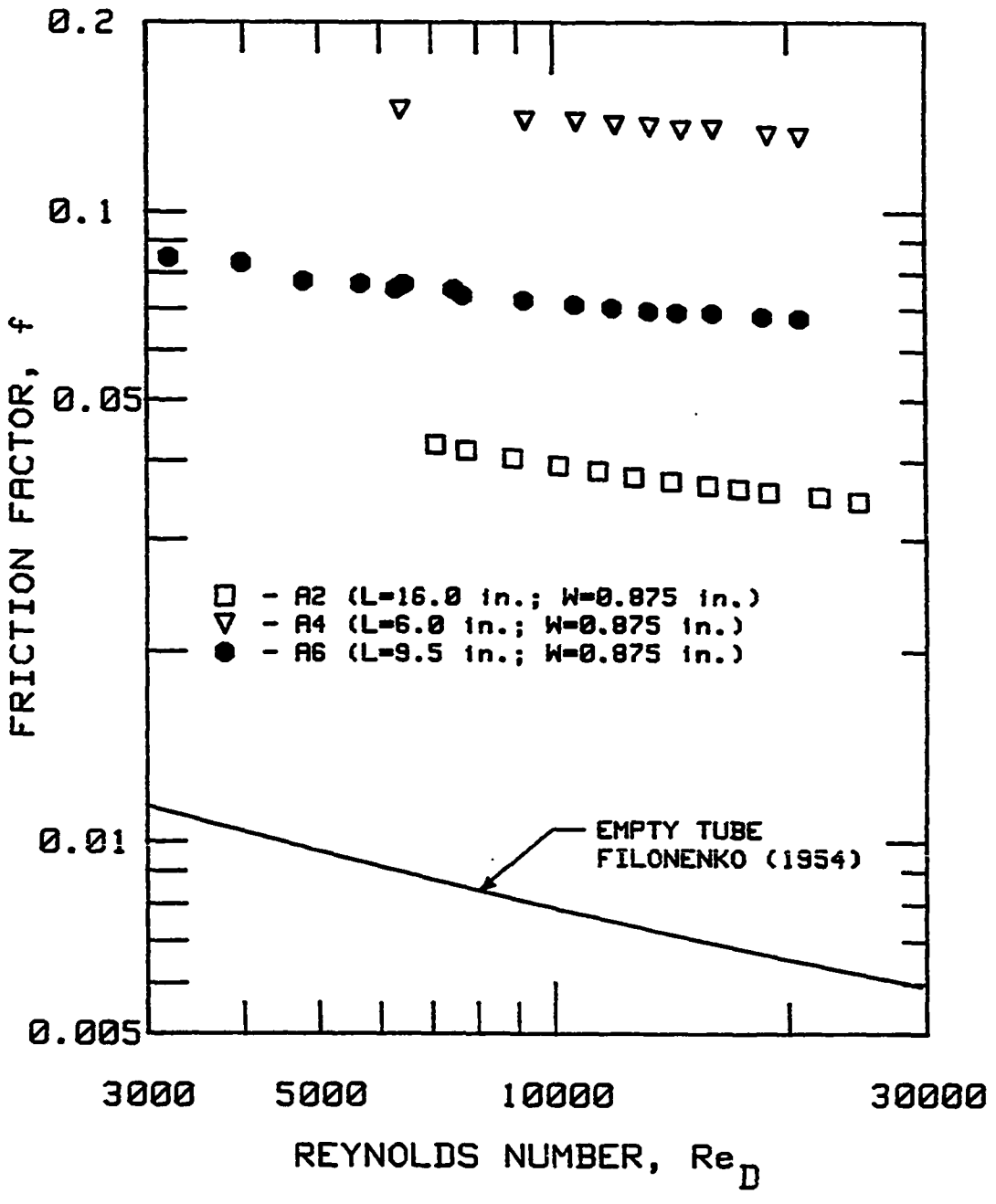

FIGURE 2.27. Effect of insert pitch on friction factor. Insert width = 0.875 in.

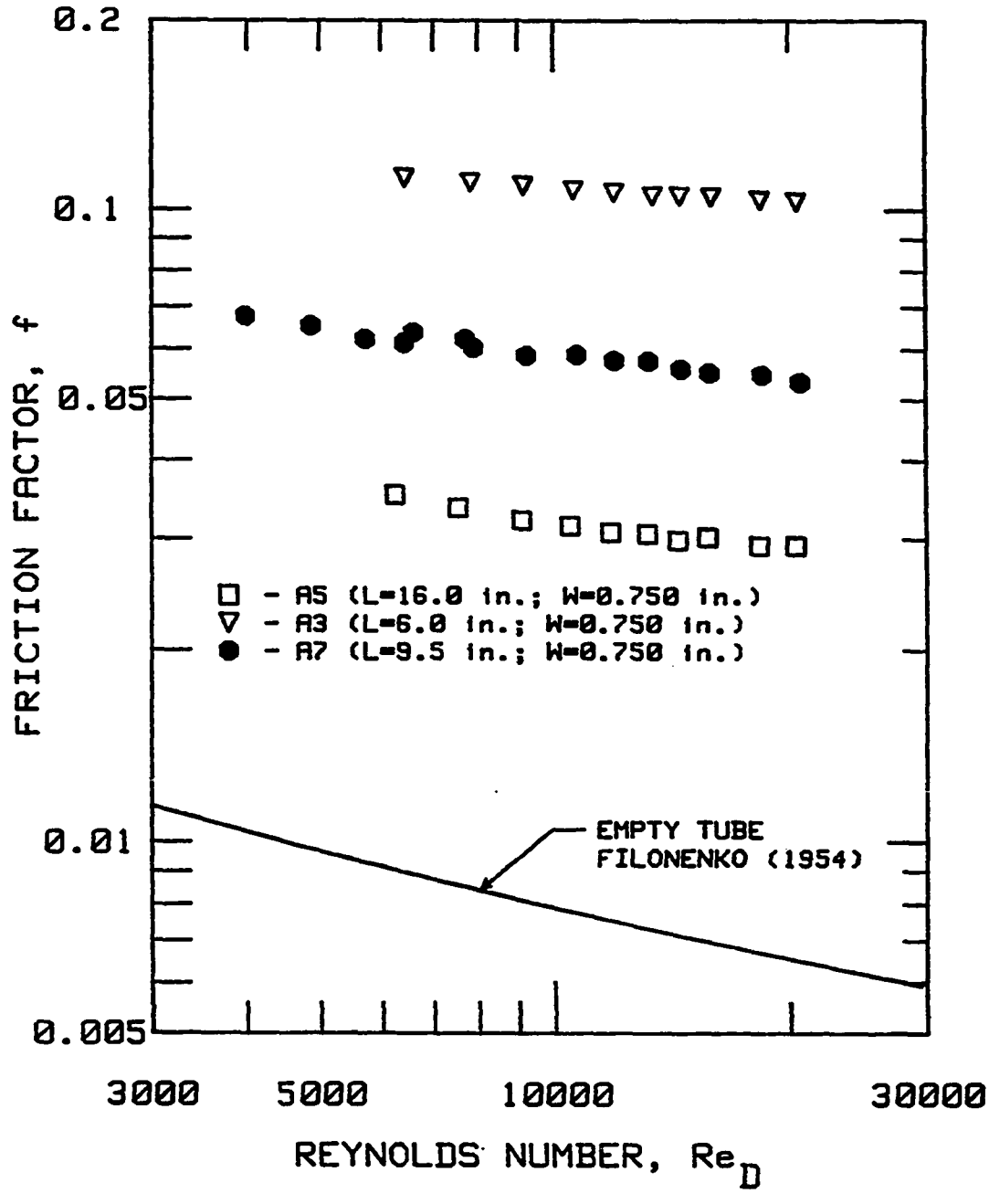

FIGURE 2.28. Effect of insert pitch on friction factor. Insert width = 0.75 in.

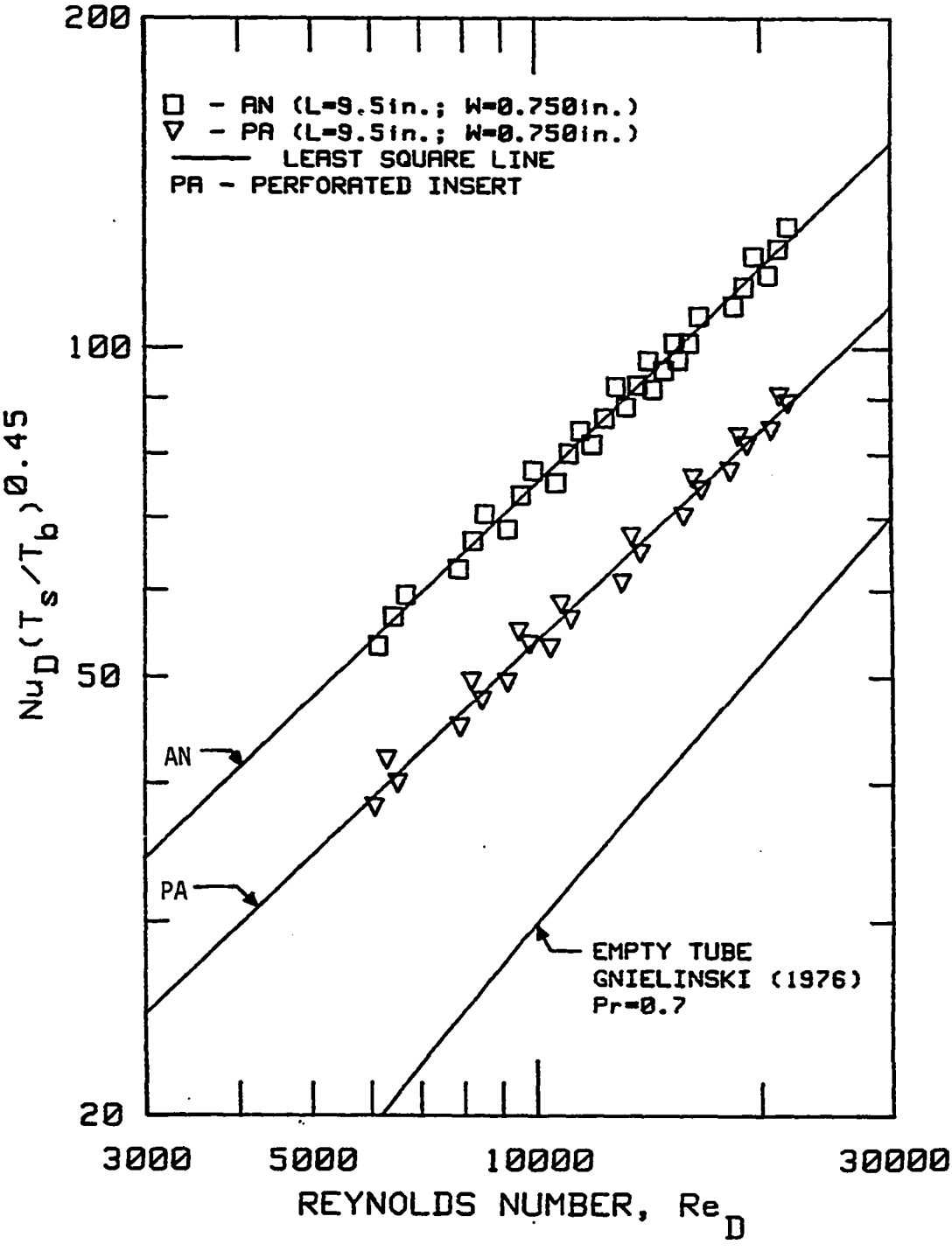

FIGURE 2.29. Effect of insert perforations on heat-transfer coefficient

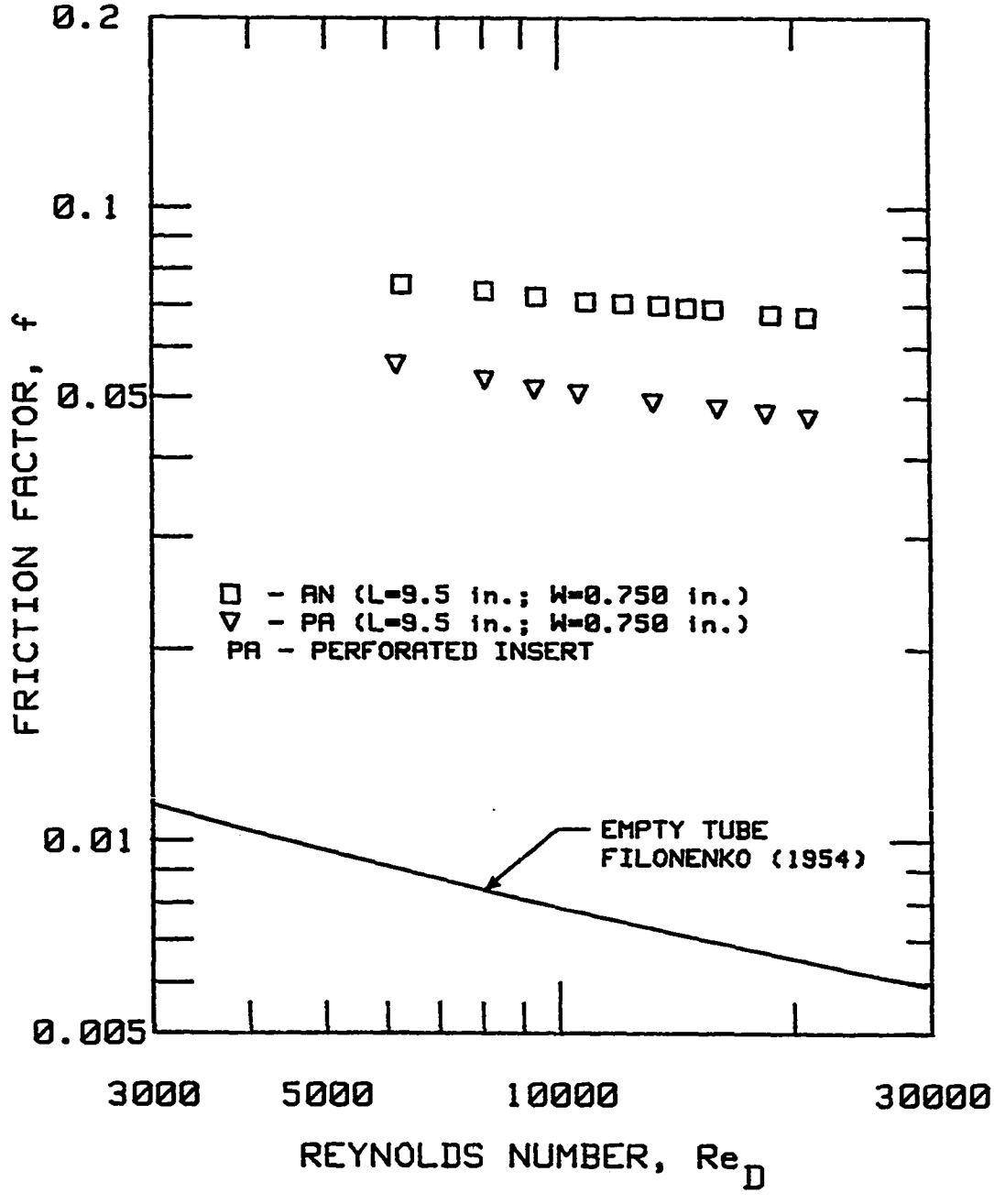

FIGURE 2.30. Effect of insert perforations on friction factor

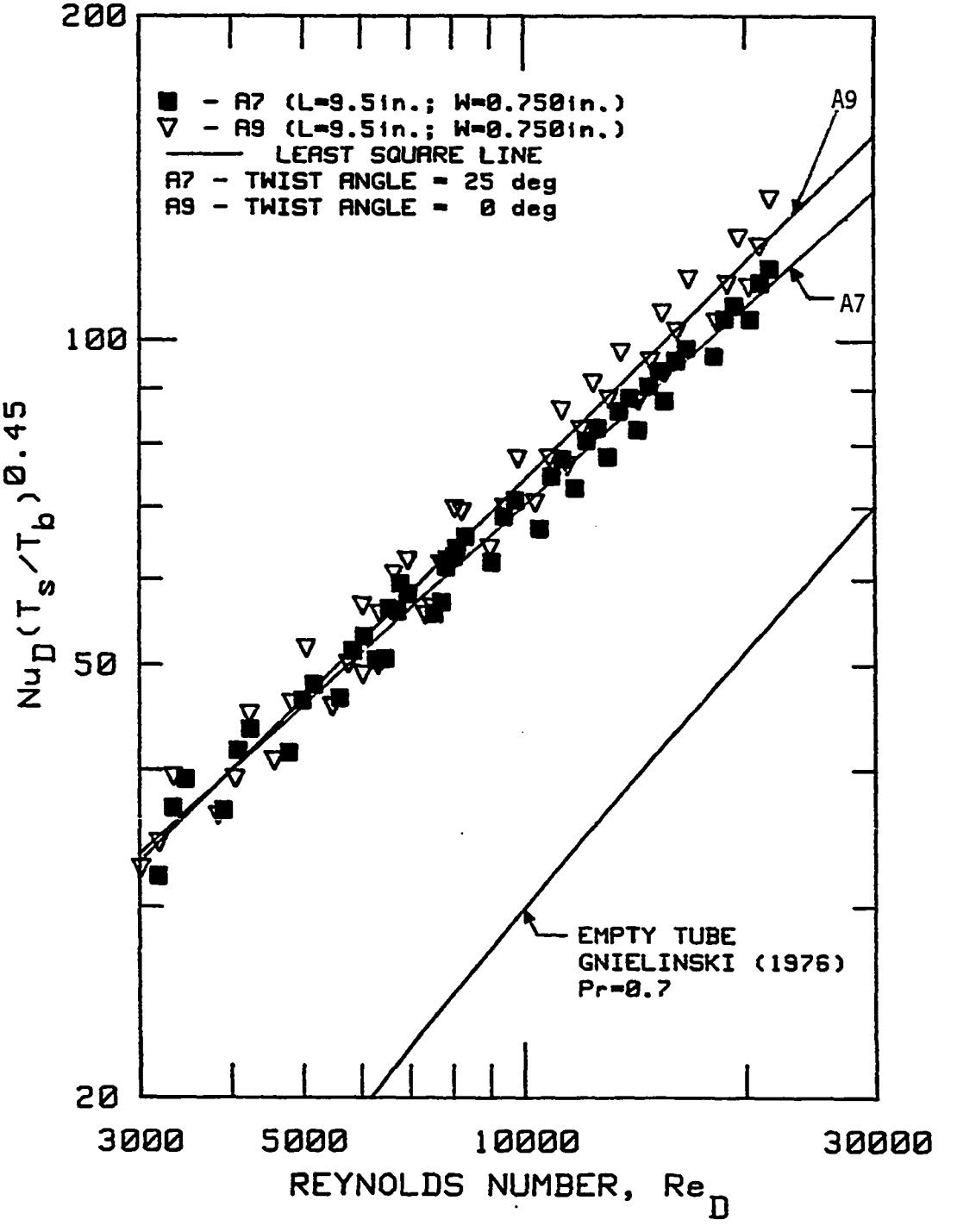

FIGURE 2.31. Effect of insert twist angle on heat-transfer coefficient

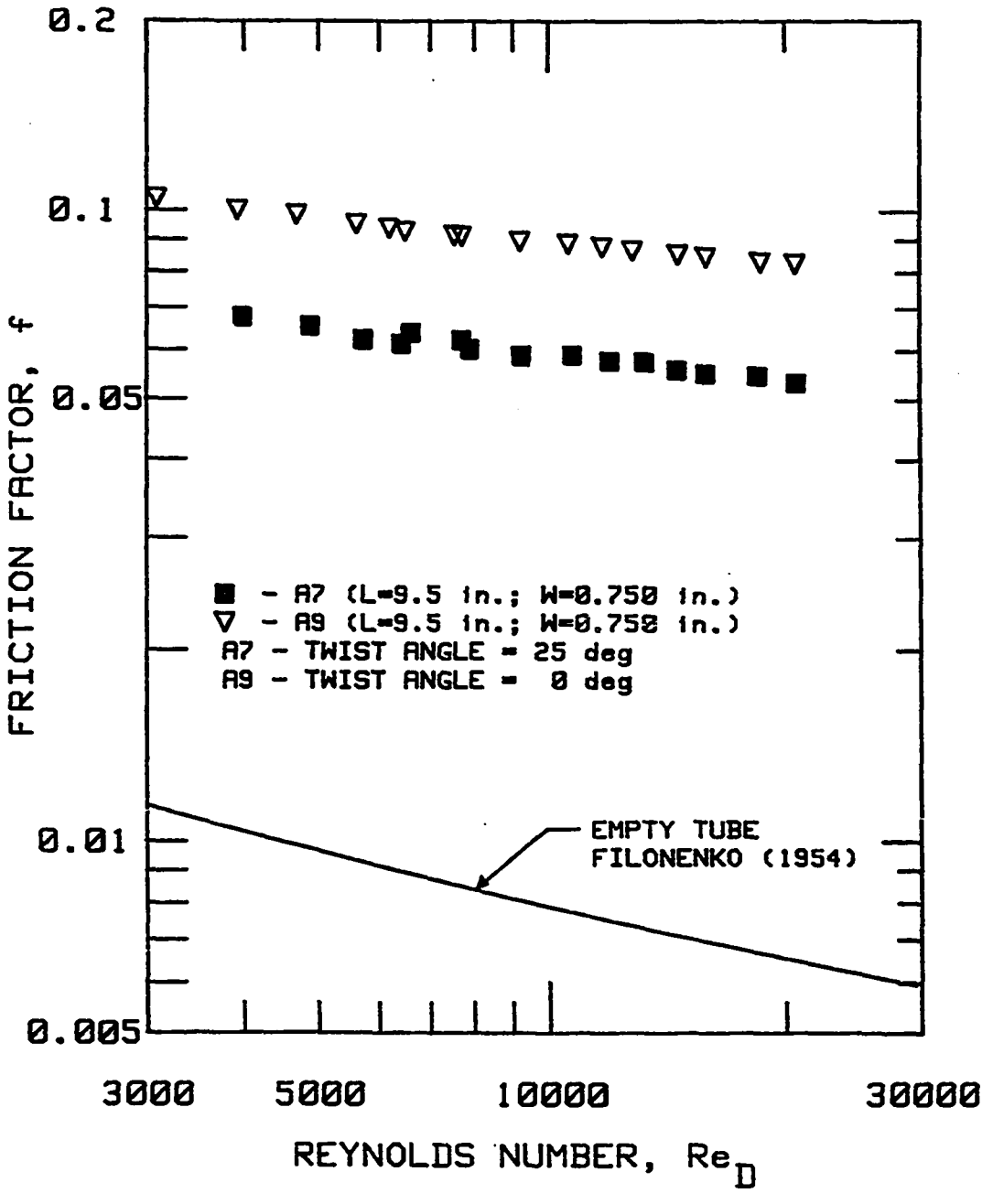

FIGURE 2.32. Effect of insert twist angle on friction factor

distribution characteristic of a long, insulated pipe. As mentioned before, the heat-transfer data from the first segment of the test section are generally lower on the coordinates of Nusselt number versus Reynolds number than the data from the other segments because fully developed enhanced conditions have not been attained in the first segment. Also, it is found that the insert length-to-diameter ratios in most insert applications are rather short. Hence, a study of the conditions in this entrance region is appropriate in order to assess the insert length required to attain fully developed enhanced conditions.

a. Method of testing for insert entrance effects The study of the entrance region heat transfer for an insert was conducted using the same experimental test rig. Figure 2.33 shows how the insert was moved axially in the tube so its upstream end could be placed at any desired location with respect to the first and second calorimeter segments. By moving the insert to a given position, the location where the enhancement begins is known in relation to the instrumented segments. The "insert entrance length" for the any particular segment, L_i, is defined as the distance from the upstream end of the insert to the upstream end of segment i. For example, the insert entrance length for the second segment, L_2, is defined as the distance from the upstream end of the insert to the upstream end of segment 2.

Experiments were conducted for Reynolds numbers of 3000, 5000, 10,000, 15,000, and 20,000, for eight insert positions and for two inserts. Inserts A4 and A6, which were of different pitch but same

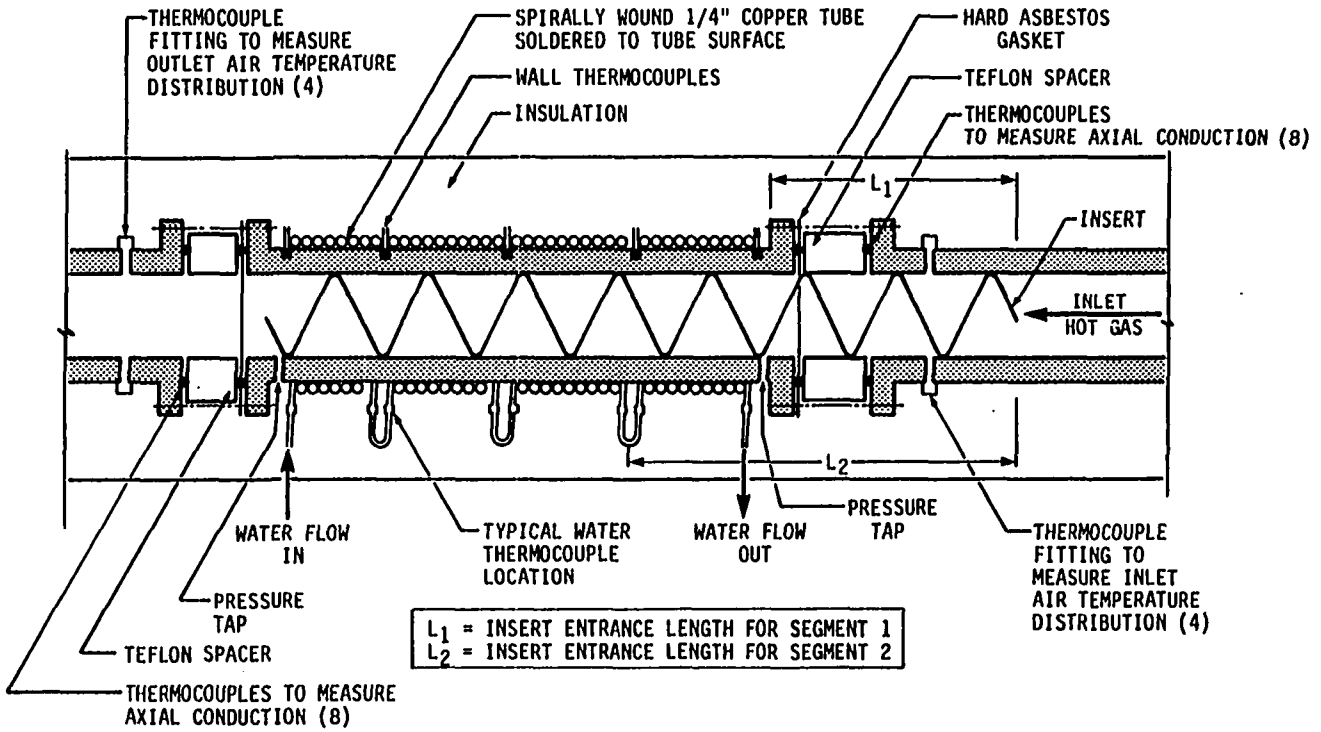

FIGURE 2.33. Location of insert to obtain entry region data

width, were tested because a pitch effect of the insert entrance length was anticipated.

b. Results and discussion The entrance region heat-transfer results are shown in Figures 2.34 and 2.35, where Nusselt numbers for segments 1, 2, and 3 are plotted against the ratio of insert entrance length to insert pitch. The figures indicate that as the ratio of insert entrance length to pitch is reduced, the heat-transfer coefficient from the hot gas to the tube decreases almost linearly. When the insert is absent from a particular segment, the Nusselt numbers correspond to the smooth tube condition for the particular Reynolds number. Both inserts indicate that a fully developed enhanced heat-transfer condition is attained at an insert entrance length to pitch ratio of about 1.5. After the fully developed enhanced condition is reached, the Nusselt number should not vary with the insert entrance length. However, the figures show that there are variations in the data at insert entrance-length-to-pitch ratios greater than 1.5 and that the fluctuations are more pronounced at higher Reynolds numbers. This could be caused by a variation in the number of contact points between the insert and the tube wall in the particular segment, which in turn depends on the location of the insert with respect to the segment.

4. Experiments to differentiate the effects of core and wall regions

The flow visualization studies on inserts reported in Chapter III indicate that the flow at the core of the tube and the flow at the wall do not mix as well as intuition suggests. Hence, it was deemed

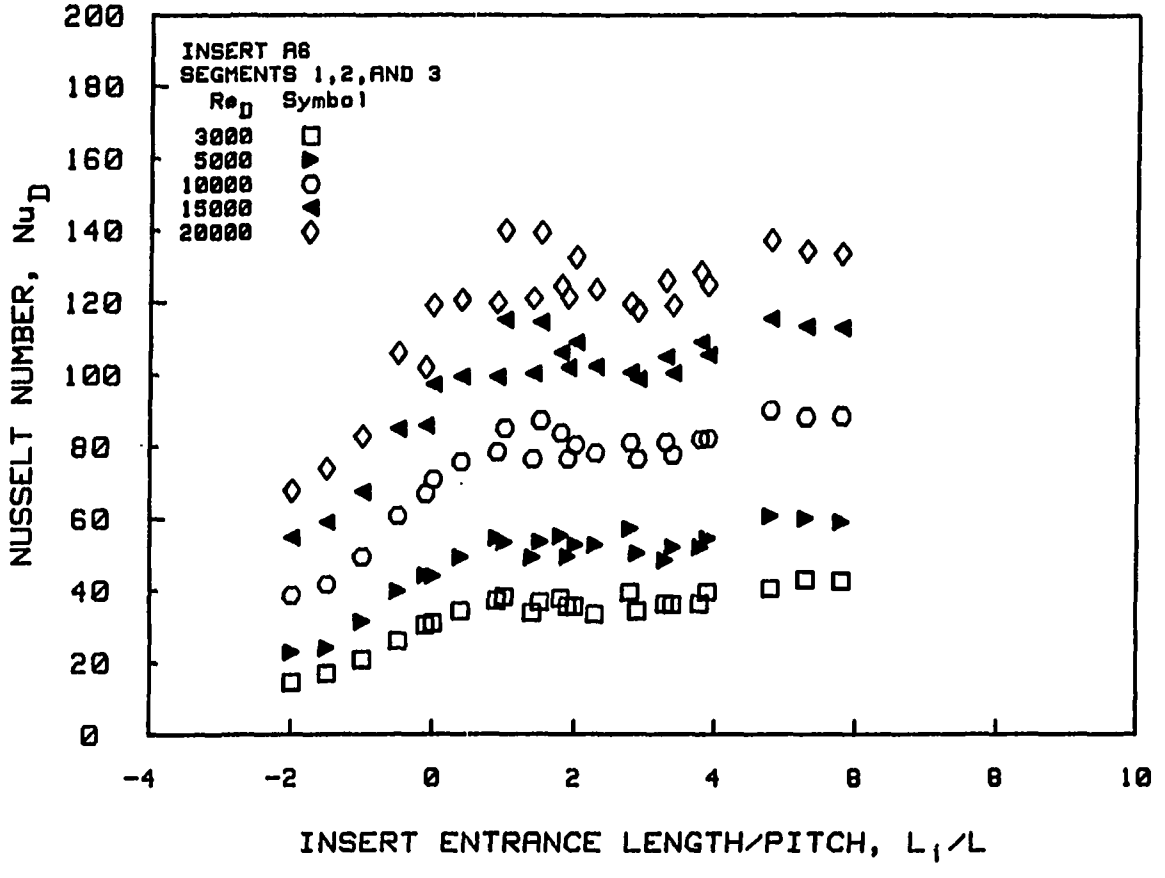

FIGURE 2.34. Insert entrance length heat-transfer data for insert A6

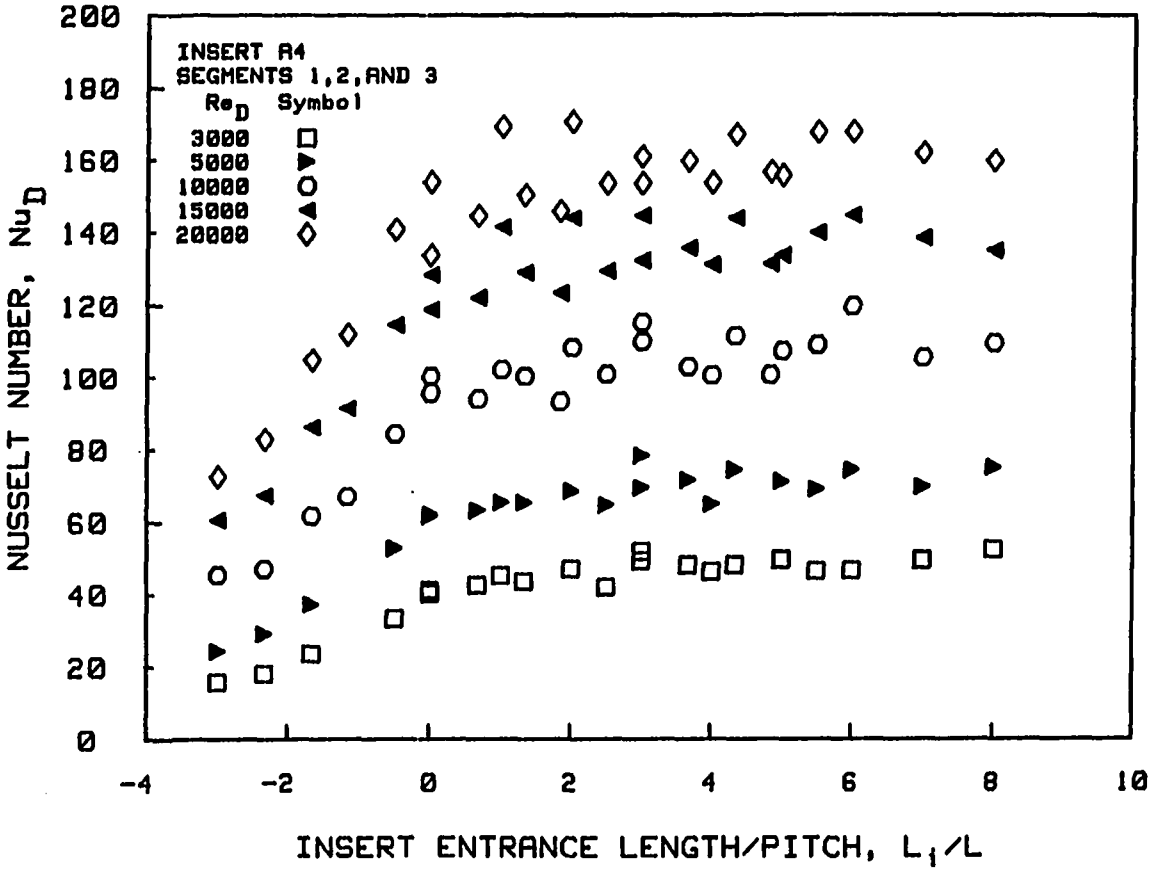

FIGURE 2.35. Insert entrance length heat-transfer data for insert A4

necessary to study the effects of the core region and the wall region separately.

a. Inserts tested To facilitate this study, the bent-strip insert A1 was cut apart to provide separate wall and core inserts AW and AC as shown in Figure 2.36. First, 1/8-in. diameter holes were drilled at three different axial locations in each of the insert sides, and three rigid 1/8-in. wires were inserted through the holes and welded to the insert. Then the insert was cut axially into three sections by using a band saw. Spacers were welded to keep the two wall sections in their correct locations, thereby forming the insert AW. Similarly, spacers were welded to keep the core section in the center of the tube to make the core region insert AC. The core section insert AC had a width of 2/3 times the diameter. These two inserts were separately tested for heat transfer and pressure drop.

b. Results and discussion Figures 2.37 and 2.38 give the heat-transfer and pressure-drop data for the core region insert AC and the wall region insert AW. These data are compared with insert A1, the original insert from which the two sectional inserts were made. Figure 2.37 shows that the core region insert enhances the heat transfer more than the wall region insert. Although the flow visualization studies in Chapter III of this study indicate that the flow along the wall is not much disturbed by the entire insert, the results of this chapter indicate that the core region plays a significant, if not dominant, role in enhancing the heat transfer. However, it is likely that the core

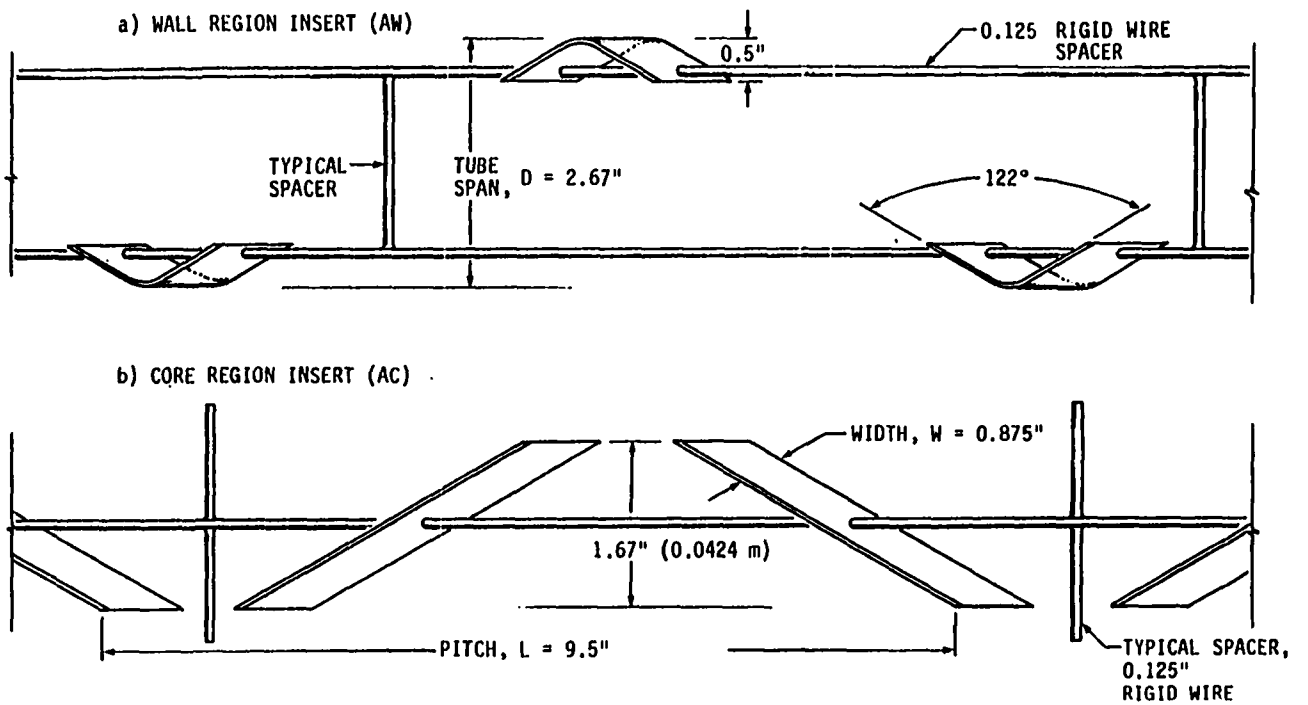

FIGURE 2.36. Inserts AW and AC. Fabricated to test core and wall region separately

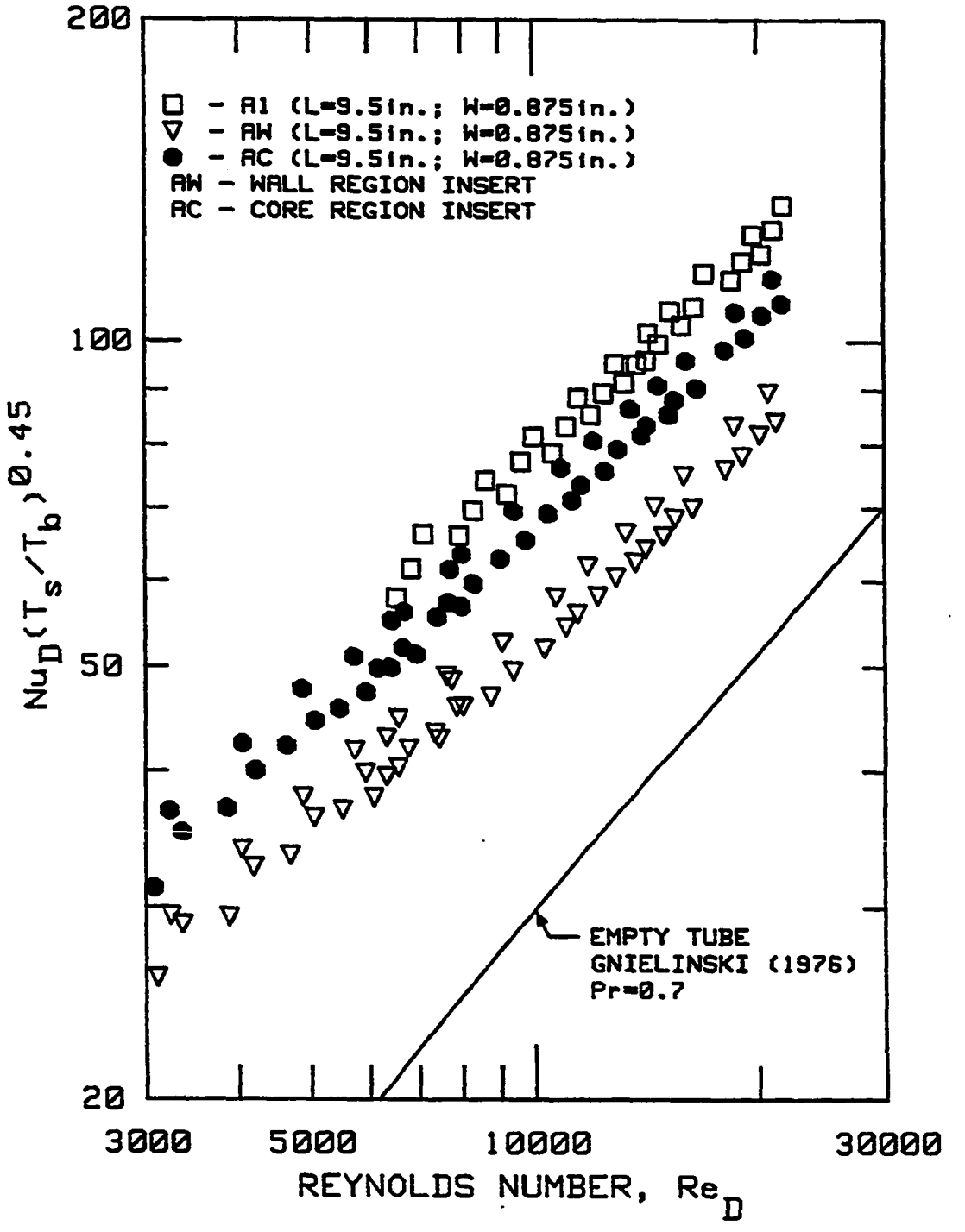

FIGURE 2.37. Heat-transfer data for the core (AC) and wall (AW) region inserts compared with data for insert A1

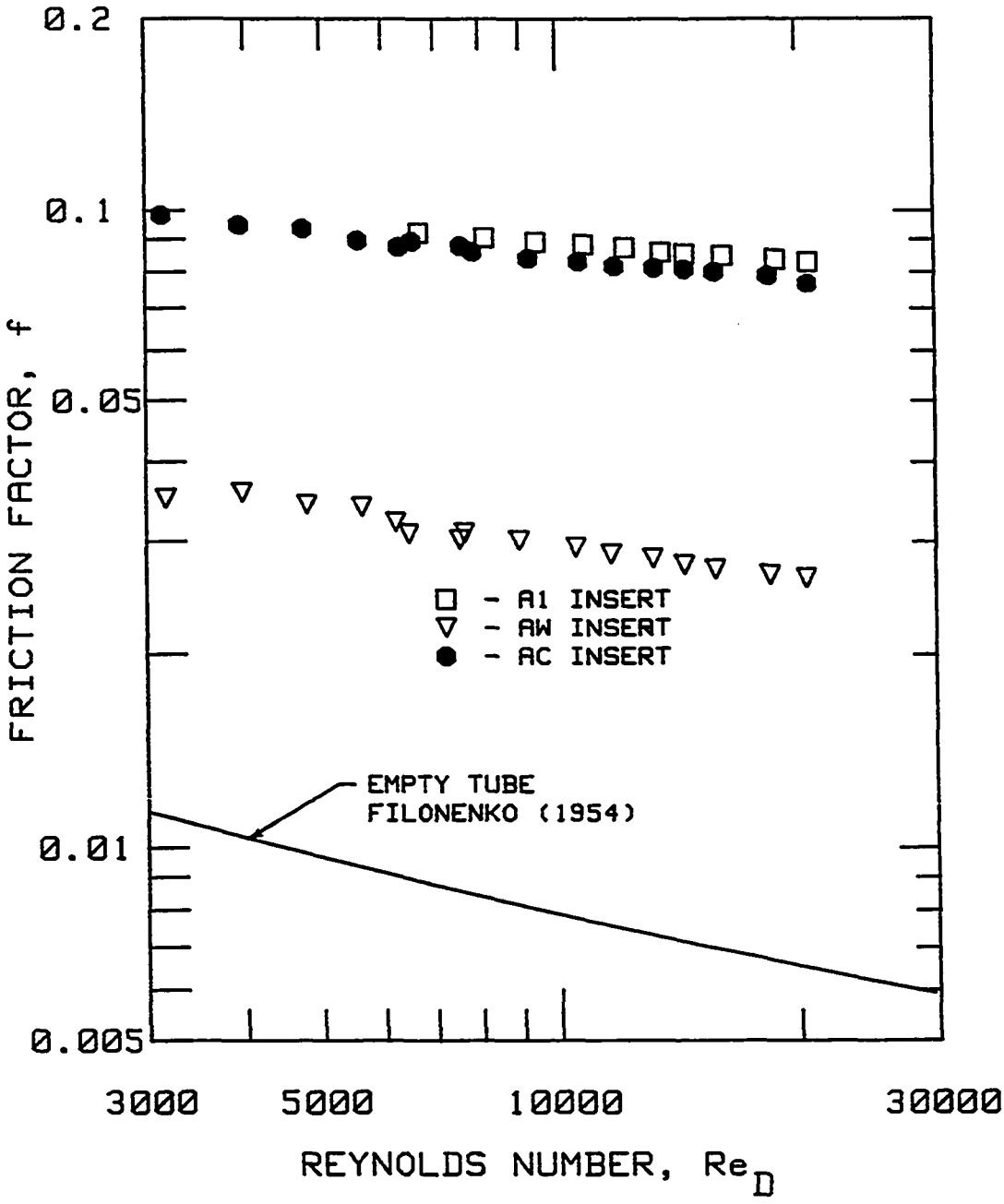

FIGURE 2.38. Pressure-drop data for the core (AC) and wall (AW) region inserts compared with data for insert A1

insert performs better on its own than the core region of the full insert because of the eddies shed from the noncontinuous sharp-edged strips. Figure 2.38 also shows the same sort of results for the case of the friction factor, with insert AC exhibiting nearly the same friction factors as the full insert.

D. General Correlations and Performance Evaluations

1. Empirical correlation of data

A statistical approach (Ostle and Mensing, 1975) was used to find a correlation by assuming a model and minimizing the least squares differences in the dependent variables to fit all the data that had been obtained for the unperforated inserts. The data of insert A9 (with twist angle 0°) was also not considered in the correlation. The following equation models were used for the correlations:

$$Nu_D = A\ (Re_D)^B\ (L/D_i)^C\ (W/D_i)^D\ (T_s/T_b)^{-0.45} \tag{2.15}$$

$$f = A\ (Re_D)^B\ (L/D_i)^C\ (W/D_i)^D \tag{2.16}$$

where A, B, C, and D are constants. In the above equations, Nu_D is based on sectional-average heat transfer, while f is based on pressure drop across the whole test section. In Equation 2.15, the Prandtl number is not considered in the correlation because there is no appreciable variation in Pr in the experiments conducted. Therefore, the correlation developed is valid only at a Pr of 0.7 (i.e., for most

gases). A property variation correction was not considered in the correlations because the variation of temperature ratio, T_s/T_b, was not large enough. However, the heat-transfer correlation was corrected for bulk properties by using the exponent suggested by Gnielinski (1976).

To obtain the values of the constants, a matrix approach to multiple linear regression was used. The methodology of this approach is given in Appendix F.

Due to the apparent entry length behavior, two equations of the same model were necessary to predict the heat transfer. One equation is used to predict the heat transfer in the "entry region," which is defined as the region from the upstream end of the insert to 1.5 times the insert pitch. The second equation predicts the heat transfer in the "fully developed region," which is defined as the region after an insert length of 1.5 times the insert pitch. The estimates of the constants, exponents and limits at 95% confidence levels are given in Table 2.2. R^2 is the correlation coefficient for each of the regression equations. The values of A, B, C, and D are valid in the following range of variables:

Re_D = 3000 - 20,000

Pr ≈ 0.7

L/D_i = 2 - 6

W/D_i = 0.15 - 0.40

Figures 2.39 and 2.40 show the correspondence between predicted and

TABLE 2.2. Estimates and uncertainties of constants in correlation equations

Equation (Region)	Estimates and Uncertainties Nu_D (Entry)	Nu_D (Developed)	f (Full)
A	$0.222^{+0.0045}_{-0.0044}$	$0.540^{+0.0029}_{-0.0029}$	$4.350^{+0.0996}_{-0.0973}$
B	0.695 ±0.0004	0.649 ±0.0001	-0.100 ±0.0004
C	-0.347 ±0.0009	-0.391 ±0.0003	-1.286 ±0.0011
D	0.319 ±0.0031	0.503 ±0.0007	1.320 ±0.0030
R^2	0.9551	0.9714	0.9984

experimental heat-transfer data for the entry region and developed region, respectively. Figure 2.41 shows the correspondence between the predicted and experimental pressure-drop data. The correlations predict most data within ±10%. The correlation obtained above was tested by applying it to data for insert B, shown in Figure 2.42, which was tested by Junkhan et al. (1985). Insert B was made by another commercial manufacturer and is bent in a different fashion from the other inserts in the present study. Figures 2.43, 2.44, and 2.45 compare the experimental heat-transfer and friction-factor data of insert B with the correlations. The friction-factor prediction is excellent, but the correlation overpredicts the heat transfer by about 10% in the developed region and underpredicts the heat transfer in the entry region by about 10%. This could be due to the fashion the insert B is bent at the tube wall as shown in Figure 2.42.

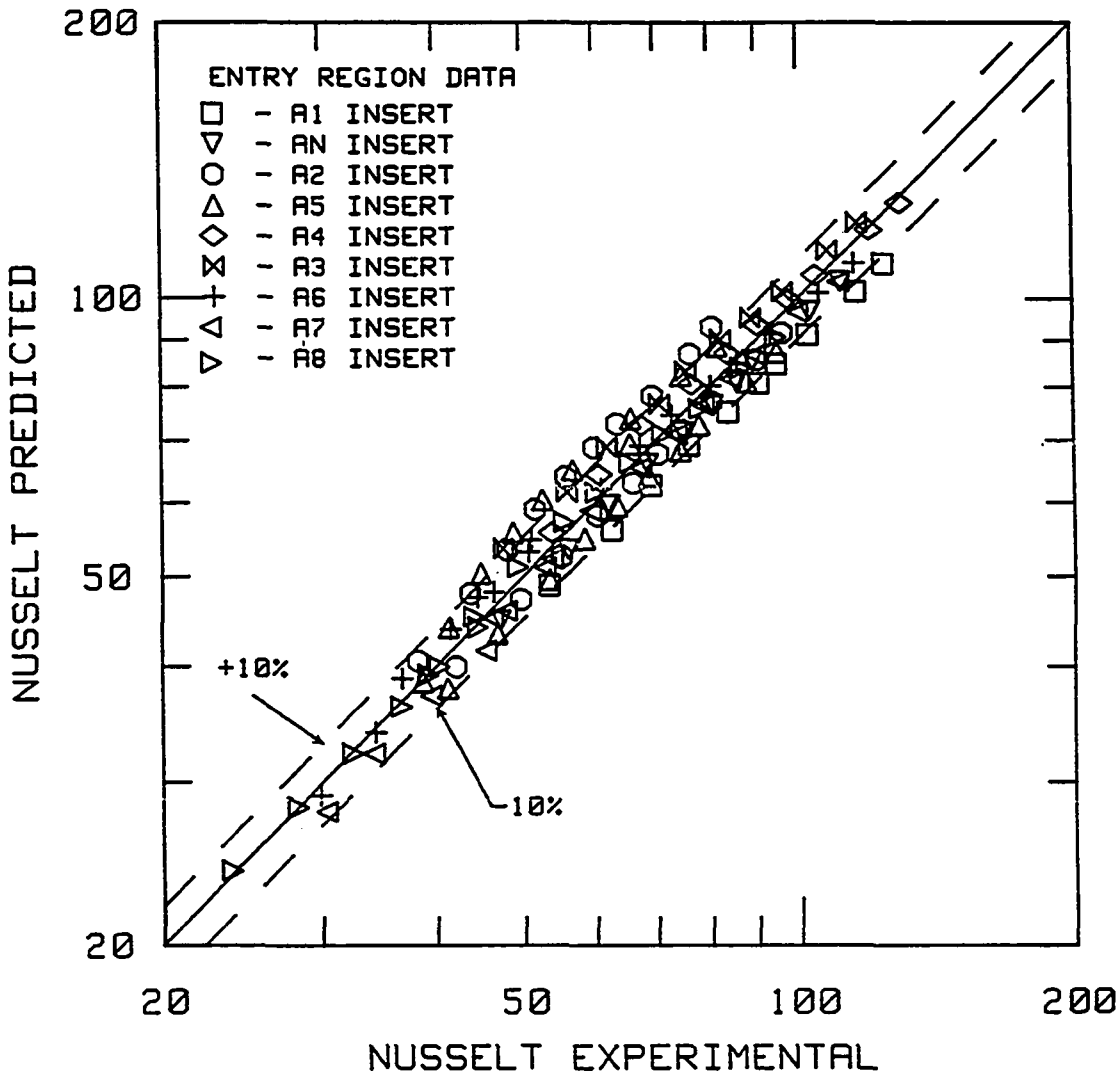

FIGURE 2.39. Predicted data for the entry region Nusselt number (Equation 2.15) compared with the experimental data for 9 inserts

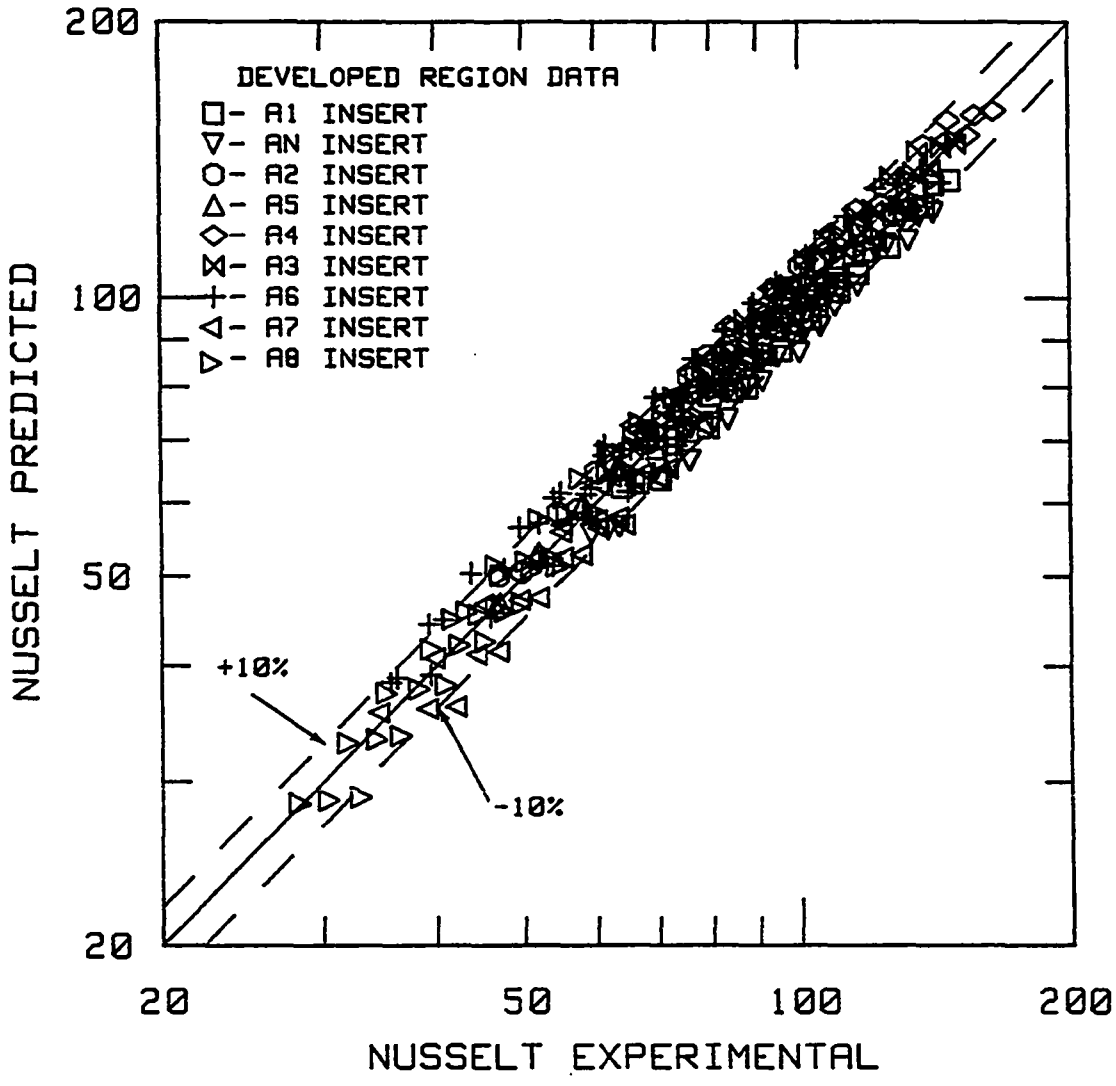

FIGURE 2.40. Predicted data for the developed region Nusselt number (Equation 2.15) compared with the experimental data for 9 inserts

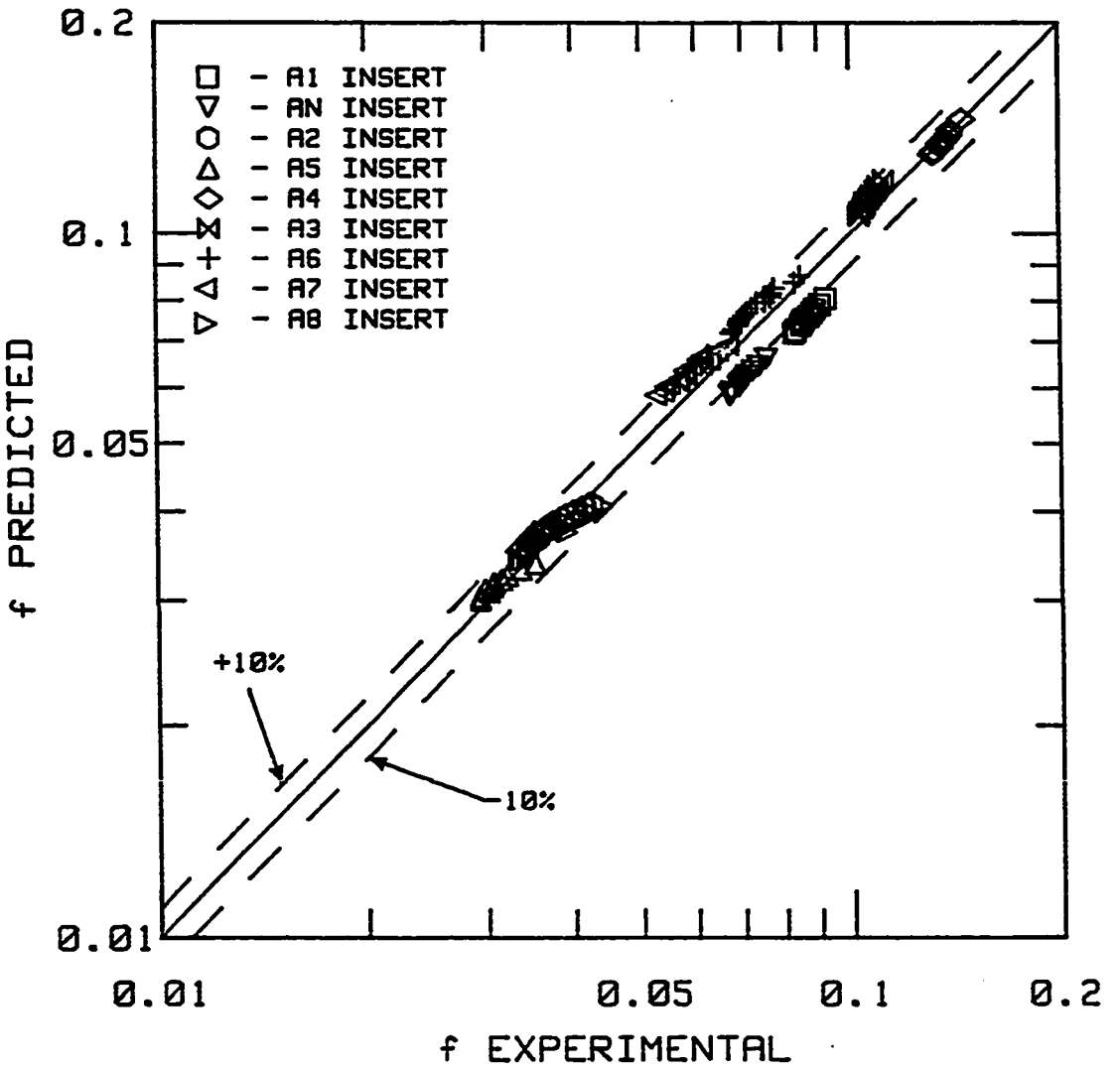

FIGURE 2.41. Predicted friction-factor data (Equation 2.16) compared with the experimental data for 9 inserts

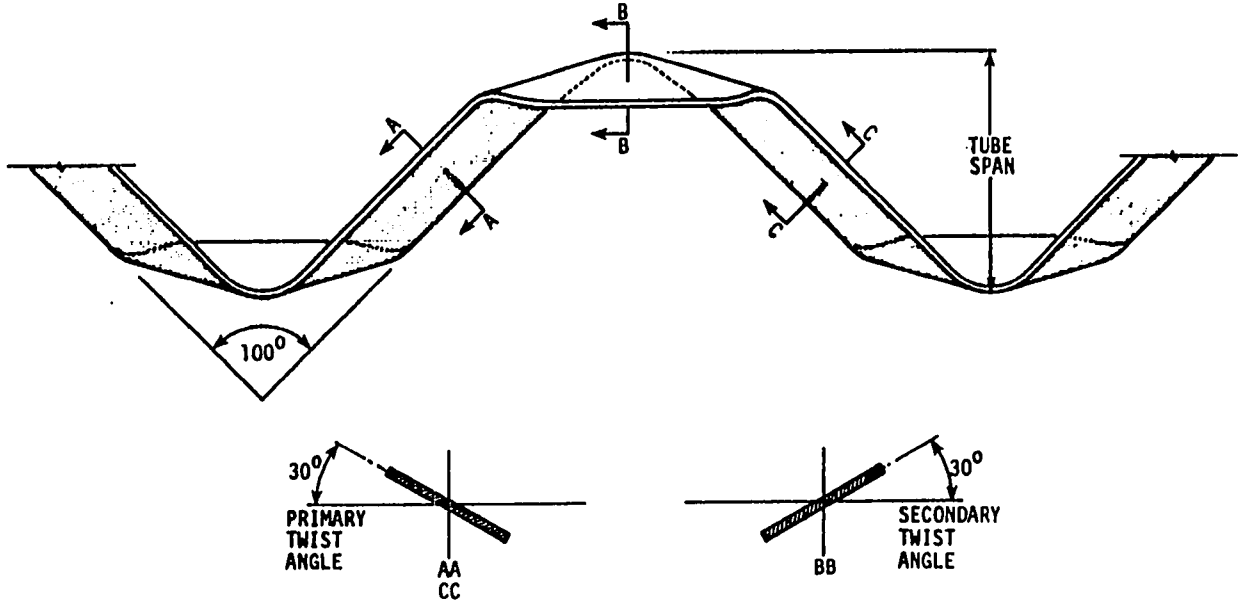

FIGURE 2.42. Geometry of insert B tested by Junkhan et al. (1985)

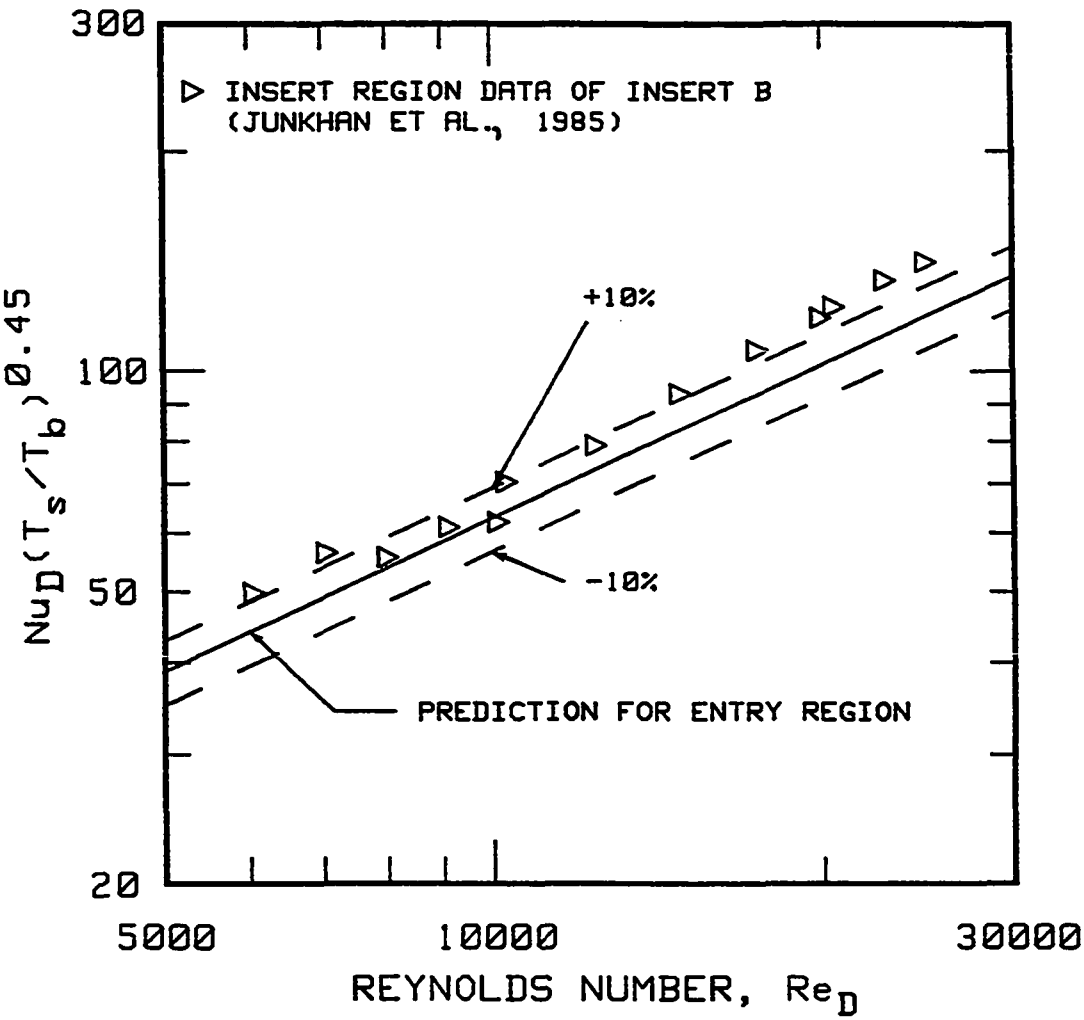

FIGURE 2.43. Insert B entry region heat-transfer data compared with prediction

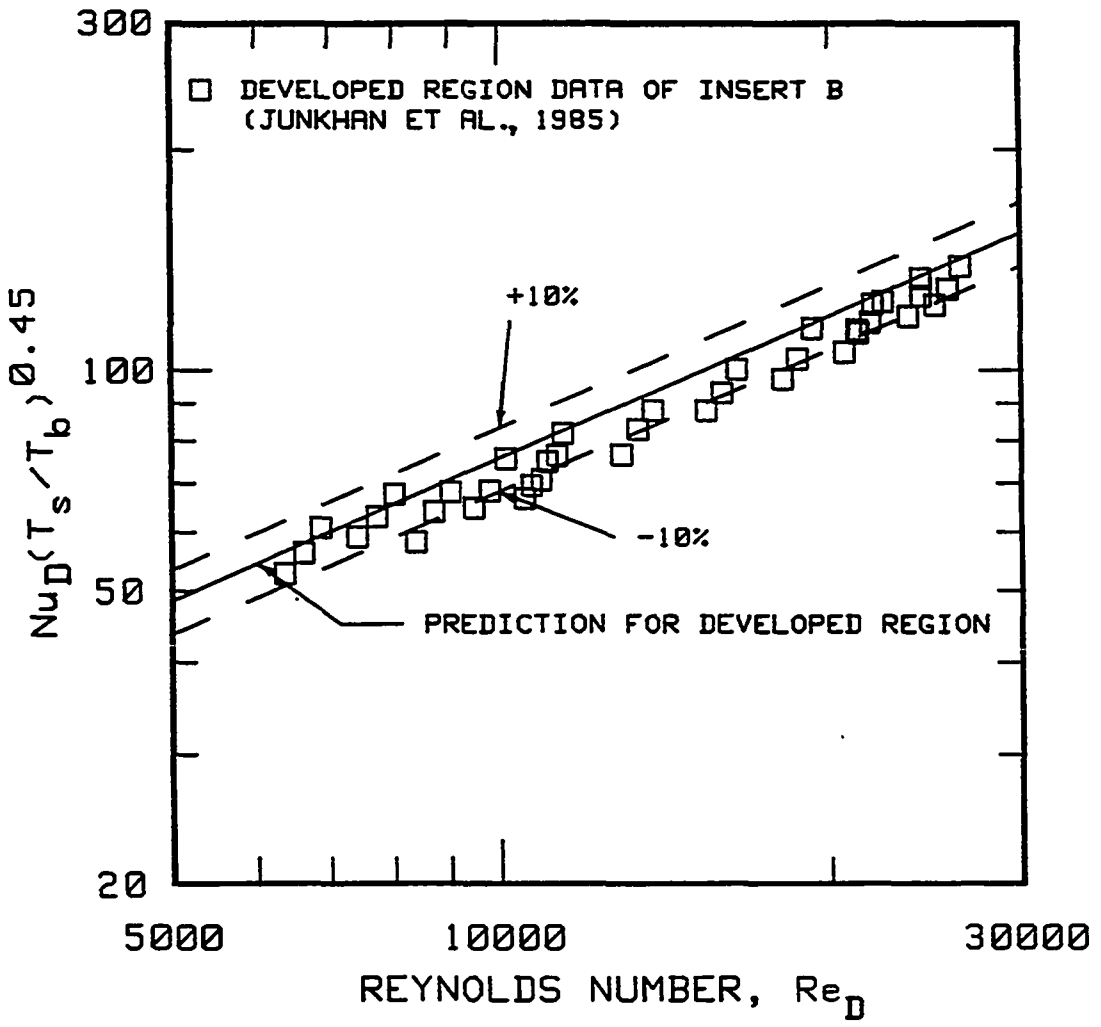

FIGURE 2.44. Insert B developed region heat-transfer data compared with prediction

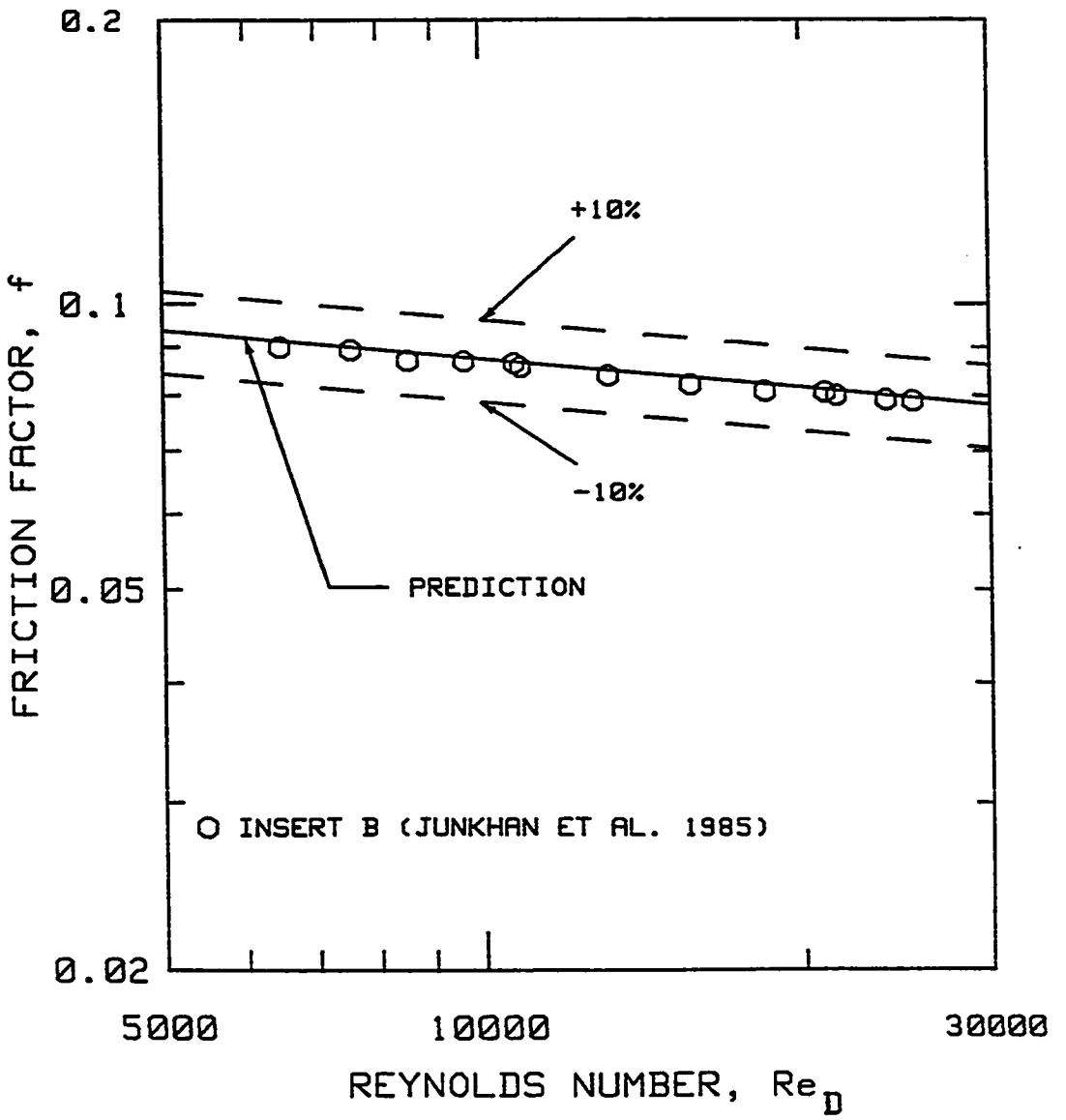

FIGURE 2.45. Insert B friction data compared with prediction

2. Performance evaluation

The results presented earlier show that bent-strip inserts augment heat transfer as much as 200% or more. However, the pressure-drop increase accompanying the enhancement in heat transfer is considerably higher. Figures 2.46 and 2.47 show the trends of heat-transfer enhancement and the increase in pressure drop with the variation in width and pitch of the insert. In these figures, the reference Nusselt number, Nu_s, is obtained by using the Gnielinski correlation at the same Reynolds number and a Prandtl number of 0.7. Figure 2.46, for a constant $Re_D = 10000$ and $L/D_i = 4.0$, shows a very steep increase in the friction factor but only a marginal increase in heat transfer as the width-to-tube-diameter ratio increases. Figure 2.47, again drawn at a constant $Re_D = 10000$ and $W/D_i = 0.4$, shows a drastic increase in the friction factor and a marginal increase in heat transfer as the pitch-to-diameter ratio is reduced. At first glance, these results indicate that using bent-strip inserts may not be considered practical. However, to actually evaluate and compare the performance of the bent-strip inserts, one must use one or more performance evaluation criteria (PEC) as described by Bergles et al. (1974).

Two performance evaluation criteria are applicable in enhancing convective heat transfer from hot gases in tubes using bent-strip inserts. They are:

1. Increasing heat duty with the basic geometry and pressure drop fixed (R_2) and

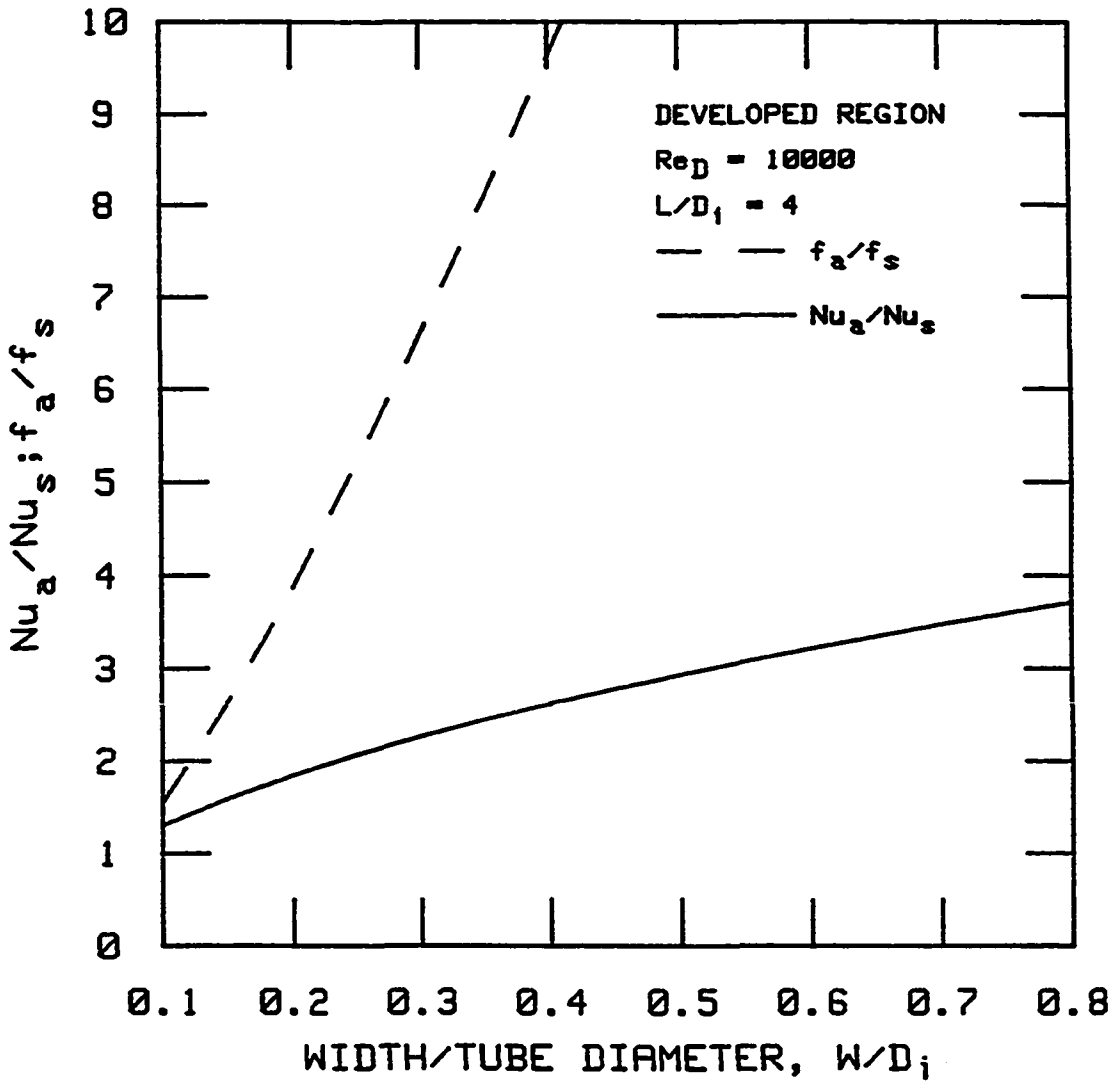

FIGURE 2.46. Predicted heat-transfer and friction-factor enhancement as a function of width-to-tube-diameter ratio

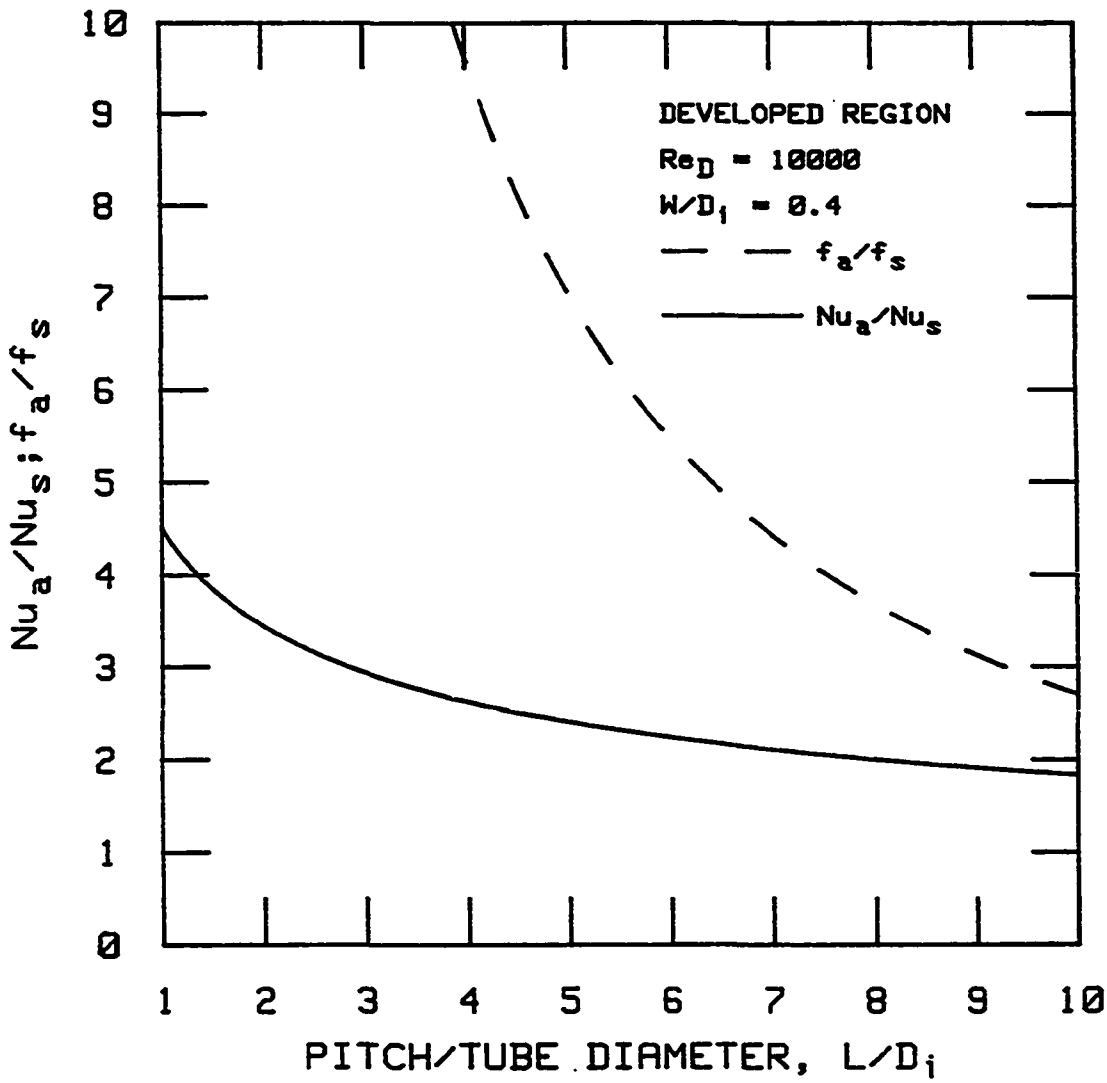

FIGURE 2.47. Predicted heat-transfer and friction-factor enhancement as a function of pitch-to-tube-diameter ratio

2. Increasing heat duty with the the basic geometry and pumping power constant (R_3).

The notations for the criteria are the same used by Bergles et al. (1974). In the case of fire-tube boiler applications, improved efficiency is attained by reducing stack temperature and increasing heat duty without having a very drastic increase in pressure drop (Yaverbaum, 1979). Therefore, R_2 would be more appropriate in fire-tube boiler applications. In forced draft systems, the criterion R_3 would be more appropriate.

The criterion R_2, defined as the increase in heat duty for constant pressure drop and basic geometry, can be written as

$$R_2 = \left[\frac{h_a}{h_o}\right]_{(\Delta p, \Delta T, L_t, D_i, N, T_{ai})} = \frac{q_a}{q_o} = \frac{Nu_a}{Nu_o} \tag{2.17}$$

The pressure drop is

$$\Delta p = 4f\ (L/D_i)\ \rho_a\ u_m^2/2 = \text{constant} \tag{2.18}$$

which becomes

$$f_a\ Re_a^2 = f_o\ Re_o^2 \tag{2.19}$$

as the constraint for PEC R_2.

For a given Re_a and insert geometry, f_a was calculated by using the empirical correlation (Equation 2.14) developed in the previous section. The Filonenko (1954) correlation

$$f_o = [\ 1.58\ \ell n(Re_D) - 3.28\ ]^{-2} \qquad (2.14)$$

was used in Equation 2.19 to obtain an equivalent Re_o. A trial-and-error method was necessary to solve for the Re_o that satisfies the constraint Equation 2.19.

The equivalent Nu_o was obtained using the Gnielinski (1976) correlation

$$Nu_o \left(\frac{T_s}{T_b}\right)^{0.45} = \frac{(f/2)(Re_D - 1000)Pr}{1 + 12.7\sqrt{(f/2)(Pr^{2/3} - 1)}} \qquad (2.13)$$

with Pr = 0.7. Finally, PEC R_2 was evaluated by obtaining the ratio Nu_a/Nu_o. Nu_a was calculated by using the empirical correlation (Equation 2.15) developed earlier for the given Re_a and insert geometry.

The R_3 performance evaluation criterion, which is defined as the ratio of heat duty under constant pumping power and geometry conditions, is

$$R_3 = \left[\frac{h_a}{h_o}\right](P,\Delta T,L_t,D_i,N,T_{ai}) = \frac{q_a}{q_o} = \frac{Nu_a}{Nu_o} \qquad (2.20)$$

Pumping power is given by

$$P = N u_m A_x\ 4f\ (L/D_i)\ \rho_a\ u_m^2/2 = \text{constant} \qquad (2.21)$$

which becomes

$$A_x\ f_a\ Re_a^3 = A_x\ f_o\ Re_o^3 \qquad (2.22)$$

This is the constraint equation for the R_3 criterion. The same method described earlier was used to calculate an equivalent Re_o, and Nu_a/Nu_o was evaluated for a given Re_a and insert geometry.

The performance evaluation results were obtained by using the correlations given for the developed region of the flow. Note that the PEC data are evaluated under idealized conditions where temperature changes along the tube and thermal resistance other than that of the gas-side have been disregarded; however, they demonstrate the qualitative advantages of the use of bent-strip inserts.

The optimum performance condition (flow and/or insert geometry) for the R_2 criterion was estimated by plotting PEC R_2 against Reynolds number Re_a for three different L/D_i and W/D_i ratios. For a constant $W/D_i = 0.3$, three values of L/D_i, 2.0, 4.0, and 6.0 were considered in Figure 2.48. In Figure 2.49, three values of W/D_i, 0.2, 0.3, and 0.4, were considered for a fixed value of $L/D_i = 4.0$. From both of these figures it is apparent that R_2 is strongly dependent on the Reynolds number. Also, for the constant pressure-drop criterion, the advantages of the bent-strip inserts are found only at lower Reynolds numbers. Decreasing pitch or increasing width reduces the enhancement effectiveness. Moreover, the variation in pitch seems to have a larger impact on the effectiveness than the variation in width.

To estimate the optimum performance conditions according to the constant pumping power (R_3) criterion, the variation of R_3 with Reynolds number, W/D_i, and L/D_i is plotted in Figures 2.50 and 2.51. Again, R_3

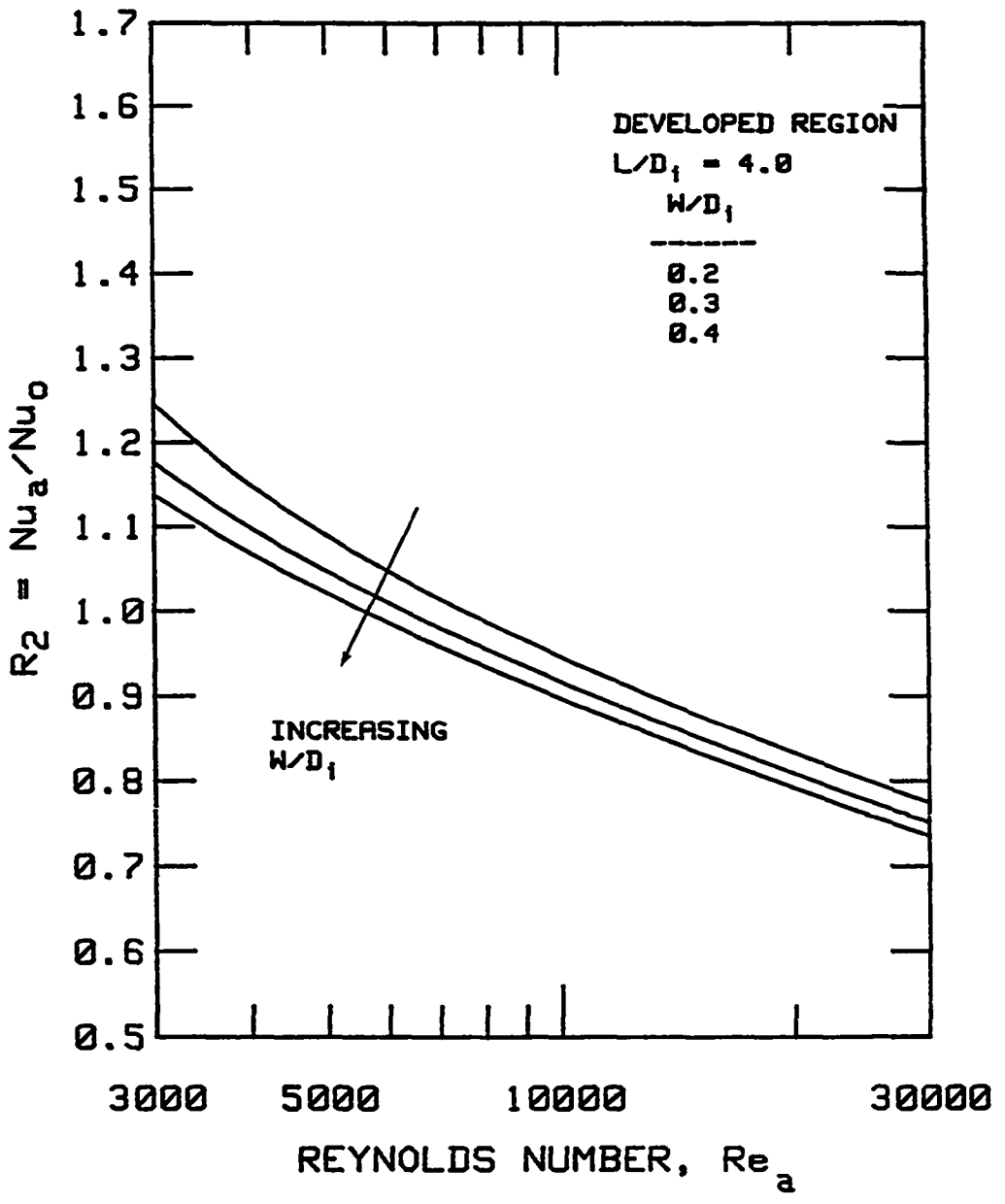

FIGURE 2.48. Effect of Reynolds number and W/D_i on R_2

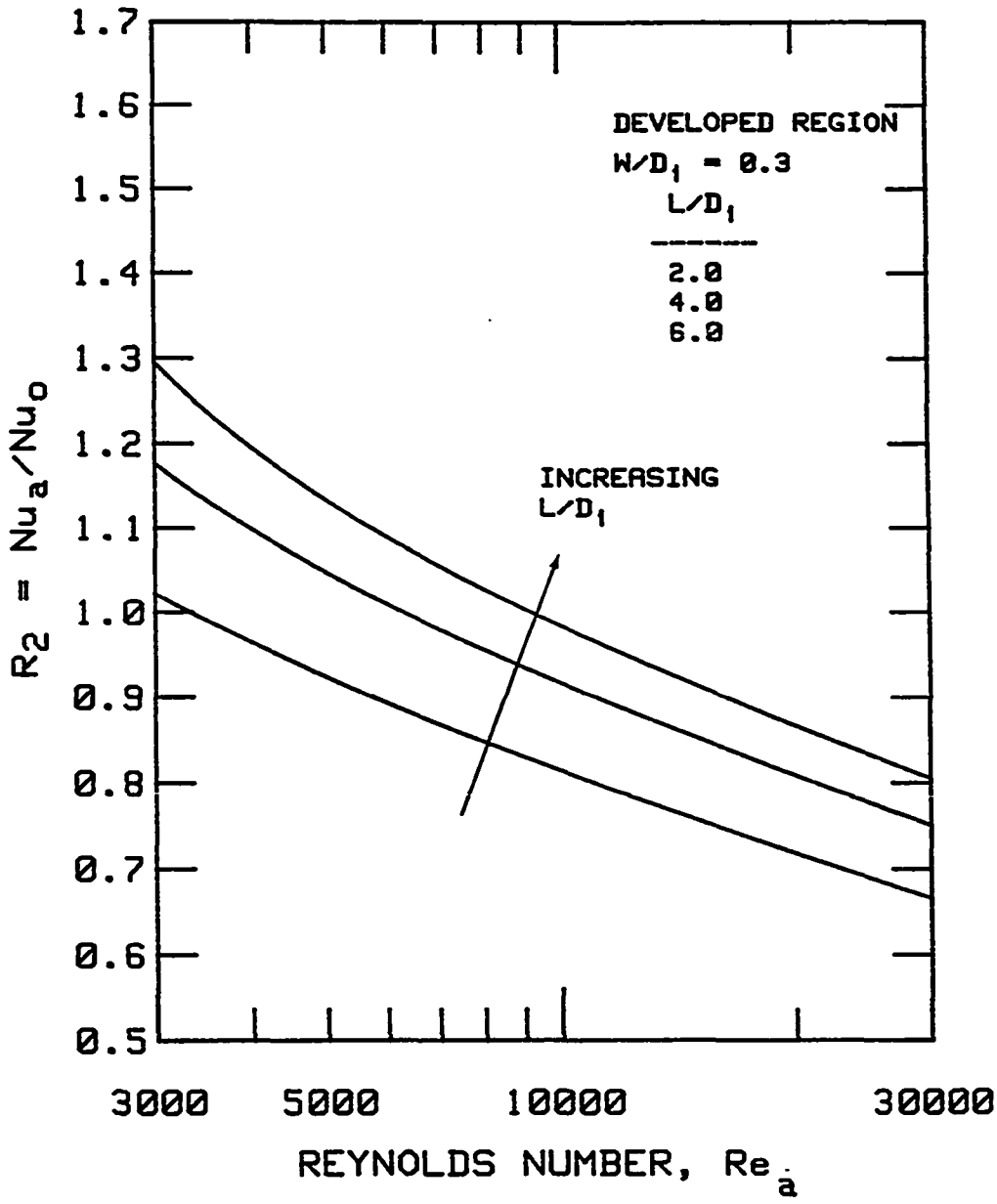

FIGURE 2.49. Effect of Reynolds number and L/D_i on R_2

shows a strong dependence on the Reynolds number, but with the use of this criterion, a much larger Reynolds number range (3000-30,000) is available for favorable applications of the bent-strip insert. Also, the enhancement effectiveness increases with increases in width; however, the variation in pitch has hardly any effect on the enhancement effectiveness.

Although the R_2 and R_3 PEC criteria yield encouraging results, the actual improvement is likely to be much lower. In the case of a computer simulation of a commercial heating boiler by Didion and Chern (1984) that used the turbulator results obtained by Junkhan et al. (1982), the results indicate that the bent-strip inserts increase the boiler seasonal efficiency by about 6%. These results are rather disappointing considering the high heat-transfer enhancement obtained in this study. One must realize, however, that in the computer simulation the inserts were placed only in 60% of the last pass due to practical limitations, and also that the majority of the heat transfer occurs in the fire box of the fire-tube boiler. Yaverbaum (1979) indicates that when inserts are used, allowances have to be made to ensure sufficient air flow for complete combustion. Yaverbaum also indicates that after inserts are installed in boilers, the burner control needs to be readjusted to obtain optimum efficiency.

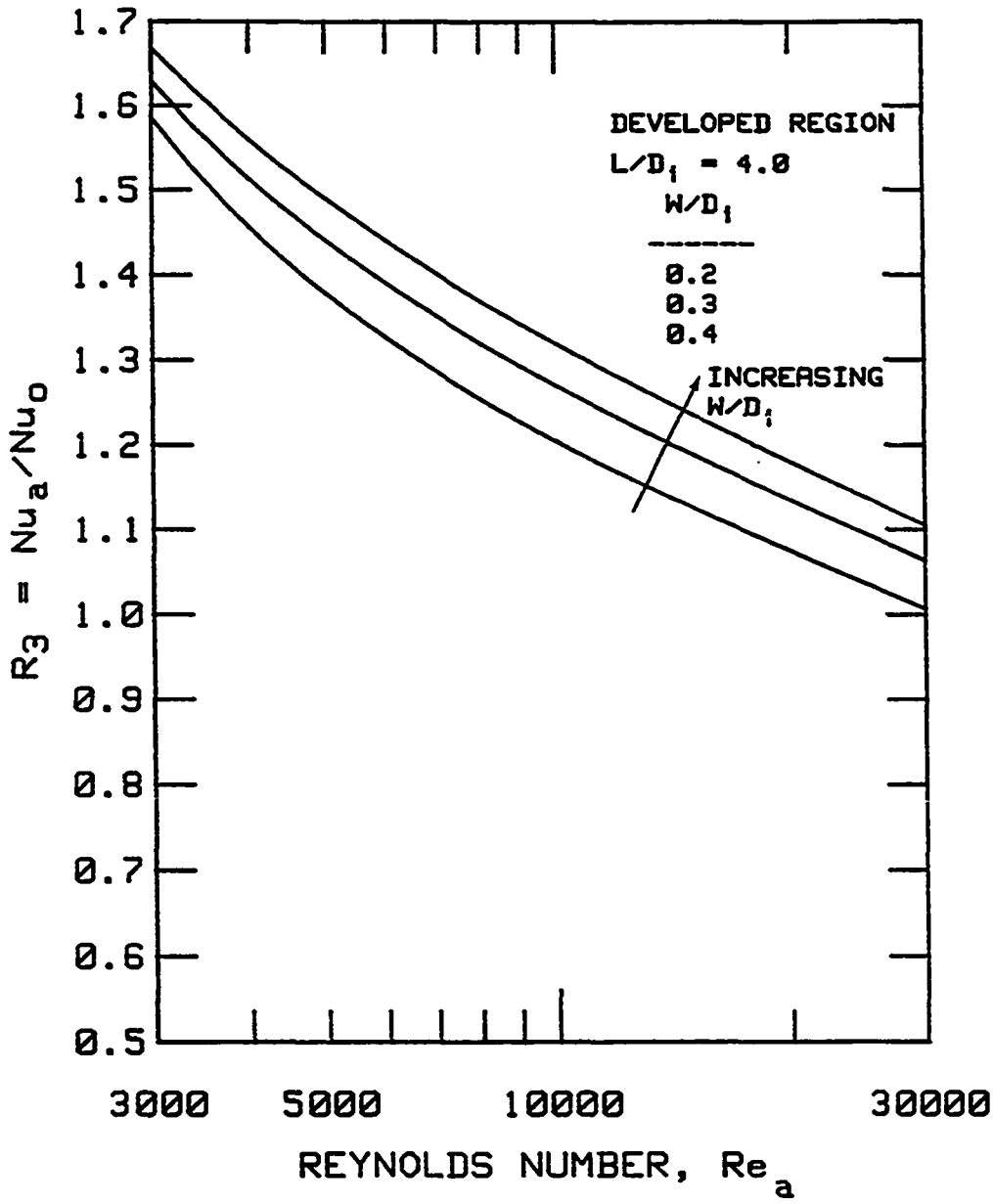

FIGURE 2.50. Effect of Reynolds number and W/D_i on R_3

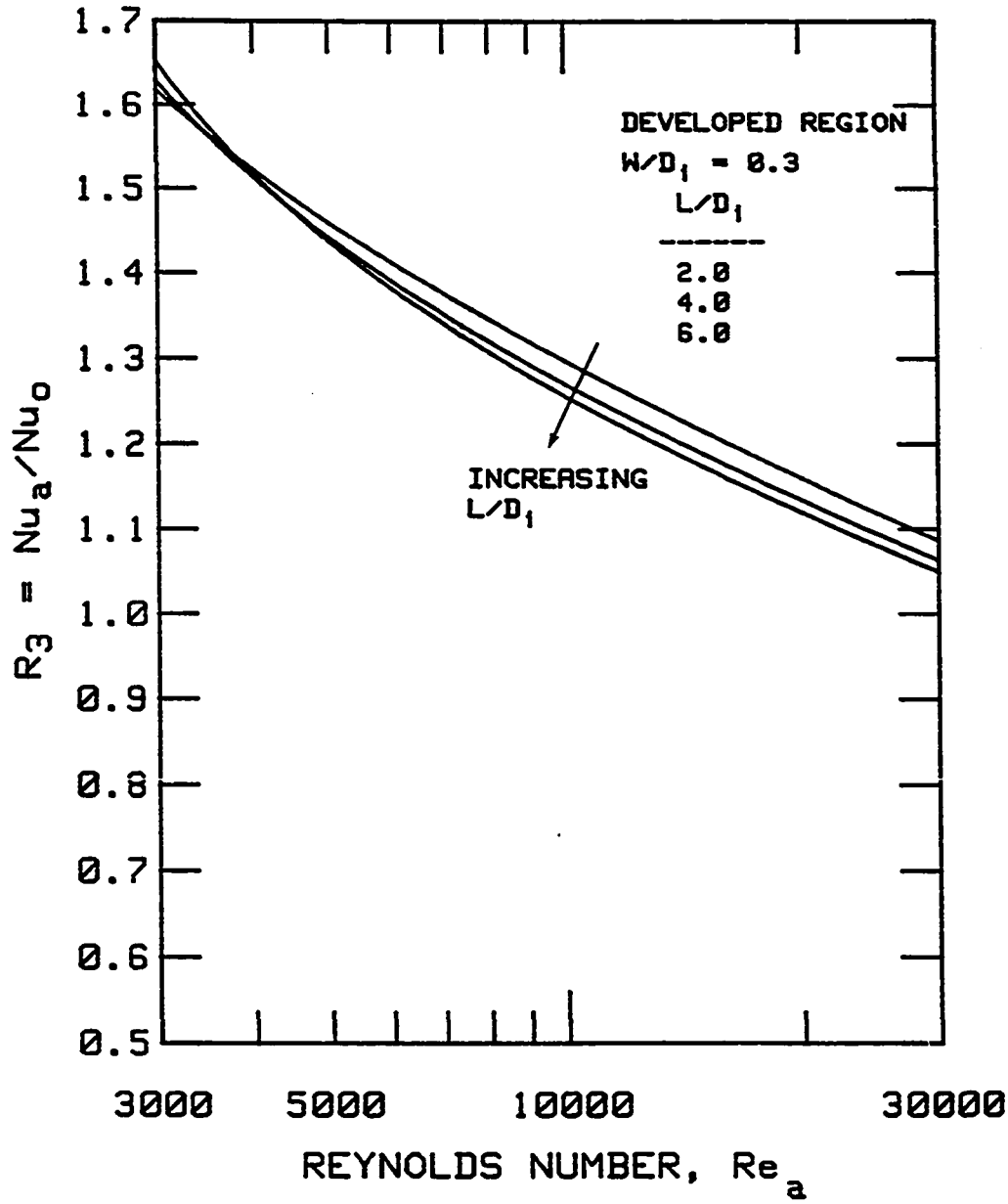

FIGURE 2.51. Effect of Reynolds number and L/D_i on R_3

III. FLOW VISUALIZATION

A. General

Flow visualization is considered one of the most effective methods to study and comprehend the basic physical nature of any flow condition. To better understand the enhancement mechanism and to study the flow patterns created by the bent-strip insert, two techniques of flow visualization were used. One technique consisted of injecting a colored dye in water flowing in a test apparatus and of photographing the dye motion (Merzkirch, 1974; Yang, 1977). The other technique was based on the observation of flow patterns on the wall of a plastic tube. The patterns of fluid flow adjacent to the tube wall were made visible by coating the wall with an oil/lamp-black mixture and using air as the working fluid (Tien, 1978; Tien and Sparrow, 1979; Motwani, 1984).

B. Flow Visualization Experiments

1. Water/dye-injection technique

The apparatus to view the dye motion in water flow consisted of a constant-head water tank which fed water through a smooth nozzle into a 5 ft long, 0.75-in. diameter clear plastic tube, as shown in Figure 3.1. The tank was divided into two sections by a wall of ceramic spheres, which acted as a baffle. The baffle assured an undisturbed water supply to the plastic tube. It was possible to obtain a Re_D range of 100 to 3000 by varying the flow rate using the needle valve at the exit. The flow rate was determined using a weigh tank.

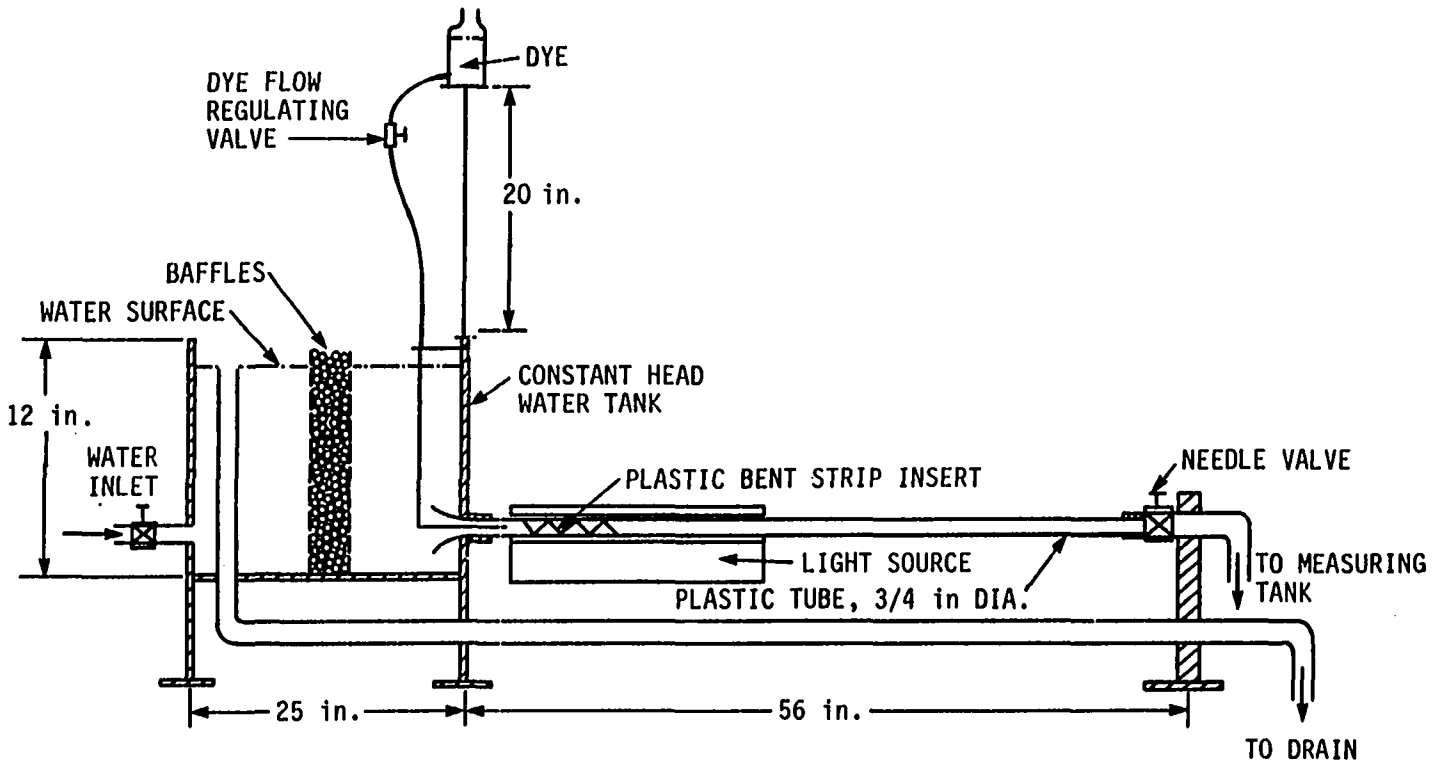

FIGURE 3.1. Water/dye flow visualization setup

A bent-strip insert similar to Figure 2.9 was made of plastic to fit the tube. The dye, a mixture of concentrated food coloring powder and water, was fed into the water by gravity with the flow rate adjusted by a restrictor to match the dye and water velocities. The dye was inserted by means of hypodermic needle tubing near the center of the tube upstream of the insert and at the wall. When fed at the wall, the dye was inserted either at the side facing the viewer or at the top. In some experiments, two different color dyes were used in water to study the flow in the center of the tube and at the wall simultaneously. Still photographs of the flow pattern were taken with a camera focused on the area of interest in the tube and with a fluorescent tube as a light source. Photographs were taken with 400 ASA color print film at shutter speeds ranging from 1/125 to 1/1000 second. Photographs could be obtained in either a vertical or horizontal plane. In order to study variations in the flow patterns as a function of time, the dye motions were videotaped with a portable Panasonic video cassette recorder. The videotape could be played back at a slower speed or stopped to look at single frame snapshots.

2. Oil/lamp-black technique

Visualization of the flow patterns adjacent to the wall was also accomplished by using the oil/lamp-black technique. The heat transfer experimental setup described in Chapter II was used with some modifications. Initially, the calorimeter test section was removed and replaced with a 2.70-in. diameter hard glass tube, and unheated air was

used as the working fluid. The flow-visualization technique consisted of evenly coating half the inside of the glass tube with a thin film of a mixture of oil and lamp black. Although, several types of oil with various weight ratios of oil to lamp black were tried, the best results were obtained with a rust removing oil in a weight ratio of oil to lamp black of about 4:1. The excess oil/lamp black was removed once the surface had been evenly coated. The assembly was immediately installed in the flow system, the blower was started, and the air was allowed to flow through the tube for about 20 minutes. Re_D was adjusted to about 25,000. Under the action of the shear stress exerted by the air on the tube wall, the mixture is made to flow along the wall in the flow direction. The resulting black and white pattern of streaks represent the average flow field near the surface. In a stagnation region, the oil and lamp black mixture remains as it was initially applied, while a region clear of the mixture indicates a region of high shear stress. The flow patterns thus formed on the glass were photographed.

To enhance the photographic results, the author used a different scheme. In this case, a 2.75 in. i.d. plastic tube was used instead of the glass tube. A second, slightly smaller diameter plastic tube, 2.5 in. i.d. by 2.75 in. o.d. and 5 ft in length, was split longitudinally into two halves. White, plasticized adhesive paper was secured to the inner surfaces of the two halves. First, the insert was placed between the two half tubes which were then reassembled and inserted in the 2.75 in. i.d. plastic tube. Next, the inner white

surface of the reassembled two halves was coated with a mixture of oil and lamp-black. Finally, the entire assembly was installed in the flow system. The air was allowed to flow through the test section for about 20 minutes. The assembly was then taken out of the flow system, and the split halves were removed from the outer tube so that photographs could be taken of the flow patterns formed on the white contact paper. Black and white 400 ASA film was used to photograph these patterns.

C. Observations of Flow Phenomena

Figure 3.2(a) shows one of the photographs obtained from the dye-injection apparatus with the camera lens axis in a horizontal plane and with dye injection in the center of the tube. The flow pattern in Figure 3.2(a) shows that the core flow at a Reynolds number of 1667 begins to be substantially mixed at the core of the tube within two insert pitch lengths.

Figure 3.2(b) shows the flow patterns when the dye is inserted at the wall with the same camera orientation and at a Reynolds number of 1667. Note that the wall flow does not appear to be affected to a great extent by the bent-strip insert at this Reynolds number. This observation is somewhat contradictory to the thermal-hydraulic results obtained by using the separate core and wall region inserts. The core-region insert tests indicate that the core region of the insert disturbs the wall flow even more than the wall region insert. Figure 3.2(c) shows a view obtained with the camera lens axis in a vertical plane with

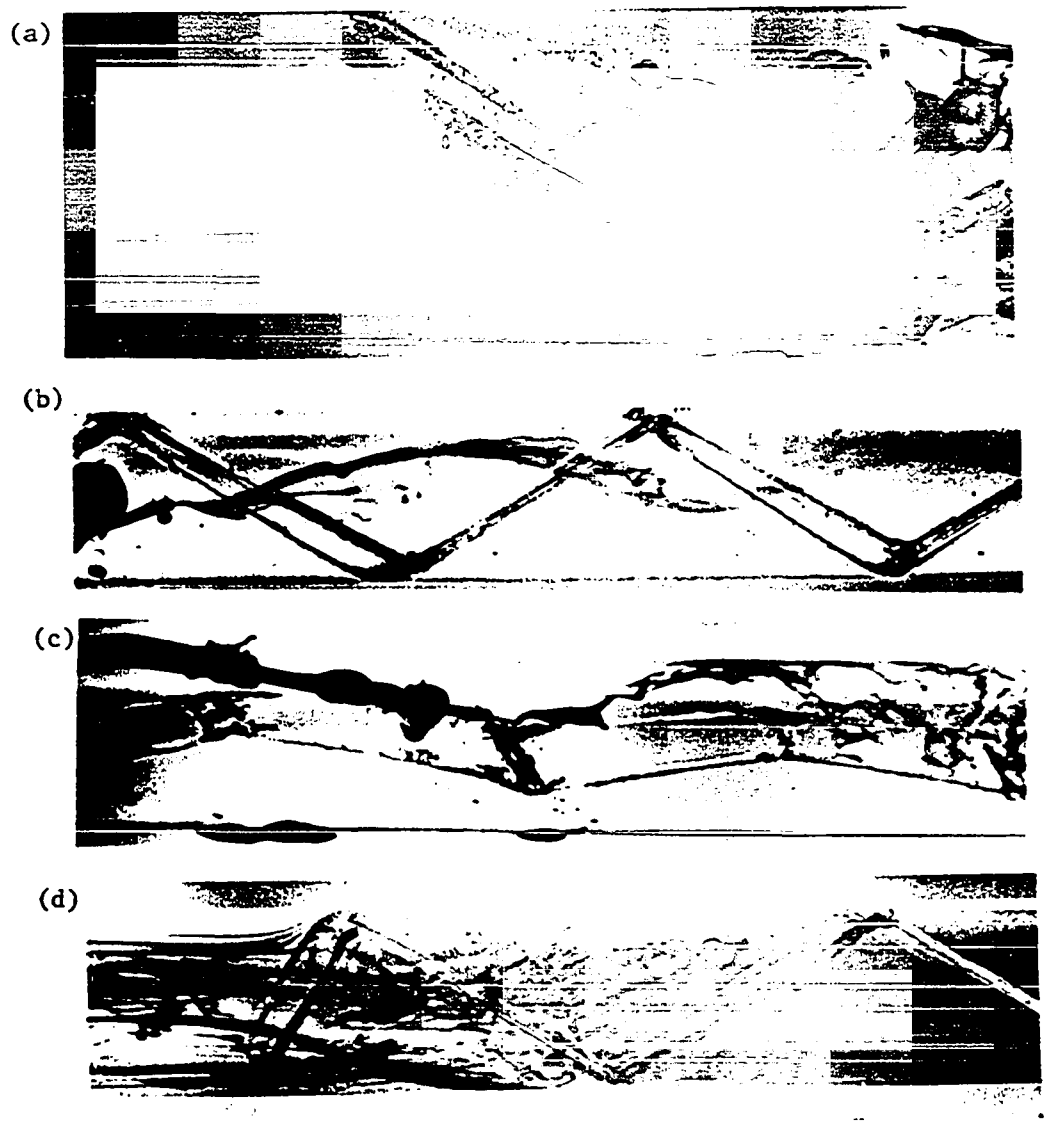

FIGURE 3.2. Flow patterns obtained by using the water/dye-injection flow visualization technique. $Re_D = 1667$

the dye injection from the top, and with the strip in the vertical orientation. Here, the wall layer at the top gets disturbed by the bluff-body-like flow downstream of the strip where it is in contact with the tube wall.

Simultaneous insertion of two colors of dye in Figure 3.2(d) shows these flow patterns at the same time. In this case, the camera lens axis was in the horizontal plane. The blue dye was inserted at the center of the tube ahead of the insert while the red dye was inserted at the wall just ahead of the insert. The blue dye at the center was fully mixed almost immediately because of the insert while the red dye required about two pitch diameters from the beginning of the insert to mix with the core. This suggests that an entrance effect exists and that the earlier assumption of the flow being fully developed by the end of the first segment (1-2 pitch lengths) in the heat-transfer/pressure-drop experiment is valid.

As mentioned before, the flow patterns obtained by the dye injection technique were videotaped. Some observations that could not be photographed but that are seen by re-playing the videotape include:

- The flow at the wall spirals along the surface, indicating the presence of secondary swirl flow.
- The flow at the wall and the flow at the core do not mix as rapidly as anticipated in 1-2 pitch lengths.
- By injecting the dye at the wall upstream of the insert, it is seen that the bent-strip insert affects the wall layer after a

length of 1-2 insert pitches. This indicates the presence of a developing length.

- At high turbulent core velocities the wall layer remains comparatively unmixed and very laminar at locations upstream of the insert. However, at the same flow rate and in the presence of the insert, the sublayer at the wall appears to very turbulent and chaotic. This behavior is also observed away from the insert contact with the tube wall.
- It is possible to see streaks of dye from the wall layer being lifted away into the core region at random intervals. The frequency of lifting appears to increase at higher velocities.

Figures 3.3, 3.4, 3.5, and 3.6 show the flow patterns obtained by using the oil/lamp-black technique with the glass tube. These flow patterns are at the wall around the point of contact between the tube wall and the bent-strip insert. In all four figures, the plane passing through the center of the insert is in the vertical orientation. Figures 3.3 and 3.5 were photographed in the horizontal direction through the uncoated side of the glass tube. Figures 3.4 and 3.6 shows the same view as Figures 3.3 and 3.5 from below the glass tube.

Figures 3.7(a), 3.7(b), and 3.7(c) are flow patterns obtained at a Reynolds number of 25,000 by using the oil/lamp-black technique. They show, respectively, the first contact point between the wall and the insert, the space between the first and second contact points, and the

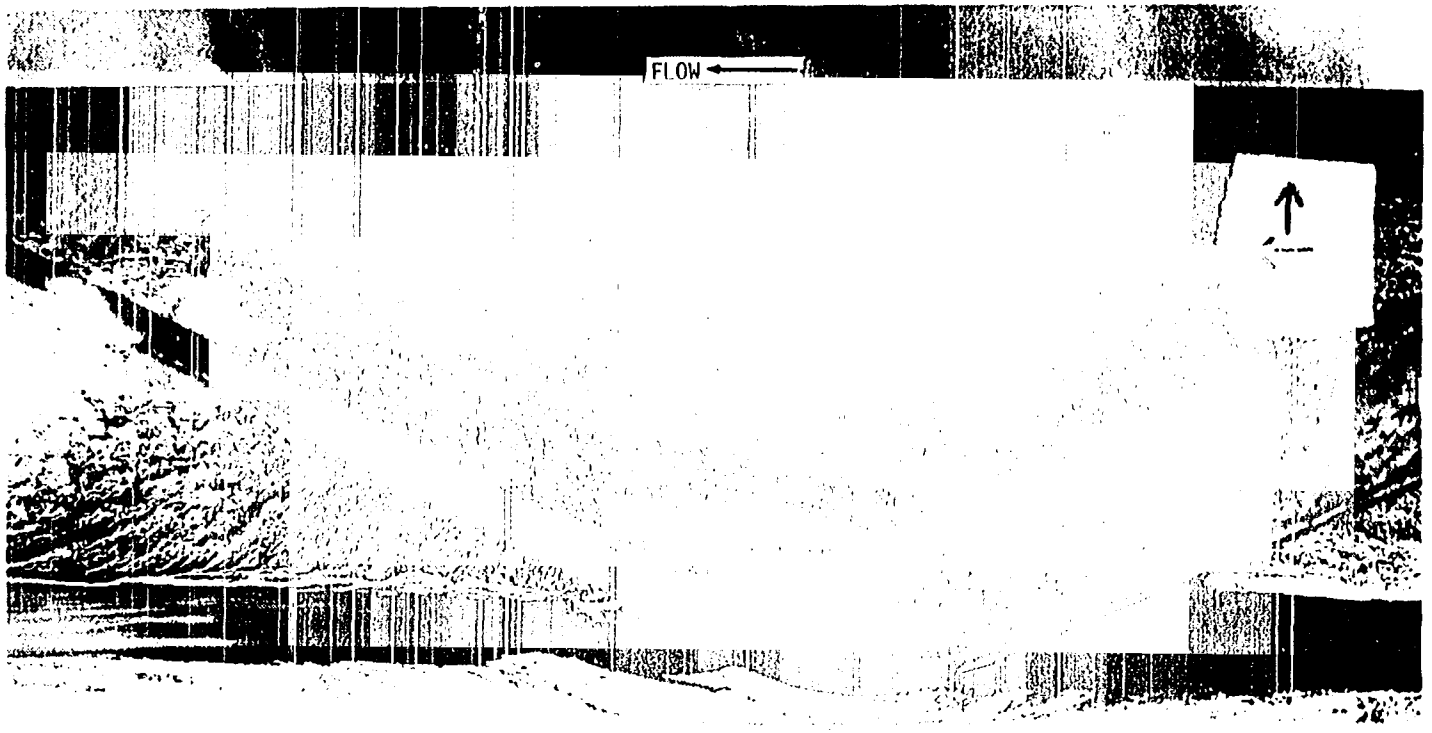

FIGURE 3.3. Flow patterns obtained by using the oil/lamp-black technique with the glass tube. Photographed from the front

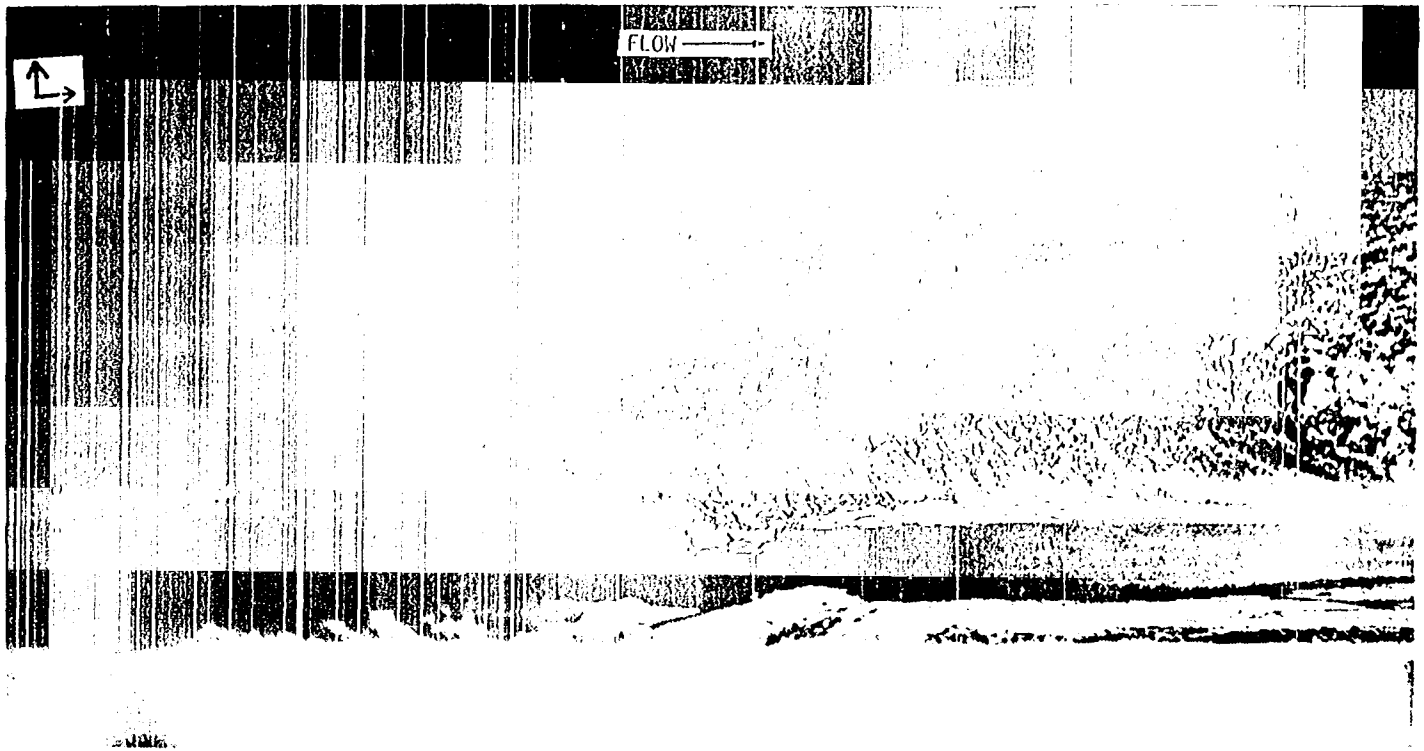

FIGURE 3.4. Flow patterns obtained by using the oil/lamp-black technique with the glass tube. Photographed from under the tube

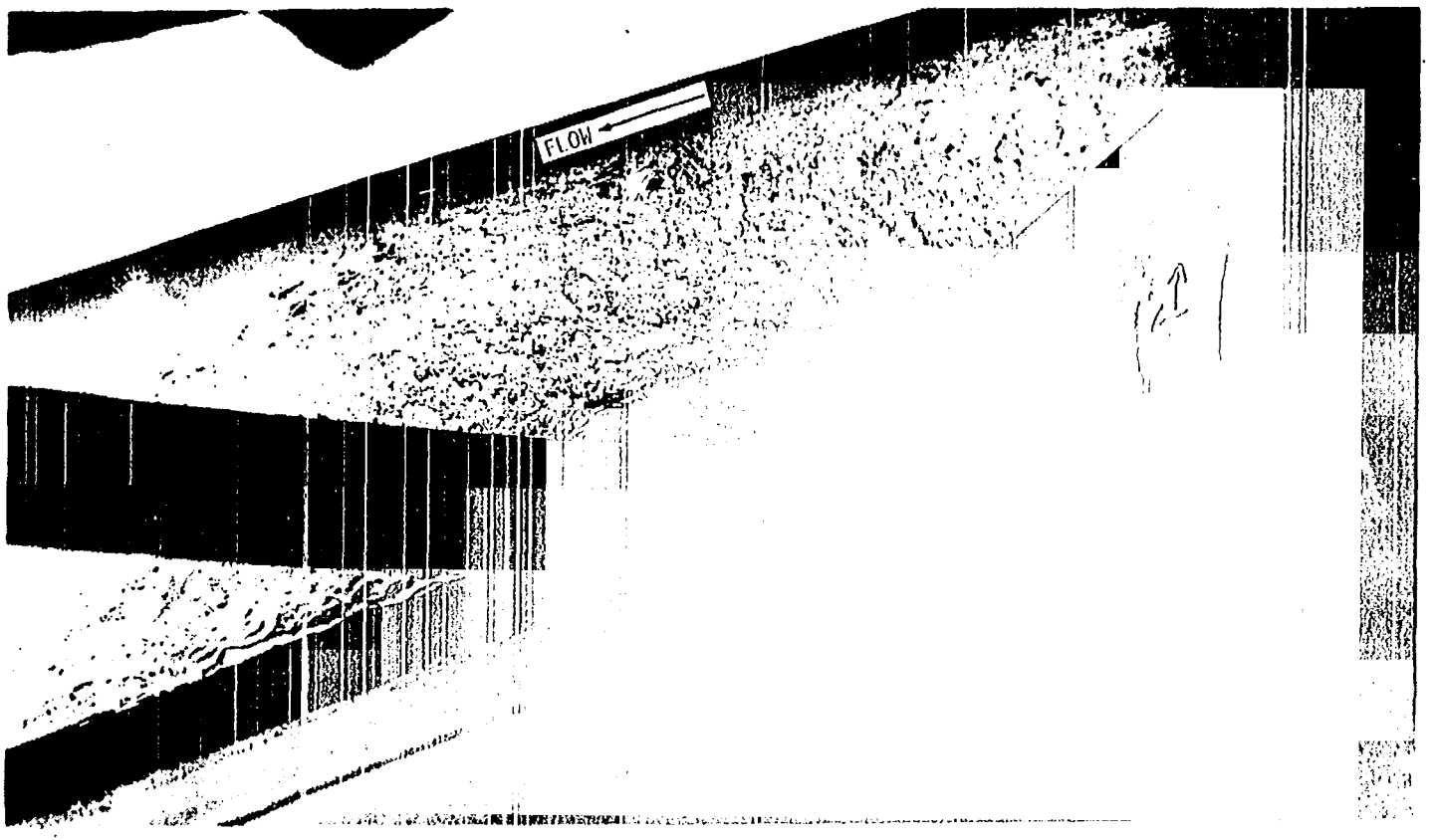

FIGURE 3.5. Flow patterns obtained by using the oil/lamp-black technique with the glass tube. Photographed from the front

FIGURE 3.6. Flow patterns obtained by using the oil/lamp-black technique with the glass tube. Photographed from under the tube

second contact point of the insert and the tube wall. The tube center line and the approximate location of the contact points of the tube wall and the insert--noted by the white rectangle--have been marked on the figures. Note that the insert touches the tube wall only at the two extremities and that there is thin gap between the insert and the tube wall at the contact area.

The photographs in Figures 3.3 through 3.7 show that most flow disturbance patterns occur near the contact points of the bent-strip turbulator and the tube wall. Since the flow patterns are caused by shear stresses at the wall, the patterns indicate that the shear stresses near the contact points of the inserts and the tube are much higher than at other regions of the wall. The flow patterns also indicate that the flow at the wall gets turned in the direction of the twist of the insert and that the effect of the insert appears at a distance of about 30% of pitch upstream of the contact point. After the contact point, the flow returns back to its original axial position within a downstream distance of about 15% of pitch. In the radial direction, the insert is seen to affect the flow pattern to about 30° from the plane of the insert. Further, it can be observed that between the two contact points, the flow at the wall is not greatly affected by the tape. That is, the flow on one side of the wall does not "feel" the effects of the insert contacting the wall on the diametrically opposite side.

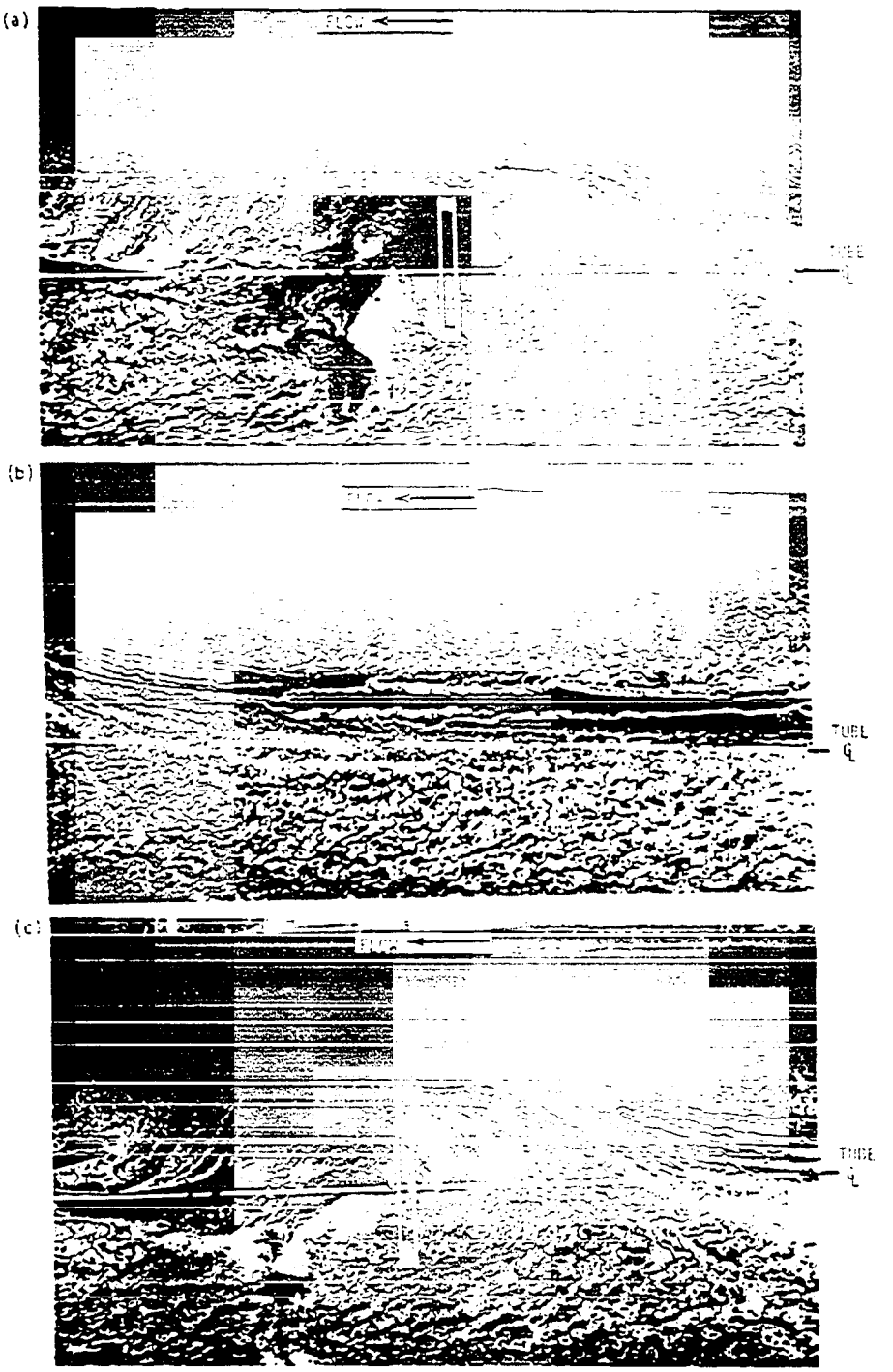

FIGURE 3.7. Flow patterns obtained by using the oil/lamp-black technique with the split plastic tube

In conclusion, both flow visualization techniques show that the flow at the wall is affected most where the bent strip insert comes in contact with the tube wall. Nevertheless from the water/dye-injection technique, it appears that in the regions where the bent strip does not touch the tube wall, the wall sublayer tends to be turbulent and very choppy. Also, mixing of the core and wall regions seems to occur when the sublayer gets ejected into the core region. The observation of the streaks of dye being ejected from the wall into the core region underscores the possibility of using a surface renewal/penetration theory to model the heat-transfer process when it is enhanced by bent-strip inserts.

IV. SURFACE RENEWAL/PENETRATION MODEL OF HEAT TRANSFER

A. Background

The surface renewal/penetration model has been applied to a wide variety of transport problems. Applications include mass transfer across a liquid-gas interface (Higbie, 1935; Danckwerts, 1951), mass transfer across a solid-fluid interface (Hanratty, 1956; Toor and Marchello, 1958; Harriot, 1962; Pinczewski and Sideman, 1974), heat transfer between a surface and a turbulent fluid (Toor and Marchello, 1958; Thomas, 1970a; Thomas and Fan, 1971; Thomas, 1982; Ibrahim and Thomas, 1983), heat transfer in a fluidized bed (Chung et al., 1972), boiling heat transfer (Han and Griffith, 1965; Mikic and Rohsenow, 1969), scraped surface heat transfer (Harriot, 1958; Azoory and Bott, 1970; Hagge and Junkhan, 1975) and condensation heat transfer in a tube with a static mixer (Fan et al., 1978). Most of the above authors have had reasonable success in using the surface renewal/penetration theory to model the heat transfer. In at least one case, pressure drop has also been modelled (Meek and Baer, 1970).

B. Turbulence Burst Phenomena

The turbulent structure near a surface has been an area of active research for a long time. Early experimental studies of Kline et al. (1967), Popovich and Hummel (1967), and Corino and Brodkey (1969) have indicated that flow very near the wall (i.e., in the wall sublayer) is not laminar but is disturbed by small velocity fluctuations.

Kline et al. (1967), using the dye-injection and hydrogen-bubble flow-visualization techniques, have shown that the turbulent structure in the near wall region exhibits recognizable and reproducible patterns--lately known as "coherent structures"--of events. These events consist of a gradual lift up of a layer at the wall (also called "streaks") and a rapid ejection where the low-speed streaks move rapidly away from the wall. In later experiments, Kim et al. (1971) termed this ejection process as "bursting".

Corino and Brodkey (1969) reporting from visual studies of motion pictures of the trajectories of small suspended particles in the flow, substantiated the same idea as Kline et al. (1967) in a slightly different fashion. The sequence of events involved in the turbulent transfer process consists of (i) formation of a low-speed packet of fluid near the wall region; (ii) interaction of a much larger high-speed fluid with the low-speed packet of fluid (also known as "sweep") so that the low-speed packet is accelerated; (iii) a rapid ejection where the low-speed packet moves away from the wall with intense, abrupt, and chaotic movements.

Offen and Kline (1974, 1975) reiterated the work of Kline et al. (1967) and also suggested that the lifting up of the wall layer may be a result of vortex pairing that results from the interaction of the vortices of the previous burst and the lifting up streak. Visual and hot-wire anemometry studies by Head and Bandyopadhyay (1981) indicate that the boundary layer action consists of vortex loops, horseshoes, or

hairpins arrayed at a characteristic angle of approximately 45° to the wall. They also conclude that the shape of the vortices is dependent on the Reynold number. Some later experiments conducted by Falco (1982) show that the turbulent production process is closely associated with the formation and evolution of a localized flow module called a pocket flow module. Pockets form in the wall region of the turbulent boundary layer as a result of the wall interaction of vortex-ring-like eddies that originate in the outer flow.

Parallel to the flow-visualization experiments, many investigators (Rao et al., 1971; Blackwelder and Kaplan, 1976; Willmarth and Bogar, 1977; Willmarth and Sharma, 1984) have studied the turbulent structure at the wall by using hot-wire anemometry. Results of Rao et al. indicate that the mean observed frequency of bursting is related to the outer flow variables and not with the wall flow variables. Willmarth and Sharma indicate similar results where the burst frequency they measured does not depend on the Reynolds number when scaled with wall parameters. They add, however, that the burst frequency increases with the Reynolds number when scaled with outer variables.

The realities, myths, and present state of the coherent structure of turbulence are surveyed in a recent paper by Hussain (1983). Despite many differences of opinion among experimentalists regarding observed details and methods used to study the coherent structure of wall turbulence, there is considerable agreement on the basic occurrence of events such as low-speed layers and their lift up and on the high

contribution to transport properties by the ejection and sweep phases of bursting. An idealized schematic picture of the turbulent burst process is shown in Figure 4.1. Grass (1971) describes how relatively large packets of low velocity fluid adjacent to the wall surface are periodically ejected from the wall region into the turbulent core region. Satisfaction of continuity requires that the fluid ejected must be replaced by a fresh inrush of fluid from the core having the properties associated with the turbulent core. During the period of time the fluid packet is in the vicinity of the surface, transient molecular transport (or conduction in the case of heat transfer) is said to occur. This basic principle is used to develop a model of heat transfer from gases in tubes with bent-strip inserts.

C. The Surface Renewal Model

The following development of a surface renewal/penetration model for heat transfer in a tube in the presence of bent-strip inserts assumes that

1. A packet of fluid at bulk temperature, driven towards the wall by the insert action and by unsteady turbulent motion, replaces another packet of fluid and comes into contact with the wall.
2. During the contact time, heat is transferred predominantly by transient conduction from the fluid to the wall.

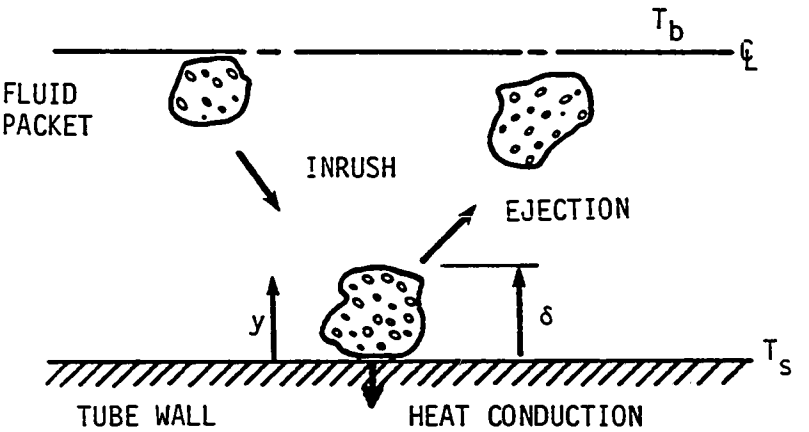

FIGURE 4.1. Turbulent burst process showing action of a fluid packet

The fluid packet remains in contact with the wall for a certain length of time before it is replaced by another packet of fluid from the core region. During this time, the following equation describes the transient conduction between the wall and the packet of fluid:

$$\frac{\partial T}{\partial t} = \alpha \frac{\partial^2 T}{\partial y^2} \tag{4.1}$$

It is realistic to assume that the temperature of the packet remains at a constant value of T_i beyond a certain characteristic length δ from the tube wall, which is the thickness of the fluid packet as shown in Figure 4.1. T_i represents the temperature of eddies at first instant of renewal. The initial and boundary conditions describing this transfer process are

$$\begin{aligned} T &= T_i \quad \text{at } t = 0 \text{ and } y > 0 \\ T &= T_s \quad \text{at } t > 0 \text{ and } y = 0 \\ T &= T_i \quad \text{at } t > 0 \text{ and } y = \delta \end{aligned} \tag{4.2}$$

The solution of Equation 4.1 subject to the conditions given by Equation 4.2 is presented in Appendix G. The final result is

$$\frac{T - T_s}{T_i - T_s} = \frac{y}{\delta} - \frac{2}{\pi} \sum_{n=1}^{\infty} \left[\frac{1}{n} \sin\left(\frac{n\pi y}{\delta}\right) \exp\left(\frac{-\alpha n^2 \pi^2}{\delta}\right) \right] \tag{4.3}$$

If $q_i(t)$ is the instantaneous heat-transfer rate at the wall at contact time t, then

$$q_i(t) = -k \left. \frac{\partial T}{\partial y} \right|_{y=0} \tag{4.4}$$

and the mean heat-transfer rate is given by the summation of the heat-transfer contribution by all the packets of fluids of different ages

$$q = \int_0^\infty q_i(t)\, P(t)\, dt \tag{4.5}$$

where P(t) is the contact-time distribution function of the fluid packets. Because of the highly mixed flow in the tube caused by the presence of the insert (observed in the flow-visualization experiments), it is reasonable to assume that the fluid packets on the surface are replaced in a completely random manner. Under this assumption, the distribution function according to Danckwerts (1951) is

$$P(t) = s \exp(-st) \tag{4.6}$$

where s is the frequency of renewal of the fluid packets.

Considering an approach very similar to that followed by Fan et al. (1978), the frequency of renewal of the fluid packets is assumed to be proportional to the number of times the fluid gets "deflected" by the insert in a given length and to the "amount" of fluid that gets deflected by the insert per unit mean residence time t_m of the fluid in the tube. The sketch of the insert in Figure 2.9 shows that the fluid gets deflected by the insert twice in one pitch L, and therefore, in a given length L_s, the fluid gets deflected $2L_s/L$ times. The proportion

of the total flow that gets deflected by the insert should be related to the fraction of the total cross-sectional area that is blocked by the projected area of the insert. This fraction is given by $[W\cos(\gamma)D]/(\pi D^2/4)$ which reduces to $4W\cos(\gamma)/\pi D$. Therefore, the frequency of renewal can be written as

$$s = C_1 \left[\left(\frac{2L_s}{L}\right)\left(\frac{4W\cos(\gamma)}{\pi D_i}\right)\left(\frac{1}{t_m}\right)\right] \tag{4.7}$$

where C_1 is a proportionality constant.

Combining Equations 4.3 to 4.6 gives the following expression (Appendix F):

$$q = -(T_s - T_i)\sqrt{(sk\rho c_p)}\coth\left(\frac{s\delta^2}{\alpha}\right)^{\frac{1}{2}} \tag{4.8}$$

For moderate Prandtl-number fluids such as air or gas, T_i may be replaced by T_b. (This is not a good assumption for low-Prandtl number fluids where the energy transfer during the flight of eddies from the bulk stream to the wall region can be significant (Thomas, 1970b).) Thus, changing T_i to T_b and converting the heat-transfer rate to heat-transfer coefficient by using the usual definitions, the following equation is obtained:

$$h = -\left(\frac{q}{T_b - T_s}\right) = -\left(\frac{q}{T_i - T_s}\right) = \sqrt{(sk\rho c_p)}\coth\left(\frac{s\delta^2}{\alpha}\right)^{\frac{1}{2}} \tag{4.9}$$

For sufficiently large values of δ,

$$\coth\left(\frac{s\delta^2}{\alpha}\right)^{\frac{1}{2}} \simeq 1 \tag{4.10}$$

This assumption reduces Equation 4.9 to

$$h = \sqrt{(sk\rho c_p)} \tag{4.11}$$

Equation 4.11 is identical to the equations developed by other users of the surface renewal/penetration model.

Substituting Equation 4.7 for s in Equation 4.11 yields

$$h = C_1 \left[\left(\frac{2L_s}{L}\right)\left(\frac{4W\cos(\gamma)}{D_i}\right)\left(\frac{k\rho c_p}{t_m}\right)\right]^{\frac{1}{2}} \tag{4.12}$$

To calculate h using the basic surface renewal model by applying Equation 4.12, the mean residence time of the fluid packets in the tube must be known. Logically, the mean residence time, t_m, of the fluid in the tube must be inversely proportional to the mean velocity, u_m, of the fluid and proportional to the length of the tube, L_s. Thus

$$t_m = C_2\left(\frac{L_s}{u_m}\right) \tag{4.13}$$

where C_2 is another proportionality constant. Substituting Equation 4.13 into Equation 4.12 and rearranging terms, the expression for the heat-transfer coefficient is obtained as

$$h = C\left[\left(\frac{8W\cos(\gamma)}{L}\right)\left(\frac{k\rho c_p u_m}{D_i}\right)\right]^{\frac{1}{2}} \tag{4.14}$$

where $C = C_1C_2$.

Converting to dimensionless terms ($Nu_D = hD_i/k$, $Re_D = \rho u_m D_i/\mu$, and $Pr = \mu c_p/k$) the final form of the model is obtained:

$$Nu_D = C\left(\frac{8W\cos(\gamma)}{\pi L}\right)^{\frac{1}{2}} Re_D^{0.5}\, Pr^{0.5} \tag{4.15}$$

D. Comparison of Model with Experimental Results and Discussion

Equation 4.15 indicates that an increase in width, W, or a decrease in pitch, L, or twist angle, γ, results in an increase in heat transfer. These trends compare well with the experimental results presented in Chapter II as shown in Figures 2.21, 2.23, 2.25, 2.26, 2.29, and 2.31. For example, the data in Figures 2.21 and 2.23 show a 6% increase in Nusselt number for an increase of 17% in width. Similarly, Figure 2.25 indicates a 15% increase in Nusselt number for a 37% decrease in pitch.

Since the constant C depends on the fluid properties and flow conditions, an exact numerical value for the constant C could not be obtained analytically by using the surface renewal model. Nevertheless, a linear regression analysis based on Equation 4.15 yielded a value of $C = 2.06$. The intercept was forced to go through the origin so as to

fit the model. The experimental results are compared in Figure 4.2 according to Equation 4.15. The line thus obtained is shown on Figure 4.2. The agreement is within ±20%. It is noted, however, that the deviation is greater at higher Nu_D, i.e., higher Re_D.

To show the variation of heat transfer coefficient with insert geometry, the experimental data and prediction are plotted on a logarithmic plot of Nusselt number as a function of Reynolds number in Figures 4.3-4.5. Figures 4.3, 4.4, and 4.5 show the effect of pitch, L, width, W, and twist angle, γ, respectively. The figures also indicate that the Reynold number exponent of 0.5 in the model is too low. However, several users of the basic surface renewal model also use a exponent of 0.5 (Thomas and Mohler, 1971). The surface renewal/penetration theory assumes (i) the inrush of fluid penetrates down to the wall itself and (ii) the ejected fluid packets gets completely mixed with the bulk fluid and attains the bulk properties; but as described by Hagge and Junkhan (1974), several investigators argue that these assumptions do not hold in practice. To overcome these shortcomings, several methods--including empirical methods--have been used, where constants are added to the existing exponent of Re_D of Pr. These constants take care of the inaccuracies of the model and are dependent on fluid properties and flow geometry. Moreover, these constants have to be evaluated experimentally. Since the analytical model described by Equation 4.15 is very similar to the empirical correlation given by Equation 2.15 in Chapter II, it was considered not

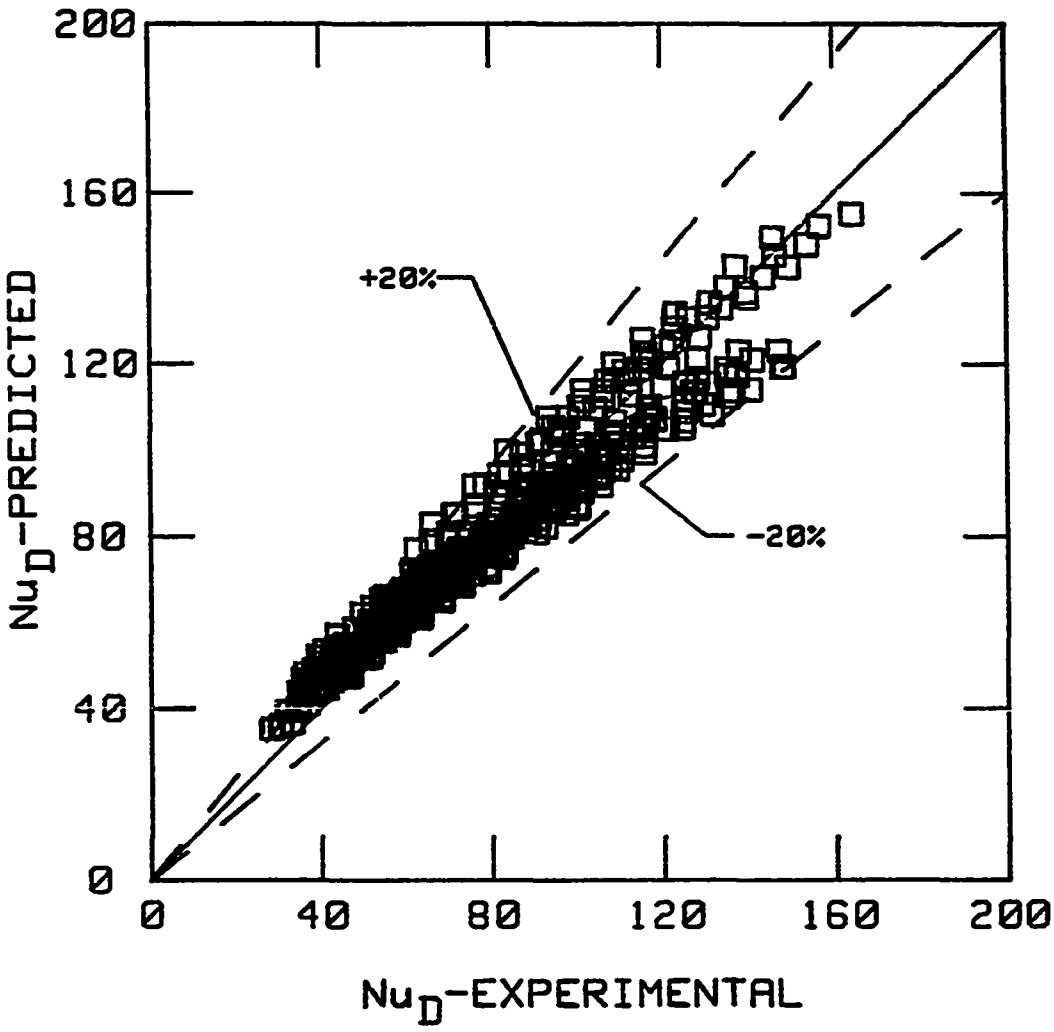

FIGURE 4.2. Scatter plot of Equation 4.15 with experimental data

necessary to further carry out an empirical evaluation of constants in the analytical model.

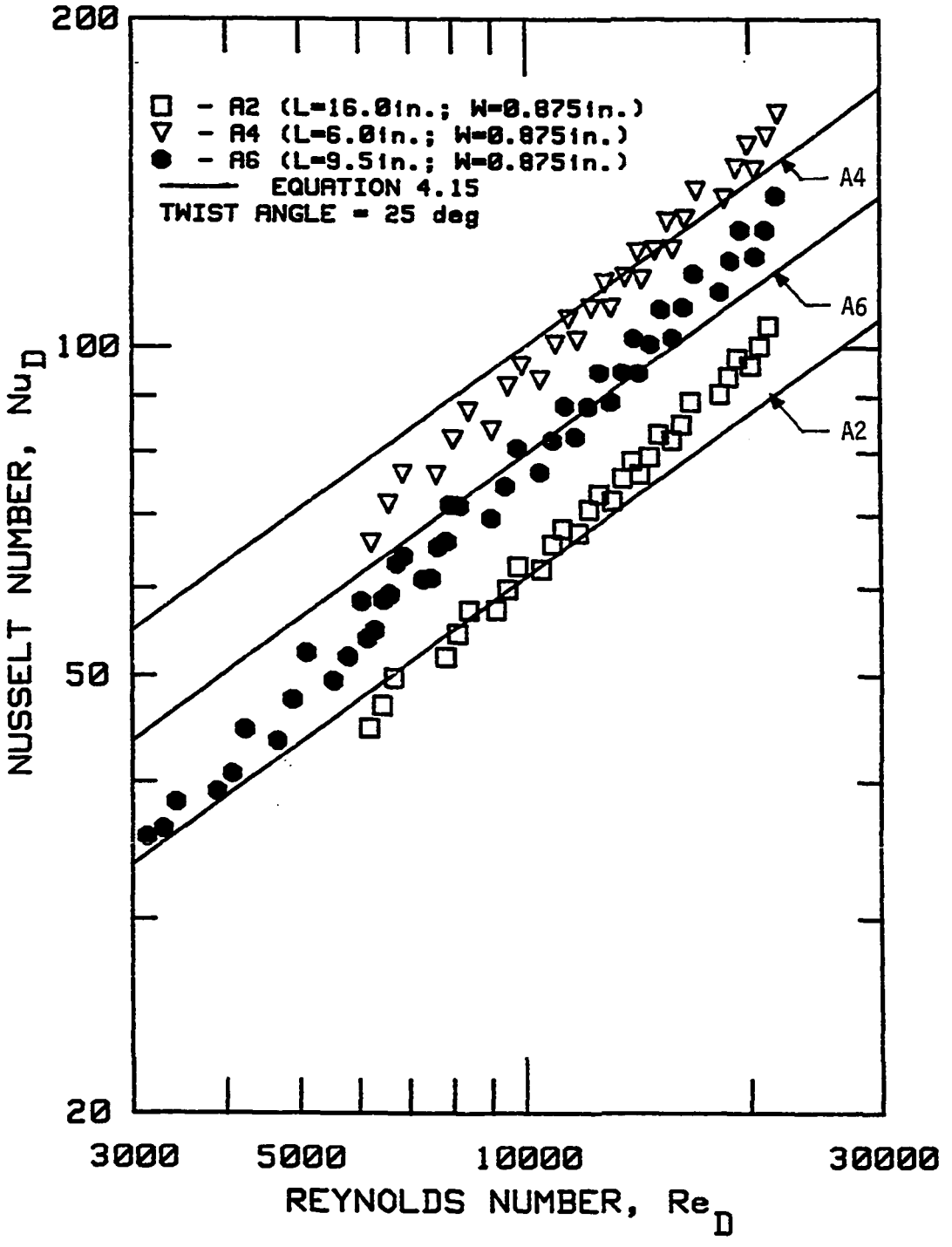

FIGURE 4.3. Effect of insert pitch, L, on Nusselt number and comparison with Equation 4.15

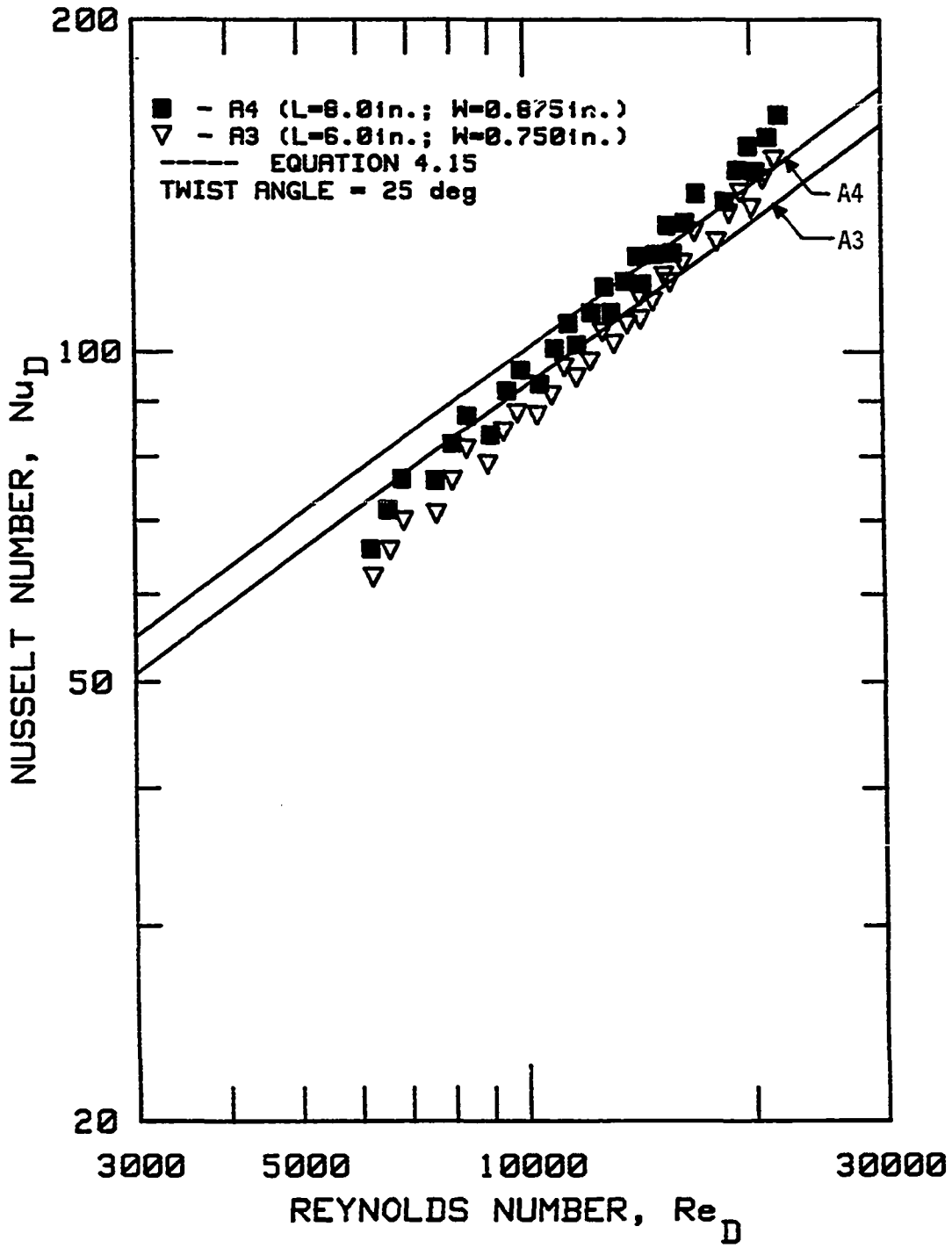

FIGURE 4.4. Effect of insert width, W, on Nusselt number and comparison with Equation 4.15

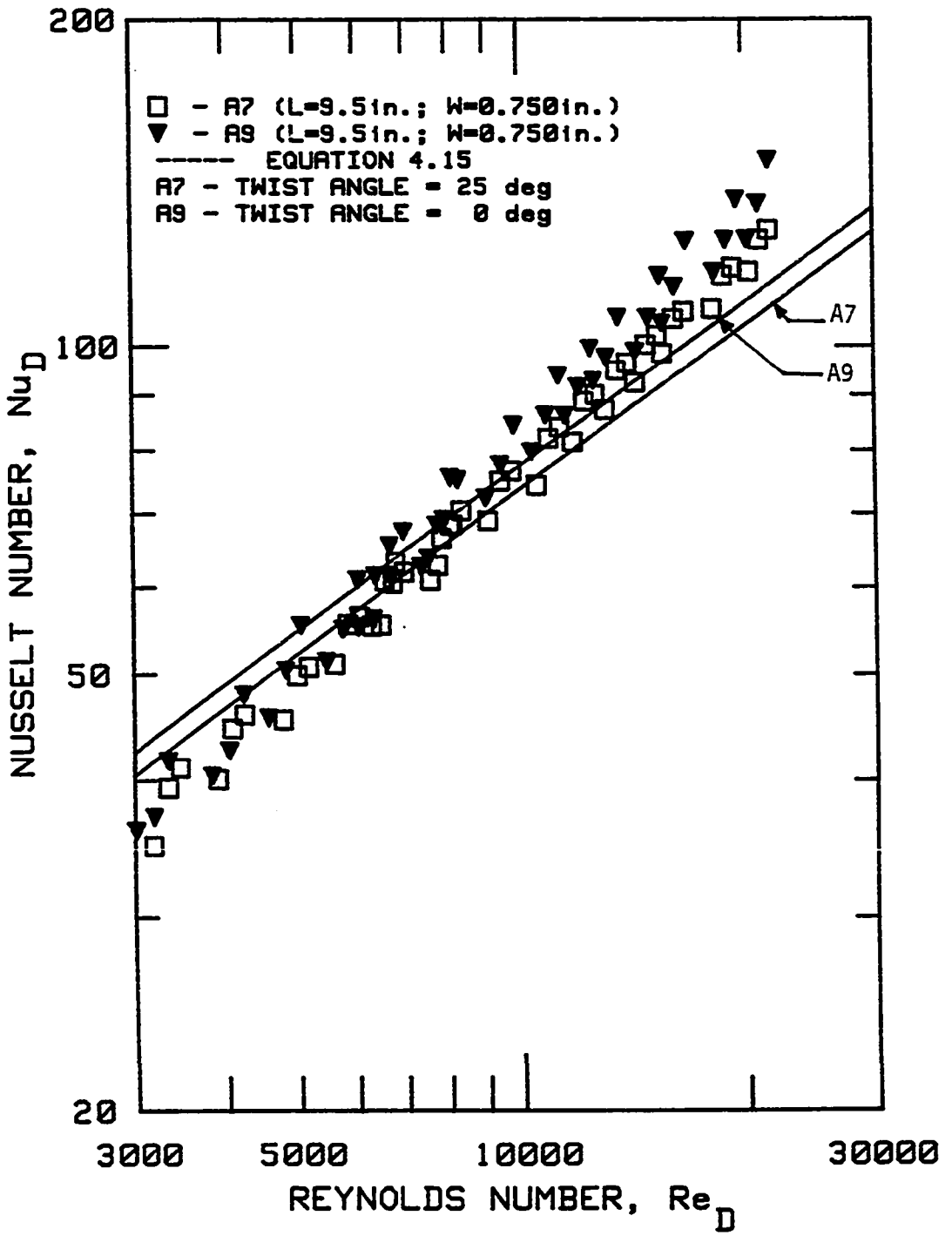

FIGURE 4.5. Effect of insert twist angle, γ, on Nusselt number and comparison with Equation 4.15

V. CONCLUSIONS AND RECOMMENDATIONS

A. Conclusions

The present study investigated the enhancement of in-tube single phase convective heat transfer in gases by means of turbulence-producing bent-strip inserts. Different geometrical variations of a bent-strip insert were tested to obtain heat-transfer and pressure-drop data. Flow-visualization studies were conducted to view the flow patterns created by the insert and thus try to understand the mechanism of enhancement. Finally, the surface renewal/penetration theory was used to obtain an analytically based model for heat transfer. The following conclusions were drawn:

1. The present investigation is the first comprehensive study conducted on enhancement of gas-side heat transfer by using bent-strip inserts.
2. The heat-transfer and pressure-drop results for bent-strip inserts confirm that there is significant increase in heat transfer; however, a considerable pressure drop penalty is incurred. A maximum heat-transfer enhancement of about 300% was achieved with an accompanying pressure-drop increase of about 1800%. The heat-transfer increases are substantially higher than the enhancement level achieved by using wire-coil or twisted-tape inserts.

3. The performance of bent-strip inserts shows that high enhancement in heat-transfer coefficient cannot be achieved with moderate increase in pressure drop.
4. The thermal-hydraulic experiments indicate that Nu_D and f are directly dependent on the pitch and width of a bent-strip insert.
5. The experimental investigations reveal an area of lesser level of augmentation at the entrance region of the insert. An insert length of one and one-half times insert pitch is estimated to be necessary before developed enhanced heat transfer is attained. This is in contrast to an entrance region in a empty tube where heat transfer in the entrance region is higher than in the developed region of the empty tube.
6. The thermal-hydraulic results also point out that the core region of the insert is responsible for the major portion of the heat-transfer enhancement.
7. Empirical correlations are presented for heat transfer and friction factor that are applicable for the design of in-tube enhancement using bent-strip inserts for cooling of hot gases. In the case of heat transfer, different correlations are given for the entrance region and developed region of the flow.

8. For conditions investigated, performance evaluation studies indicate that under a constant pumping power constraint, favorable enhancement is available in the Reynolds number range of 3000 to 30,000. However, under a constant pressure drop constraint, favorable enhancement is available only in the lower Reynolds number range of about 3000 to 5000. Hence, bent-strip inserts are not recommended at higher Reynolds number flows and in cases where allowances cannot be made for high pressure drops.
9. Flow-visualization studies suggest the existence of a swirl flow at the wall and also points out that maximum shear stresses occurs near the contact points of the insert and the tube wall.
10. Flow patterns also confirm the existence of an entry length region corresponding to a distance of about one to two times the insert pitch.
11. The water/dye-injection flow-visualization technique suggests a surface penetration/surface renewal type mechanism at the wall.
12. A semiempirical model using surface renewal/surface penetration theory describes the heat transfer data with reasonable accuracy.

B. Recommendations for Future Work

1. Due to the high pressure-drop penalty, it may be advantageous to use bent-strip inserts in laminar and transition heat-transfer applications. Flow-visualization studies have indicated that even in laminar Reynolds number ranges, the bent-strip insert tends to "turbulize" the flow. Heat-transfer and pressure-drop data in the laminar and transition range would be a valuable extension to this study.
2. Using bent-strip inserts in liquids may have possible applications and should be investigated.
3. In high temperature, real-life applications, an accurate radiant heat-transfer model is required. The measurement of the heat-transfer coefficient from the gas to the insert will be required to obtain more accurate radiation results.
4. By attaining higher gas temperatures, the effect of bulk properties can be evaluated. The effect of variable properties will be useful in fire-tube boiler applications, where the operating temperatures are much higher.
5. Fundamental studies of velocity and temperature profiles in the tube would give more insight into the mechanism of enhancement. Also, the surface renewal frequency could be estimated by using surface film hot-wire anemometry. This would facilitate the development of an independent method to predict the heat transfer by analytical means.

VI. REFERENCES

Azoory, S., and Bott, T. R. 1970. "Local Heat Transfer Coefficients in a Model 'Falling Film' Scraped Surface Exchanger." Canadian Journal of Chemical Engineering 48:373-377.

Beckermann, C. 1984. "Analysis of Submerged Combustion Chamber Gas-Fired Water Heaters." M.S. Thesis, Purdue University, West Lafayette, Indiana.

Bergles, A. E., Blumenkrantz, A. R., and Taborek, J. 1974. "Performance Evaluation Criteria for Enhanced Heat Transfer Surfaces." Heat Transfer 1974, The Proceedings of the Fifth International Heat Transfer Conference, Tokyo, Vol. 2, pp. 239-243. The Japan Society of Mechanical Engineers, Tokyo.

Bergles, A. E., Nirmalan, V., Junkhan, G. H., and Webb, R. L. 1983. "Bibliography on Augmentation of Convective Heat and Mass Transfer-II." HTL-31, ISU-ERI-Ames-84222, DE-8401848, Iowa State University, Ames.

Blackwelder, R. F., and Kaplan, R. E. 1976. "On the Wall Structure of the Turbulent Boundary Layer." Journal of Fluid Mechanics 76(Part 1):89-112.

Chung, B. T. F., Fan, L. T., and Hwang, C. L. 1972. "A Model of Heat Transfer in Fluidized Beds." Journal of Heat Transfer 94:105-110.

Colburn, A. P., and King, W. J. 1931. "Relationship Between Heat Transfer and Pressure Drop." Industrial and Engineering Chemistry 23:919-923.

Corino, E. R., and Brodkey, R. S. 1969. "A Visual Investigation of the Wall Region in Turbulent Flow." Journal of Fluid Mechanics 37(Part 1):1-30.

Danckwerts, P. V. 1951. "Significance of Liquid-Film Coefficients in Gas Absorption." Industrial Engineering Chemistry 43:1460-1467.

Didion, D. A., and Chern, L. 1984. "Prediction of Performance for a Fire-Tube Boiler with and without Turbulators." U. S. Department of Commerce, National Bureau of Standards, Maryland.

Evans, S. I., and Sarjant, R. J. 1951. "Heat Transfer and Turbulence in Gases Flowing Inside Tubes." Journal of the Institute of Fuel 24:216-227.

Falco, R. E. 1982. "A Synthesis and Model of Turbulence Structure in the Wall Region." Structure of Turbulence in Heat and Mass Transfer, pp. Edited by Z. P. Zaric. Hemisphere Publishing Corporation, New York.

Fan, L. T., Lin, S. T., and Azer, N. Z. 1978. "Surface Renewal Model of Condensation Heat Transfer in Tubes with In-Line Static Mixers." International Journal of Heat and Mass Transfer 21:849-854.

Feingold, A. 1966. "Radiant-Interchange Configuration Factors between Various Selected Plane Surfaces." Proceedings of the Royal Society (London) Series A, 292(1428):51-60.

Filonenko, G. K. 1954. Teploenergetika 1(4):40-44.

Gnielinski, V. 1976. "New Equations for Heat and Mass Transfer in Turbulent Pipe and Channel Flow." International Chemical Engineering 16:359-368.

Grass, A. J. 1971. "Structural Features of Turbulent Flow over Smooth and Rough Boundaries." Journal of Fluid Mechanics 50(Part 2):233-355.

Hagge, J. K., and Junkhan, G. H. 1974. "Experimental Study of a Method of Mechanical Augmentation of Convective Heat Transfer Coefficients in Air." HTL-3, ISU-ERI-Ames-74158, Iowa State University, Ames.

Hagge, J. K., and Junkhan, G. H. 1975. "Mechanical Augmentation of Convective Heat Transfer in Air." Journal of Heat Transfer 97:516-520.

Han, C. Y., and Griffith, P. 1965. "The Mechanisms of Heat Transfer in Nucleate Pool Boiling, Parts I and II." International Journal of Heat and Mass Transfer 8:887-913.

Hanratty, T. J. 1956. "Turbulent Exchange of Mass Momentum with a Boundary." AIChE Journal 2:359-362.

Harriot, P. 1958. "Heat Transfer in Scraped-Surface Exchangers." Chemical Engineering Progress Symposium Series 55(29):137-139.

Harriot, P. 1962. "A Random Eddy Modification of the Penetration Theory." Chemical Engineering Science 17:149-154.

Head, M. R., and Bandyopadhyay. P. 1981. "New Aspects of Turbulent-Boundary Layer Structure." Journal of Fluid Mechanics 107:297-238.

Higbie, R. 1935. "The Rate of Absorption of a Pure Gas into a Still Liquid During Period of Short Exposure." Transactions of the American Institute of Chemical Engineers 31:365-388.

Hussain, A. K. M. F. 1983. "Coherent Structures--Reality and Myth." The Physics of Fluids 26:2816-2850.

Ibrahim M. B., and Thomas, L. C. 1983. "A Surface Renewal/Classical Analysis of Turbulent Convection Heat Transfer." Transactions of the Canadian Society of Mechanical Engineers 7(4):170-177.

Junkhan, G. H., Bergles, A. E., Nirmalan, V., and Ravigururajan, T. 1982. "Tests of Turbulators for Fire-Tube Boilers." HTL-29, ISU-ERI-Ames-83130, FESA-E-83023, Iowa State University, Ames.

Junkhan, G. H., Bergles, A. E., Nirmalan, V., and Ravigururajan, T. 1985. "Investigation of Turbulators for Fire Tube Boilers." Journal of Heat Transfer 107:354-360.

Kim, H. T., Kline, S. J., and Reynolds, W. C. 1971. "The Production of Turbulence Near a Smooth Wall in a Turbulent Boundary Layer." Journal of Fluid Mechanics 50(Part 1):133-160.

Kirov, N. Y. 1949. "Turbulence Promoters in Boiler Smoke Tubes." Journal of the Institute of Fuel 22:192-196.

Kline, J., Reynolds, W. C., Schraub, F. A., and Runstadler, P. W. 1967. "The Structure of Turbulent Boundary Layers." Journal of Fluid Mechanics 30(part 4):741-773.

Kline, S., and McClintock, F. A. 1953. "Describing Uncertainties in Single-Sample Experiments." Mechanical Engineering 75:3-8.

Kreith, F. 1962. Radiation Heat Transfer for Spacecraft and Solar Power Plant Design. International Textbook Company, Scranton, Pennsylvania.

McDonald, R. J., Batey, J. E., Allen, T. W., and Hoppe, R. J. 1979. "Direct Efficiency Measurement and Analysis of Residential Oil-Fired Boiler Systems." Brookhaven National Laboratory, Report No. BNL 51171.

Meek, R. L., and Baer, A. D. 1970. "The Periodic Viscous Sublayer in Turbulent Flow." AIChE Journal 16:841-847.

Merzkirch, W. 1974. Flow Visualization. Academic Press, New York.

Mikic, B. B., and Rohsenow, W. M. 1969. "A New Correlation of Pool-Boiling Data Including the Effects of Heating Surface Characteristics." Journal of Heat Transfer 91:245-250.

Mills, A. F. 1962. "Experimental Investigation of Turbulent Heat Transfer in the Entrance Regions of a Circular Conduit." Journal of Mechanical Engineering Science 4:63-67.

Morcos, S. M. 1974. "Combined Forced and Free Laminar Convection in Horizontal Tubes." Ph.D. Dissertation, Iowa State University, Ames

Motwani, D. G. 1984. "Experimental Studies in Convective Heat Transfer from Rectangular Plates Inclined at Different Angles of Attack and Yaw." Ph.D. Thesis, Indian Institute of Technology, Bombay, India.

Offen, G. R., and Kline, S. J. 1974. "Combined Dye-Streak and Hydrogen-Bubble Visual Observations of a Turbulent Boundary Layer." Journal of Fluid Mechanics 62(Part 2):223-239.

Offen, G. R., Kline, S. J. 1975. "A Proposed Model of the Bursting Process in Turbulent Boundary Layers." Journal of Fluid Mechanics 70(Part 2):209-228.

Ostle, B., and Mensing, R. W. 1975. Statistics in Research. Third Edition. Iowa State University Press, Ames, Iowa.

Pinczewski, W. V., and Sideman, S. 1974. "A Model for Mass (Heat) Transfer in Turbulent Tube Flow. Moderate and High Schimdt (Prandtl) Numbers." Chemical Engineering Science 29:1969-1976.

Popovich, A. T., and Hummel, R. L. 1967. "Experimental Study of the Viscous Sublayer in Turbulent Pipe Flow." AIChE Journal 13:854-860.

Rao, N. K., Narasimha, R., and Badri Narayanan, M. A. 1971. "The 'Bursting' Phenomenon in a Turbulent Boundary Layer." Journal of Fluid Mechanics 48(Part 2):339-352.

Royds, R. 1921. Heat Transmission by Radiation, Conduction, and Convection. First Edition. Constable and Company, London.

Shah, R. K., and Johnson, R. S. 1981. "Correlations for Fully Developed Turbulent Flow through Circular and Noncircular Channels." Proceedings of the 6th National Heat Transfer Conference, Madras, India.

Thomas, L. C. 1970a. "A Pseudo-Surface Rejuvenation Model for Turbulent Heat Transfer." Proceedings of the Sixth Southeastern Seminar on Thermal Sciences, North Carolina State University, Raleigh, North Carolina, April 1970.

Thomas, L. C. 1970b. "Temperature Profiles for Liquid Metals and Moderate-Prandtl-Number Fluids." Journal of Heat Transfer 92:565-567.

Thomas, L. C. 1982. "A Turbulent Burst Model for Energy Transfer in the Wall Region." Heat Transfer 1982, Proceeding of the Seventh International Heat Transfer Conference, Munich, Vol. 3, pp. 307-312. Hemisphere Publishing Corporation, New York.

Thomas, L. C., and Fan, L. T. 1971. "Adaptation of the Surface Rejuvenation Model to Turbulent Heat and Mass Transfer at a Solid-Fluid Interface." Industrial Engineering Chemistry Fundamentals 10:135-139.

Thomas, L. C., and Mohler, R. A. 1971. "Mathematical Model for Close Clearance Heat Exchangers." American Society of Mechanical Engineers, Paper No. 71-HT-32.

Thorsen, R., and Landis, F. 1968. "Friction and Heat Transfer Characteristics in Turbulent Swirl Flow Subjected to Large Transverse Temperature Gradients." International Journal of Heat and Mass Transfer 90:87-97.

Tien, K. K. 1978. "Heat/Mass Transfer Characteristics and Fluid Flow Patterns for Air Flow about an Inclined and Yawed Flat Plates." Ph.D. Thesis, Department of Mechanical Engineering, University of Minnesota, Minneapolis.

Tien, K. K., and Sparrow, E. M. 1979. "Local Heat Transfer and Fluid Flow Characteristics for Air Flow Oblique or Normal to a Square Plate." International Journal of Heat and Mass Transfer 22:349-360.

Toor, H. L., and Marchello, J. M. 1958. "Film-Penetration Model for Mass and Heat Transfer." AIChE Journal 4:97-101.

Watanabe, K., Taira, T., and Mori, Y. 1984. "Heat Transfer Augmentation in Tubular Flow by Twisted Tapes at High Temperatures and Optimum Performance." Heat Transfer Japanese Research 12(3):1-31.

Whitham, J. M. 1896. "The Effect of Retarders in Fire Tubes of Steam Boilers." Street Railway Journal 12:374.

Willmarth, W. W., and Bogar, T. J. 1977. "Survey and New Measurements of Turbulent Structure Near the Wall." The Physics of Fluids 20(10):S9-S21.

Willmarth, W. W., and Sharma, L. K. 1984. "Study of Turbulent Structure with Hot Wires smaller than Viscous Length." Journal of Fluid Mechanics 142:121-149.

Yang, W.-J. 1977. "Flow Visualization Studies in the United States and Canada." Flow Visualization, Proceedings of the International Symposium on Flow Visualization, Tokyo, pp. 41-62. Hemisphere Publishing Corporation, New York.

Yaverbaum, L. H. 1979. Energy Saving by Increasing Boiler Efficiency. Noyes Data Corporation, Park Ridge, New Jersey.

VII. ACKNOWLEDGEMENTS

In every Ph.D. endeavor, the final credit goes to the author. I can only say "I did it but not without help from many." I sincerely appreciate my major professors George H. Junkhan and Arthur E. Bergles for introducing me to the art and science of "augmenting heat transfer." I am deeply indebted to them for their guidance, assistance and invaluable advice throughout my program at ISU.

I also wish to thank Professor William J. Cook, Professor James C. Hill, and Professor Bruce R. Munson, the members of my advisory committee, for agreeing to be on my committee and their ready assistance at various points during my Ph.D. program.

My thanks are due to the various sources of financial assistance which supported me during my stay at ISU. They are the Department of Energy, Stuart Radiator Company, the U.S. Army, the American Society of Heating, Refrigerating, and Air-Conditioning Engineers (ASHRAE), and last, but not least, the Engineering Research Institute.

I would like to acknowledge Mr. Hap Steed for all his technical assistance, Mr. Gay Scandrett for his technical help and for teaching me to play racquet ball, and Ms. Carla Holbrook for typing all the reports and for bringing cookies for us in the lab. Also, my gratitude goes to the many colorful personalities, past and present, in ME and ISU for making my stay at ISU a memorable one.

Finally, I like to thank the most important person in my life, my wife Dushy, for putting up with me through the ups and downs of my Ph.D. program.

VIII. APPENDIX A: COMPUTER PROGRAM FOR DATA ACQUISITION AND REDUCTION

```
10    ! ------------------------------------------------------------------
20    !
30    !              DATA ACQUISITION PROGRAM FOR TWISTED TAPE
40    !                   INSERTS IN FIRE TUBE BOILERS
50    !
60    !                            JANUARY 1985
70    !
80    ! ------------------------------------------------------------------
90    !
100   OPTION BASE 1
110   DIM Date$[20],Operator$[20],Type$[20],Typex$[2],Run(20)
120   DIM Dataout(18),Datain(44),Rawdata(44),Re_or(7),Cons_or(7)
130   DIM Segment(4,11),Ptemp$(36)[28],Ppres$(6)[28],Pkey$(2)[48]
140   DIM Pred$(18)[48],Pseg$(4,5)[48],File$[6],Sub(14)
150   DIM Pcorr_nu$(12)[48],Corr_nu(4)
160   !
170   ! ------------------------------------------------------------------
180   !
190   !      DEFINITION OF VARAIBLES
200   !
210   ! ------------------------------------------------------------------
220   !
230         ! Date$.........date of run
240         ! Operator$.....name of operator
250         ! Type$.........type of twisted tape
260         ! Run_no........run number for specific tape
270         ! Dataout(1).....air density at orifice, lbm/cu-ft
280         ! Dataout(2).....air viscosity at orifice, lbm/hr-ft
290         ! Dataout(3).....air mass flow rate, lbm/hr
300         ! Dataout(4).....average inlet air temperature, deg.F
310         ! Dataout(5).....average outlet air temperature, deg.F
320         ! Dataout(6).....air temperature drop, deg.F
330         ! Dataout(7).....specific heat of air, Btu/lbm-deg.F
340         ! Dataout(8).....heat transfer from air, Btu/hr
350         ! Dataout(9).....heat transfer to water thru #4, Btu/hr
360         ! Dataout(10)....heat transfer to water thru #3, Btu/hr
370         ! Dataout(11)....heat transfer to water thru #2, Btu/hr
380         ! Dataout(12)....heat transfer to water thru #1, Btu/hr
390         ! Dataout(13)....total heat transfer to water, Btu/hr
400         ! Dataout(14)....upstream temp drop across teflen, deg.F
410         ! Dataout(15)....downstream temp drop across teflen, deg.F
420         ! Dataout(16)....axial conduction from upstream, Btu/hr
430         ! Dataout(17)....axial conduction from downstream, Btu/hr
440         ! Dataout(18)....energy balance
450         !
460         !
470         ! Datain(1).......test sec. wall temp 1-top, deg.F
480         ! Datain(2).......test sec. wall temp 1-nearside, deg.F
490         ! Datain(3).......test sec. wall temp 1-farside, deg.F
500         ! Datain(4).......test sec. wall temp 2-top, deg.F
510         ! Datain(5).......test sec. wall temp 2-nearside, deg.F
520         ! Datain(6).......test sec. wall temp 2-farside, deg.F
530         ! Datain(7).......test sec. wall temp 3-top, deg.F
540         ! Datain(8).......test sec. wall temp 3-nearside, deg.F
550         ! Datain(9).......test sec. wall temp 3-farside, deg.F
560         ! Datain(10).....test sec. wall temp 4-top, deg.F
570         ! Datain(11).....test sec. wall temp 4-nearside, deg.F
580         ! Datain(12).....test sec. wall temp 4-farside, deg.F
590         ! Datain(13).....test sec. wall temp 5-top, deg.F
600         ! Datain(14).....test sec. wall temp 5-nearside, deg.F
```

```
610         ! Datain(15).....test sec. wall temp 5-farside, deg.F
620         ! Datain(16).....water inlet-4, deg.F
630         ! Datain(17).....water outlet-4, deg.F
640         ! Datain(18).....water inlet-3, deg.F
650         ! Datain(19).....water outlet-3, deg.F
660         ! Datain(20).....water inlet-2, deg.F
670         ! Datain(21).....water outlet-2, deg.F
680         ! Datain(22).....water inlet-1, deg.F
690         ! Datain(23).....water outlet-1, deg.F
700         ! Datain(24).....air inlet-1, deg.F
710         ! Datain(25).....air inlet-2, deg.F
720         ! Datain(26).....air inlet-3, deg.F
730         ! Datain(27).....air inlet-4, deg.F
740         ! Datain(28).....air outlet-1, deg.F
750         ! Datain(29).....air outlet-2, deg.F
760         ! Datain(30).....air outlet-3, deg.F
770         ! Datain(31).....air outlet-4, deg.F
780         ! Datain(32).....room temperature, deg.F
790         ! Datain(33).....temp across teflon-upstream-1, deg.F
800         ! Datain(34).....temp across teflon-upstream-2, deg.F
810         ! Datain(35).....temp across teflon-downstream-1, deg.F
820         ! Datain(36).....temp across teflon-downstream-2, deg.F
830         ! Datain(37).....atmospheric reference pressure, in.water
840         ! Datain(38).....static pressure-inlet heater box, in.water
850         ! Datain(39).....pressure drop-orifice, in.water
860         ! Datain(40).....static pressure-outlet orifice, in.water
870         ! Datain(41).....pressure drop-test section, in.water
880         ! Datain(42).....static pressure-down stream test sec., in.water
890         ! Datain(43).....atmospheric pressure, in.Hg
900         ! Datain(44).....water flow rate, lmb/hr
910         !
920         !
930         ! SegmentX(1).....outlet air temp in segment X
940         ! SegmentX(2).....specific heat of air in segment X
950         ! SegmentX(3).....average wall temp-upstream in segment X
960         ! SegmentX(4).....average wall temp-downstream in segment X
970         ! SegmentX(5).....overall heat transfer coeff. in segment X
980         ! SegmentX(6).....air-side heat transfer coeff. in segment X
990         ! SegmentX(7).....thermal conductivity of air in segment X
1000        ! SegmentX(8).....Nusselt number of air in segment X
1010        ! SegmentX(9).....viscosity of air in segment X
1020        ! SegmentX(10)....Prandtl number of air in segment X
1030        ! SegmentX(11)....Reynold number in segment X
1040        !
1050        !
1060  !
1070  !  ------------------------------------------------------------------
1080  !
1090  !       ASSIGNMENT OF MULTIPLEXER CHANNELS TO ANALOG INPUTS
1100  !
1110  ! ------------------------------------------------------------------
1120  !
1130        !
1140        !   Mux Channel                    Input
1150        !       0                pressure transducer output
1160        !       I                      Datain(I)
1170        !
1180  ! ------------------------------------------------------------------
1190  !
1200  !     Instrument Configuration Codes
```

```
1210  !
1220  ! ------------------------------------------------------------------------
1230  !
1240  DIM Rdg(20)
1250  DIM Dmm$(3)[30]
1260  Dmm$(1)="F1R1Z0FL0M0T2" ! dcv,range=10,auto-0=off,filter=off
1270  Dmm$(2)="HSM00ZL1M2RS110STNT3Q" ! 10 Readings and get mean
1280  Dmm$(3)="HSM00ZL1M2RS120STNT3Q" ! 20 Readings and get mean
1290  !
1300  ! ------------------------------------------------------------------------
1310  !
1320  !       Control of the Printer
1330  !
1340  ! ------------------------------------------------------------------------
1350  !
1360  Key=701
1370  DISP "SET PAPER AT TOP OF PAGE"
1380  PAUSE
1390  WRITE BIN Key;27,110
1400  !
1410  ! ------------------------------------------------------------------------
1420  !
1430  !               Input of Run Type
1440  !
1450  ! ------------------------------------------------------------------------
1460  !
1470  INPUT "DATE?",Date$
1480  INPUT "OPERATOR?",Operator$
1490  INPUT "TYPE OF INSERT?",Type$
1500  !
1510  ! ------------------------------------------------------------------------
1520  !
1530  !             Calculation of Radiation Area and Shape Factors
1540  !
1550  ! ------------------------------------------------------------------------
1560  !
1570  Sigma=1.712E-9
1580  INPUT "Length Of Insert?",Length
1590  INPUT "Pitch of Insert?",Pitch
1600  INPUT "Width of Insert?",Width
1610  IF Pitch<>9.5 THEN 1650
1620  Rad_con=Sigma/(1/.964+1/.7-1+(1/.9-1)*2*20.4375*Width/149.94)
1630  Area1=20.4375*Width*2/144
1640  Area11=(Length-53.625)/17.875*20.4375*Width*2/144
1650  IF Pitch<>16 THEN 1690
1660  Rad_con=Sigma/(1/.9994+1/.7-1+(1/.9-1)*2*18.8491*Width/149.94)
1670  Area1=18.8491*Width*2/144
1680  Area11=(Length-53.625)/17.875*18.8491*Width*2/144
1690  IF Pitch<>6 THEN 1730
1700  Rad_con=Sigma/(1/.9+1/.7-1+(1/.9-1)*2*25.2791*Width/149.94)
1710  Area1=25.2791*Width*2/144
1720  Area11=(Length-53.625)/17.875*25.2791*Width*2/144
1730  IF (Pitch<>9.5) AND (Pitch<>16) AND (Pitch<>6) THEN 1590
1740  !
1750  ! ------------------------------------------------------------------------
1760  !
1770  !           Operating conditions monitoring sequence
1780  !
1790  ! ------------------------------------------------------------------------
1800  !
```

```
1810 Rerun: INPUT "ENTER RUN NUMBER?",Run_no
1820  INPUT "FLOW RANGE (1) 6000-20000 or (2) 3000-6000 ? 1 or 2 ",Or_key
1830  INPUT "ATMOSPHERIC PRESSURE, in IN.Hg?",Datain(43)
1840  OUTPUT 709 USING Mux;32
1850 Mux: IMAGE #,"C",ZZ,"E"
1860  Dvm=1 ! Flag for averaging 10 or 20 readings
1870  OUTPUT 722;Dmm$(2)
1880  OUTPUT 722;Dmm$(1)
1890  GOSUB Reading
1900  Rawdata(32)=Rdg
1910  Temp_data=Rawdata(32)*1000
1920  Datain(32)=149.1995+44.1465*Temp_data+.0548*Temp_data^2-.0015*Temp_data^3
1930  OUTPUT 709 USING Mux;0
1940  OUTPUT 722;Dmm$(2)
1950  OUTPUT 722;Dmm$(1)
1960  FOR I=1 TO 2
1970  BEEP
1980  DISP "SET SCANNIVALVE AT CHANNEL ",I
1990  PAUSE
2000  GOSUB Reading
2010  Rawdata(36+I)=Rdg
2020  Datain(I+36)=-1.139*Rawdata(37)+1.139*Rawdata(I+36)
2030  NEXT I
2040  BEEP
2050  DISP "SET SCANNIVALVE AT CHANNEL 3"
2060  PAUSE
2070  Pflag=1
2080 Repeat_mass:!
2090  ON KEY #0 GOTO Monit
2100  GOSUB Reading
2110  Rawdata(39)=Rdg
2120  Datain(39)=-1.139*Rawdata(37)+1.139*Rawdata(39)
2130  IF Pflag=1 THEN INPUT "MAXIMUM PRESSURE REACHED? Yes=1,No=0",Yes_no
2140  IF (Pflag=1) AND (Yes_no=0) THEN Next
2150  IF (Pflag=1) AND (Yes_no=1) THEN INPUT "PRESSURE IN in.H2O?",Datain(36+I)
2160 Next: DISP "TO MONITER TEMP: PAUSE;CONT Monit EXECUTE OR HIT k0"
2170  IF Pflag=1 THEN Pflag=0
2180  GOSUB Orifice
2190  Dataout(3)=Mass
2200  OUTPUT 16 USING Scrfmt1;Dataout(3)
2210 Scrfmt1: IMAGE "MASS FLOW RATE OF AIR = ",3D.3D," lbm/hr"
2220  GOTO Repeat_mass
2230 Monit: !
2240  PRINT CHR$(27)&CHR$(69)
2250  DISP "SET AIR TEMPERATURE"
2260  BEEP
2270 Repeat_temp: OUTPUT 722;Dmm$(1)
2280  OUTPUT 722;Dmm$(2)
2290  ON KEY #1 GOTO Take_data
2300  DISP "TO TAKE DATA PAUSE AND CONT Take_data EXECUTEOR HIT k1"
2310  OUTPUT 709 USING Mux;24
2320  GOSUB Reading
2330  Rawdata(24)=Rdg
2340  Temp_data=Rawdata(24)*1000
2350  Datain(24)=149.1995+44.1465*Temp_data+.0548*Temp_data^2-.0015*Temp_data^3
2360  OUTPUT 16 USING Scrfmt2;Datain(24)
2370 Scrfmt2: IMAGE "AVERAGE INLET AIR TEMPERATURE = ",3D.3D," deg.F"
2380  FOR I=1 TO 10
2390  OUTPUT 722;Dmm$(1)
2400  OUTPUT 709 USING Mux;23
```

```
2410  GOSUB Reading
2420  Rawdata(23)=Rdg
2430  Temp_data=Rawdata(23)*1000
2440  Datain(23)=149.1995+44.1465*Temp_data+.0548*Temp_data^2-.0015*Temp_data^3
2450  OUTPUT 16 USING Scrfmt3;Datain(23)
2460 Scrfmt3: IMAGE "OUTLET WATER TEMPERATURE = ",3D.3D," deg.F"
2470  NEXT I
2480  GOTO Repeat_temp
2490  !
2500  ! ------------------------------------------------------------------
2510  !
2520  !       DATA COLLECTION AND CONVERTING TO TRUE VALUES
2530  !
2540  ! ------------------------------------------------------------------
2550  !
2560  !         Thermocouple readings
2570  !
2580  ! ------------------------------------------------------------------
2590  !
2600 Take_data: PRINT CHR$(27)&CHR$(69)
2610  DISP "TAKING DATA. PLEASE BE PATIENT"
2620  OUTPUT 722;Dmm$(2)
2630  FOR I=1 TO 36
2640  OUTPUT 722;Dmm$(1)
2650  OUTPUT 709 USING Mux;I
2660  GOSUB Reading
2670  Rawdata(I)=Rdg
2680  Temp_data=Rawdata(I)*1000
2690  Datain(I)=149.1995+44.1465*Temp_data+.0548*Temp_data^2-.0015*Temp_data^3
2700  NEXT I
2710  !
2720  ! ------------------------------------------------------------------
2730  !
2740  !           Pressure Readings
2750  !
2760  ! ------------------------------------------------------------------
2770  !
2780  OUTPUT 709 USING Mux;0
2790  Dvm=2
2800  OUTPUT 722;Dmm$(3)
2810  FOR I=1 TO 6
2820  OUTPUT 722;Dmm$(1)
2830  BEEP
2840  DISP "SET SCANNIVALVE ON CHANNEL ",I
2850  PAUSE
2860  GOSUB Reading
2870  Rawdata(36+I)=Rdg
2880  Datain(36+I)=-1.139*Rawdata(37)+1.139*Rawdata(36+I)
2890  IF I=3 THEN INPUT "HAS MAX PRESSURE BEEN REACHED? Yes=1, No=0",Yes_no
2900  IF (I=3) AND (Yes_no=0) THEN Next1
2910  IF (I=3) AND (Yes_no=1) THEN INPUT "PRESSURE IN in.H2O?",Dataout(36+I)
2920 Next1: NEXT I
2930  Dvm=1
2940  BEEP
2950  INPUT "WATER FLOW RATE? in lbm/hr",Datain(44)
2960  !
2970  ! ------------------------------------------------------------------
2980  !
2990  !         DATA REDUCTION
3000  !
```

```
3010  ! ------------------------------------------------------------------
3020  !
3030  Dataout(4)=(Datain(24)+Datain(25)+Datain(26)+Datain(27))/4
3040  Dataout(5)=(Datain(28)+Datain(29)+Datain(30)+Datain(31))/4
3050  Dataout(6)=Dataout(4)-Dataout(5)
3060  Avg_air_temp=(Dataout(4)+Dataout(5))/2+459.67
3070  Dataout(7)=.2231+3.42E-5*Avg_air_temp-2.93E-9*Avg_air_temp^2
3080  GOSUB Orifice
3090  Dataout(3)=Mass
3100  Dataout(8)=Dataout(3)*Dataout(6)*Dataout(7)
3110  Dataout(9)=Datain(44)*(Datain(17)-Datain(16))
3120  Dataout(10)=Datain(44)*(Datain(19)-Datain(18))
3130  Dataout(11)=Datain(44)*(Datain(21)-Datain(20))
3140  Dataout(12)=Datain(44)*(Datain(23)-Datain(22))
3150  Dataout(13)=Dataout(12)+Dataout(11)+Dataout(10)+Dataout(9)
3160  Dataout(14)=Datain(36)-Datain(35)
3170  Dataout(15)=Datain(33)-Datain(34)
3180  Dataout(16)=.759255*Dataout(14)
3190  Dataout(17)=1.071844*Dataout(15)
3200  Dataout(18)=(Dataout(13)-Dataout(16)-Dataout(17))/Dataout(8)
3210  !
3220  ! ------------------------------------------------------------------
3230  !
3240  !     Nusselt Number Calculation
3250  !
3260  ! ------------------------------------------------------------------
3270  !
3280  !       For Segment I
3290  !
3300  FOR I=4 TO 1 STEP -1
3310  IF I=4 THEN Sub(3)=Dataout(5)
3320  IF I<>4 THEN Sub(3)=Segment(I+1,1)
3330  IF I=1 THEN Area=Area11
3340  IF I<>1 THEN Area=Area1
3350  Sub(2)=Dataout(3)
3360  IF I=1 THEN Sub(5)=Dataout(12)-Dataout(16)
3370  IF I=2 THEN Sub(5)=Dataout(11)
3380  IF I=3 THEN Sub(5)=Dataout(10)
3390  IF I=4 THEN Sub(5)=Dataout(9)-Dataout(17)
3400  Sub(6)=Segment(I,3)=(Datain(3*I-2)+Datain(3*I-1)+Datain(3*I))/3
3410  Sub(7)=Segment(I,4)=(Datain(3*I+1)+Datain(3*I+2)+Datain(3*I+3))/3
3420  IF I=1 THEN Sub(8)=.971429
3430  IF I=2 THEN Sub(8)=1.030303
3440  IF I=3 THEN Sub(8)=1.007407
3450  IF I=4 THEN Sub(8)=.992701
3460  CALL Nusselt(Sub(*),Corr_nu(I),Rad_con,Area,Qr(I),T_ins(I))
3470  Segment(I,1)=Sub(1)
3480  Segment(I,2)=Sub(4)
3490  Segment(I,5)=Sub(8)
3500  Segment(I,6)=Sub(9)
3510  Segment(I,7)=Sub(10)
3520  Segment(I,8)=Sub(11)
3530  Segment(I,9)=Sub(12)
3540  Segment(I,10)=Sub(13)
3550  Segment(I,11)=Sub(14)
3560  NEXT I
3570  !
3580  ! ------------------------------------------------------------------
3590  !            friction factor calculation
3600  ! ------------------------------------------------------------------
```

```
3610  !
3620  Density1=(1.3259*Datain(43)+.097527*Datain(42))/(Dataout(4)+459.67)
3630  Density2=(1.3259*Datain(43)+.097527*(Datain(42)-Datain(41)))/(Dataout(5)+4
59.67)
3640  Delp_mom=(25.71876*Dataout(3))^2*(1/Density1-1/Density2)/(3600^2*32.174)
3650  Delp_tot=Datain(41)*5.2024+Delp_mom
3660  Cf=31432.11228*Delp_tot*Datain(43)/(Dataout(3)^2*(Dataout(4)+Dataout(5)+92
0))
3670  OUTPUT 16 USING Scrfmt5;Dataout(18)
3680 Scrfmt5: IMAGE "ENERGY BALANCE = ",2D.4D
3690  INPUT "IS ENERGY BALANCE OK? Yes=1, No=0",Yes_no
3700  IF Yes_no=0 THEN Repeat_mass
3710  !
3720  ! ------------------------------------------------------------------
3730  !
3740  !        PRINTING OUT THE RAW AND REDUCED DATA
3750  !
3760  ! ------------------------------------------------------------------
3770  !
3780  WRITE BIN Key;32,32
3790  WRITE BIN Key;27,49
3800  WRITE BIN Key;32,32,32,32,32,32,32,32,32,32,32,32,32,32,32,32,32,32,32,32,32,32
3810  WRITE BIN Key;32,32,32,32,32,32,32,32,32,32,32,32,32,32,32,32,32,32,32,32,32,32
3820  WRITE BIN Key;32,32,32,32,32,32,32,32,32,32,32,32,32,32,32,32,32,32,32,32,32,32
3830  WRITE BIN Key;32,32,32
3840  WRITE BIN Key;27,49
3850  EOL Key;CHR$(9)
3860  WRITE BIN Key;13
3870  OUTPUT Key USING Pfmt1;Type$,Run_no
3880 Pfmt1: IMAGE L,2X,"TYPE OF TAPE: ",20A,3X,"RUN NUMBER: ",3D
3890  OUTPUT Key USING Pfmt2;Date$,Operator$
3900 Pfmt2: IMAGE L,2X,"DATE: ",15A,3X,"OPERATOR: ",15A
3910 Pline: IMAGE #,L,"-------------------------------------------------------
-----"
3920 Plinel: IMAGE L,"-------------------------------------------------------
---"
3930  OUTPUT Key USING Plinel;
3940  WRITE BIN Key;9
3950  OUTPUT Key;"                              RAW DATA"
3960  OUTPUT Key USING Plinel;
3970  WRITE BIN Key;9
3980  OUTPUT Key;"                           TEMPERATURE DATA"
3990  WRITE BIN Key;9
4000  OUTPUT Key USING "#,K";"Location              Scanner      Reading          T
emperature"
4010  OUTPUT Key USING Plinel;
4020  WRITE BIN Key;9
4030  OUTPUT Key USING "#,K";"                      Channel        Volts
  deg.F"
4040  WRITE BIN Key;9
4050  OUTPUT Key;"                           REDUCED RUN DATA"
4060  OUTPUT Key USING Pline;
4070  OUTPUT Key USING Plinel;
4080  Ptemp$(1)="Test.Sec.wall 1-top      1    "
4090  Ptemp$(2)="Test.Sec.wall 1-ns       2    "
4100  Ptemp$(3)="Test.Sec.wall 1-fs       3    "
4110  Ptemp$(4)="Test.Sec.wall 2-top      4    "
4120  Ptemp$(5)="Test.Sec.wall 2-ns       5    "
4130  Ptemp$(6)="Test.Sec.wall 2-fs       6    "
4140  Ptemp$(7)="Test.Sec.wall 3-top      7    "
```

```
4150  Ptemp$(8)="Test.Sec.wall 3-ns      8   "
4160  Ptemp$(9)="Test.Sec.wall 3-fs      9   "
4170  Ptemp$(10)="Test.Sec.wall 4-top     10  "
4180  Ptemp$(11)="Test.Sec.wall 4-ns      11  "
4190  Ptemp$(12)="Test.Sec.wall 4-fs      12  "
4200  Ptemp$(13)="Test.Sec.wall 5-top     13  "
4210  Ptemp$(14)="Test.Sec.wall 5-ns      14  "
4220  Ptemp$(15)="Test.Sec.wall 5-fs      15  "
4230  Ptemp$(16)="Water inlet-4           16  "
4240  Ptemp$(17)="Water outlet-4          17  "
4250  Ptemp$(18)="Water inlet-3           18  "
4260  Ptemp$(19)="Water outlet-3          19  "
4270  Ptemp$(20)="Water inlet-2           20  "
4280  Ptemp$(21)="Water outlet-2          21  "
4290  Ptemp$(22)="Water inlet-1           22  "
4300  Ptemp$(23)="Water outlet-1          23  "
4310  Ptemp$(24)="Air inlet-1             24  "
4320  Ptemp$(25)="Air inlet-2             25  "
4330  Ptemp$(26)="Air inlet-3             26  "
4340  Ptemp$(27)="Air inlet-4             27  "
4350  Ptemp$(28)="Air outlet-1            28  "
4360  Ptemp$(29)="Air outlet-2            29  "
4370  Ptemp$(30)="Air outlet-3            30  "
4380  Ptemp$(31)="Air outlet-4            31  "
4390  Ptemp$(32)="Room temperature        32  "
4400  Ptemp$(33)="Teflon up stream-1      33  "
4410  Ptemp$(34)="Teflon up stream-2      34  "
4420  Ptemp$(35)="Teflon down stream-1    35  "
4430  Ptemp$(36)="Teflon down stream-2    36  "
4440 Pfmt3: IMAGE #,L,28A,5D.6D,8X,5D.6D
4450  Ppres$(1)="Atmospheric reference    1  "
4460  Ppres$(2)="St. inlet heater box     2  "
4470  Ppres$(3)="Pres. drop orifice       3  "
4480  Ppres$(4)="St. down str. orifice    4  "
4490  Ppres$(5)="Pres. drop test sec.     5  "
4500  Ppres$(6)="St. up str. test sec.    6  "
4510  Pkey$(1)="Atmospheric pressure                    in.Hg    "
4520  Pkey$(2)="Water flow rate                        lmb/hr    "
4530 Pfmt4: IMAGE #,L,48A,5D.5D
4540 Pfmt41: IMAGE L,48A,5D.5D
4550  Pred$(1)="Air density at orifice              lbm/cu.ft    "
4560  Pred$(2)="Air viscosity at orifice            lbm/hr-ft    "
4570  Pred$(3)="Air mass flow rate                     lbm/hr    "
4580  Pred$(4)="Average inlet air temperature           deg.F    "
4590  Pred$(5)="Average outlet air temperature          deg.F    "
4600  Pred$(6)="Air temperature drop                    deg.F    "
4610  Pred$(7)="Specific heat of air           Btu/lbm-deg.F    "
4620  Pred$(8)="Heat transfer from air                 Btu/hr    "
4630  Pred$(9)="Heat transfer to water thru # 4        Btu/hr    "
4640  Pred$(10)="Heat transfer to water thru # 3       Btu/hr    "
4650  Pred$(11)="Heat transfer to water thru # 2       Btu/hr    "
4660  Pred$(12)="Heat transfer to water thru # 1       Btu/hr    "
4670  Pred$(13)="Total heat trnsfer to water           Btu/hr    "
4680  Pred$(14)="Upstream temp. drop across teflon      deg.F    "
4690  Pred$(15)="Downstream temp. drop across teflon    deg.F    "
4700  Pred$(16)="Axial conduction from upstr. end      Btu/hr    "
4710  Pred$(17)="Axial conduction from dnstr. end      Btu/hr    "
4720  Pred$(18)="Energy balance                                  "
4730  FOR I=1 TO 18
4740  OUTPUT Key USING Pfmt3;Ptemp$(I),Rawdata(I),Datain(I)
```

```
4750  OUTPUT Key USING Pfmt41;Pred$(I),Dataout(I)
4760  NEXT I-
4770  Pseg$(1,1)="Inlet air temperature at 1              deg.F     "
4780  Pseg$(1,2)="Heat tran. coeff.-1       Btu/sq.ft-hr-deg.F     "
4790  Pseg$(1,3)="Nusselt number-1                                 "
4800  Pseg$(1,4)="Prandtl number-1                                 "
4810  Pseg$(1,5)="Reynolds number-1                                "
4820  Pseg$(2,1)="Inlet air temperature at 2              deg.F     "
4830  Pseg$(2,2)="Heat tran. coeff.-2       Btu/sq.ft-hr-deg.F     "
4840  Pseg$(2,3)="Nusselt number-2                                 "
4850  Pseg$(2,4)="Prandtl number-2                                 "
4860  Pseg$(2,5)="Reynolds number-2                                "
4870  Pseg$(3,1)="Inlet air temperature at 3              deg.F     "
4880  Pseg$(3,2)="Heat tran. coeff.-3       Btu/sq.ft-hr-deg.F     "
4890  Pseg$(3,3)="Nusselt number-3                                 "
4900  Pseg$(3,4)="Prandtl number-3                                 "
4910  Pseg$(3,5)="Reynolds number-3                                "
4920  Pseg$(4,1)="Inlet air temperature at 4              deg.F     "
4930  Pseg$(4,2)="Heat tran. coeff.-4       Btu/sq.ft-hr-deg.F     "
4940  Pseg$(4,3)="Nusselt number-4                                 "
4950  Pseg$(4,4)="Prandtl number-4                                 "
4960  Pseg$(4,5)="Reynolds number-4                                "
4970  Pcorr_nu$(1)="Nu*F(L/D)*(Tw/Tb)^.45; (1)                       "
4980  Pcorr_nu$(2)="Nu*F(L/D)*(Tw/Tb)^.45; (2)                       "
4990  Pcorr_nu$(3)="Nu*F(L/D)*(Tw/Tb)^.45; (3)                       "
5000  Pcorr_nu$(4)="Nu*F(L/D)*(Tw/Tb)^.45; (4)                       "
5010  Pcorr_nu$(5)="Radiation Correction (1)              Btu/hr    "
5020  Pcorr_nu$(6)="Radiation Correction (2)              Btu/hr    "
5030  Pcorr_nu$(7)="Radiation Correction (3)              Btu/hr    "
5040  Pcorr_nu$(8)="Radiation Correction (4)              Btu/hr    "
5050  Pcorr_nu$(9)="Insert Temperature   (1)               deg.F    "
5060  Pcorr_nu$(10)="Insert Temperature   (2)               deg.F   "
5070  Pcorr_nu$(11)="Insert Temperature   (3)               deg.F   "
5080  Pcorr_nu$(12)="Insert Temperature   (4)               deg.F   "
5090  FOR I=1 TO 3
5100  OUTPUT Key USING Pfmt3;Ptemp$(6*(I-1)+19),Rawdata(6*(I-1)+19),Datain(6*(I-
1)+19)
5110  OUTPUT Key USING Pfmt41;Pseg$(I,1),Segment(I,1)
5120  OUTPUT Key USING Pfmt3;Ptemp$(6*(I-1)+20),Rawdata(6*(I-1)+20),Datain(6*(I-
1)+20)
5130  OUTPUT Key USING Pfmt41;Pseg$(I,2),Segment(I,6)
5140  OUTPUT Key USING Pfmt3;Ptemp$(6*(I-1)+21),Rawdata(6*(I-1)+21),Datain(6*(I-
1)+21)
5150  OUTPUT Key USING Pfmt41;Pseg$(I,3),Segment(I,8)
5160  OUTPUT Key USING Pfmt3;Ptemp$(6*(I-1)+22),Rawdata(6*(I-1)+22),Datain(6*(I-
1)+22)
5170  OUTPUT Key USING Pfmt41;Pcorr_nu$(I),Corr_nu(I)
5180  OUTPUT Key USING Pfmt3;Ptemp$(6*(I-1)+23),Rawdata(6*(I-1)+23),Datain(6*(I-
1)+23)
5190  OUTPUT Key USING Pfmt41;Pseg$(I,4),Segment(I,10)
5200  OUTPUT Key USING Pfmt3;Ptemp$(6*(I-1)+24),Rawdata(6*(I-1)+24),Datain(6*(I-
1)+24)
5210  OUTPUT Key USING Pfmt41;Pseg$(I,5),Segment(I,11)
5220  NEXT I
5230  OUTPUT Key USING Pline;
5240  OUTPUT Key USING Pfmt41;Pseg$(4,1),Segment(4,1)
5250  WRITE BIN Key;9
5260  OUTPUT Key USING "#,K";"                          PRESSURE DATA"
```

```
5270  OUTPUT Key USING Pfmt41;Pseg$(I,2),Segment(I,6)
5280  WRITE BIN Key;9
5290  OUTPUT Key USING "#,K";"Location            Scannivalve  Reading
 Pressure"
5300  OUTPUT Key USING Pfmt41;Pseg$(I,3),Segment(I,8)
5310 Pcf:  IMAGE L,"Coefficient of friction, Cf                    ",5D.6D
5320  WRITE BIN Key;9
5330  OUTPUT Key USING "#,K";"                          Channel     Volts
   in.H2O"
5340  OUTPUT Key USING Pfmt41;Pcorr_nu$(I),Corr_nu(I)
5350  OUTPUT Key USING Pline;
5360  OUTPUT Key USING Pfmt41;Pseg$(I,4),Segment(I,10)
5370  OUTPUT Key USING Pfmt3;Ppres$(1),Rawdata(1+36),Datain(1+36)
5380  OUTPUT Key USING Pfmt41;Pseg$(I,5),Segment(I,11)
5390  OUTPUT Key USING Pfmt3;Ppres$(2),Rawdata(2+36),Datain(2+36)
5400  OUTPUT Key USING Pcf;Cf
5410  OUTPUT Key USING Pfmt3;Ppres$(3),Rawdata(3+36),Datain(3+36)
5420  OUTPUT Key USING Pline1;
5430 Pfmt31: IMAGE L,28A,5D.6D,8X,5D.6D
5440  FOR I=1 TO 3
5450  OUTPUT Key USING Pfmt3;Ppres$(I+3),Rawdata(I+3+36),Datain(I+3+36)
5460  OUTPUT Key USING Pfmt41;Pcorr_nu$(I+4),Qr(I)
5470  NEXT I
5480 OUTPUT Key USING Pline;
5490  OUTPUT Key USING Pfmt41;Pcorr_nu$(8),Qr(4)
5500  WRITE BIN Key;9
5510  OUTPUT Key USING "#,K";"                        KEYBOARD INPUTS"
5520  OUTPUT Key USING Pfmt41;Pcorr_nu$(9),T_ins(1)-459.67
5530  OUTPUT Key USING Pfmt4;Pkey$(1),Datain(43)
5540  OUTPUT Key USING Pfmt41;Pcorr_nu$(10),T_ins(2)-459.67
5550  OUTPUT Key USING Pfmt4;Pkey$(2),Datain(44)
5560  OUTPUT Key USING Pfmt41;Pcorr_nu$(11),T_ins(3)-459.67
5570  OUTPUT Key USING Pline;
5580  OUTPUT Key USING Pfmt41;Pcorr_nu$(12),T_ins(4)-459.67
5590  !
5600  ! ------------------------------------------------------------------
5610  !
5620  !       RECORDING OF RAW AND REDUCED DATA ON DISK
5630  !
5640  ! ------------------------------------------------------------------
5650  !
5660  MASS STORAGE IS ":F8,0"
5670  BEEP
5680  DISP "DATA READY TO BE RECORDED ON DISK. IF OK CONT"
5690  PAUSE
5700  DISP "INSERT DISK INTO DISK DRIVE 0 AND CONT"
5710  PAUSE
5720  Type1$=""
5730  FOR I=1 TO LEN(Type$)
5740  IF Type$[I,I]="" THEN Out
5750  Type1$=Type1$&Type$[I,I]
5760 Out: NEXT I
5770  File$="FR"&VAL$(Run_no)&Type1$
5780  OUTPUT 16;"FILE NAME IS ",File$
5790  INPUT "IS FILENAME OK? Yes=1, No=0 ",Yes_no
5800  IF Yes_no=0 THEN Name
5810  IF LEN(File$)>6 THEN Name
5820  GOTO Out1
5830 Name: LINPUT "ENTER THE CORRECT FILENAME PLEASE",File$
5840 Out1: CREATE File$,5
```

```
5850  ASSIGN #1 TO File$
5860  PRINT #1;Date$,Operator$,Type$,Run_no,Rawdata(*),Datain(*),Dataout(*)
5870  PRINT #1;Segment(*)
5880  CHECK READ #1
5890  PROTECT File$,"Firetube"
5900  OUTPUT Key USING Pfmt5;File$
5910 Pfmt5: IMAGE L, "DATA RECORDED ON DISK: FILE NAME IS ",6A
5920  WRITE BIN Key;12
5930  BEEP
5940  INPUT "ANOTHER RUN? Yes=1, No=0",Yes_no
5950  IF Yes_no=1 THEN Rerun
5960  DISP "BYE FOR NOW"
5970  STOP
5980  END
5990  !
6000  !
6010  ! ------------------------------------------------------------------------
6020  !
6030  !       SUBROUTINE TO CALCULATE THE MASS FLOW RATE OF AIR
6040  !
6050  ! ------------------------------------------------------------------------
6060  !
6070 Orifice: !
6080  Dataout(1)=(1.3259*Datain(43)+.97527*Datain(38))/(Datain(32)+459.67)
6090  Dataout(2)=2.6866E-3*(Datain(32)+459.67)^1.5/(Datain(32)+658.37)
6100 Orifice_data1: !
6110  DATA 12.2525,7,15000,.02612,25000,.02601,35000,.02596,50000,.02591,75000,.
02585
6120  DATA 100000,.02582,150000,.02579
6130 Orifice_data2: !
6140  DATA 20.3718,6,15000,.00942,25000,.00938,35000,.00935,50000,.009325,75000,
.009305
6150  DATA 100000,.009295
6160  IF Or_key=1 THEN RESTORE Orifice_data1
6170  IF Or_key=2 THEN RESTORE Orifice_data2
6180  READ Re_cons,Or_num
6190  FOR I=1 TO Or_num
6200  READ Re_or(I),Cons_or(I)
6210  NEXT I
6220  Re=Re_or(1)
6230  Cons=Cons_or(1)
6240 Constant: Mass=12932.9505*Cons*SQR(Dataout(1)*Datain(39))
6250 Re_check=Re_cons*Mass/Dataout(2)
6260  IF ABS(Re_check-Re)<1 THEN RETURN
6270  FOR I=1 TO 6
6280  IF Re_check<Re_or(1) THEN Extrapolate
6290  IF Re_check>Re_or(I) THEN Interpolate
6300  NEXT I
6310 Interpolate: Cons=Cons_or(I)+(Re_check-Re_or(I))*(Cons_or(I+1)-Cons_or(I))/
(Re_or(I+1)-Re_or(I))
6320  Re=Re_check
6330  GOTO Constant
6340 Extrapolate: Cons=Cons_or(I)+(Re_check-Re_or(I))*(Cons_or(I+1)-Cons_or(I))/
(Re_or(I+1)-Re_or(I))
6350  Re=Re_check
6360  GOTO Constant
6370  !
6380  !
6390  !
6400  ! ------------------------------------------------------------------------
```

```
6410  !
6420  !       SUBROUTINE TO TAKE 10/20 READINGS AND FIND THE MEAN
6430  !          USING THE VOLTMETER INTERNAL PROGRAM MODE
6440  !
6450  ! ------------------------------------------------------------------------
6460  !
6470 Reading: !
6480   SET TIMEOUT 7;2000  ! If it hangs up
6490   ON INT #7,1 GOSUB Clear_dvm
6500   OUTPUT 722;"X1"
6510   St_ct=0  ! Timer set to zero
6520   STATUS 722;Status
6530   St_ct=St_ct+1 ! Timer counter
6540   IF St_ct>800 THEN REMOTE 722! If it misses the program execution end noti
ce
6550   IF St_ct>800 THEN 6500
6560   IF Status<>66 THEN 6520
6570   OUTPUT 722;"SO0REM"
6580   ENTER 722;Rdg
6590  RETURN
6600 Clear_dvm: !
6610  DISP "CLEARING VOLTMETER"
6620  CLEAR 722
6630  REMOTE 722
6640  IF Dvm=1 THEN OUTPUT 722;Dmm$(2)
6650  IF Dvm=2 THEN OUTPUT 722;Dmm$(3)
6660  OUTPUT 722;Dmm$(1)
6670  RETURN
6680  !
6690  !
6700  ! ------------------------------------------------------------------------
6710  !
6720  !       SUBROUTINE TO CALCULATE Nu, Re and Pr FOR EACH SEGMENT
6730  !
6740  ! ------------------------------------------------------------------------
6750  !
6760  !
6770  SUB Nusselt(Sub(*),Corr_nu,Rad_con,Area,Qr,T_ins)
6780  Sub(1)=Sub(3)
6790 Iterate: Avg_air_temp=(Sub(1)+Sub(3))/2+459.67
6800  Sub(4)=.2231+3.42E-5*Avg_air_temp-2.93E-9*Avg_air_temp^2
6810  IF ABS(Sub(1)-(Sub(3)+Sub(5)/Sub(4)/Sub(2)))<.1 THEN Done
6820  Sub(1)=Sub(3)+Sub(5)/Sub(4)/Sub(2)
6830  GOTO Iterate
6840 Done: Tb=(Sub(1)+Sub(3))/2+459.67
6850  Len_con=Sub(8)
6860  Sub(8)=Sub(8)*Sub(5)*LOG((Sub(3)-Sub(7))/(Sub(1)-Sub(6)))/.990256/(Sub(3)-
Sub(7)-(Sub(1)-Sub(6)))
6870  Sub(9)=1/(1/Sub(8)-.004783)
6880  T_in1=Tb
6890  T_ins=Tb-Rad_con/Sub(9)*(T_in1^4-((Sub(7)+Sub(6))/2+459.62)^4)
6900  IF ABS(T_in1-T_ins)<.1 THEN Done1
6910  T_in1=T_ins
6920  GOTO 6890
6930 Done1: Qr=Rad_con*(T_in1^4-((Sub(7)+Sub(6))/2+459.67)^4)*Area
6940  Qc=Sub(5)-Qr
6950  Sub(8)=Len_con*Qc*LOG((Sub(3)-Sub(7))/(Sub(1)-Sub(6)))/.990256/(Sub(3)-Sub
(7)-(Sub(1)-Sub(6)))
6960  Ha=1/(1/Sub(8)-.004783)
6970  IF ABS(Ha-Sub(9))<.01 THEN Done2
```

```
6980   Sub(9)=Ha
6990   GOTO 6880
7000 Done2: Sub(9)=Ha
7010   Sub(10)=1.3466E-2+2.2323E-5*(Sub(1)+Sub(3))/2
7020   Sub(11)=2.67*Sub(9)/12/Sub(10)
7030   Sub(12)=2.6286E-3*Avg_air_temp^1.5/(Avg_air_temp+198.7)
7040   Sub(13)=Sub(12)*Sub(4)/Sub(10)
7050   Sub(14)=5.722425*Sub(2)/Sub(12)
7060   Corr_nu=Sub(11)*(((Sub(6)+Sub(7))/2+459.67)/((Sub(1)+Sub(3))/2+459.67))^.4
5
7070   SUBEND
7080   !
```

IX. APPENDIX B: MEASUREMENT OF INSERT TEMPERATURE TO VERIFY ASSUMPTIONS MADE TO ESTIMATE RADIANT HEAT TRANSFER FROM THE INSERT

A. Measurement of Insert Temperature

As mentioned in the data-reduction procedure, the radiation heat transfer from the insert to the tube was estimated by using the following assumptions:

1. The convective heat transfer coefficient at the wall, h_a, is equal to the insert convective heat-transfer coefficient, h_i.
2. Under steady-state conditions, the convective heat transfer from the hot gas to the insert is equal to the radiation from the insert to the tube wall.
3. Axial heat conduction along the insert length is negligible.
4. Radiation from the hot gas to the wall or to the insert is negligible.

To verify whether these assumptions are valid, eleven 28 gage chromel/alumel thermocouples were attached to insert A6 at various axial locations to measure the insert temperature. Five of these thermocouples were attached at locations corresponding to the ends of the four calorimeter segments of the test section. The other six thermocouples were placed at different locations in the insert length corresponding to segment 3 of the test section. This was thus done to obtain a radial and axial average insert temperature in segment 3.

To attach the thermocouple to the insert at each location, a 0.125 in. diameter hole was drilled partway into the insert. The

thermocouple bead was then placed in the hole and was filled with silver solder. The lead wire was brought along the length of the insert for a few inches and then axially along the side of the insert towards the downstream end of the test section. Once all the thermocouples were attached to the insert, the insert was pushed into the test section. The eleven thermocouple lead wires were brought out from the test section between the teflon and asbestos spacer at the downstream test section end and connected to the thermocouple reference junction.

To permit measurement of the eleven extra thermocouples, a Hewlett Packard Scanner HP 3488A was used in addition to the other instrumentations described earlier. The standard heat-transfer experiments were conducted, and in addition the insert temperatures were also measured for 14 different air-side Reynolds numbers.

B. Results and Verification of Assumptions

Using the simple radiation model given in Equation 2.6, the radiant energy transfer from the insert to the wall in segment 3 was calculated. Figure B.1 compares the measured insert temperature and the estimated insert temperature on the basis of the assumptions given earlier and using Equation 2.8 given below.

$$q_{r,4} = \frac{\sigma(T_{i,4}^{4} - T_{s,4}^{4})\, A_i}{1/F_{i-s} + (1/\varepsilon_i - 1) + (1/\varepsilon_s - 1)(A_i/A_s)} \qquad (2.8)$$

The figure indicates that the actual insert temperature is about 22°F

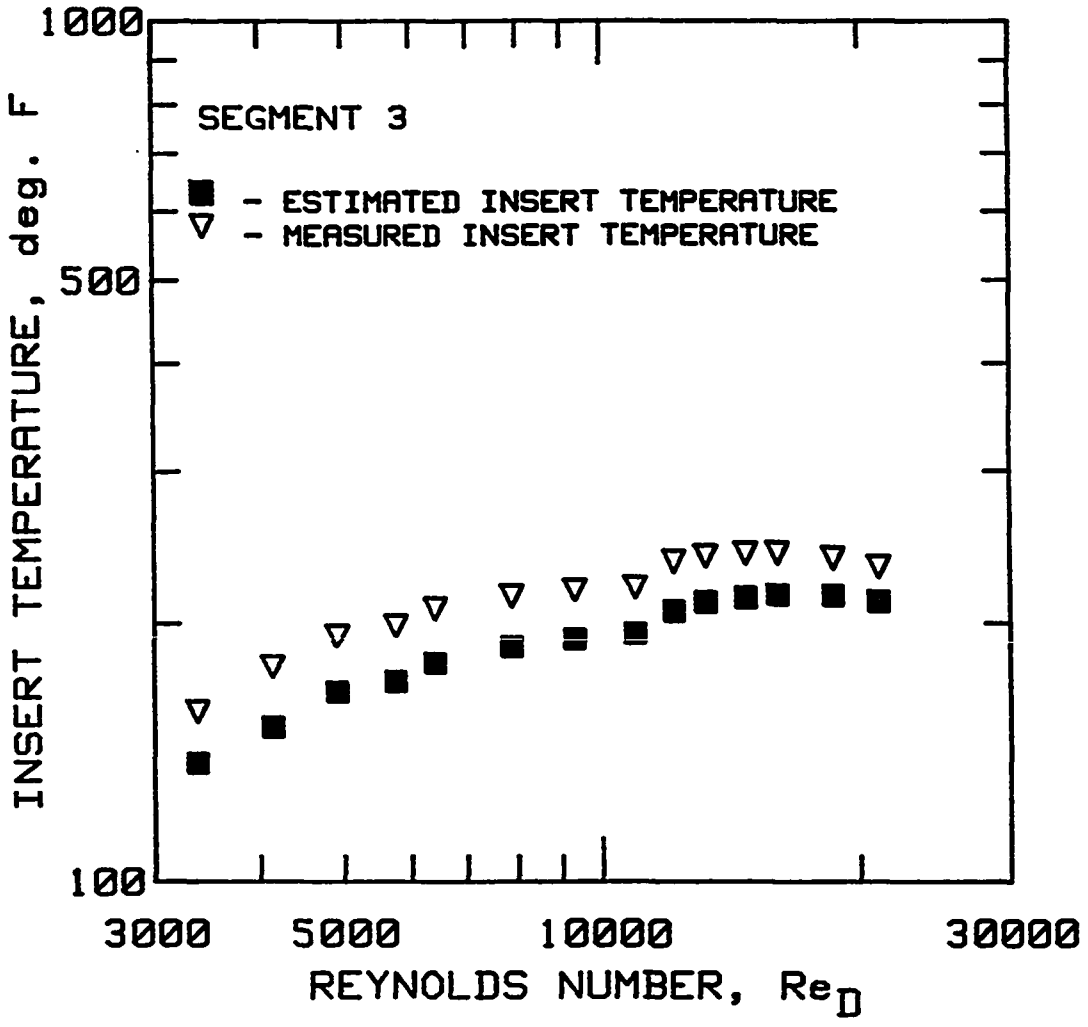

FIGURE B.1. Comparison of estimated and measured insert temperatures

higher than the estimated insert temperature. The apparent discontinuity in the data occur due to variation in inlet air temperature. In Figure B.2, the estimated and the measured components of radiant heat transfer are plotted as functions of Reynolds number. The figure shows that the estimation procedure based on the assumptions underpredicts the radiant component of energy transfer by about 30%. Again, the discontinuity in the data occurs due to the variation in inlet air temperature. This points out that radiation from the insert is strongly dependent on the air temperature. To obtain a better estimate of radiation heat transfer by using the same model, a more accurate estimate of the insert convective heat-transfer coefficent (and thereby insert temperature) is necessary. This is also confirmed by Beckermann (1984), who indicates that the variations in insert emissivity, ε_i, and shape factor, F_{i-s}, do not affect the radiant heat transfer appreciably. However, he points out that the radiant component of heat transfer is very much dependent on insert temperature.

Although there is a discrepancy of about 30% in the radiant heat-transfer component due to the assumptions made, this error affects the convective heat transfer component in this investigation by only about 1% to 2% as seen in Figures B.3. In the uncertainty analysis given in Appendix C, the uncertainty in the radiant component was assumed to be 50%. With this pessimistic assumption, the uncertainty in Nusselt number worked out to be about 6%. Therefore, in this experimental investigation, the radiant transfer from insert to the wall is not a major component of the energy transfer. The convective heat transfer

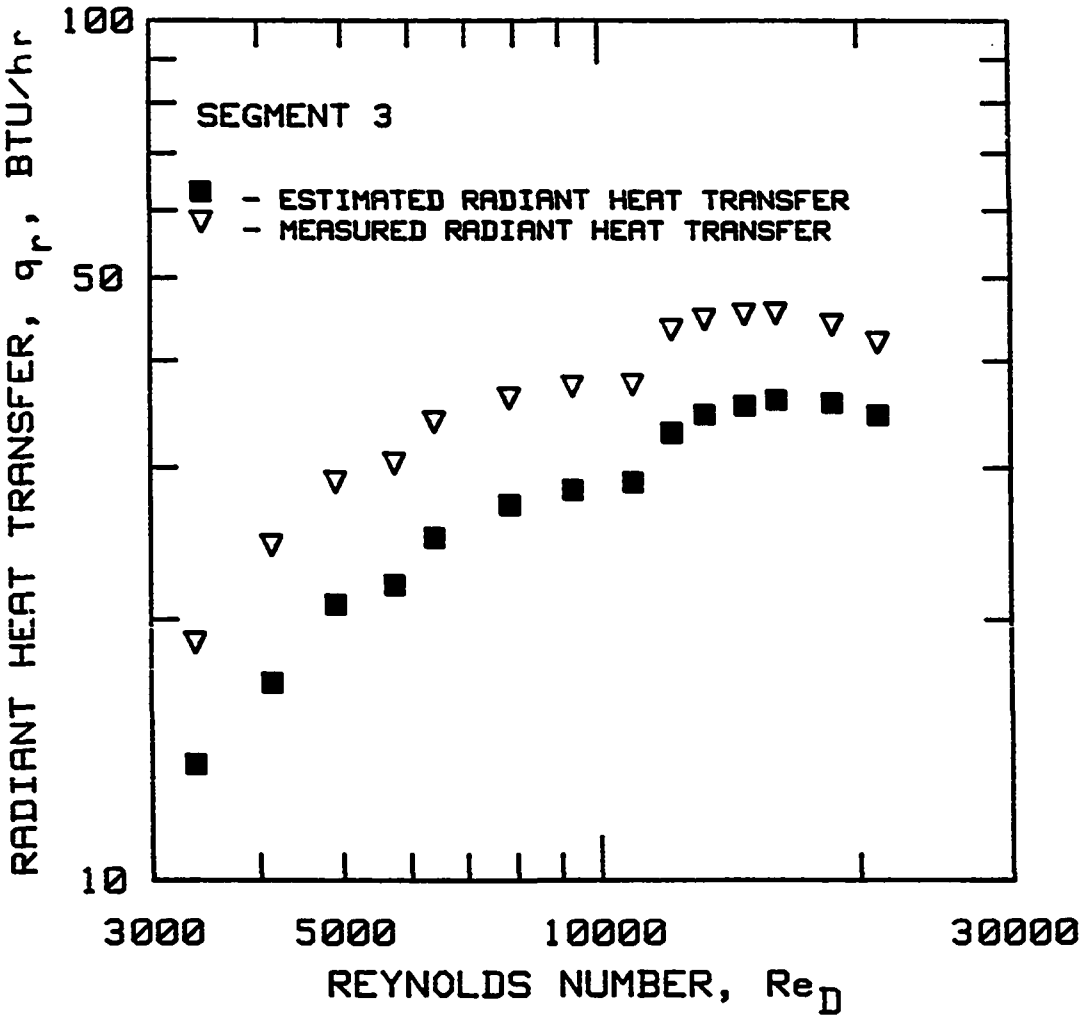

FIGURE B.2. Comparison of radiant heat transfer evaluated by estimation and measurement of insert temperature

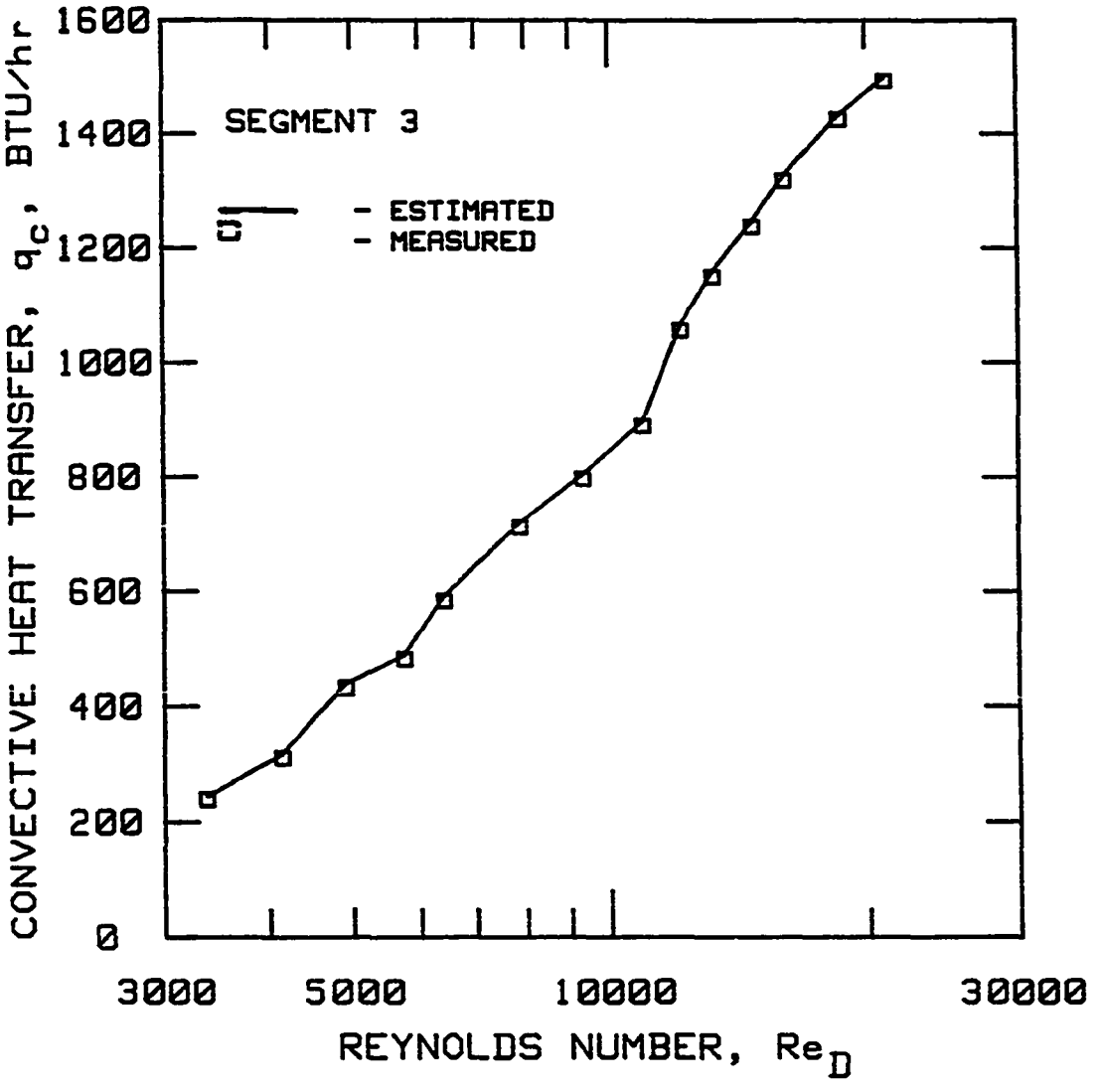

FIGURE B.3. Comparison of convective heat transfer evaluated by estimation and measurement of insert temperature

coefficients evaluated in study represent only the convective component of heat transfer from the hot gas to tube wall. Nevertheless, in actual fire-tube boiler type applications where the gas temperature could be as high as 1500°F, the radiant transfer from the insert would be considerably higher. This would further enhance the heat transfer from the hot gas to the tube wall in addition to the convective heat transfer enhancement obtained by using bent-strip inserts.

X. APPENDIX C: SAMPLE CALCULATION AND ERROR ANALYSIS

Given below are the equations used for the calculation of experimentally determined quantities necessary for the determination of the Nusselt number in one segment of the calorimeter as well as of the friction factor for the whole test section. Also included is an uncertainty analysis of each calculated quantity obtained by using the method of Kline and McClintock (1953).

The expression for the uncertainty W in a calculated result found from a linear function of variables is

$$W_Z = \left[\sum_{i=1}^{n} \left(\frac{\partial Z}{\partial x_i} W_{X_i} \right)^2 \right]^{\frac{1}{2}} \qquad (C.1)$$

where X_i is any of n parameters of which quantity Z is a function.

In the following calculations, the properties of water were calculated by using equations given by Morcos (1974). Morcos had given uncertainties in using his equations, and these values were used in the error analysis. It is also assumed that the uncertainties in the properties of air is ±1%. The measurement uncertainties used in this investigation are based primarily on manufacturers' specifications and in some cases from the calibration data. The following are the uncertainties in measured quantities:

air temperature = ±3°F

water temperature = ±0.2°F

wall temperature = ±0.2°F

water flow rate = ±0.75 lbm/hr

pressure = ±0.01 in. H_2O

The air density ρ_a at the orifice is calculated by using the equation

$$\rho_a = \frac{p_{atm} + p_{st}}{R\ T_{atm}} \tag{C.2}$$

which with conversion factors for compatible units becomes

$$\rho_a = \frac{70.731\ p_{atm} + 5.2024\ p_{st}}{53.35\ T_{atm}} \quad lbm/ft^3 \tag{C.3}$$

The uncertainty in ρ_a is given by

$$W_\rho = \frac{1}{53.35\ T_{atm}} \left[\left(70.731\ W_{p_{atm}}\right)^2 + \left(5.2024\ W_{p_{st}}\right)^2 + \left(\frac{(70.731\ p_{atm} + 5.2024\ p_{st})}{T_{atm}}\ W_{T_{atm}} \right)^2 \right]^{\frac{1}{2}} \tag{C.4}$$

p_{atm} = 28.985 in. Hg

p_{st} = 0.41 in. H_2O

T_{atm} = 78.96 °F

ρ_a = 0.07197 lbm/ft^3

W_{ρ_a} = 0.00012 lbm/ft^3

The mass-flow rate of air is calculated by using the following equation:

$$m_a = C_D \rho_a \left(\frac{\Delta p_{or}}{\rho_a} \right) \tag{C.5}$$

which with conversion factors for compatible units become

$$m_a = 12932.95\ C_D \sqrt{(\rho_a\ \Delta p_{or})} \tag{C.6}$$

Then, the uncertainty in m_a is given by

$$W_{m_a} = 12932.95 \left[\left(\sqrt{(\Delta p_{or} \rho_a)}\ W_{C_D} \right)^2 + \left(\frac{C_D}{2} \sqrt{\frac{\Delta p_{or}}{\rho_a}}\ W_{\rho_a} \right)^2 + \left(\frac{C_D}{2} \frac{\rho_a}{\Delta p_{or}} W_{\Delta p_{or}} \right)^2 \right]^{\frac{1}{2}} \tag{C.7}$$

$C_D = 0.02599$

$\Delta p_{or} = 1.249$ in. H_2O

$m_a = 100.75$ lbm/hr

$W_{m_a} = 2.06$ lbm/hr

The heat gained by water in a particular segment (in this case the fourth segment) of the calorimeter is

$$q_{w,4} = m_w\ c_{pw,4}\ (T_{w2,4} - T_{w1,4}) \tag{C.8}$$

and the uncertainty in heat gained by water is given by

$$W_{q_{w,4}} = \left[\left(m_w\, c_{pw,4}\, W_{\Delta T_{w,4}}\right)^2 + \left(c_{pw,4}\, \Delta T_{w,4}\, W_{m_w}\right)^2 + \left(m_w\, \Delta T_{w,4}\, W_{c_{pw,4}}\right)^2\right]^{\frac{1}{2}} \tag{C.9}$$

where $\Delta T_{w,4}$ is the temperature drop $(T_{w2,4} - T_{w1,4})$.

$m_w = 80.34$ lbm/hr

$c_{pw,4} = 1.0005$ BTU/lbm-°F

$\Delta T_{w,4} = 10.27$°F

$q_{w,4} = 825.44$ BTU/hr

$W_{q_{w,4}} = 33.06$ BTU/hr

The relation used to calculate heat gained by conduction by the first segment in the calorimeter is

$$q_{cd} = k_t\, A_t \left(\frac{\Delta T_t}{\Delta X}\right) \tag{C.10}$$

and the uncertainty in q_{cd} is given by

$$W_{q_{cd}} = \left[\left(\frac{k_t\, A_t}{\Delta X}\, W_{\Delta T_t}\right)^2 + \left(\frac{A_t\, \Delta T_t}{\Delta X}\, W_{k_t}\right)^2 + \left(\frac{k_t\, \Delta T_t}{\Delta X}\, W_{A_t}\right)^2 + \left(-\frac{k_t\, A_t\, \Delta T_t}{\Delta X}\, W_{A_t}\right)^2\right]^{\frac{1}{2}} \tag{C.11}$$

$k_t = 1.77$ BTU/hr-ft-°F

$A_t = 0.05$ ft^2

$\Delta T_t = 54.27$°F

$\Delta X = 1.0$ in.

$q_{cd} = 58.17$ BTU/hr

Assuming W_{k_t}, W_{A_t}, $W_{\Delta X} \lll W_{\Delta T}$

$W_{q_{cd}} = 0.62$ BTU/hr

Therefore, the actual heat gained by water from hot air in segment 4 is

$$q_{wc,4} = q_{w,4} - q_{cd} \tag{C.12}$$

and the uncertainty in $q_{wc,4}$ is given by

$$W_{q_{wc,4}} = W_{q_{w,4}} + W_{q_{cd}} \tag{C.13}$$

$q_{wc,4} = 767.28$ BTU/hr

$W_{q_{c,4}} = 33.68$ BTU/hr

The outlet air temperature for the first segment in the calorimeter was calculated by using the following equation:

$$T_{a1,4} = T_{a2,4} - \frac{q_{wc,4}}{c_{pa,4}\, m_a} \tag{C.14}$$

The uncertainty in $T_{a2,4}$ is given by

$$W_{T_{a1,4}} = \left[\left(W_{T_{a2,4}}\right)^2 + \left(\frac{1}{c_{pa,4}\, m_a} W_{q_{wc,4}}\right)^2 + \left(\frac{q_{wc,4}}{c_{pa,4} m_a^2} W_{m_a}\right)^2 + \left(- \frac{q_{wc,4}}{m_a\, c_{pa,4}^2} W_{c_{pa,4}}\right)^2\right]^{\frac{1}{2}} \quad (C.15)$$

$T_{a2,4} = 169.60°F$

$c_{pa,4} = 0.2439$ BTU/lbm-°F

$T_{a1,4} = 200.88°F$

$W_{T_{a2,4}} = 3.38°F$

The log-mean temperature difference is obtained by using the standard equation given below.

$$\Delta T_{LMTD} = \frac{\Delta T_1 - \Delta T_2}{\ell n\left(\frac{\Delta T_1}{\Delta T_2}\right)} = \frac{(T_{a1,4} - T_{t,4}) - (T_{a2,4} - T_{t,4})}{\ell n\left(\frac{T_{a1,4} - T_{t,4}}{T_{a2,4} - T_{t,4}}\right)} \quad (C.16)$$

The uncertainty in ΔT_{LMTD} is given by the expression

$$W_{\Delta T_{LMTD}} = \left\{\left[\frac{\ell n\left(\frac{\Delta T_1}{\Delta T_2}\right) - \left(\frac{\Delta T_1 - \Delta T_2}{\Delta T_1}\right)}{\left[\ell n\left(\frac{\Delta T_1}{\Delta T_2}\right)\right]^2} W_{\Delta T_1}\right]^2\right.$$

$$+\left[\frac{\left(\frac{\Delta T_1 - \Delta T_2}{\Delta T_2}\right) - \ell n\left(\frac{\Delta T_1}{\Delta T_2}\right)}{\left[\ell n\left(\frac{\Delta T_1}{\Delta T_2}\right)\right]^2} W_{\Delta T_2}\right]^2\Bigg\}^{\frac{1}{2}} \qquad \text{(C.17)}$$

$\Delta T_1 = 123.51°F$

$\Delta T_2 = 98.68°F$

$\Delta T_{LMTD} = 110.63°F$

$W_{\Delta T_{LMTD}} = 2.42°F$

The overall heat-transfer coefficient is calculated by using the expression

$$U = \frac{q_{wc,4} - q_{r,4}}{A_s \, \Delta T_{LMTD}} \qquad \text{(C.18)}$$

and the uncertainty in U is given by expression

$$W_U = \left[\left(\frac{1}{A_s \, \Delta T_{LMTD}} W_{(q_{wc,4}-q_{r,4})}\right)^2 + \left(\frac{-(q_{wc,4}-q_{r,4})}{A_s^2 \, \Delta T_{LMTD}} W_{A_s}\right)^2 + \left(\frac{-(q_{wc,4}-q_{r,4})}{A_s \, (\Delta T_{LMTD})^2} W_{\Delta T_{LMTD}}\right)^2\right]^{\frac{1}{2}} \qquad \text{(C.19)}$$

$A_s = 0.98 \text{ ft}^2$

$q_{r,4} = 22.31 \text{ BTU/hr}$

$U = 6.95 \text{ BTU/hr-ft}^2\text{-°F}$

Assuming a 50% uncertainty in $q_{r,4}$

$W_U = 0.43$ BTU/hr-ft^2-°F

The average heat-transfer coefficient in the first segment is calculated by

$$h_{a,4} = \left[\frac{1}{U} - \frac{D_i \ln\left(\frac{D_t}{D_i}\right)}{2k_s} \right]^{-1} \tag{C.20}$$

and the uncertainty in h_a is given by

$$W_{h_{a,4}} = \left[\left\{ \left(\frac{1}{U} - \frac{D_i \ln\left(\frac{D_t}{D_i}\right)}{2k_s} \right)^{-2} \left(\frac{-1}{U^2} \right) W_U \right\}^2 \right.$$

$$+ \left\{ \left(\frac{1}{U} - \frac{D_i \ln\left(\frac{D_t}{D_i}\right)}{2k_s} \right)^{-2} (-) \frac{\ln\left(\frac{D_t}{D_i}\right)(-) D_i^2}{2k_s} W_{D_i} \right\}^2$$

$$+ \left\{ \left(\frac{1}{U} - \frac{D_i \ln\left(\frac{D_t}{D_i}\right)}{2k_s} \right)^{-2} \frac{D_i}{2k_s D_t} W_D \right\}^2$$

$$\left. + \left\{ \left(\frac{1}{U} - \frac{D_i \ln\left(\frac{D_t}{D_i}\right)}{2k_s} \right)^{-2} (-) \frac{D_i \ln\left(\frac{D_t}{D_i}\right)}{2k_s} W_{k_s} \right\}^2 \right]^{\frac{1}{2}} \tag{C.21}$$

$D_i = 2.67$ in.

$D_t = 2.80$ in.

$k_s = 25$ BTU/hr-ft-°F

$h_{a,4} = 6.98$ BTU/hr-ft²-°F

$W_{h_{a,4}} = 0.43$ BTU/hr-ft²-°F

As explained in the data reduction procedure,

$$q_{r,4} = \frac{\sigma A_i (T_{i,4}^4 - T_{s,4}^4)}{1/F_{i-s} + (1/\varepsilon_i - 1) + (1/\varepsilon_s - 1)(A_i/A_s)} \qquad (C.22)$$

$$q_{ci,4} = h_{i,4} A_i (T_{b,4} - T_{i,4}) = q_{r,4} \qquad (C.23)$$

$\sigma = 0.1712 \times 10^{-8}$ BTU/hr-ft²-°R⁴

$F_{i-s} = 0.964$

$\varepsilon_i = 0.7$

$\varepsilon_s = 0.9$

$A_i = 0.2484$ ft²

$A_s = 1.0413$ ft²

$T_{b,4} = 185.24°F = 644.91°R$

$T_{s,4} = 74.18°F = 553.85°R$

$T_{i,4} = 632.03°R = 172.36°F$

$q_{r,4} = 22.31$ BTU/hr

The Nusselt number is obtained by using the standard definition and is given by

$$Nu_{D,4} = \frac{h_{a,4} D_i}{k_{a,4}} \tag{C.24}$$

The uncertainty in $Nu_{D,4}$ is obtained by using the following expression:

$$W_{Nu_{D,4}} = \left[\left(\frac{D_i}{k_{a,4}} W_{h_{a,4}}\right)^2 + \left(\frac{h_{a,4}}{k_{a,4}} W_{D_i}\right)^2 + \left(\frac{h_{a,4} D_i}{k_{a,4}^2} W_{k_{a,4}}\right)^2\right]^{\frac{1}{2}} \tag{C.25}$$

$k_{a,4} = 0.0176$ BTU/hr-ft-°F

$Nu_{D,4} = 88.18$

$W_{Nu_{D,4}} = 5.58$

The airside Reynolds number in the fourth segment is calculated by using

$$Re_{D,4} = \frac{4m_a}{\pi \mu_{a,4} D_i} \tag{C.26}$$

and the uncertainty in $Re_{D,4}$ is given by

$$W_{Re_{D,4}} = \frac{4}{\pi}\left[\left(\frac{1}{\mu_{a,4} D_i} W_{m_a}\right)^2 + \left(\frac{-m_a}{\mu_{a,4} D_i^2} W_{D_i}\right)^2 + \left(\frac{-m_a}{\mu_{a,4}^2 D_i} W_{\mu_{a,4}}\right)^2\right]^{\frac{1}{2}} \tag{C.27}$$

$\mu_{a,4} = 0.05103$ lbm/ft-hr

$Re_{D,4} = 11298$

$W_{Re_{D,4}} = 290$

This process of calculation is repeated by using the inlet air temperature at one segment as the outlet air temperature for the next segment (i.e., $T_{a2,3} = T_{a1,4}$). The second and third segments have no conduction correction; however, heat gain by the coolant in the first segment requires a conduction correction similar to that used for the fourth segment. By using a similar calculating procedure as given in Equations C.8 to C.27, the following values of Nusselt numbers, Reynolds numbers, and the respective uncertainties were calculated:

$$Nu_{D,3} = 82.02, \qquad W_{Nu_{D,3}} = 4.68$$

$$Re_{D,3} = 10882, \qquad W_{Re_{D,3}} = 280$$

$$Nu_{D,2} = 76.62, \qquad W_{Nu_{D,2}} = 4.56$$

$$Re_{D,2} = 10447, \qquad W_{Re_{D,2}} = 269$$

$$Nu_{D,1} = 70.80, \qquad W_{Nu_{D,1}} = 4.50$$

$$Re_{D,1} = 9989, \qquad W_{Re_{D,1}} = 258$$

The pressure drop across the calorimeter is calculated in two steps. First, by knowing the inlet and outlet air temperature, the pressure rise due to temperature drop is calculated by

$$\Delta p_c = \frac{1}{g_c} \left(\frac{m_a}{A_x}\right)^2 \left(\frac{1}{\rho_{a1}} - \frac{1}{\rho_{a2}}\right) \qquad (C.28)$$

and the uncertainty in Δp_c is given by the following expression:

$$W_{\Delta p_c} = \frac{1}{A_x g_c}\left\{\left[2m_a W_{m_a}\left(\frac{1}{\rho_{a1}} - \frac{1}{\rho_{a2}}\right)\right]^2 + \left[\frac{-m_a^2}{\rho_{a1}^2} W_{\rho_{a2}}\right]^2 + \left[\frac{-m_a^2}{\rho_{a2}^2} W_{\rho_{a2}}\right]^2\right\}^{\frac{1}{2}} \quad \text{(C.29)}$$

$\rho_{a1} = 0.0487$ lbm/ft^3

$\rho_{a2} = 0.0611$ lbm/ft^3

$g_c = 32.174 \times 3600^2$ ft/hr^2

$\Delta p_c = 0.013$ in. H_2O

$W_{\Delta p_c} = 0.003$ in. H_2O

The actual friction pressure drop is calculated by adding the measured pressure drop to the pressure rise due to momentum:

$$\Delta p_f = \Delta p + \Delta p_c \quad \text{(C.30)}$$

The uncertainty in Δp_f is given by

$$W_{\Delta p_f} = W_{\Delta p} + W_{\Delta p_c} \quad \text{(C.31)}$$

$\Delta p = 0.203$ in. H^2O

$\Delta p_f = 0.216$ in. H^2O

$W_{\Delta p_f} = 0.013$ in. H^2O

The Fanning friction factor is calculated by using the expression

$$f = \frac{8\,\Delta p_f}{g_c(\rho_{am}/2)^2 u_m^2}\,\frac{D_i}{L_t} = \frac{\pi^2\,\Delta p_f\,\rho_{am}\,D_i^5}{16\,m_a^2\,L_t} \qquad (C.32)$$

The uncertainty in f is given by

$$W_f = \frac{\pi^2}{16}\left[\left(\frac{\rho_{am}D_i^5}{m_a^2 L_t} W_{\Delta p_f}\right)^2 + \left(\frac{\Delta p_f D_i^5}{m_a^2 L_t} W_{\rho_{am}}\right)^2 + \left(\frac{\Delta p_f \rho_{am}\,5D_i^4}{m_a^2 L_t} W_{D_i}\right)^2 + \left(\frac{-\Delta p_f \rho_{am} D_i^5}{m_a^2 L_t^2} W_{L_t}\right)^2 + \left(\frac{-2\Delta p_f \rho_{am} D_i^5}{m_a^3 L_t} W_{m_a}\right)^2\right]^{\frac{1}{2}} \qquad (C.33)$$

$\rho_{am} = 0.0548$ lbm/ft^3

$L_t = 71$ in.

$f = 0.071$

$W_f = 0.004$

XI. APPENDIX D. CALCULATIONS OF ANGLES REQUIRED FOR FABRICATING THE INSERTS

Inserts A1, AN, and PA were made by a commercial manufacturer. To fabricate similar inserts with different pitches and widths, the relationship between pitch, L, twist angle, γ, longitudinal angle, ϕ, bending angle, α, and bending line angle, θ, were required.

Figure D.1 shows the three-dimensional view of the insert at the bend. Figure D.2 shows the plan view and Figure D.3 is view of the section ZZ marked in Figure D.2. The vertical plane passing through BFC in Figure D.1 is shown in Figure D.4.

Considering Figure D.2,

$$BA = 2BE = W_A/\sin(\theta) \tag{D.1}$$

where W_A is the apparent width, which is equal to W $\sin(\gamma)$.

Again, in Figure D.2,

$$EG = BE \tan(\theta)$$

Substituting for BE from Equation D.1,

$$EG = (W_A/2\sin\theta) \tan\theta = W_A/2\cos\theta \tag{D.2}$$

In Figure D.2,

$$BG = BE/\cos\theta$$

substituting for BE from Equation D.1,

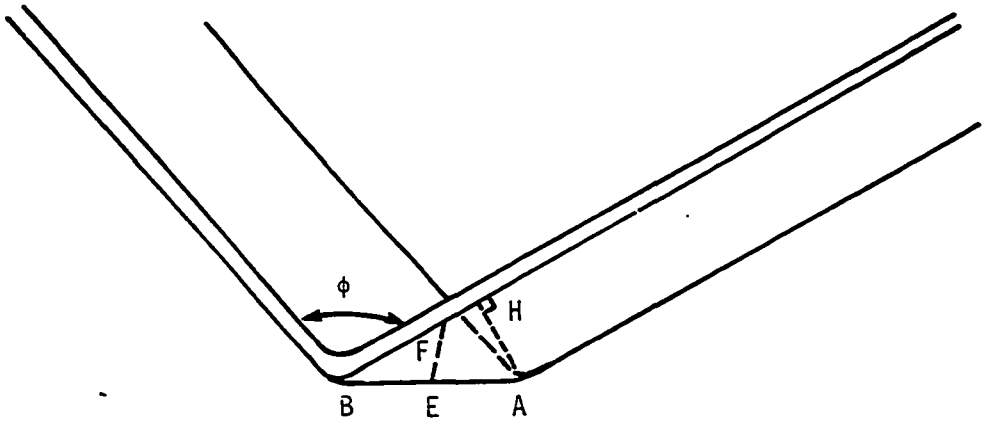

FIGURE D.1. Isometric view of the insert at a bend

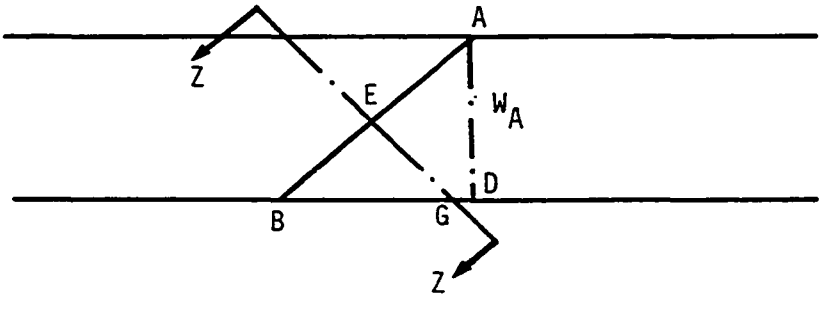

FIGURE D.2. Plan view of insert at a bend

$$BG = W_A/(2\cos\theta \sin\theta) \tag{D.3}$$

From Figure D.4,

$$FG = BG \tan\beta = W_A \tan\beta/(2\cos\theta \sin\theta) \tag{D.4}$$

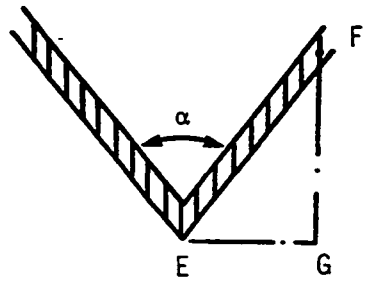

FIGURE D.3. View of section ZZ

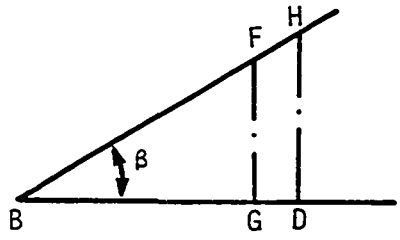

FIGURE D.4. View of vertical plane passing through BFC

Considering Figure D.3,

$$\tan(\mu) = FG/EG$$

Substituting for FG and EG from Equations D.4 and D.2, respectively,

$$\tan(\mu) = \frac{W_A \tan\beta/(2\cos\theta \sin\theta)}{W_A/(2\cos\theta)} = \frac{\tan\beta}{\sin\theta} \qquad (D.5)$$

But $\mu = 90-\alpha/2$ and $\beta = 90-\beta/2$, which gives the relationship between α, ϕ, and θ; thus

$$\cot(\alpha/2) = \frac{\cot(\phi/2)}{\sin(\theta)}$$

or

$$\tan(\alpha/2) = \sin(\theta)\,\tan(\phi/2) \qquad (D.6)$$

Figure D.5 shows the vertical plane passing through AD in Figure D.1. Point D in Figure D.5 is the same point D in Figure D.4.

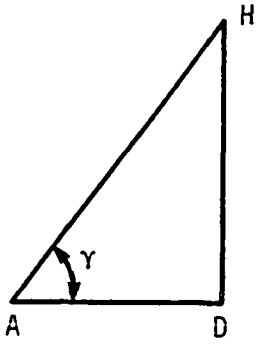

FIGURE D.5. View of vertical plane passing through AD

Considering Figure D.5,

$$\tan(\gamma) = HD/AD \qquad (D.7)$$

From Figure D.4,

$$HD = BD\,\tan\beta$$

and from Figure D.2,

$$AD = BD \tan\theta$$

Substituting for HD and AD in Equation D.7,

$$\tan(\gamma) = \frac{\tan(\beta)}{\tan(\theta)}$$

But since $\beta = 90-\phi/2$, the relationship between γ, θ, and θ is given as

$$\tan(\theta) = \frac{1}{\tan(\gamma)\ \tan(\phi/2)} \qquad (D.8)$$

The design procedure is as follows. For a particular pitch, L, the longitudinal angle ϕ can be calculated from

$$\phi/2 = \tan^{-1}(L/2D)$$

For the value of ϕ and a given twist angle, γ, the bending line angle, θ, is calculated using Equation D.6. Using this value of θ and the value of ϕ, the bending angle, α, is calculated by using Equation D.8.

To fabricate the inserts, markings at distances of $(L/2)/\sin(\phi/2)$ on a metal strip are made at angle of θ with the strip edge (as shown by line BA in Figure D.2). Then, the metal strip is bent at that line through an angle of $180-\alpha$. It should be noted that at every other marking, the strip is bent in the opposite direction.

XII. APPENDIX E: HEAT-TRANSFER AND PRESSURE-DROP DATA

Original data is available from the Heat Transfer Laboratory, Department of Mechanical Engineering, Iowa State University, Ames.

INSERT DESIGNATION: A1

SEGMENT 1			SEGMENT 2		
Re	Nu	Ts/Tb	Re	Nu	Ts/Tb
6212.2	51.25	0.768	6536.9	63.95	0.801
7571.5	59.97	0.771	7941.9	72.94	0.800
8792.0	66.49	0.761	9215.2	80.02	0.791
10128.5	73.26	0.759	10597.5	87.61	0.786
11440.4	80.65	0.763	11946.6	95.12	0.786
12722.3	87.30	0.765	13262.7	101.84	0.786
13637.8	91.37	0.766	14201.9	106.99	0.786
15264.3	99.13	0.773	15855.5	115.05	0.792
17828.4	111.64	0.771	18492.7	127.15	0.787
19599.6	119.70	0.763	20328.1	135.13	0.780

SEGMENT 3			SEGMENT 4		
Re	Nu	Ts/Tb	Re	Nu	Ts/Tb
6848.2	66.70	0.835	7124.1	70.57	0.866
8299.5	75.73	0.830	8623.5	79.49	0.858
9625.1	84.36	0.822	9998.3	87.57	0.851
11054.2	91.26	0.815	11476.1	95.61	0.842
12440.6	98.21	0.812	12902.7	103.24	0.837
13792.0	104.71	0.810	14293.3	110.72	0.833
14758.2	109.56	0.808	15288.7	116.15	0.830
16436.0	118.31	0.813	16991.9	125.68	0.834
19147.5	130.89	0.806	19780.4	137.35	0.826
21049.1	141.02	0.799	21750.4	147.09	0.819

INSERT DESIGNATION: AN

SEGMENT 1			SEGMENT 2		
Re	Nu	Ts/Tb	Re	Nu	Ts/Tb
5835.0	45.71	0.760	6138.3	59.16	0.794
7506.0	54.59	0.761	7865.9	69.67	0.790
8776.2	60.75	0.760	9173.6	75.97	0.787
10207.0	67.17	0.765	10638.4	83.80	0.788
11421.5	73.27	0.765	11890.3	90.84	0.787
12735.1	79.13	0.779	13212.6	97.84	0.796
13825.8	83.85	0.771	14343.4	101.89	0.791
14993.9	87.88	0.781	15516.6	107.90	0.797
17824.9	101.19	0.775	18431.0	121.21	0.791
19840.8	109.46	0.772	20498.7	129.53	0.788

SEGMENT 3			SEGMENT 4		
Re	Nu	Ts/Tb	Re	Nu	Ts/Tb
6434.2	61.66	0.830	6693.3	63.43	0.862
8222.4	72.68	0.822	8545.1	75.75	0.851
9570.7	80.32	0.817	9937.4	83.31	0.844
11073.0	87.79	0.815	11478.4	90.83	0.840
12362.3	94.68	0.813	12807.5	99.93	0.837
13699.5	101.30	0.817	14165.0	105.53	0.836
14860.1	104.71	0.813	15348.3	109.52	0.835
16048.1	110.72	0.816	16558.7	115.85	0.835
19042.4	124.75	0.810	19634.9	131.63	0.828
21164.6	135.40	0.807	21811.4	140.44	0.825

INSERT DESIGNATION: A2

SEGMENT 1			SEGMENT 2		
Re	Nu	Ts/Tb	Re	Nu	Ts/Tb
5913.2	42.82	0.752	6187.3	44.81	0.781
7507.0	50.73	0.752	7829.0	51.93	0.776
8774.3	56.36	0.755	9126.8	57.31	0.775
10117.4	61.82	0.755	10502.9	62.43	0.773
11375.8	67.68	0.755	11793.7	67.39	0.772
12654.5	72.22	0.758	13095.6	72.14	0.773
13783.2	76.61	0.760	14247.0	76.28	0.773
15234.4	82.73	0.757	15737.1	82.07	0.772
17699.0	92.67	0.756	18257.8	90.41	0.769
19494.0	99.01	0.755	20092.7	96.09	0.766

SEGMENT 3			SEGMENT 4		
Re	Nu	Ts/Tb	Re	Nu	Ts/Tb
6436.3	46.94	0.810	6668.0	49.70	0.837
8124.3	54.52	0.801	8404.6	57.24	0.826
9453.2	59.83	0.797	9767.1	62.79	0.819
10863.0	65.81	0.793	11211.5	68.00	0.814
12183.3	70.80	0.791	12562.4	73.12	0.811
13510.6	75.66	0.790	13918.7	78.46	0.808
14683.4	79.16	0.788	15115.5	83.04	0.805
16205.8	84.77	0.788	16666.7	88.92	0.806
18780.3	93.72	0.783	19298.5	97.62	0.799
20655.1	100.25	0.780	21216.9	104.59	0.795

INSERT DESIGNATION: A5

SEGMENT 1			SEGMENT 2		
Re	Nu	Ts/Tb	Re	Nu	Ts/Tb
5848.4	41.96	0.746	6119.4	42.63	0.772
7087.9	47.87	0.745	7395.3	47.33	0.767
8585.7	54.74	0.744	8933.6	52.82	0.764
9944.5	59.95	0.748	10318.9	57.77	0.766
11246.8	65.16	0.756	11641.7	62.29	0.770
12583.3	70.62	0.763	12997.5	66.88	0.775
13761.8	76.42	0.761	14213.7	73.05	0.772
15054.6	80.19	0.758	15532.0	76.02	0.768
17551.2	90.42	0.756	18088.0	84.77	0.766
19567.0	97.74	0.759	20138.4	91.49	0.768

SEGMENT 3			SEGMENT 4		
Re	Nu	Ts/Tb	Re	Nu	Ts/Tb
6370.6	46.51	0.798	6609.8	47.02	0.823
7679.9	51.56	0.791	7953.9	51.87	0.814
9256.2	57.85	0.785	9570.9	58.01	0.807
10668.5	63.19	0.785	11011.5	63.28	0.805
12012.7	68.32	0.787	12381.1	68.42	0.804
13388.5	73.32	0.789	13779.0	72.97	0.805
14644.5	79.45	0.784	15076.8	79.04	0.798
15985.5	82.70	0.781	16443.2	83.14	0.795
18593.4	90.69	0.777	19105.6	92.63	0.790
20678.4	97.73	0.778	21229.0	100.47	0.790

INSERT DESIGNATION: A4

SEGMENT 1			SEGMENT 2		
Re	Nu	Ts/Tb	Re	Nu	Ts/Tb
5886.8	46.18	0.752	6216.8	65.94	0.791
7224.4	52.85	0.749	7609.8	76.08	0.783
8573.4	59.45	0.745	9009.3	83.71	0.776
9996.0	67.00	0.753	10469.5	93.21	0.780
11240.0	73.22	0.758	11745.2	101.43	0.783
12526.9	79.04	0.765	13056.2	108.66	0.787
13793.7	85.25	0.770	14348.9	115.47	0.790
15220.6	91.36	0.780	15788.6	123.29	0.800
17888.8	103.81	0.775	18539.0	137.19	0.793
19657.1	111.77	0.774	20355.4	145.79	0.790

SEGMENT 3			SEGMENT 4		
Re	Nu	Ts/Tb	Re	Nu	Ts/Tb
6555.2	71.58	0.832	6852.0	76.31	0.869
8016.5	82.11	0.819	8384.9	87.13	0.853
9469.7	91.92	0.814	9890.4	96.06	0.847
10973.2	100.65	0.811	11443.9	106.12	0.841
12286.6	108.64	0.810	12799.3	114.76	0.838
13626.6	116.04	0.811	14173.3	122.37	0.836
14945.8	122.84	0.812	15524.7	130.62	0.835
16395.4	131.33	0.822	16980.7	139.52	0.844
19233.7	146.32	0.813	19909.5	153.72	0.834
21103.2	156.59	0.810	21837.2	164.19	0.830

INSERT DESIGNATION: A3

SEGMENT 1			SEGMENT 2		
Re	Nu	Ts/Tb	Re	Nu	Ts/Tb
5946.0	42.62	0.747	6262.3	62.14	0.782
7264.9	49.95	0.747	7630.8	70.94	0.778
8527.2	55.76	0.747	8935.1	78.65	0.775
9921.7	63.13	0.745	10379.5	87.24	0.773
11235.7	68.22	0.752	11719.7	94.50	0.776
12646.5	74.42	0.756	13162.3	101.62	0.778
13714.4	79.67	0.758	14256.4	107.02	0.780
15056.5	85.94	0.757	15644.0	115.76	0.776
17404.6	96.04	0.751	18067.0	126.24	0.770
19439.4	103.65	0.762	20121.2	135.22	0.779

SEGMENT 3			SEGMENT 4		
Re	Nu	Ts/Tb	Re	Nu	Ts/Tb
6593.5	65.76	0.820	6887.5	69.90	0.856
8018.8	76.02	0.812	8375.8	81.29	0.845
9369.9	84.28	0.807	9770.5	87.63	0.839
10860.5	91.04	0.804	11305.7	96.62	0.834
12232.5	97.87	0.804	12713.2	104.26	0.831
13709.6	105.92	0.804	14228.0	112.39	0.830
14827.5	111.16	0.805	15368.6	117.41	0.830
16271.5	120.62	0.799	16878.0	128.85	0.822
18770.3	133.86	0.794	19447.1	139.74	0.818
20846.5	143.64	0.801	21548.5	149.41	0.823

INSERT DESIGNATION: A6

SEGMENT 1			SEGMENT 2		
Re	Nu	Ts/Tb	Re	Nu	Ts/Tb
2953.7	30.93	0.776	3138.0	35.67	0.818
3674.4	35.76	0.771	3888.4	39.22	0.808
4430.6	38.96	0.762	4675.8	43.65	0.796
5261.9	44.06	0.757	5543.7	49.45	0.790
5826.4	47.28	0.744	6145.6	53.99	0.779
5972.3	48.98	0.751	6292.9	54.94	0.782
6975.0	53.76	0.767	7309.4	61.08	0.789
7136.1	54.41	0.744	7501.2	61.24	0.775
8570.8	64.06	0.746	8989.2	69.50	0.773
9989.3	70.80	0.747	10447.9	76.62	0.772
11193.6	76.64	0.752	11679.8	82.58	0.775
12511.2	83.96	0.758	13028.0	88.97	0.777
13671.2	89.48	0.768	14200.0	94.52	0.783
15190.1	97.29	0.764	15766.5	101.97	0.784
17641.9	109.34	0.765	18282.6	112.52	0.781
19693.9	119.04	0.766	20383.2	121.31	0.781

SEGMENT 3			SEGMENT 4		
Re	Nu	Ts/Tb	Re	Nu	Ts/Tb
3297.1	36.27	0.857	3428.6	38.35	0.890
4075.3	40.71	0.844	4239.3	44.72	0.877
4901.5	47.57	0.831	5108.8	52.44	0.864
5803.3	51.99	0.823	6043.7	58.37	0.854
6444.4	58.50	0.815	6718.7	63.14	0.849
6593.6	59.24	0.814	6874.0	64.18	0.846
7635.1	65.35	0.814	7950.6	71.45	0.840
7846.6	66.18	0.807	8170.1	71.37	0.840
9381.6	74.35	0.803	9755.2	80.59	0.832
10882.0	82.02	0.800	11298.2	88.18	0.828
12143.7	88.00	0.799	12592.8	94.70	0.825
13521.9	94.67	0.799	14005.3	101.82	0.822
14713.3	100.56	0.801	15225.5	108.35	0.820
16311.5	108.88	0.806	16842.8	116.89	0.829
18892.5	120.18	0.800	19495.9	128.33	0.821
21035.9	128.29	0.799	21683.5	137.93	0.819

INSERT DESIGNATION: A7

SEGMENT 1			SEGMENT 2		
Re	Nu	Ts/Tb	Re	Nu	Ts/Tb
3008.6	31.10	0.782	3184.1	34.86	0.826
3700.0	35.37	0.784	3900.2	40.12	0.822
4546.8	40.92	0.781	4779.8	45.51	0.815
5349.6	46.84	0.783	5611.8	51.12	0.814
6020.9	48.42	0.786	6294.9	55.37	0.815
6197.4	49.94	0.790	6472.8	55.47	0.816
7271.8	55.28	0.798	7565.3	60.88	0.819
7427.9	56.35	0.787	7743.6	62.80	0.809
8684.5	62.32	0.771	9056.2	68.93	0.795
10111.0	70.34	0.767	10526.8	74.26	0.790
11299.2	76.78	0.761	11764.5	81.38	0.783
12523.7	82.25	0.759	13026.0	87.15	0.779
13789.0	88.05	0.758	14324.3	92.39	0.777
15017.2	93.72	0.758	15586.5	98.37	0.776
17549.4	104.31	0.759	18176.4	108.25	0.775
19682.1	114.90	0.762	20356.1	117.10	0.777

SEGMENT 3			SEGMENT 4		
Re	Nu	Ts/Tb	Re	Nu	Ts/Tb
3336.9	39.41	0.866	3466.1	41.10	0.901
4081.0	44.65	0.857	4238.4	45.98	0.890
4991.1	49.91	0.849	5177.4	50.79	0.880
5851.2	55.56	0.844	6066.4	56.46	0.872
6554.6	60.81	0.844	6793.0	63.21	0.871
6732.4	60.52	0.842	6971.6	61.93	0.868
7846.0	66.46	0.842	8110.8	68.37	0.865
8047.9	68.30	0.833	8335.9	70.38	0.856
9412.7	74.94	0.820	9748.2	76.56	0.846
10923.6	82.00	0.813	11305.8	84.00	0.837
12208.2	88.76	0.807	12632.6	90.06	0.831
13508.7	94.84	0.802	13974.1	96.35	0.824
14838.8	100.23	0.799	15338.8	102.31	0.820
16135.2	106.02	0.796	16668.7	107.68	0.817
18780.0	116.15	0.794	19371.0	118.14	0.813
21002.3	125.35	0.794	21638.7	127.92	0.812

INSERT DESIGNATION: A8

SEGMENT 1			SEGMENT 2		
Re	Nu	Ts/Tb	Re	Nu	Ts/Tb
2947.4	24.86	0.771	3098.2	28.48	0.806
3695.4	29.43	0.768	3873.3	32.17	0.797
4460.2	33.84	0.765	4664.7	35.54	0.790
5240.8	38.28	0.758	5477.4	39.73	0.783
5834.3	41.11	0.749	6094.9	41.91	0.773
6067.4	42.22	0.760	6325.4	43.48	0.781
6987.7	46.62	0.762	7269.3	47.56	0.781
7159.5	46.47	0.746	7456.1	46.84	0.768
8590.6	52.28	0.752	8915.6	52.41	0.770
10104.3	58.66	0.759	10458.2	58.05	0.774
11262.5	63.49	0.762	11639.2	62.28	0.775
12618.6	68.95	0.770	13014.2	67.35	0.780
14206.7	74.82	0.791	14598.9	73.45	0.799
15413.4	81.44	0.781	15853.1	77.81	0.790
17789.3	90.31	0.776	18283.6	85.41	0.784
19779.8	98.51	0.769	20326.6	91.24	0.778

SEGMENT 3			SEGMENT 4		
Re	Nu	Ts/Tb	Re	Nu	Ts/Tb
3236.9	30.62	0.841	3361.4	33.25	0.873
4038.2	34.65	0.828	4190.9	36.83	0.857
4855.0	38.58	0.817	5036.5	41.28	0.844
5696.6	42.71	0.809	5906.1	45.63	0.836
6335.8	44.84	0.798	6568.2	48.01	0.825
6567.9	46.95	0.805	6804.4	50.21	0.829
7536.0	51.39	0.801	7799.4	54.79	0.824
7732.6	50.66	0.792	8003.2	54.13	0.817
9222.2	56.29	0.790	9526.6	60.08	0.812
10792.2	62.15	0.791	11124.3	65.30	0.811
11995.1	66.36	0.791	12353.5	70.75	0.808
13389.7	71.53	0.794	13768.8	75.58	0.810
14975.2	78.29	0.811	15356.7	81.85	0.824
16268.8	83.31	0.802	16689.3	86.54	0.816
18751.0	91.40	0.795	19225.7	94.88	0.809
20839.2	97.79	0.789	21361.4	101.79	0.803

INSERT DESIGNATION: A9

SEGMENT 1			SEGMENT 2		
Re	Nu	Ts/Tb	Re	Nu	Ts/Tb
2800.9	32.02	0.741	3013.3	36.00	0.795
3583.2	37.70	0.740	3830.8	40.41	0.787
4283.9	41.45	0.733	4567.5	45.66	0.776
5157.8	46.37	0.732	5477.2	51.36	0.772
5638.5	49.06	0.727	6035.3	55.22	0.765
5980.4	51.07	0.730	6332.8	56.18	0.768
6962.5	57.13	0.731	7354.7	62.60	0.766
7113.5	58.59	0.729	7517.5	63.70	0.763
8526.3	68.16	0.730	8987.8	72.29	0.762
9858.6	75.76	0.733	10361.7	79.67	0.763
10950.6	82.50	0.739	11485.2	86.07	0.767
12010.4	89.32	0.747	12570.5	92.69	0.772
13742.3	96.43	0.744	14350.4	98.77	0.767
14924.6	102.24	0.743	15570.6	104.99	0.765
17600.4	115.84	0.753	18299.7	116.91	0.771
19540.4	125.18	0.761	20267.0	125.35	0.777

SEGMENT 3			SEGMENT 4		
Re	Nu	Ts/Tb	Re	Nu	Ts/Tb
3191.5	37.03	0.842	3340.3	41.69	0.882
4042.3	42.67	0.829	4228.2	47.93	0.868
4823.1	50.44	0.818	5055.0	55.43	0.857
5766.6	55.00	0.811	6030.7	60.97	0.848
6360.3	61.42	0.804	6660.3	65.42	0.841
6658.0	61.48	0.805	6960.5	67.37	0.842
7719.2	68.29	0.801	8063.5	75.48	0.836
7391.7	69.02	0.798	8243.4	75.12	0.833
9412.0	77.51	0.794	9813.2	84.31	0.827
10828.5	86.14	0.793	11276.7	93.73	0.825
11978.9	91.48	0.795	12452.4	99.40	0.824
13088.8	97.53	0.797	13589.7	106.29	0.824
14918.8	106.22	0.791	15477.4	116.08	0.818
16180.3	113.44	0.788	16786.8	125.04	0.814
18960.4	125.22	0.790	19621.1	136.46	0.813
20958.5	135.22	0.795	21658.9	148.25	0.815

INSERT DESIGNATION: PA

SEGMENT 1			SEGMENT 2		
Re	Nu	Ts/Tb	Re	Nu	Ts/Tb
5806.4	41.97	0.756	6061.9	42.55	0.780
7599.4	49.93	0.762	7896.7	50.27	0.779
8819.9	55.88	0.750	9165.1	55.63	0.768
10078.3	60.42	0.756	10443.1	59.65	0.772
12606.1	71.56	0.761	13023.1	68.35	0.773
15283.1	81.86	0.764	15754.3	78.70	0.774
17671.8	91.22	0.767	18188.1	86.65	0.773
20105.4	101.23	0.769	20667.9	94.46	0.774

SEGMENT 3			SEGMENT 4		
Re	Nu	Ts/Tb	Re	Nu	Ts/Tb
6298.4	46.29	0.806	6516.5	43.49	0.830
8179.9	54.76	0.798	8451.0	52.07	0.817
9493.6	61.13	0.788	9811.5	58.88	0.808
10787.7	64.68	0.790	11120.3	62.07	0.808
13418.9	74.83	0.787	13808.5	71.58	0.802
16202.7	84.70	0.787	16646.0	82.04	0.800
18683.6	92.74	0.782	19181.7	90.48	0.792
21205.5	101.02	0.782	21749.2	98.99	0.791

INSERT DESIGNATION: AW

SEGMENT 1			SEGMENT 2		
Re	Nu	Ts/Tb	Re	Nu	Ts/Tb
2973.7	23.10	0.778	3111.7	28.41	0.810
3722.7	25.54	0.775	3881.2	32.44	0.802
4507.8	30.27	0.774	4693.5	37.01	0.798
5302.0	33.97	0.769	5513.5	40.89	0.792
5833.5	36.11	0.739	6083.2	42.66	0.764
6106.2	36.90	0.770	6334.6	43.92	0.791
7122.7	40.96	0.772	7373.4	48.26	0.790
7175.3	41.86	0.742	7461.0	48.50	0.762
8437.5	46.69	0.744	8751.9	53.04	0.761
9976.2	52.08	0.740	10331.1	58.95	0.756
11081.6	56.36	0.750	11450.6	63.24	0.761
12547.3	60.98	0.762	12927.9	67.93	0.772
13760.5	65.68	0.766	14161.3	72.03	0.774
15063.9	69.49	0.762	15495.9	77.07	0.771
17637.3	79.14	0.757	18130.7	85.71	0.766
19660.8	85.68	0.762	20181.9	92.06	0.769

SEGMENT 3			SEGMENT 4		
Re	Nu	Ts/Tb	Re	Nu	Ts/Tb
3247.0	31.78	0.844	3365.7	30.70	0.875
4044.7	36.78	0.832	4192.7	34.92	0.860
4883.4	41.26	0.825	5057.6	39.01	0.850
5729.8	45.80	0.818	5929.9	43.01	0.843
6337.0	47.69	0.793	6571.1	44.03	0.821
6569.2	49.11	0.814	6787.5	45.48	0.837
7632.6	53.83	0.811	7876.7	49.82	0.832
7754.9	54.11	0.785	8033.3	50.52	0.809
9074.7	58.77	0.781	9383.2	54.69	0.802
10695.6	64.98	0.775	11044.2	60.29	0.796
11833.8	69.29	0.776	12207.0	64.54	0.792
13321.8	74.06	0.785	13705.3	68.96	0.800
14574.6	78.34	0.786	14978.4	72.97	0.800
15942.0	83.75	0.784	16375.6	77.58	0.798
18635.4	93.28	0.779	19127.8	86.74	0.793
20716.4	100.01	0.780	21242.4	93.34	0.792

INSERT DESIGNATION: AC

SEGMENT 1			SEGMENT 2		
Re	Nu	Ts/Tb	Re	Nu	Ts/Tb
2903.0	29.93	0.773	3078.2	34.22	0.816
3634.1	35.03	0.760	3852.6	40.83	0.802
4395.5	40.10	0.764	4642.5	46.71	0.800
5177.0	44.17	0.756	5457.2	50.83	0.791
5872.2	48.71	0.768	6164.7	55.11	0.799
6102.3	49.09	0.755	6412.7	55.56	0.788
7089.9	54.67	0.771	7414.9	61.56	0.796
7334.5	57.09	0.765	7679.5	63.64	0.792
8629.1	63.25	0.755	9026.9	70.22	0.780
9994.5	71.94	0.751	10445.1	77.53	0.776
11105.7	77.99	0.746	11598.9	82.64	0.771
12482.9	84.94	0.747	13015.6	89.23	0.770
13645.9	90.01	0.749	14205.0	93.91	0.770
14905.5	96.03	0.750	15497.0	99.17	0.769
17444.8	108.76	0.751	18103.3	110.51	0.769
19644.0	118.24	0.755	20347.1	118.93	0.771

SEGMENT 3			SEGMENT 4		
Re	Nu	Ts/Tb	Re	Nu	Ts/Tb
3235.1	39.36	0.858	3365.2	36.95	0.894
4052.7	45.83	0.843	4220.2	42.45	0.878
4873.1	51.65	0.837	5070.0	47.49	0.869
5720.6	55.70	0.826	5947.9	50.77	0.857
6439.5	59.95	0.830	6680.3	55.74	0.859
6705.4	61.40	0.822	6959.7	55.16	0.853
7728.2	67.06	0.823	8009.2	61.17	0.848
8009.4	69.32	0.820	8306.3	64.25	0.846
9409.9	76.55	0.808	9757.5	70.93	0.834
10874.9	84.16	0.802	11267.2	77.48	0.827
12065.3	89.41	0.797	12491.8	82.70	0.823
13519.7	95.82	0.795	13984.0	89.42	0.819
14737.0	100.93	0.793	15230.4	93.63	0.815
16059.6	106.64	0.791	16584.2	99.24	0.813
18728.1	118.54	0.789	19315.4	110.85	0.810
21013.2	127.28	0.790	21643.3	119.32	0.809

INSERT DESIGNATION: A1

Re	Cf
6680.4	0.0921
8109.1	0.0904
9407.6	0.0889
10814.1	0.0882
12182.6	0.0872
13517.6	0.0858
14471.7	0.0853
16136.9	0.0848
18812.2	0.0836
20681.8	0.0829

INSERT DESIGNATION: A4

Re	Cf
6377.7	0.1452
9235.7	0.1397
10720.7	0.1391
12017.8	0.1376
13345.7	0.1366
14653.2	0.1350
16096.3	0.1353
18892.7	0.1325
20738.2	0.1316

INSERT DESIGNATION: AN

Re	Cf
6275.2	0.0757
8034.9	0.0738
9364.5	0.0724
10849.2	0.0710
12120.4	0.0705
13453.1	0.0700
14594.4	0.0694
15779.3	0.0690
18733.3	0.0676
20828.9	0.0671

INSERT DESIGNATION: A3

Re	Cf
6422.4	0.1122
7822.6	0.1102
9150.7	0.1091
10616.9	0.1076
11975.3	0.1066
13436.6	0.1053
14541.7	0.1052
15962.5	0.1047
18422.2	0.1036
20488.9	0.1031

INSERT DESIGNATION: A2

Re	Cf
7075.1	0.0425
7741.3	0.0416
8868.7	0.0404
10156.6	0.0394
11411.1	0.0386
12690.9	0.0377
14184.6	0.0371
15795.3	0.0366
17288.4	0.0361
18919.3	0.0357
21917.0	0.0351
24591.7	0.0345

INSERT DESIGNATION: A5

Re	Cf
6237.0	0.0352
7529.2	0.0336
9086.6	0.0321
10485.9	0.0315
11820.6	0.0307
13187.1	0.0305
14424.2	0.0298
15753.8	0.0302
18334.6	0.0293
20403.2	0.0293

INSERT DESIGNATION: A6

Re	Cf
11902.5	0.0703
13266.6	0.0695
14452.5	0.0692
20699.1	0.0676
10654.3	0.0711
18578.2	0.0680
16027.7	0.0690
9174.2	0.0722
7663.5	0.0735
6283.8	0.0755
7467.5	0.0753
6433.2	0.0768
5663.2	0.0769
4779.2	0.0776
3969.4	0.0830
3204.3	0.0846

INSERT DESIGNATION: A7

Re	Cf
3979.9	0.0676
4873.8	0.0653
5719.8	0.0622
6415.8	0.0613
6593.6	0.0637
7698.5	0.0620
7888.8	0.0601
9225.4	0.0586
10716.8	0.0588
11976.1	0.0576
13258.1	0.0574
14572.7	0.0557
15851.9	0.0550
18469.2	0.0546
20669.8	0.0532

INSERT DESIGNATION: A9

Re	Cf
3086.5	0.1043
3921.1	0.1000
4682.4	0.0984
5608.1	0.0951
6186.1	0.0937
6482.9	0.0926
7525.0	0.0911
7691.5	0.0909
9184.8	0.0893
10581.4	0.0885
11716.8	0.0875
12814.8	0.0865
14622.2	0.0853
15865.6	0.0845
18620.4	0.0830
20606.2	0.0825

INSERT DESIGNATION: A8

Re	Cf
3161.0	0.0445
13197.8	0.0349
20576.7	0.0337
18512.4	0.0340
11812.6	0.0356
16056.1	0.0346
14784.4	0.0347
10619.8	0.0360
9063.7	0.0365
7587.9	0.0378
6208.3	0.0389
7398.1	0.0395
6441.3	0.0393
5580.2	0.0399
4754.1	0.0418
3949.4	0.0432

INSERT DESIGNATION: PA

Re	Cf
6170.8	0.0563
8031.8	0.0531
9322.5	0.0515
10607.4	0.0507
13214.1	0.0490
15971.5	0.0479
18431.3	0.0471
20932.0	0.0463

INSERT DESIGNATION: AW

Re	Cf
3174.5	0.0351
3960.3	0.0359
4785.6	0.0344
5618.8	0.0341
6449.4	0.0309
7501.3	0.0302
6206.2	0.0322
7606.1	0.0310
10511.8	0.0294
11643.2	0.0286
8911.8	0.0301
13125.6	0.0282
14368.7	0.0276
15719.3	0.0271
18382.8	0.0266
20450.4	0.0263

INSERT DESIGNATION: AC

Re	Cf
3145.4	0.0984
3939.9	0.0949
4745.3	0.0937
5575.7	0.0898
6289.2	0.0876
6545.0	0.0893
7560.5	0.0878
7832.4	0.0860
9205.9	0.0838
10645.4	0.0828
11815.4	0.0816
13250.6	0.0811
14454.6	0.0808
15761.6	0.0800
18397.9	0.0789
20661.9	0.0767

XIII. APPENDIX F: MULTIPLE LINEAR REGRESSION USING MATRICES

To obtain the values of the parameters in the correlation equations, a matrix approach to multiple linear regression was used. Taking the logarithm of the correlation equations converts them to linear equations with multiple independent variables of the following form:

$$Y_i = \beta_0 + \beta_1 X_{1i} + \beta_2 X_{2i} + \ldots\ldots + \beta_p X_{pi} + \varepsilon_i, \; i = 1,\ldots n. \qquad (F.1)$$

The same model for all the n observations can be written in matrix form by defining the following matrices:

$$[Y] = \begin{bmatrix} Y_1 \\ Y_2 \\ . \\ . \\ Y_n \end{bmatrix} \quad [X] = \begin{bmatrix} 1 & X_{11} & X_{21} & \cdots & X_{p1} \\ 1 & X_{12} & X_{22} & \cdots & X_{p2} \\ . & . & . & & . \\ . & . & . & & . \\ 1 & X_{1n} & X_{2n} & & X_{pn} \end{bmatrix} \quad [\beta] = \begin{bmatrix} \beta_1 \\ \beta_2 \\ . \\ . \\ \beta_n \end{bmatrix} \quad [\varepsilon] = \begin{bmatrix} \varepsilon_1 \\ \varepsilon_2 \\ . \\ . \\ \varepsilon_n \end{bmatrix}$$

Then, the model in matrix notation is

$$[Y] = [X][\beta] + [\varepsilon] \qquad (F.2)$$

To estimate the parameters, the sum of squares is to be minimized is

$$SS = ([Y] - [X][B])^T ([Y] - [X][B]) \qquad (F.3)$$

where [B] is estimate of [β]. The normal equation can be written as

$$([X]^T [X])\ [B] = [X]^T [Y] \tag{F.4}$$

The least square estimates of [B] can be obtained by inverting the matrix $[X]^T[X]$ and is

$$[B] = ([X]^T[X])^{-1} ([X]^T[Y]) \tag{F.5}$$

The estimate of the variance is given by

$$s_E^2 = ([Y]^T[Y] - [B]^T[X]^T[Y])/(n-p-1) \tag{F.6}$$

Also, the variances and covariances of the b's are easily expressed in matrix notation by

$$[V]([B]) = ([X]^T[X])\quad \sigma_E^2 \tag{F.7}$$

If [C] is defined as $([X]^T[X])^{-1}$ and the estimated variance s_E^2 is used as the estimate of σ_E^2, the variance of b_h is

$$s_{b_h}^2 = c_{hh}\, s_E^2, \quad h = 1,2,\ldots p \tag{F.8}$$

where c_{hh} are the elements in matrix [C].

Based on the assumption of normal distribution, 100γ percent confidence interval for b_h is given by

$$\begin{matrix} U \\ L \end{matrix} = b_h \pm t_{[(1+\gamma)/2](n-p-1)}\, s_{b_h}, \quad h = 1,2,..p \tag{F.9}$$

The correlation coefficient, R^2, is given by the following equation

$$R^2 = \frac{[B]^T[X][Y] - n(\Sigma Y_i)^2}{[Y]^T[Y] - n(\Sigma Y_i)^2} \qquad \text{(F.10)}$$

where ΣY_i is given by the (1,1) element in the matrix $[X]^T[X]$.

The equations in this appendix were by solved using the Heat Transfer Laboratory HP 9845B Desktop Computer which has the capability to handle matrix arithmetic without any involved programming.

XIV. APPENDIX G. MATHEMATICAL SOLUTIONS USED IN THE SURFACE RENEWAL/PENETRATION MODEL

The solution of

$$\frac{\partial T}{\partial t} = \alpha \frac{\partial^2 T}{\partial y^2} \tag{G.1}$$

with the following initial and boundary conditions:

$$\begin{aligned} T &= T_i \quad \text{at } t = 0 \text{ and } y > 0 \\ T &= T_w \quad \text{at } t > 0 \text{ and } y = 0 \\ T &= T_i \quad \text{at } t > 0 \text{ and } y = \delta \end{aligned} \tag{G.2}$$

is obtained by using the method of separation of variables.

First, the variables are transformed into nondimensional variables by defining

$$T = \frac{T - T_w}{T_i - T_w} \qquad \text{and} \qquad Y = y/\delta \ .$$

The differential equation can then be written as

$$\frac{\partial T}{\partial t} = \frac{\alpha}{\delta^2} \frac{\partial^2 T}{\partial Y^2} \tag{G.3}$$

and the initial and boundary conditions become

$$T[Y,0] = 1$$

$$T[0,t] = 0$$

$$T[1,t] = 1$$

To obtain a homogeneous boundary condition, a new variable W, is defined as $W = T - Y$. The differential equation becomes

$$\frac{\partial W}{\partial t} = \frac{\alpha}{\delta^2} \frac{\partial^2 W}{\partial Y^2} \tag{G.4}$$

with initial and boundary conditions

$$W(t = 0,\ Y > 0) = 1 - Y$$

$$W(t > 0,\ Y = 0) = 0$$

$$W(t > 0,\ Y = 1) = 0$$

To solve the above equation, the method of separation of variables is used. Defining

$$W(t,Y) = U(t)\ V(Y) \tag{G.5}$$

the differential equation becomes

$$V(Y) \frac{\partial U(t)}{\partial t} = \frac{\alpha}{\delta^2}\ U(t) \frac{\partial^2 V(Y)}{\partial Y^2}$$

$$\frac{U'}{\alpha U} = \frac{V''}{V} \tag{G.6}$$

In the above equation, the left member is clearly independent of Y, and therefore, the right member also is independent of Y. Similarly the left and right members must be independent of t.

Therefore,

$$\frac{U'}{(\alpha/\delta^2)U} = \frac{V''}{V} = \xi = \text{a constant}$$

For $\xi > 0$ the solutions turn out to be trivial.

Therefore,

for $\xi < 0$, i.e. $\xi = -\beta^2$

$$V'' + \beta^2 V = 0, \quad V(0) = V(1) = 0$$

$$V = A \cos(\beta Y) + B \sin(\beta Y)$$

$$V(0) = 0 \rightarrow A = 0$$

$$V = B \sin(\beta Y)$$

$$V(1) = B \sin(\beta) = 0$$

Here, $B \neq 0$, as it would imply a trivial solution.

Therefore,

$$\sin(\beta) = 0, \quad \text{or} \quad \beta = n\pi, \quad \text{where } n = 0,1,2 \ldots$$

$$V = B \sin(n\pi Y)$$

$$= B_n \sin(n\pi Y), \quad n = 0,1,2 \ldots$$

The solution of

$$\frac{U'}{(\alpha/\delta^2)U} = -\beta^2$$

$$\frac{U'}{U} = -\frac{\alpha\beta^2}{\delta^2}$$

$$\ln U = -\frac{\alpha\beta^2 t}{\delta^2} + C_1$$

$$U = C \exp\left(-\frac{\alpha\beta^2 t}{\delta^2}\right)$$

Combining U and V

$$W = UV = D_n \sin(n\pi Y) \exp\left(-\frac{\alpha\beta^2 t}{\delta^2}\right), \quad n = 0,1,2.....$$

where $D_n = C\ B_n$,

or

$$W = \sum_{n=1}^{\infty} D_n \sin(n\pi Y) \exp\left(-\frac{\alpha\beta^2 t}{\delta^2}\right)$$

since each value of n is a solution.

For the initial condition, t = 0

$$W = 1 - Y = \sum_{n=1}^{\infty} D_n \sin(n\pi Y) \exp\left(-\frac{\alpha\beta^2 t}{\delta^2}\right)$$

Using Fourier series

$$D_n = \frac{2}{1} \int_0^1 (1 - Y) \sin(n\pi Y) dY$$

$$= 2 \int_0^1 \sin(n\pi Y) dY - 2 \int_0^1 Y \sin(n\pi Y) dY$$

$$= 2 \left(-\right) \frac{\cos(n\pi Y)}{n\pi} \Bigg|_0^1 - 2 \left(-\right) \frac{Y \cos(n\pi Y)}{n\pi} \Bigg|_0^1 + 2 \int_0^1 \left(-\right) \frac{\cos(n\pi Y)}{n\pi} dY$$

$$= \frac{2}{n\pi} \left[-\cos(n\pi) + 1\right] - \frac{2}{n\pi} \left[-\cos(n\pi)\right] + 2 \left[\frac{\sin(n\pi Y)}{n^2\pi^2}\right]_0^1$$

$$= 2/n\pi$$

$$W = \sum_{n=1}^{\infty} \frac{2}{n\pi} \sin(n\pi Y) \exp\left(-\frac{\alpha\beta^2 t}{\delta^2}\right) \qquad (G.7)$$

Substituting back for W

$$T - Y = \sum_{n=1}^{\infty} \frac{2}{n\pi} \sin(n\pi Y) \exp\left(-\frac{\alpha n^2\pi^2 t}{\delta^2}\right)$$

$$\frac{T - T_w}{T_i - T_w} = \sum_{n=1}^{\infty} \frac{2}{n\pi} \sin(n\pi Y) \exp\left(-\frac{\alpha n^2\pi^2 t}{\delta^2}\right)$$

$$\frac{T - T_w}{T_i - T_w} = \frac{y}{\delta} + \sum_{n=1}^{\infty} \frac{2}{n\pi} \sin(n\pi Y) \exp\left(-\frac{\alpha n^2 \pi^2 t}{\delta^2}\right) \qquad (G.8)$$

The instantaneous heat-transfer rate is given by

$$q_i(t) = -k \left.\frac{dT}{dy}\right|_{y=0} \qquad (G.9)$$

The mean heat transfer rate is

$$q = \int_0^{\infty} q_i(t)\, P(t)\, dt \qquad (G.10)$$

where

$$P(t) = s \exp(-st) \qquad (G.11)$$

Substituting G.8 into G.9

$$q_i(t) = -k(T_i - T_w)\left[\frac{1}{\delta} + \frac{2}{\pi} \sum_{n=1}^{\infty} \frac{1}{n} \cos\left(\frac{n\pi y}{\delta}\right)\left(\frac{n\pi}{\delta}\right) \exp\left(-\frac{\alpha n^2 \pi^2 t}{\delta^2}\right)\right]\Bigg|_{y=0}$$

$$= -k(T_i - T_w)\left[\frac{1}{\delta} + \frac{2}{\delta} \sum_{n=1}^{\infty} \exp\left(-\frac{\alpha n^2 \pi^2 t}{\delta^2}\right)\right]$$

$$q = \int_0^{\infty} -\frac{k}{\delta}(T_i - T_w)\left[\frac{1}{\delta} + 2 \sum_{n=1}^{\infty} \exp\left(-\frac{\alpha n^2 \pi^2 t}{\delta^2}\right) s e^{-st}\right] dt$$

$$q = -\frac{k}{s\delta}(T_i - T_w)\int_0^\infty \left[e^{-st} + 2\sum_{n=1}^{\infty} \exp\left(-s + \frac{\alpha n^2\pi^2}{\delta^2}\right)t \right] dt$$

$$q = -\frac{k}{s\delta}(T_i - T_w)\left[\frac{e^{-st}}{-s}\Bigg|_0^\infty + 2\sum_{n=1}^{\infty} \frac{\exp\left(-s + \frac{\alpha n^2\pi^2}{\delta^2}\right)t}{-s + \frac{\alpha n^2\pi^2}{\delta^2}}\Bigg|_0^\infty \right]$$

$$q = -\frac{ks}{\delta}(T_i - T_w)\left[\frac{1}{s} + 2\sum_{n=1}^{\infty} \frac{\delta^2}{s\delta^2 + \alpha n^2\pi^2} \right]$$

$$q = -\frac{ks}{\delta}(T_i - T_w)\left[\frac{1}{s} + 2\sum_{n=1}^{\infty} \frac{\delta^2/\alpha}{s\delta^2/\alpha + n^2\pi^2} \right]$$

$$q = -\frac{ks}{\delta}(T_i - T_w)\left[\frac{1}{s} + \frac{2s\delta^2}{s\alpha}\sum_{n=1}^{\infty} \frac{1}{s\delta^2/\alpha + n^2\pi^2} \right]$$

Letting $Z^2 = s\delta^2/\alpha$ and substituting Z into the above equation,

$$q = -\frac{k}{\delta}(T_i - T_w)\left[1 + 2Z^2\sum_{n=1}^{\infty} \frac{1}{Z^2 + n^2\pi^2} \right]$$

$$q = -\frac{k}{\delta}(T_i - T_w)\, Z\left[\frac{1}{Z} + 2Z\sum_{n=1}^{\infty} \frac{1}{Z^2 + n^2\pi^2} \right]$$

But,

$$\coth(Z) = \frac{1}{Z} + 2Z \sum_{n=1}^{\infty} \frac{1}{Z^2 + n^2\pi^2}$$

Therefore,

$$q = -\frac{k}{\delta} (T_i - T_w) Z \coth(Z)$$

$$q = -\frac{k}{\delta} (T_i - T_w) \left(\frac{s\delta^2}{\alpha}\right)^{\frac{1}{2}} \coth\left(\frac{s\delta^2}{\alpha}\right)^{\frac{1}{2}}$$

$$q = -\frac{k}{\delta} (T_i - T_w) \left(\frac{s\rho c_p}{k}\right)^{\frac{1}{2}} \coth\left(\frac{s\delta^2}{\alpha}\right)^{\frac{1}{2}}$$

$$q = -(T_i - T_w) (sk\rho c_p)^{\frac{1}{2}} \coth\left(\frac{s\delta^2}{\alpha}\right)^{\frac{1}{2}} \qquad \text{(G.12)}$$